Synthesis, Oxidation and Photophysics of Perfluoroborated Tetrakis(pyrophosphito)diplatinate (II) and Density Functional Theory (DFT) Study of Electrochemical CO_2 Reduction by Mn Catalysts

Thesis by
Yan Choi Lam

In Partial Fulfillment of the Requirements for the degree
of
Doctor of Philosophy

CALIFORNIA INSTITUTE OF TECHNOLOGY
Pasadena, California
2015
(Defended 9th March 2015)

ACKNOWLEDGEMENTS

My life and work at Caltech has been greatly blessed by the many people Providence has brought into my life. Indeed, this thesis is greatly enriched by the many colleagues and collaborators I have had the privilege of working with, as is evident in the very extensive author list in Chapter II.

I'd like to thank first and foremost my scientific collaborators. It was a joy to work with Alec and Gretchen, serious scientists who are also kind and fun to be with. I have had a very fruitful collaboration with Prof. Antonín Vlček. Thank you, Tony; I have benefited much from your diligence, patience and expertise. Through Tony, I have also had the privilege of working with some great collaborators in the Czech Republic. I'd like especially to thank Standa and Jan for their warm welcome when I visited Prague in 2012. The other students and researchers at the J. Heyrovský Institute of Physical Chemistry, too, were gracious hosts. I regret only that my visit was really too short, and look forward to a day when I can visit again.

Much the same can be said of my time at the University of Regensburg. I have benefited much from interacting with Hartumt and Thomas, among the other wonderful people and scientists I met at Regensburg. I hope to visit again.

Back in Pasadena, the Bercaw, Gray, and Goddard groups (especially the Catalysis and JCAP sub-groups) have been wonderful colleagues; I owe to them almost everything I know today about chemistry. No doubt some are—quite justly—disappointed that I have not been a better student; I apologize for this and other transgressions, and hope that our

time together will prove to be a starting point for many years of friendship and learning from each other, perhaps even scientific collaboration.

I came to Caltech with no previous experience, and little knowledge, of time-resolved spectroscopy, photophysics, or computational chemistry. Thank you, John, Harry and Bill, for giving me the opportunity to learn and freedom to explore. I hope I have not been a major disappointment. I am also indebted to the many people who have kindly and patiently imparted their knowledge and skill to me—to Alec for teaching me time-resolved electronic spectroscopy and luminescence spectroscopy, to many members of the Bercaw group for various laboratory techniques, to Smith who taught me everything I know about computational chemistry, to Jay (Winkler) for his patience in teaching me photophysics and what little coding in MATLAB I know.

The "supporting" staff have been fantastic. Our crystallographers Larry Henling and Mike Takase solved and refined the structures presented here. Pat, Rick, and Shirley have taken such care of administrative minutiae that I have had little to worry about on that front; they are also such pleasant and humorous people to be with. The phenomenal non-faculty staff at Caltech deserve a special mention. I have mentioned Smith and Jay Winkler; I have also learned much from Jay Labinger and Bruce. I hope someday to become half as intelligent and knowledgeable as they are.

John, Harry, and Bill have, each in his own way, been great advisers, who have had great patience with me when progress was slow. (I wish I was a better advisee.) John and Harry have modeled for me scientists great not only in their expertise, but especially in

humor, generosity, and kindness towards all. I am especially touched that Harry knows and greets some of our custodial staff by name. Bill has been enthusiastic about my work on CO_2 reduction from day one, and given me much freedom to explore various aspects of this chemistry. I especially appreciate his chemical intuitions and willingness to take on seemingly impossible challenges with gusto. ("CO_2 reduction on Cu makes the phonebook? Bring it on!" This is surely a poor paraphrase, but one gets the general idea.)

However much graduate school may feel like a cloister, even life in the lab is not all about science. Accordingly, I have enjoyed friendship with my colleagues and many others. Sibo was a great roommate, classmate, and friend, with whom I enjoyed hiking and many other things. Smith has been a great mentor, but also much more besides. Congratulations, Ross, you have managed not only to obtain a PhD degree, but also to marry and start a family (not necessarily in that order). Ian and Alex showed me how it is possible not only to be dedicated scientists, but also have an active social life and care for junior members of the group. Sam's boisterous loudness has added so much life and fun to our little part of MSC. The Cp-All-Stars were an amazing group to hang out and play with, softball being largely a pretext for socializing.

Outside of Caltech, the good people of Trinity Baptist Church have been a source of encouragement and perspective. The patient endurance of those who are living through sickness and other trials puts my complaints and worries into perspective. Tim, Tania, Jonathan, Genti and Amos have been especially dear friends and brothers and sisters. Dwayne and Malana, Joe and Elsa, and Robert and Mami, have loved me like family.

Many thanks, too, for the countless prayers unheard except in Heaven; I am convinced that I have escaped many evils through them.

My brothers and sisters at iPraise, too, have been a source of joy and companionship. Thanks for the many rides you have offered me. Before I bought my car (from one of them), they were my only occasion to enjoy decent Chinese food (nowhere to be found in Pasadena!). The EBCM "diaspora" are always in my thoughts and prayers. I rejoice especially to see the arrows God has put in your quivers; may your children grow up in the fear and love of the LORD.

My loving parents have been supportive all along, as have my aunts and uncles even if I have a hard time explaining to them what I do. My sister's wedding was a highlight of my last year in graduate school, and serving as emcee at her wedding a great joy. May you and Ashley spend many happy years together, and may your quiver be filled as all-wise Providence deems best.

Finally, *summa cum laude* to the One Triune God, who has neither dealt with me as my sins deserve nor withheld His grace for me. All the inadequacies in this thesis and in my time here at Caltech are naturally *mea culpa*, and much credit for any good belongs to my advisors, collaborators, colleagues and classmates, but all glory belongs to the Source of all knowledge and goodness.

夫能保爾無蹶、立爾於其有榮之前、歡然無瑕、唯一上帝、我之救者、願榮威權力、由我主耶穌基督歸之、先乎萬古、以迄於今、至於世世、阿們。

ABSTRACT

In the first part of this thesis (Chapters I and II), the synthesis, characterization, reactivity and photophysics of per(difluoroborated) tetrakis(pyrophosphito)diplatinate(II) (Pt(POP-BF_2)) are discussed. Pt(POP-BF_2) was obtained by reaction of $[Pt_2(POP)_4]^{4-}$ with neat boron trifluoride diethyl etherate ($BF_3 \cdot Et_2O$). While Pt(POP-BF_2) and $[Pt_2(POP)_4]^{4-}$ have similar structures and absorption spectra, they differ in significant ways. Firstly, as discussed in Chapter I, the former is less susceptible to oxidation, as evidenced by the reversibility of its oxidation by I_2. Secondly, while the first excited triplet states (T_1) of both Pt(POP-BF_2) and $[Pt_2(POP)_4]^{4-}$ exhibit long lifetimes (ca. 10 μs at room temperature) and substantial zero-field splitting (40 cm^{-1}), Pt(POP-BF_2) also has a remarkably long-lived (1.6 ns at room temperature) singlet excited state (S_1), indicating slow intersystem crossing (ISC). Fluorescence lifetime and quantum yield (QY) of Pt(POP-BF_2) were measured over a range of temperatures, providing insight into the slow ISC process. The remarkable spectroscopic and photophysical properties of Pt(POP-BF_2), both in solution and as a microcrystalline powder, form the theme of Chapter II.

In the second part of the thesis (Chapters III and IV), the electrochemical reduction of CO_2 to CO by $[(L)Mn(CO)_3]^-$ catalysts is investigated using density functional theory (DFT). As discussed in Chapter III, the turnover frequency (TOF)-limiting step is the dehydroxylation of $[(bpy)Mn(CO)_3(CO_2H)]^{0/-}$ (bpy = bipyridine) by trifluoroethanol (TFEH) to form $[(bpy)Mn(CO)_4]^{+/0}$. Because the dehydroxylation of $[(bpy)Mn(CO)_3(CO_2H)]^-$ is faster, maximum TOF (TOF_{max}) is achieved at potentials sufficient to completely reduce $[(bpy)Mn(CO)_3(CO_2H)]^0$ to $[(bpy)Mn(CO)_3(CO_2H)]^-$. Substitution of bipyridine with

bipyrimidine reduces the overpotential needed, but at the expense of TOF_{max}. In Chapter IV, the decoration of the bipyrimidine ligand with a pendant alcohol is discussed as a strategy to increase CO_2 reduction activity. Our calculations predict that the pendant alcohol acts in concert with an external TFEH molecule, the latter acidifying the former, resulting in a ~ 80,000-fold improvement in the rate of TOF-limiting dehydroxylation of $[(L)Mn(CO)_3(CO_2H)]^-$.

An interesting strategy for the co-upgrading of light olefins and alkanes into heavier alkanes is the subject of Appendix B. The proposed scheme involves dimerization of the light olefin, operating in tandem with transfer hydrogenation between the olefin dimer and the light alkane. The work presented therein involved a Ta olefin dimerization catalyst and a silica-supported Ir transfer hydrogenation catalyst. Olefin dimer was formed under reaction conditions; however, this did not undergo transfer hydrogenation with the light alkane. A significant challenge is that the Ta catalyst selectively produces highly branched dimers, which are unable to undergo transfer hydrogenation.

FOREWORD

Portions of this thesis have been published in peer-reviewed journals, and there are plans to publish other portions. The spectroscopy and photophysics of Pt(POP-BF_2) in MeCN solution, here incorporated into Chapter II, were published in *Journal of the American Chemical Society* in 2012,[1] although the fitting of temperature-dependent non-radiative decay rates to an Arrhenius expression discussed in that article has not been incorporated. Instead, we here discuss a few quantum mechanical models for understanding non-radiative decay in microcrystalline Pt(POP-BF_2) over a 5-310 K temperature range. Additionally, we were recently notified that our work on Mn-catalyzed CO_2 reduction to CO, forming most of Chapter III, has been accepted for publication in *ACS Catalysis*.[2]

The high resolution and time-resolved spectroscopy of microcrystalline Pt(POP-BF_2), which forms the remainder of Chapter II (and for which the experiments were conducted primarily at the University of Regensburg by Dr. Thomas Hofbeck; I performed most of the data analysis and wrote the manuscript), is in the last stages of manuscript preparation, as is the work presented in Chapter IV.

---

[1] Alec C. Durrell; Gretchen E. Keller; Yan-Choi Lam; Jan Sýkora; Antonín Vlček, Jr.; and Harry B. Gray, *Structural control of $^1A_{2u}$ to $^3A_{2u}$ intersystem crossing in diplatinum (II,II) complexes, J. Am. Chem. Soc.* **2012**, *134*, 14201-14207.

[2] Yan Choi Lam, Robert J. Nielsen, Harry B. Gray, and William A. Goddard, III, *A Mn Bipyrimidine Catalyst Predicted To Reduce CO_2 at Lower Overpotential, ACS Catal.* **2015**, *5*, 2521−2528.

TABLE OF CONTENTS

Chapter I

Synthesis and Oxidation of Per(difluoroborated)-tetrakis(pyrophosphito)diplatinate(II) ($[Pt_2(pop\text{-}BF_2)_4]^{4-}$)

Y.C. Lam; J. A. Labinger; J. E. Bercaw; H. B. Gray

Abstract

Salts of per(difluoroborated) tetrakis(pyrophosphito)diplatinate(II) ([*n*-$Bu_4N]_4[Pt_2(^{BF2}POP)_4]$, **3a**, and $[Ph_4As]_4[Pt_2(^{BF2}POP)_4]$, **3b**) were obtained by reaction of [*n*-$Bu_4N]_4[Pt_2(POP)_4]$ (**1a**) and $[Ph_4As]_4[Pt_2(POP)_4]$ (**1b**) with neat boron trifluoride diethyl etherate. The structure of **3b** and the absorption spectrum of **3a** closely resemble those of **1**. Reaction of I_2 with **3a** and **3b** yielded [*n*-$Bu_4N]_4[Pt_2(^{BF2}POP)_4I_2]$ (**4a**) and $[Ph_4As]_4[Pt_2(^{BF2}POP)_4I_2]$ (**4b**) (Pt-Pt, 2.7223 Å; Pt-I, 2.7292 Å), respectively. Unlike $[Pt_2(POP)_4I_2]^{4-}$, $[Pt_2(^{BF2}POP)_4I_2]^{4-}$ is in equilibrium with $[Pt_2(^{BF2}POP)_4]$ and I_2 in acetonitrile solution. Reaction of **3a** with [*n*-$Bu_4N][Br_3]$ gives [*n*-$Bu_4N]_4[Pt_2(^{BF2}POP)_4Br_2]$ (**5a**); the Pt-Pt (2.692 Å) and Pt-Br (2.534 Å) distances in $[Ph_4As]_4[Pt_2(^{BF2}POP)_4Br_2]$ (**5b**) are slightly shorter than those in [*n*-$Bu_4N]_4[Pt_2(POP)_4Br_2]$.

Introduction

Face-to face binuclear complexes of Pt(II),[1] Ir(I)[2] and Rh(I)[3] have been extensively investigated, owing in part to their rich spectroscopic, photophysical, and photochemical properties. An MO model accounts for the electronic structures of these complexes: overlap of the *n* d_{z^2} and (*n+1*) p_z orbitals from two d^8 square planar units generates two bonding (dσ, pσ) and two antibonding orbitals (dσ*, pσ*); the dσ and dσ* orbitals are filled, whereas the pσ and pσ* orbitals are vacant (Figure 1). A weak metal-metal bond in the ground state is attributable to *n* d_{z^2} and (*n+1*) p_z mixing.[4]

Tetrakis(μ-pyrophosphito)diplatinate(II), $[Pt_2(\mu\text{-}P_2O_5H_2)_4]^{4-}$ (**1**), commonly referred to as "platinum-pop",[1] is the archetypal d^8-d^8 complex.[5,6] Electronic excitation of **1** produces a triplet (^{3}[**1**]) that phosphoresces at 514 nm with a lifetime of 9 μs.[7] Data from vibrational spectra and time-resolved crystallography demonstrate convincingly that the strength of the Pt-Pt bond in ^{3}[**1**] is greatly enhanced relative to that in the ground state, as predicted by the MO model (Figure 1b).[8]

---

[1] a) Roundhill, D. M.; Che, C. M. and Gray, H. B., *Acc. Chem. Res.* **1989**, *22*, 55-61; b) A. P. Zipp, *Coord. Chem. Rev.* **1988**, *84*, 47

[2] a) Smith, T. P., PhD Dissertation, California Institute of Technology, 1982; b) Smith, D. C., PhD Dissertation, California Institute of Technology, 1989

[3] a) Lewis, N. S.; Mann, K. R.; Gordon, J. G. II and Gray, H. B., *J. Am. Chem. Soc.* **1976**, *98*, 7461-7463; b) Mann, K. R.; Thich, J. A.; Bell, R. A.; Coyle, C. L. and Gray, H. B., *Inorg. Chem.* **1980**, *19*, 2462-2468

[4] a) Mann, K. R.; Gordon, J. G.; and Gray, H. B.., *J. Am. Chem. Soc.* **1975**, *97*, 3553-3555; b) Nocera, D. G.; Maverick, A. W.; Winkler, J. R.; Che, C.-M. and Gray, H. B., *ACS Symp. Ser.* **1983**, *No. 211*, 21-23; c) Bercaw, J. B.; Durrell, A. C.; Gray, H. B.; Green, J. C.; Hazari, N.; Labinger, J. A. and Winkler, J. R., *Inorg. Chem.* **2010**, *49*, 1801-1810

[5] Sperline, R. P.; Dickson, M. K. and Roundhill, D. M., *J. Chem. Soc., Chem. Comm.***1977,** 62-63

[6] Filomena Dos Remedios Pinto, M. A., Sadler, P. J., Neidle, S., Sanderson, M. R., Subbiah, A., and Kuroda R., *J. Chem. Soc., Chem. Comm.***1980,** 13-15. Corrections made by Marsh, R. E., and Herbstein, F. H., *Acta Crystallogr., Sect. B* **1983**, *39*, 280-287

[7] Stiegman, A. E., Rice, S. F., Gray, H. B. and Miskowski, V. M., *Inorg. Chem.* **1987**, *26*, 1112-1116

[8] a) Rice, S. F. and Gray, H. B., *J. Am. Chem. Soc.* **1983**, *105*, 4571-4575; b) Stein, *P.;* Dickson, *M. K. and* D. M. Roundhill, *J. Am. Chem. Soc.* **1983**, *105*, 3489-3494; c) Che, C.M.; Butler, L. G.; Gray, H. B.; Crooks, R. M. and

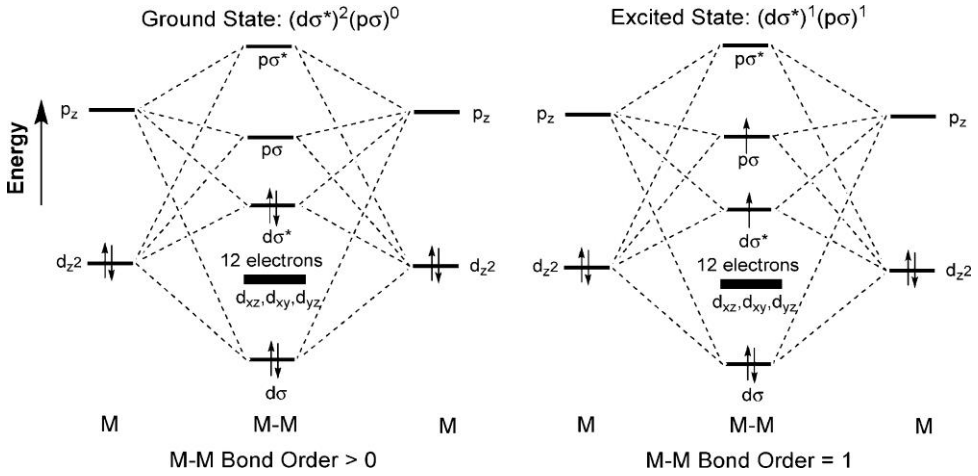

Figure 1: Electronic structures of a d^8-d^8 complex in its ground (left) and lowest triplet excited state (right).[5c]

Woodruff, W. H., *J. Am. Chem. Soc.* **1983**, *105*, 5492; d) Kim, C. D.; Pillet, S.; Wu, G.; Fullagar, W. L. and Coppens, P., *Acta Crystallogr. Sect. A* **2001**, *58*, 133*; e) Yasuda, N.; Uekusa, H. and Ohashi, Y., Bull. Chem. Soc. Jpn. **2004**, 77, 933-944; f)* Van der Veen, R. M.; Milne, C. J.; El Nahhas, A.; Lima, F. A.; Pham, V-T; Best, J.; Weinstein, J. A.; Borca, C. N.; Abela, R.; Bressler, C. and Chergui, M., *Angew. Chem. Int. Ed.* **2009**, *48*, 2711 –2714

Owing in part to its long lifetime, ^{3}[**1**] is able to abstract hydrogen atoms from stannanes, germanes, silanes,[9] alcohols,[9c,d,10] and hydrocarbons.[10c,d] It also reacts with alkyl and aryl halides,[9c,d,11] giving the Pt(III,III) alkyl or aryl halide $[Pt_2(\mu\text{-}P_2O_5H_2)_4RX]^{4-}$ and/or the Pt(III,III) dihalide $[Pt_2(\mu\text{-}P_2O_5H_2)_4X_2]^{4-}$ along with an organic radical coupling product R_2. A reaction of special interest is the photocatalytic dehydrogenation of isopropanol to acetone,[11a] which requires two photons, one to generate ^{3}[**1**] and a second to trigger reductive elimination of H_2 from the photogenerated dihydride $[Pt_2(\mu\text{-}P_2O_5H_2)_4H_2]^{4-}$. Reactions of **1** with halogens or alkyl iodides yield axially substituted diplatinum(III) complexes.[12]

Few analogues of **1** have been reported. In one such complex, $Pt_2(PCP)_4^{4-}$ (**2**), a methylene unit replaces the oxygen bridge between the phosphorous donor atoms.[13] While **1** and **2** have very similar structural and spectroscopic characteristics, triplet ^{3}[**2**] has a shorter lifetime at room temperature than ^{3}[**1**].[14] Of relevance here is that Harvey prepared and partially characterized a fluoroborated analogue of **1** in which an average of six protons

---

[9] a) Vlcek, A. and Gray, H. B., *J. Am. Chem. Soc.* **1987,** *109,* 286-287; b) Vlcek, A. and Gray, H. B., *Inorg. Chem.* **1987,** *26,* 1997-2001; c) Roundhill, D. M.; Atherton, S. J. and Shen Z-P, *J. Am. Chem. Soc.* **1987,** *109,* 6076-6079; d) Roundhill, D. M.; Shen, Z.-P.; King, C. and Atherton, S. J., *J. Phys. Chem.* **1988**, *92*, 4088-4094

[10] a) Che, C.-M.; Lee, W.-M.; Cho, K-C.; Harvey, P. D. and Gray, H. B., *J. Phys. Chem.*, **1989**, *93*, 3095–3099; b) Harvey, E. L.; Stiegman, A. E.; Vlcek, A. and Gray, H. B., *J. Am. Chem. Soc.* **1987,** *109,* 5233-5235; c) Sweeney, R. J.; Harvey, E. L. and Gray, H. B., *Coord. Chem. Rev.* **1990**, *105*, 23-34

[11] a) Roundhill, D. M., *J. Am. Chem. Soc.* **1985,** *107,* 4354-4356; b) Roundhill, D. M. and Atherton, S. J., *Inorg. Chem.* **1986,** *25,* 4071-4072; c) Roundhill, D. M., Dickson, M. K. and Atherton, S. J., *J. Organometallic Chem.* **1987,** *335,* 413-422

[12] a) Che, C.-M.; Schaefer, W. P.; Gray, H. B.; Dickson, M. K.; Stein, P. B. and Roundhill, D. M., *J. Am. Chem. Soc.* **1982,** *104,* 4253-4255; b) Che, C.-M.; Mak, T. C. and Gray, H. B., *Inorg. Chem.* **1984,** *23,* 4386-4388

[13] King, C., Auerbach, R. A., Fronczek, F. R., and Roundhill, D. M., *J. Am. Chem. Soc.* **1986,** *108,* 5626-5627

[14] King, C.; Yin, Y.; McPherson, G. L.; and Roundhill, D. M., *J. Phys. Chem.* **1989,** *93,* 3451-3455

were replaced with BF_2 groups, $[n\text{-}Bu_4N]_4\,[Pt_2P_8O_{20}H_2B_6F_{12}]$.[15] As with **2**, this compound exhibited spectroscopic characteristics very similar to those of **1**.[15] By improving the fluoroboration method, we have obtained a product anion (**3**) in which all protons of **1** have been replaced with bridging BF_2 groups (Figure 2). **3** displays remarkable photophysical properties, most notably a long-lived (τ = 2 ns at room temperature) singlet state (see Chapter II). [16]

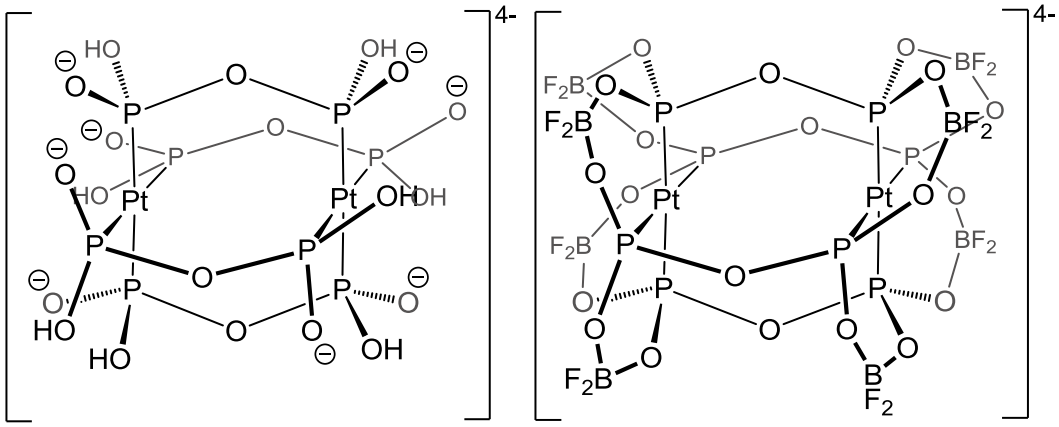

Figure 2: Structures of complex anions **1** (left) and **3** (right).

[15] Harvey, E. L., Caltech PhD. Dissertation, 1990

[16] Durrell, A. C.; Keller, G. E.; Lam, Y. C.; Sýkora, J.; Vlček , A. Jr.; and Gray, H. B., *J. Am. Chem. Soc.* **2012**, *134*, 14201−14207

Results and Discussion

Structures. $[n\text{-}Bu_4N]_4[Pt_2(^{BF_2}POP)_4]$ (**3a**) was prepared by dissolving $[n\text{-}Bu_4N]_4[Pt_2(POP)_4]$ (**1a**) in neat boron trifluoride diethyl etherate and stirring the solution for two days at room temperature (Scheme 1). The same method was used to synthesize $[Ph_4As]_4[Pt_2(^{BF_2}POP)_4]$ (**3b**); this compound and its derivatives were used for crystallographic analyses.

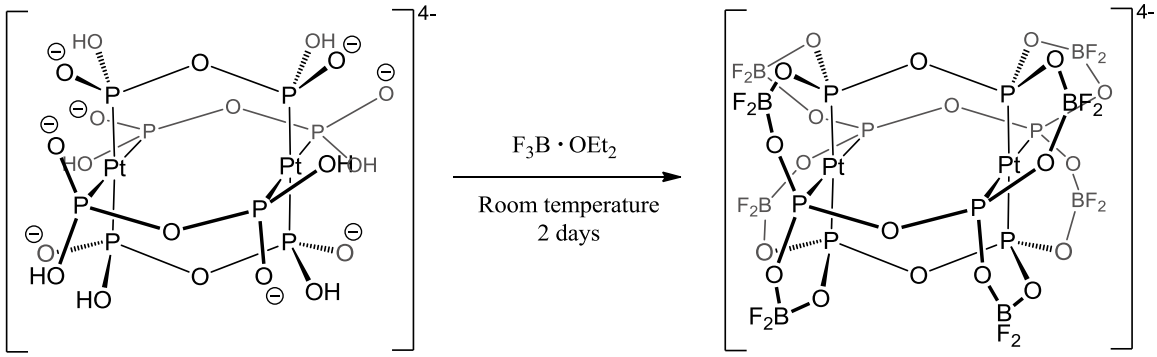

Scheme 1: Synthesis of complex anion **3**.

The ^{31}P-NMR spectrum of **3** (**3a**) features a single broad singlet at 58.8 ppm, with a P-^{195}Pt coupling constant of 2204 Hz, compared with 66.8 ppm and 2978 Hz for **1**; the singlet is broader than that of **1**, likely due to coupling to quadrupolar ^{11}B. The ^{19}F-NMR spectrum exhibits features attributable to two diastereotopic fluorines coupled to each other and broadened by coupling to quadrupolar ^{11}B. The structure of **3b** is shown in

Figure 3 (crystallographic data are in Supporting Information). Selected bond distances for **3b**, $K_4[Pt_2(POP)_4]$,[6] and $[(Bn)(Ph)Me_2N]_4[Pt_2(POP)_4]$[8e] are set out in Table 1. **3b** has a Pt-Pt separation of 2.8873(11) Å, somewhat shorter than in **1** ($K_4[Pt_2(POP)_4]$: 2.925(1) Å, $[(Bn)(Ph)Me_2N]_4[Pt_2(POP)_4]$: 2.9203(2) Å); Pt-P distances (2.294 Å average) are also shorter ($K_4[Pt_2(POP)_4]$: 2.321(4) Å, $[(Bn)(Ph)Me_2N]_4[Pt_2(POP)_4]$: 2.3360(8) Å, averaged).

Table 1: Selected bond distances (Å) for $[Ph_4As]_4[Pt_2(^{BF2}POP)_4]$ (**3b**), $K_4[Pt_2(POP)_4]$, and $[(Bn)(Ph)Me_2N]_4[Pt_2(POP)_4]$.

Bond	$[Ph_4As]_4[Pt_2(^{BF_2}POP)_4]$ (**3b**)	$K_4[Pt_2(POP)_4]$ [6]	$[(Bn)(Ph)Me_2N]_4[Pt_2(POP)_4]$ [8e]
Pt-Pt	2.8873(11)	2.925(1)	2.9203(2)
Pt-P (average)	2.294	2.321(4)	2.3360(8)
P-O(-P) (average)	1.614	1.622(12/14)	1.638(3)

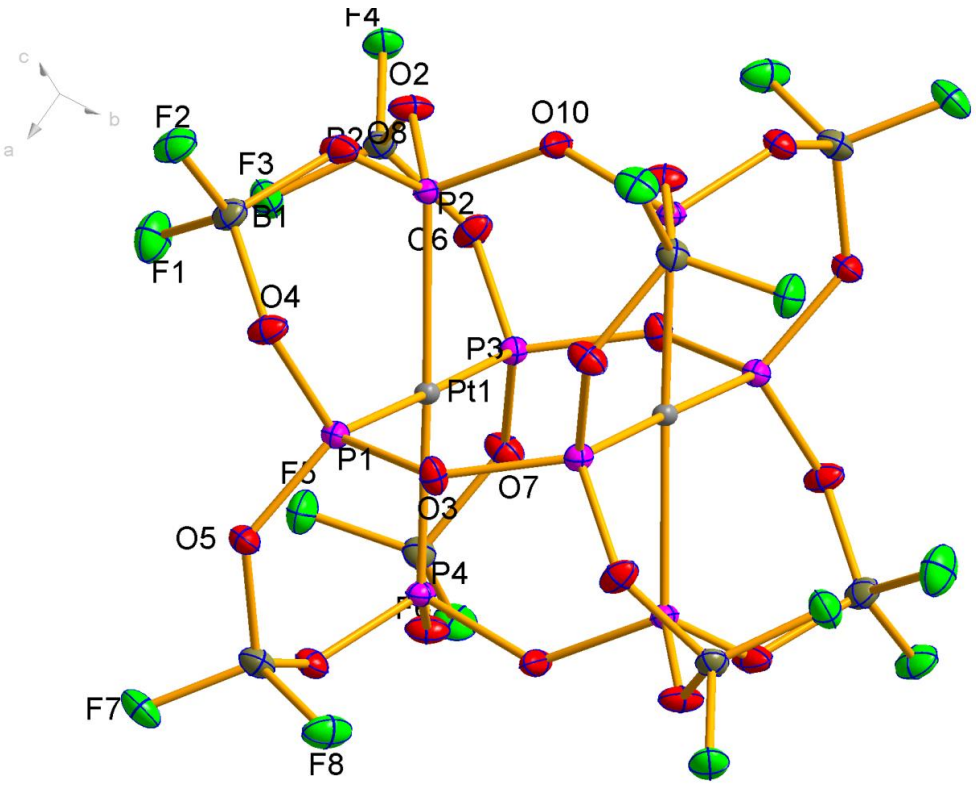

Figure 3: Structure of $[Pt_2(^{BF2}POP)_4]^{4-}$ (**3**) in $[Ph_4As]_4[Pt_2(^{BF2}POP)_4]$ (**3b**) crystals. A crystallographic center of inversion coincides with the geometric center of the anion.

Oxidative Addition Reactions. In analogy with **1**,[17] **3** reacts with excess iodine to give $[Pt_2(^{BF_2}POP)_4I_2]^{4-}$ (**4**) as the sole product. When **4** is isolated by precipitation with ether and then redissolved in acetonitrile, however, it partially converts to **3** and unidentified product(s). In an acetonitrile solution with ca. 40-fold excess of chloride, **4** completely converts to **3**. These results suggest that the reaction between **3** and iodine to form **4** is reversible, the equilibrium lying in the direction of **4**; the back reaction is favored by the presence of chloride, which combines with iodine to form $[I_2Cl]^-$ (Scheme 2). This reversibility contrasts with **1**, whose reaction with iodine is not readily reversible.

$$[Pt_2(^{BF_2}POP)_4I_2]^{4-} \rightleftharpoons [Pt_2(^{BF_2}POP)_4]^{4-} + I_2 \xrightleftharpoons{Cl^-} [Pt_2(^{BF_2}POP)_4]^{4-} + [I_2Cl]^-$$

Scheme 2: Reversible reaction of **3** with I_2 to form **4**.

The reaction of **3a** with [n-Bu_4N][Br_3] produces [n-Bu_4N]$_4$[$Pt_2(^{BF_2}POP)_4Br_2$] (**5a**); its reaction with bromine yields **5a**, but also a large quantity of unidentified products. The latter behavior contrasts with that of **1**, whose reaction with bromine cleanly yields [n-Bu_4N]$_4$[$Pt_2(POP)_4Br_2$].[17] Reaction of **3b** with [Ph_4As][Br_3] gives [Ph_4As]$_4$[$Pt_2(^{BF_2}POP)_4Br_2$] (**5b**).

Unlike **1**, which reacts quickly with iodomethane to form [n-Bu_4N]$_4$[$Pt_2(^{BF_2}POP)_4(CH_3)I$],[12a] **3a** does not react with iodomethane at room temperature. Our finding of inertness toward a powerful electrophile such as iodomethane together with

[17] Alexander, K. A.; Bryan, S. A.; Fronczek, F. R.; Fultz, W. C.; Rheingold, A. L.; Roundhill, D. M.; Stein, P. and Watkins, S. F., *Inorg. Chem.* **1985**, *24*, 2803-2808

the reversibility of its reaction with iodine clearly shows that **3** is less prone to oxidative addition than **1**, owing to the electron-withdrawing character of the perdifluoroborated pyrophosphite ligands. Bond lengths in the structures of $[Ph_4As]_4[Pt_2(^{BF2}POP)_4I_2]$ (**4b**, Figure 4) and $[Ph_4As]_4[Pt_2(^{BF2}POP)_4Br_2]$ (**5b,** Figure 5) are given in Table 2 and Table 3. Relative to the analogous oxidative addition products of **1**, **4**, and **5** have shorter Pt-Pt, Pt-P, and Pt-X bonds, indicative of somewhat stronger bonding in these compounds.

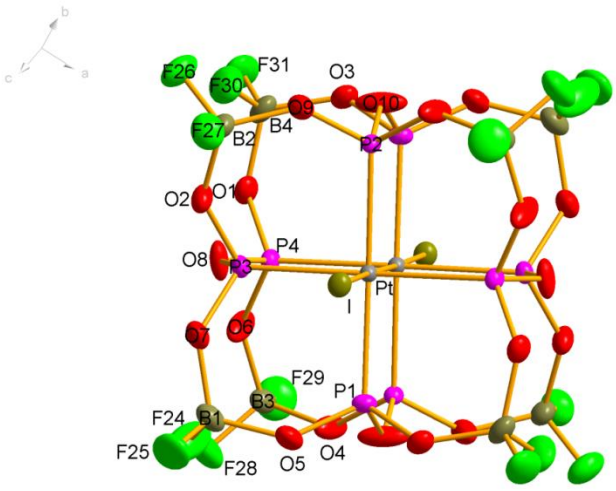

Figure 4: Structure of $[Pt_2(^{BF_2}POP)_4I_2]^{4-}$ in $[Ph_4As]_4[Pt_2(^{BF_2}POP)_4I_2]$ (4b) crystals. A crystallographic center of inversion coincides with the geometric center of the anion.

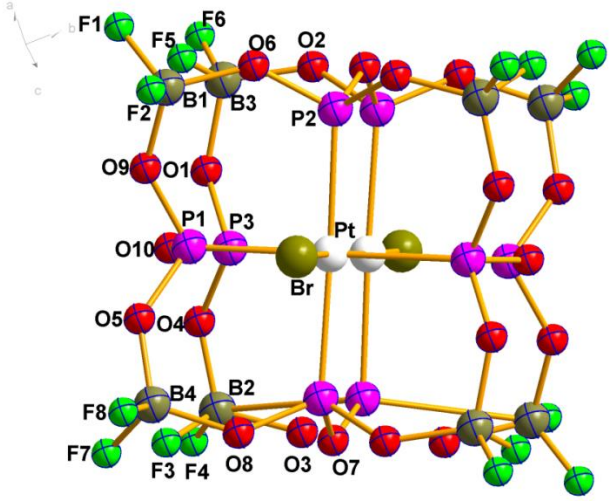

Figure 5: Structure of $[Pt_2(^{BF_2}POP)_4I_2]^{4-}$ in $[Ph_4As]_4[Pt_2(^{BF_2}POP)_4Br_2]$ (5b) crystals. A crystallographic center of inversion coincides with the geometric center of the anion.

Table 2: Selected bond distances (Å) for $[Ph_4As]_4[Pt_2(^{BF_2}POP)_4I_2]$ (**4b**), $K_4[Pt_2(POP)_4I_2]$, and $K_2[n\text{-}Bu_4N]_2[Pt_2(POP)_4I_2]$. Numbers in parentheses are the uncertainties; numbers in square brackets are the root-mean-square deviations of the individual values from their mean.

Bond	$[Ph_4As]_4[Pt_2(^{BF_2}POP)_4I_2]$ (**4b**)	$K_4[Pt_2(POP)_4I_2]$[17]	$K_2[n\text{-}Bu_4N]_2[Pt_2(POP)_4I_2]$[17]
Pt-Pt	2.7223	2.754(1)	2.742(1)
Pt-P	2.319	2.348(1)	2.343[6](2)
Pt-I	2.7292	2.746(1)	2.721(1)

Table 3: Selected bond distances (Å) for $[Ph_4As]_4[Pt_2(^{BF_2}POP)_4Br_2]$ (**5b**) and $[(n\text{-}Bu_4N]_4[Pt_2(POP)_4Br_2]$. Numbers in parentheses are the uncertainties; numbers in square brackets are the root-mean-square deviations of the individual values from their mean.

Bond	$[Ph_4As]_4[Pt_2(^{BF_2}POP)_4Br_2]$ (**5b**)	$[n\text{-}Bu_4N]_4[Pt_2(POP)_4Br_2]$[17]
Pt-Pt	2.692	2.716(1)
Pt-P (average)	2.323[1]	2.362[3](2)
Pt-Br	2.534	2.572(1)

Experimental Section

General. Unless stated otherwise, all manipulations were conducted under an inert atmosphere using standard glove box or Schlenk line techniques, all chemicals were obtained from Sigma-Aldrich Corporation, and solvents were dried using activated alumina columns according to Grubbs' method.[18] Perdeuterated acetonitrile (d_3-MeCN) was obtained from Cambridge Isotopes Laboratories, stored over activated 3 Å molecular sieves overnight, degassed, and passed through activated alumina. Boron trifluoride diethyl etherate ($F_3B{\cdot}OEt_2$) was distilled under vacuum, stored, and used under an inert atmosphere. Iodine was sublimed. $K_4[Pt_2(POP)_4]$,[19] [*n*-$Bu_4N]_4[Pt_2(POP)_4]$ (**1a**),[20] and $[Ph_4As]_4[Pt_2(POP)_4]$ (**1b**)[19] were prepared as previously reported. Tetraphenylarsonium tribromide ($[Ph_4As][Br_3]$) was synthesized by mixing aqueous solutions of tetraphenylarsonium chloride ($[Ph_4As][Cl]$), sodium bromide, and bromine; the resulting red precipitate was collected by filtration, washed with more deionized water, and dried under vacuum overnight.

Physical Methods. NMR spectra were recorded on a Varian 300 MHz Mercury or 500 MHz Inova spectrometer. ^{1}H NMR chemical shifts were referenced to residual protio-solvents as determined relative to Me_4Si (δ = 0 ppm); ^{19}F NMR chemical shifts were referenced to an external $CFCl_3$ standard (δ = 0 ppm); ^{31}P NMR chemical shifts were referenced to an external 85% H_3PO_4 standard (δ = 0 ppm). Elemental analyses were

---

[18] Pangborn, A. B.; Giardello, M. A.;Grubbs, R. H.; Rosen, R. K. and Timmers, F. J., *Organometallics* **1996**, *15*, 1518-1520

[19] Che, C.M.; Butler, L. G.; Grunthaner, P. J. and Gray, H. B., *Inorg. Chem.* **1985**, *24*, 4662-4665

[20] Bennett, M. A.; Bhargava, S. K.; Bond, A. M.; Bansal, V.; Forsyth, C. M.; Guo, S.-X. and Priver, S. H., *Inorg. Chem.* **2009**, *48*, 2593-2604

performed by Robertson Microlit, Madison, NJ. X-ray crystallographic data were collected on a Bruker KAPPA APEX II instrument, with the crystals mounted on a glass fiber with Paratone-N oil. Structures were determined using direct methods as implemented in the Bruker AXS software package.

Perfluoroborated Compounds.

Tetrabutylammonium Per(difluoroborated)tetrakis(μ-pyrophosphito) diplatinate (II) (**3a**)

Under a dry argon atmosphere, 400 mg **1a** (0.21 mmol) was dissolved in about 3 mL neat $F_3B{\cdot}OEt_2$, and stirred at room temperature for two days. The solvent was removed by vacuum distillation, and the solid was washed with dry, degassed THF. The residue was dissolved in acetonitrile, the solution filtered through Celite, and the product precipitated with THF. The luminescent green powder was washed with more THF to yield 350 mg product (0.15 mmol, 73%). The product could be further purified by vapor diffusion of diethyl ether into an acetonitrile solution of the product. Samples suitable for photophysical measurements were prepared by two recrystallizations.

^{1}H NMR (300 MHz, CD_3CN) δ 3.08-3.14 (m, 2 H), 1.57-1.69 (m, 2 H), 1.39 (quintet, J= 8 Hz, 2 H), 1.00 (t, J= 8 Hz, 3 H); ^{19}F NMR (282 MHz, CD_3CN) δ -133.54, (d, J= 62Hz), -138.78 (d, J= 62Hz); ^{31}P NMR (121 MHz, CD_3CN) δ 58.81 ($J_{P\text{-}Pt}$= 3112Hz)

Tetraphenylarsonium Per(difluoroborated)tetrakis(μ-pyrophosphito) diplatinate (II) (**3b**)

3b was synthesized in exactly in the same way as **3a**, except that the mixture was initially heated to 50^{o}C for about 30 min to completely dissolve **1b**. Samples suitable for crystallographic analysis were prepared by crystallization, as detailed for **3a**. ^{19}F- and ^{31}P-NMR spectra were the same as those for **3a**.

^{1}H NMR (300 MHz, CD_3CN) δ 7.99 (t, J = 7 Hz, 2 H), 7.76-7.91 (m, 3 H)

Refined crystal structure has been deposited at the Cambridge Crystallographic Data Center, reference number CCDC 1049647.

Tetrabutylammonium Per(difluoroborated)tetrakis(μ-pyrophosphito) diplatinate (III) Diiodide (**4a**)

To a solution of 84 mg **3a** (36 μmol) in about 1 mL d_3-MeCN was added 99 mg (39 μmol, 11 equivalents) of iodine in about 10 mL acetonitrile. The luminescent green solution turned orange; ^{19}F- and ^{31}P-NMR of this solution indicated clean formation of **4a** after 30 min at room temperature.

^{1}H NMR (300 MHz, CD_3CN) δ 3.08-3.14 (m), 1.57-1.69 (m), 1.39 (quintet, J= 8 Hz), 1.00 (t, J= 8 Hz); ^{19}F NMR (282 MHz) δ -134.50 (d, J = 60.5 Hz), -138.34 (d, J = 60.5 Hz); ^{31}P NMR (121 MHz) δ 0.45 ($J_{P\text{-}Pt}$= 2204Hz)

To isolate **4a**, diethyl ether was added to the solution, forming a red precipitate. The precipitate was collected by filtration through Celite and washed with further portions of diethyl ether. The product was extracted into acetonitrile, and the solution was evaporated to dryness to obtain a red product (56 mg). ^{19}F- and ^{31}P-NMR analysis of this product, however, indicated a mixture of **4a**, an unidentified product, and **3a**.

Tetraphenylarsonium Per(difluoroborated)tetrakis(μ-pyrophosphito) diplatinate (III) Diiodide (**4b**)

The title compound was synthesized in an analogous manner as **4a**, with **3b** as starting material. Crude product was isolated by precipitation with diethyl ether. Crystals suitable for crystallographic analysis were obtained by diffusion of diethyl ether into a concentrated

acetonitrile solution. A preliminary crystal structure has been obtained, and is pending refinement. ^{19}F- and ^{31}P-NMR spectra were the same as those for **4a**, while the ^{1}H-NMR spectrum was the same as that for **3b**.

Tetrabutylammonium Per(difluoroborated)tetrakis(μ-pyrophosphito) diplatinate (III) Dibromide (**5a**)

To a solution of 82 mg **3a** (35 μmol) in about 2 mL acetonitrile was added 37.5 mg tetrabutylammonium tribromide (78 μmol, 2.2 equivalents). The solution was stirred for 2.5 hours. Solvent was removed under reduced pressure, and the residue was washed with THF to yield 58 mg of **5a** (23 μmol, 67%) as a yellowish-orange solid.

^{1}H NMR (300 MHz, CD_3CN) δ 3.08-3.14 (m), 1.57-1.69 (m), 1.39 (quintet, J= 8 Hz), 1.00 (t, J= 8 Hz); ^{19}F NMR (282 MHz, CD_3CN) δ -135.47(d, *J* = 60 Hz), -138.56 (d, *J* = 60 Hz); ^{31}P NMR (121 MHz, CD_3CN) δ 6.47 ($J_{P\text{-}Pt}$= 2157Hz)

Tetraphenylarsonium Per(difluoroborated)tetrakis(μ-pyrophosphito) diplatinate (III) Dibromide (**5b**)

17 mg of **3b** (5.9 μmol) and 7.5 mg (12 μmol, 2 equivalents) of tetraphenylarsonium tribromide ($[Ph_4As][Br_3]$) were dissolved in 0.7 mL d_3-MeCN to form an orange solution. The solvent was removed under reduced pressure, and the residue was washed with THF to yield an orange solid, which was dissolved in acetonitrile. Crystals suitable for crystallographic analysis were obtained by diffusion of diethyl ether into this solution. A preliminary crystal structure has been obtained, and is pending refinement. ^{19}F- and ^{31}P-NMR spectra were the same as those for **5a**.

Chapter II

Photophysics of $[Pt_2(pop\text{-}BF_2)_4]^{4-}$: Spectroscopy and Decay Pathways of the Lowest Singlet and Triplet Excited States

Y.C. Lam; T. Hofbeck; A. C. Durrell; G. E. Keller; J. Sýkora; M. Kalbáč; S. Zalis; J. Winkler, Jr.; A. Vlček, Jr.; H. Yersin; H. B. Gray

Abstract

Fluorescence, phosphorescence, and corresponding excitation spectra of microcrystalline per(difluoroboro)tetrakis(pyrophosphito)diplatinate(II) ($[Bu_4N]_4[Pt_2(\mu\text{-}P_2O_5(BF_2)_2)_4]$, abbreviated Pt(pop-$BF_2$)) have been obtained over a range of temperatures, 1.3 - 310 K. Emission spectra at 10 K exhibit vibrational fine structure with a 123 cm^{-1} progression attributable to ground-state Pt-Pt stretching, in agreement with experimental and DFT-calculated non-resonant Raman spectra. Vibrational progressions observed in the excitation spectra reveal higher Pt-Pt stretching energies in the $^1A_{2u}$ (160 cm^{-1}) and $^3A_{2u}$ (168 cm^{-1}) $d\sigma^*p\sigma$ excited states. The overall photoluminescence quantum yield approaches unity, independent of temperature. The fluorescence quantum yield and lifetime decrease with increasing temperature, while the phosphorescence quantum yield increases commensurately. The optically populated $^1A_{2u}$ state also undergoes unusually slow (0.83 – 3.3 ns) intersystem crossing to the lowest triplet $^3A_{2u}$ with strongly temperature dependent kinetics that is analyzed using the theory of radiationless multiphonon transitions. Temperature dependence of the phosphorescence lifetime reveals a $^3A_{2u}$ zero-field splitting

of ~40 cm^{-1} ($A_{1u} < E_u$) and the decay lifetimes of the spin-orbit states: 8.6 ms (A_{1u}) and 2.3 μs (E_u). Emission from A_{1u} is allowed by Herzberg-Teller spin-vibronic coupling involving a ~180 cm^{-1} vibration.

Introduction

Face-to-face d^8-d^8 complexes of Rh, Ir, and Pt exhibit remarkable spectroscopic, photophysical, and photochemical properties, owing to dramatic variations in metal-metal interactions in their ground and lowest electronic excited states.[1-4] In particular, tetrakis(μ-pyrophosphito)diplatinate(II) ($[Pt_2(\mu\text{-}P_2O_5H_2)_4]^{4-}$, abbreviated as Pt(pop)) has been investigated extensively.[1-3,5]

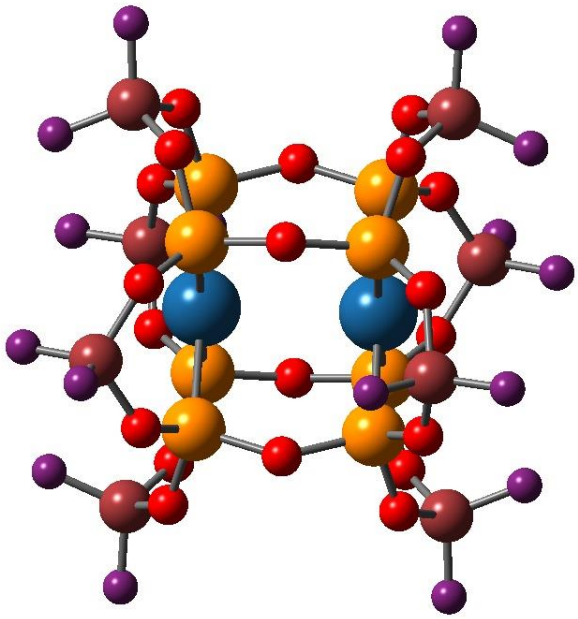

Figure 1. DFT-optimized structure of the lowest-energy C_{2h} conformer of Pt(pop-BF_2) in vacuum. Color code: Pt (blue), P (orange), O (red), B (brown), F (violet).

The $d\sigma^* \rightarrow p\sigma$ excitation[1,3,6] gives a singlet state of A_{2u} symmetry which undergoes intersystem crossing (ISC) to the corresponding triplet ($^3A_{2u}$), with a room-temperature lifetime ranging from 2 to 30 ps, depending on the solvent.[7-9] (Symmetry labels refer to the D_{4h} point group of the $Pt_2(POP)_4$ core.) Because this excitation populates a Pt-Pt bonding orbital, the Pt-Pt interaction is strengthened, as was documented by time-resolved X-ray

diffraction and EXAFS (the Pt-Pt bond contracts by 0.28-0.31 Å upon excitation).[10] In addition, Franck-Condon analysis of low-temperature emission spectra as well as transient Raman spectra show that the Pt-Pt stretching frequency is higher in both dσ*pσ states ($^1A_{2u}$,$^3A_{2u}$) (145 cm^{-1} in $^1A_{2u}$; 150 cm^{-1} in $^3A_{2u}$, vs. 110 cm^{-1} in the ground state).[3,6,7,11,12] Owing in part to its relatively long lifetime (ca. 10 μs), the $^3A_{2u}$ excited state participates in a rich array of electron transfer and atom transfer reactions.[1,3-5]

Replacing the terminal hydrogen atoms of Pt(pop) by BF_2 groups produces $[Pt_2(\mu\text{-}P_2O_5(BF_2)_2)_4]^{4-}$, abbreviated as Pt(pop-$BF_2$). The structure of the perfluoroborated complex is more rigid and the Pt-Pt unit is better shielded from the environment (Figure 1).[13] Here we report investigations of solution photophysics, which revealed that Pt(pop-BF_2) exhibits strong fluorescence and phosphorescence. The decay rate of the former matches the rise of the latter, and is dominated by singlet to triplet intersystem crossing (ISC). ISC in Pt(pop-BF_2) is much slower than in Pt(pop). Furthermore, spectroscopic investigations of microcrystalline Pt(pop-BF_2) over an exceptionally broad temperature range (1.5 – 310 K) furnished the Pt-Pt stretching vibrational energies in the ground state ($^1A_{1g}$) and two lowest excited states ($^1A_{2u}$, $^3A_{2u}$), providing insight into the splitting of $^3A_{2u}$ into A_{1u} and E_u states under the influence of spin-orbit coupling. In addition, the temperature-dependent kinetics of the fluorescence and phosphorescence decay was studied, shedding new light on the mechanisms whereby the singlet and triplet dσ*pσ states decay to the ground-state.

Results and Discussion

Electronic Absorption Spectroscopy

The absorption spectrum of Pt(pop-BF_2) in MeCN solution exhibits an intense band at 365 nm (ε = 37500 $M^{-1}cm^{-1}$) attributable to the $d\sigma^* \rightarrow p\sigma$ ($^1A_{1g} \rightarrow {}^1A_{2u}$) transition; by comparison, Pt(pop) has a similar absorption feature at 372 nm (Figure 2 and Table 1).[6,7,12] The corresponding spin-forbidden $d\sigma^* \rightarrow p\sigma$ transition ($^1A_{1g} \rightarrow {}^3A_{2u}$) gives rise to a ~270× weaker band at 454 nm, virtually identical with that of Pt(pop).[12] Both complexes show a series of relatively weak UV bands. The 2100-3200 cm^{-1} blue shifts upon perfluoroboration are in line with the LMCT character indicated by TD-DFT calculations on Pt(pop).[13,14,15,16]

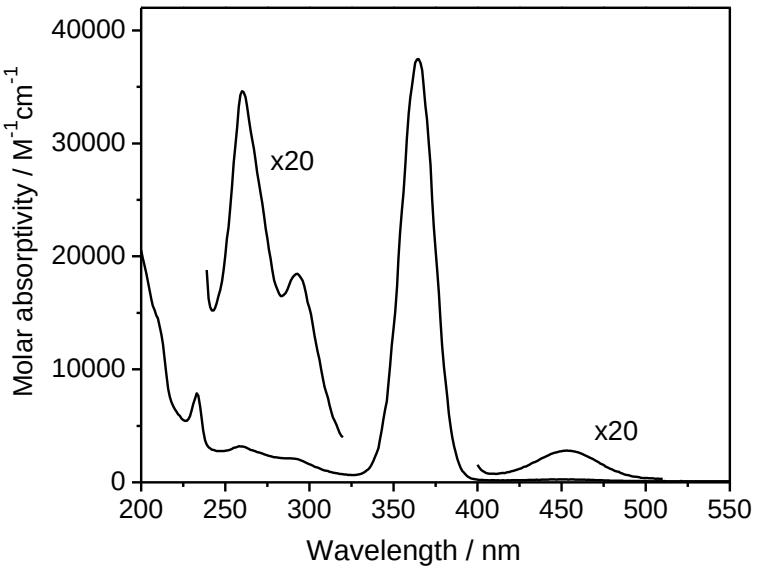

Figure 2. Absorption spectrum of Pt(pop-BF_2) in MeCN solution.

Table 1. Absorption and emission properties of Pt(pop-BF_2) and Pt(pop) in MeCN solution.

Pt(pop-BF_2)	Pt(pop)[a]	Assignment [b]
Absorption, nm (ε, $M^{-1}cm^{-1}$)		
233 (7880)	246 (3770)	LMCT [c]
260 (3180)	285 (2550)	LMCT [c]
291 (2110)	315 (1640)	LMCT [c]
365 (37500)	372 (33400)	$^1(d\sigma^*\rightarrow p\sigma)\ ^1A_{1g}\rightarrow{}^1A_{2u}$
454 (140)	454 (155)	$^3(d\sigma^*\rightarrow p\sigma)\ ^1A_{1g}\rightarrow{}^3A_{2u}$
Emission, nm (lifetime at 21 °C)		
393 (1.6 ns)	398 (~8 ps)	$^1(p\sigma\rightarrow d\sigma^*)\ ^1A_{2u}\rightarrow{}^1A_{1g}$
512 (8.4 μs)	511 (9.4 μs)	$^3(p\sigma\rightarrow d\sigma^*)\ ^3A_{2u}\rightarrow{}^1A_{1g}$
Emission Stokes shift, cm^{-1}		
1760	2230	Fluorescence
2460	2500	Phosphorescence

[a] Absorption data and emission lifetimes from ref. 7, emission wavelengths from ref. 16. [b] Based on refs. 7, 13, 14. [c] The principal excitations are directed to the pσ LUMO accompanied by smaller contributions from Pt-localized excitations.

Solution Photoluminescence

The emission spectra of Pt(pop-BF_2) and Pt(pop) differ greatly in the relative intensities of $p\sigma\rightarrow d\sigma^*$ fluorescence and phosphorescence. The spectrum of Pt(pop-BF_2) at room temperature shows intense $^3A_{2u}\rightarrow{}^1A_{1g}$ phosphorescence at 512 nm and equally strong $^1A_{2u}\rightarrow{}^1A_{1g}$ fluorescence at 393 nm (Figure 3 and Table 1). Owing to phosphorescence quenching by traces of O_2, the intensity ratio of the two bands depends on sample preparation; a limiting phosphorescence:fluorescence peak-intensity ratio of 1.15 at 21 °C was obtained from a solution degassed under high vacuum. While Pt(pop) in MeCN also shows strong phosphorescence at 511 nm, the fluorescence at 398 nm is extremely weak,[7,17] as documented quantitatively by emission quantum yields: whereas room-temperature phosphorescence yields of the two complexes are comparable, the fluorescence

yield is three orders of magnitude larger for Pt(pop-BF_2) than for Pt(pop) (2.7×10^{-1} and 1.5×10^{-4}, respectively).[7]

The excitation spectra of Pt(pop-BF_2) measured at 405 and 512 nm are virtually identical and match perfectly the strong $^1A_{1g}\rightarrow{}^1A_{2u}$ absorption band at 363 nm (Figure 4); and the phosphorescence:fluorescence peak-intensity ratio is independent of excitation wavelength from 350 to 380 nm. Both the fluorescence band intensity and quantum yield decrease with increasing temperature, accompanied by a concomitant increase in phosphorescence intensity and yield (Figures 3 and 8, and Table 2). The total emission quantum yield of *ca*. 0.75 is temperature-independent (Table 2), implying direct conversion of the fluorescent state ($^1A_{2u}$) to the phosphorescent state ($^3A_{2u}$).

This conclusion was confirmed by observing virtually identical single-exponential kinetics of fluorescence decay and phosphorescence rise—measured under identical conditions except for detection wavelengths (405 and 512 nm, respectively)—both occurring with a 1.6 ns lifetime (Figures 5, 6, and 7). This result was double-checked using two different techniques: time-correlated single photon counting (TCSPC) (373 nm, ~80 ps excitation, Figure 5) and streak camera (355 nm, 50 ps excitation, Figures 6 and 7). Our findings clearly demonstrate that $^1A_{2u}\rightarrow{}^3A_{2u}$ intersystem crossing (ISC) in Pt(pop-BF_2) is slow but occurs without any apparent intermediates.

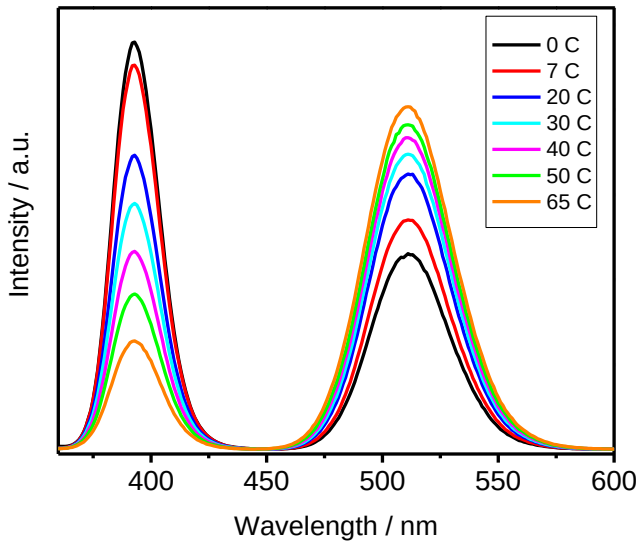

Figure 3. Temperature dependence of the emission spectrum of Pt(pop-BF_2) in MeCN solution. Excitation at 355 nm.

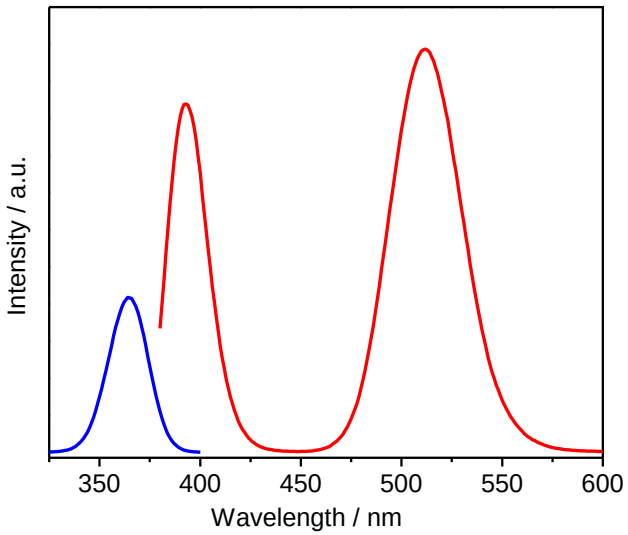

Figure 4. Red: emission spectrum of Pt(pop-BF_2), excitation wavelength 373 nm. Blue: normalized excitation spectra of in MeCN obtained at λ_{em} = 405 and 512 nm (the two spectra are indistinguishable). Measured in a MeCN solution at 21 °C, degassed at 4×10^{-5} mbar.

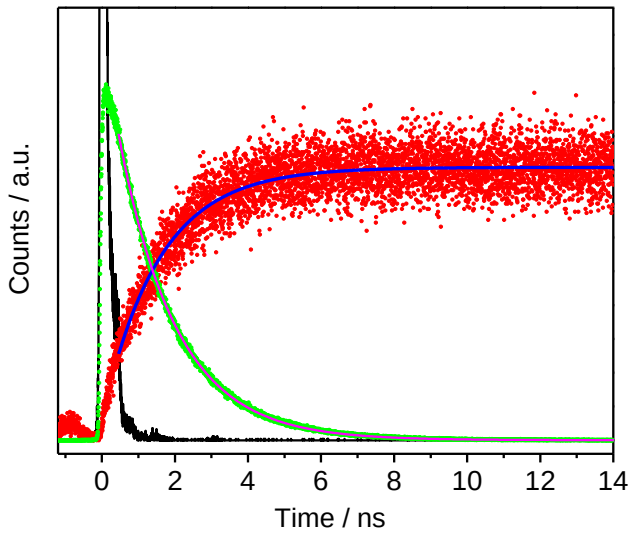

Figure 5. Phosphorescence rise at 512 nm (red) and fluorescence decay at 405 nm (green) of Pt(pop-BF_2) in MeCN, shown together with a 373 nm excitation-pulse profile (black). Measured using TCSPC. The blue and magenta curves are single-exponential fits in the 0.3–17.2 ns interval with lifetimes of 1.56±0.02 and 1.58±0.001 ns, respectively.

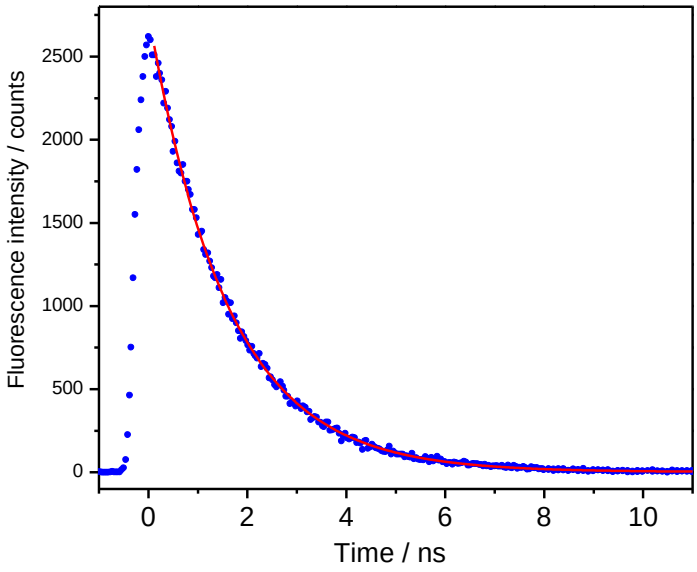

Figure 6. Fluorescence decay of Pt(pop-BF_2) in MeCN measured with a streak camera, excited at 355 nm, 10 ps. Emission in the 400-415 nm range was selected by a bandpass filter. Red curve: single-exponential fit with τ = 1.58±0.01 ns.

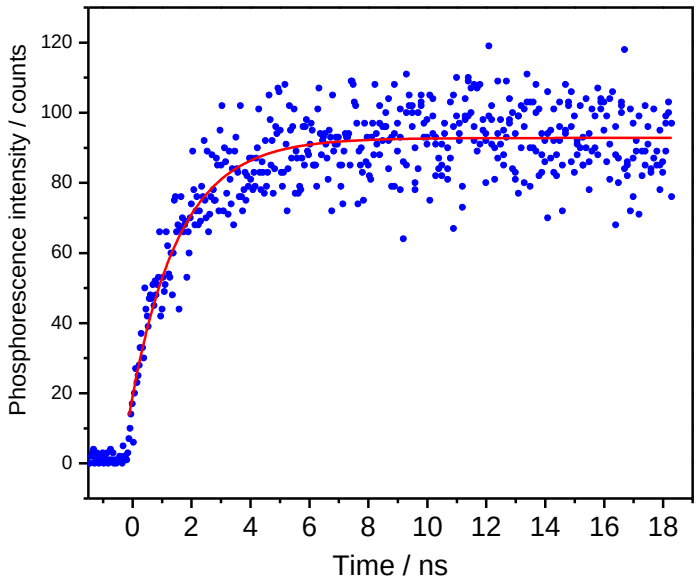

Figure 7. Phosphorescence rise of Pt(pop-BF_2) in MeCN measured with a streak camera, excited at 355 nm, 1 ps pulse. Emission wavelengths >500 nm were selected by a cut-off filter. Red curve: single-exponential fit with τ = 1.62±0.09 ns.

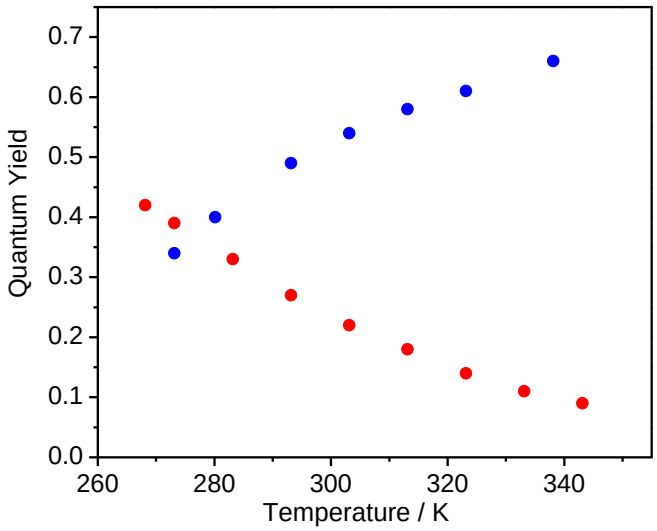

Figure 8. Temperature-dependence of the fluorescence (red) and phosphorescence (blue) quantum yield of Pt(pop-BF_2) in MeCN.

Table 2. The temperature dependence of Pt(pop-BF_2) fluorescence (ϕ_{fl}) and phosphorescence (ϕ_{ph}) quantum yields. Measured in degassed MeCN solution.

T [°C]	T [K]	ϕ_{fl}	ϕ_{ph}	$\phi_{fl} + \phi_{ph}$
-5	268.15	0.42	-	-
0	273.15	0.39	0.34	0.73
7	280.15	-	0.40	-
10	283.15	0.33	-	-
20	293.15	0.27	0.49	0.76
30	303.15	0.22	0.54	0.76
40	313.15	0.18	0.58	0.76
50	323.15	0.14	0.61	0.75
60	333.15	0.11	-	-
65	338.15	-	0.66	-
70	343.15	0.09	-	-

Table 3. Temperature dependence of Pt(pop-BF_2) fluorescence lifetime. The values were obtained by deconvolution of the TCSPC signal and the actual excitation pulse profile. The nonradiative $^1A_{2u}$ decay rate constants k_{nr} were calculated as $1/\tau - k_r$, assuming $k_r = 1.7\times10^8$ s^{-1}.

t [°C]	T [K]	τ_1 [ns]	τ [ns]	A_1 [%]	A_2 [%]	k_{nr} [10^8 s^{-1}]
3.4	276.55	0.29	2.20	5	95	2.8
12.0	285.15	0.12	1.86	8	95	3.7
20.8	293.95	0.20	1.56	9	91	4.7
30.2	303.35	0.20	1.28	9	91	6.1
39.4	312.55	0.14	1.03	10	90	8.0
49.7	322.85	0.12	0.81	11	89	10.6
60.6	333.75	0.08	0.63	12	88	14.2
70.9	344.05	0.06	0.50	13	87	18.3

The Pt(pop-BF_2) room-temperature fluorescence lifetime of 1.6 ns is about 100-times longer than the 8–18 ps lifetimes reported for Pt(pop) in MeCN[7] and similar solvents.[8,10] Figure 6 shows that the Pt(pop-BF_2) fluorescence decay is strongly temperature-dependent, and the kinetics are predominantly single-exponential (lifetimes are collected in Table 3).[i]

Photoluminescence of Microcrystalline Pt(pop-BF_2)

Similar to its photophysical properties in MeCN solution, Pt(pop-BF_2) powder exhibits both fluorescence and phosphorescence (401 nm and 530 nm, respectively, at room temperature, see Figure 9). Fluorescence and phosphorescence quantum yields decrease and increase, respectively, with increasing temperature (Figures 9 and 10), whereas the total photoluminescence quantum yield stays nearly constant, close to unity (Figure 10, Table 4). The fluorescence band undergoes a small blue-shift upon decreasing the temperature. Phosphorescence shows no observable changes in the peak wavelength and band-shape from room temperature to 10 K. Upon decreasing the temperature further to 1.5 K, it undergoes a sudden red-shift (by ca. 220 cm^{-1}) and broadening (Figure 9). This red-shift is discussed later.

[i] An additional low-amplitude 60-290 ps decay component revealed by deconvolution of the TCSPC data (Table S2) is tentatively attributed to relaxation processes.

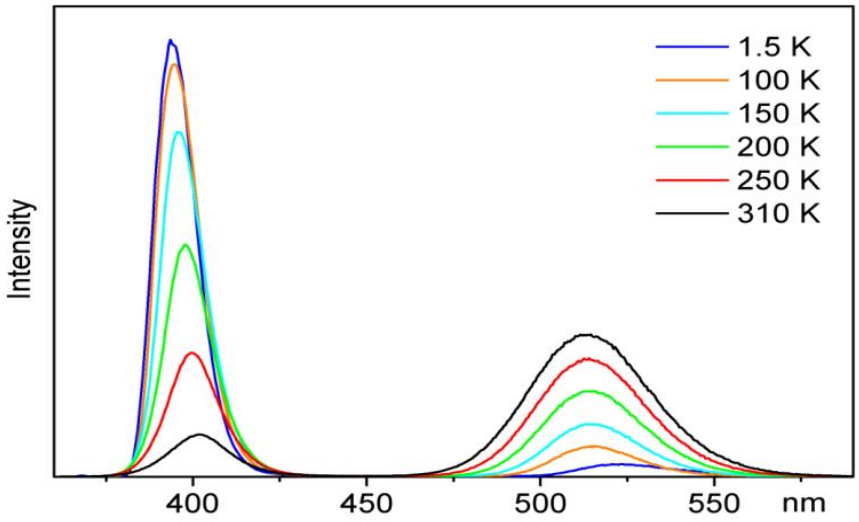

Figure 9. Photoluminescence spectra of Pt(pop-BF_2) in a microcrystalline powder at selected temperatures in the 1.5–310 K range. λ_{exc} = 355 nm.

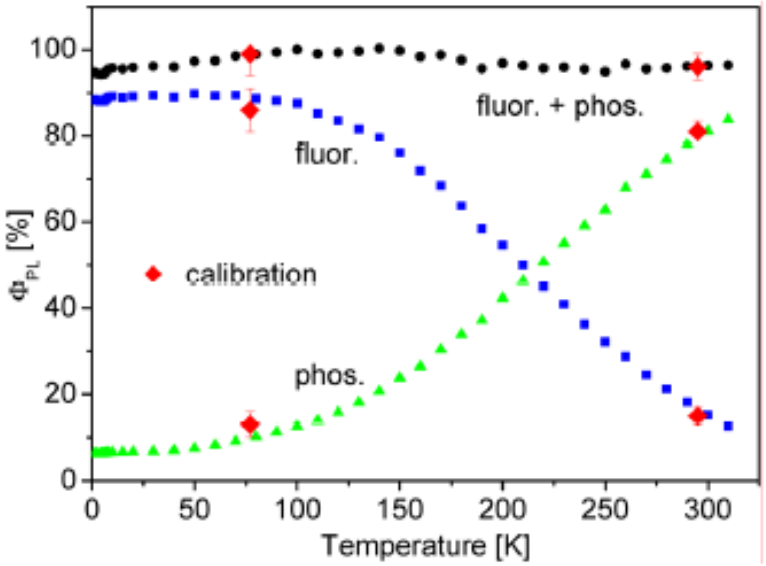

Figure 10. Temperature dependence of the fluorescence and phosphorescence quantum yields of Pt(pop-BF_2) (powder). Relative intensities were obtained from the emission spectra and calibrated by measurements in an integrating sphere (red).

Table 4. Temperature-dependence of the fluorescence and phosphorescence quantum yields of Pt(pop-BF_2) (powder). Relative intensities were obtained from the emission spectra and calibrated against measurements in an integrating sphere at 77 K and 298 K.

Temperature / K	Φ(Fluorescence)	Φ (Phosphorescence)	Φ (total)
310	0.126	0.838	0.964
300	0.152	0.811	0.964
290	0.182	0.78	0.962
280	0.212	0.745	0.957
270	0.245	0.71	0.955
260	0.287	0.679	0.966
250	0.321	0.628	0.949
240	0.363	0.591	0.955
230	0.41	0.55	0.959
220	0.45	0.507	0.957
210	0.501	0.463	0.963
200	0.546	0.422	0.968
190	0.584	0.372	0.956
180	0.637	0.338	0.976
170	0.684	0.304	0.988
160	0.719	0.265	0.984
150	0.76	0.238	0.998
140	0.795	0.207	1.002
130	0.815	0.181	0.996
120	0.835	0.158	0.993
110	0.851	0.139	0.99
100	0.875	0.125	1
90	0.881	0.112	0.994
80	0.887	0.102	0.989
70	0.894	0.091	0.985
60	0.893	0.081	0.974
50	0.898	0.075	0.973
40	0.89	0.07	0.96
30	0.894	0.068	0.961
20	0.891	0.067	0.958
15	0.889	0.066	0.956
10	0.891	0.066	0.957
8	0.89	0.065	0.955
7	0.885	0.064	0.949
6.5	0.885	0.064	0.949
6	0.88	0.063	0.944
5	0.88	0.063	0.943
4	0.88	0.062	0.943
2.5	0.882	0.062	0.944
1.5	0.885	0.063	0.948

$^1A_{2u}\rightarrow{}^1A_{1g}$ fluorescence: characterization of the lowest excited singlet state

The high-resolution fluorescence spectrum attributed[13] to $^1A_{2u}(d\sigma^*p\sigma)$ and the corresponding excitation spectrum are shown in Figure 11. A clearly resolved 123 cm^{-1} vibrational progression is observed in the fluorescence spectrum, which corresponds to the Pt-Pt stretching vibration (ν(Pt-Pt)) in the ground state, in agreement with the non-resonant Raman spectrum that exhibits a prominent band at 123 cm^{-1} (Figure 11) assigned to ν(Pt-Pt) by DFT calculations (Table 5, see also Figure 12). The Pt-Pt stretching wavenumber of Pt(pop-BF_2) is higher than for Pt(pop): 110 cm^{-1} (low temperature phosphorescence)[6] and 116-118 cm^{-1} (Raman).[17] Fluorescence excitation spectrum exhibits a strong $^1A_{1g}\rightarrow{}^1A_{2u}$ band with a 160±7 cm^{-1} progression attributable to the ν(Pt-Pt) vibration in the $^1A_{2u}$ excited state. The first excitation vibronic band coincides with the emission onset (Figure 5-right), yielding an $E_{00}(^1A_{2u})$ value of 26210 cm^{-1}.

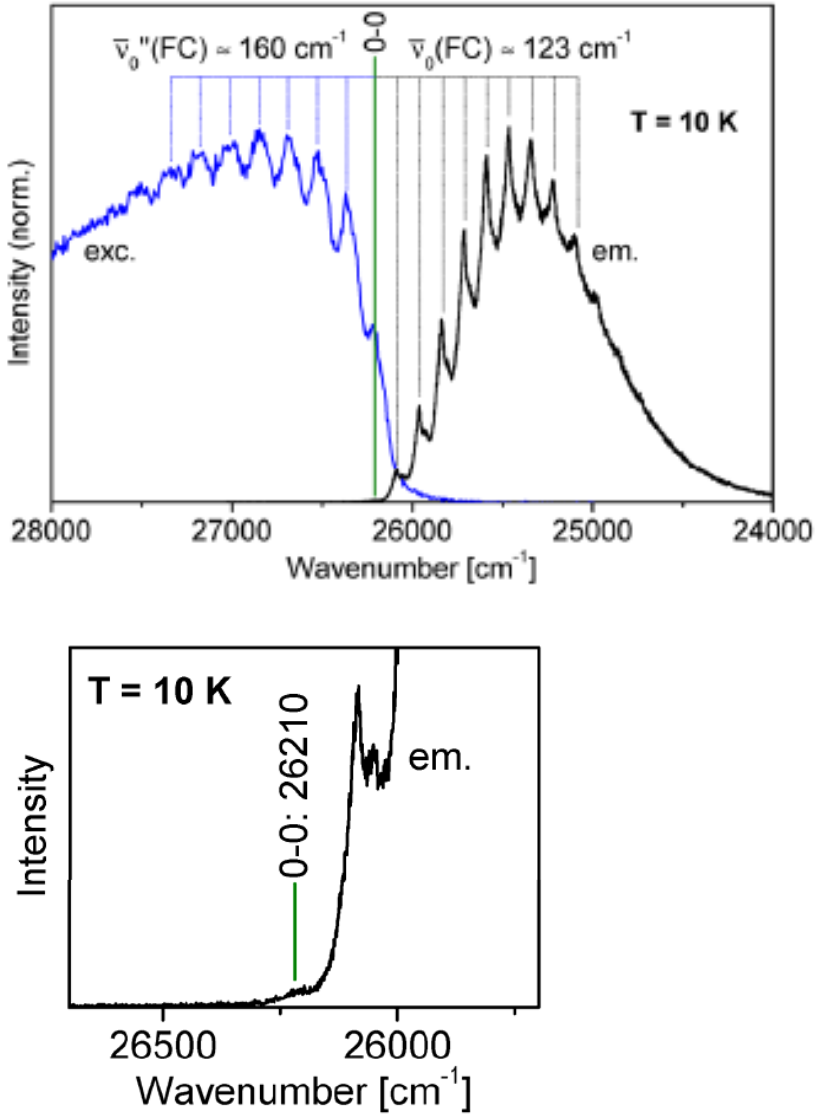

Figure 11. Top: High-resolution emission and excitation spectra of Pt(pop-BF_2) at 10 K in the $^1A_{1g} \leftrightarrow {}^1A_{2u}$ energy region; λ_{exc}(emission) = 340 nm, λ_{det}(excitation) = 430 nm, respectively. Bottom: Enlarged region of the electronic 0-0 transition in the high-resolution fluorescence spectrum. λ_{exc} = 300 nm.

Table 5. Selected experimental and DFT calculated Raman-active vibrations of Pt(pop-BF_2).

Vibrational Frequency/ cm^{-1}		Raman activity/ $Å^4Amu^{-1}$		Symmetry [a]	
Expt.	Calc'd	(calc'd)	Assignment	C_{2h}	D_{4h}
123	125	3	ν(Pt-Pt)	A_g	A_{1g}
	150	0.2	pop-BF_2 breathing	B_g	E_g
169	155	4	pop-BF_2 breathing + ν(Pt-Pt)	A_g	E_g
	158	3	pop-BF_2 breathing + ν(Pt-Pt)	A_g	E_g
~194	204	–	pop-BF_2breathing	A_g	A_{1g}
	213 or 217		skeletal def.	B_g	A_{2g}
~248	257	3	δ(P-O-P) + ν(Pt-P) + skeletal def.	B_g	B_{1g}
260	268	8	δ(P-O-P) + ν(Pt-P) + skeletal def.	A_g	A_{1g}
283	280	20	ν(Pt-P) + δ(P-O-P) + skeletal def.	A_g	A_{1g}
	327	3	skeletal def.	A_g	-
388	384	11	δ(P-O-P)	A_g	A_{1g}
576	572	8	δ(P-O-B)+ δ(O-B-O)	A_g	A_{1g}
	577	3	δ(P-O-B)+ δ(O-B-O)	A_g	-
	669	3	δ(P-O-B)+ δ(O-B-O)	A_g	E_g
	712	3	δ(P-O-P)+ δ(O-B-O)	A_g	A_{1g}
	811	20	ν(Pt-P)+ δ(P-O-P)	A_g	A_{1g}
	817	3	ν(B-O)+ ν(P-O)	A_g	-
	841 or 846	–	ν(B-O)+ ν(P-O)	B_g	A_{2g}
	961	2	ν(P-O) + ν(B-O) + skeletal def.	A_g	E_g
	961	1	ν(P-O) + ν(B-O) + skeletal def.	B_g	E_g
	1049	12	ν(B-O) +δ(P-O-P)	A_g	A_{1g}
1112	1106	5	ν(P-O)	B_g	E_g
	1123	12	ν(P-O)	A_g	E_g
	1130	7	ν(B-F)+ ν(P-O)	A_g	B_{2g}
1150	1149	3	ν(B-F)	A_g	B_{2g}
	1159	9	ν(B-F)	A_g	A_{1g}
	1176	10	ν(B-F)	A_g	A_{1g}

[a] Left column: symmetry of vibrational modes obtained for the lowest-energy C_{2h} structure. Right column: symmetry of vibrational modes in a D_{4h} point group.

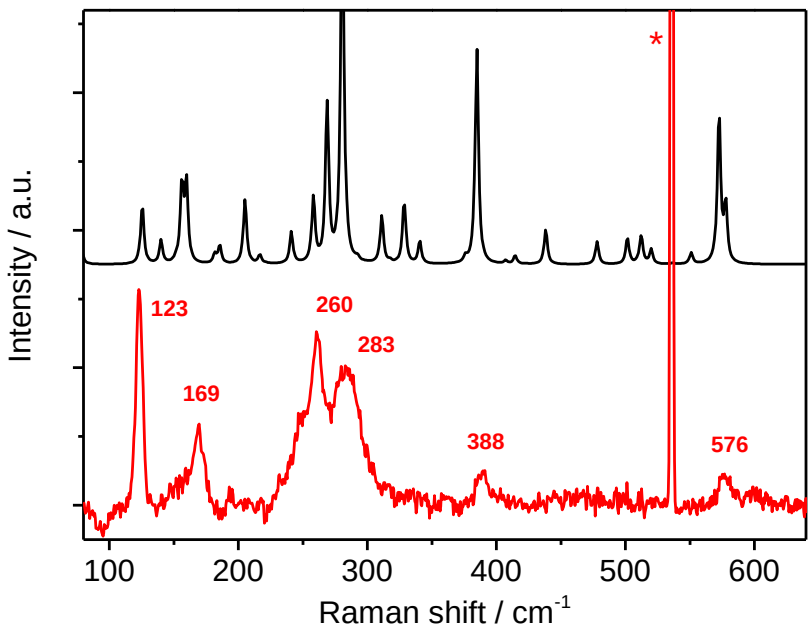

Figure 12. Raman spectra of $[Bu_4N]_4[Pt(pop\text{-}BF_2)]$. Bottom-red: experimental spectrum measured on a solid sample (λ_{exc} = 1064 nm). The intense band at 536 cm^{-1} (*) is due to Bu_4N^+. Top-black: DFT-calculated spectrum (PBE0, vacuum).

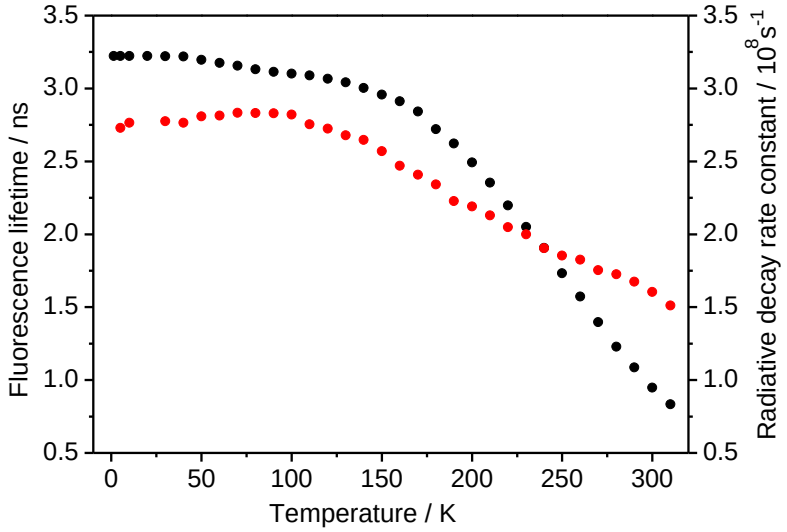

Figure 13. Temperature dependence of the fluorescence decay lifetime (red) and radiative decay rate constant (black) of $Pt(pop\text{-}BF_2)$ powder. λ_{exc} = 378 (diode laser), λ_{det} = 400 nm. (Lifetimes were obtained without deconvolution of the excitation pulse profile; $k_r = \phi_{fl}/\tau_{fl}$)

Table 6. Fluorescence lifetime and quantum yield of microcrystalline Pt(pop-BF_2) as a function of temperature. The radiative ($k_r = \phi_{fl} / \tau_{fl}$) and non-radiative ($k_{nr} = (1 - \phi_{fl}) / \tau_{fl}$) decay rates were calculated from these quantities.

Temperature [K]	τ_{fl} [ns]	Φ(Fluorescence)	k_r [10^8 s^{-1}]	k_{nr} [10^8 s^{-1}]
5	3.22	0.88	2.73	0.372
10	3.22	0.89	2.77	0.338
30	3.22	0.89	2.78	0.329
40	3.22	0.89	2.76	0.342
50	3.20	0.90	2.81	0.319
60	3.17	0.89	2.81	0.337
70	3.16	0.89	2.83	0.336
80	3.13	0.89	2.83	0.361
90	3.11	0.88	2.83	0.382
100	3.10	0.88	2.82	0.403
110	3.09	0.85	2.75	0.482
120	3.07	0.84	2.72	0.538
130	3.04	0.82	2.68	0.608
140	3.00	0.80	2.65	0.683
150	2.96	0.76	2.57	0.811
160	2.91	0.72	2.47	0.965
170	2.84	0.68	2.41	1.11
180	2.72	0.64	2.34	1.33
190	2.62	0.58	2.23	1.59
200	2.49	0.55	2.19	1.82
210	2.35	0.50	2.13	2.12
220	2.20	0.45	2.05	2.50
230	2.05	0.41	2.00	2.88
240	1.91	0.36	1.90	3.34
250	1.73	0.32	1.85	3.92
260	1.57	0.29	1.82	4.53
270	1.40	0.25	1.75	5.40
280	1.23	0.21	1.73	6.41
290	1.09	0.18	1.68	7.53
300	0.95	0.15	1.60	8.95
310	0.83	0.13	1.51	10.5

Fluorescence decay can be fitted with single-exponential kinetics (Table 6). The lifetime is nearly temperature-independent up to about 100 K and then decreases with increasing temperature (Figure 13). Fluorescence radiative decay rate constant, calculated from the lifetime and quantum yield (ϕ_{fl}/τ_{fl}), decreases ca. 1.8-times upon increasing the temperature from 100 to 310 K (Figure 13).

Non-radiative decay is approximately invariant with temperature over 5-90 K, then increases ca. 27-fold from 90 to 310 K (Table 6, Figure 14). Treating non-radiative decay as a multiphonon transition from thermally equilibrated vibrational levels of the $^1A_{2u}$ state into densely spaced vibrational levels of a final state, Englman and Jortner derived equation (1) as the expression for non-radiative decay rates in the strong coupling limit, where the potential energy surface of the final state is substantially displaced from that of $^1A_{2u}$.[19] The quantitative criterion for strong coupling is $\lambda \gg \hbar\langle\omega\rangle \tanh\left(\frac{\hbar\langle\omega\rangle}{2k_BT}\right)$.[19]

$$k_{nr} = \frac{C^2\sqrt{2\pi}}{\hbar\sqrt{\lambda k_B T^*}}\exp\left(-\frac{E_a}{k_B T^*}\right)$$
$$T^* = \frac{\hbar\langle\omega\rangle}{2k_B}\coth\left(\frac{\hbar\langle\omega\rangle}{2k_B T}\right) \qquad (1)$$

In equation (1), C denotes the electronic coupling term (often denoted H_{AB} by other authors), λ the reorganization energy, and E_a the apparent activation energy. Fitting the k_{nr} data in Table 6 (Figure 14), E_a = 2024 cm^{-1}, $\hbar\langle\omega\rangle$ = 367 cm^{-1}. Since spectroscopic evidence such as vibronic progressions indicates that $^1A_{2u}$ and $^3A_{2u}$ have similar equilibrium geometries and vibrational frequencies, they are likely weakly coupled. Equation (1), therefore, is most consistent with decay via a strongly displaced

intermediate state. Unfortunately, no information about either ΔE or λ is available from equation (1), making it impossible to determine C and the Huang-Rhys displacement parameter $S = \lambda/\hbar\langle\omega\rangle$.

Here we show that a two-channel model with physically plausible parameters can account for the observed temperature dependence. In channel 1, $^1A_{2u}$ intersystem crosses directly by a multiphonon process into $^3A_{2u}$, hence ΔE = -5750 cm^{-1} and S is small (arbitrarily taken to be 0.1 for purposes of model fitting, *vide infra*) since the $^1A_{2u}$ and $^3A_{2u}$ potential energy surfaces are almost nested (*vide supra*). In channel 2, ISC occurs into a deactivating state of triplet character, which then rapidly decays to $^3A_{2u}$. Assuming that only one vibrational mode undergoes displacement in each channel, and that the vibrations are harmonic with the same force constants in $^1A_{2u}$ and the final state,

$$k_{nr} = k_1(\Delta E_1 = -5750,\ S_1 = 0.1,\ \hbar\omega_1) + k_2(\Delta E_2,\ S_2,\ \hbar\omega_2) \qquad (2)$$

Assuming a Boltzmann distribution for the vibrational energy levels of $^1A_{2u}$,

$$k_i = \frac{2\pi H_{AB}^2}{\hbar}\frac{1}{Q}\sum_m\sum_n \exp\left(-\frac{\left(m+\frac{1}{2}\right)*\hbar\omega_i}{kT}\right) I^2_{[A,m],[B,n]}\,\delta\left(\left(m+\frac{1}{2}\right)*\hbar\omega_i - \epsilon_{B,n}\right) \qquad (3)$$

Equation (3) is an expression for the thermally weighted probability per unit time of transitioning from vibrational level *m* of $^1A_{2u}$ to vibrational level *n* of the final state ($^3A_{2u}$ or the deactivating state in channel 2). Q is the vibrational partition function, $\hbar\omega_i$ the promoting mode frequency, $I_{[A,m],[B,n]}$ the overlap integral of the vibrational wavefunctions, and $\epsilon_{B,n}$ the energy of the nth vibrational level of B, the final electronic state. The delta function arises from the conservation of energy, and consequently the only

non-zero terms occur for $n - m = \Delta E / \hbar\omega = n_0$, where n_0 is an integer. In practice, low-frequency lattice modes are always present that allow transition at $\Delta E / \hbar\omega \approx n_0$.

Recursion relations for the overlap integrals of two harmonic oscillator wave functions were derived by F. Ansbacher:[20]

$$I(m,n,\gamma) = \frac{\gamma}{\sqrt{2m}} I(m-1,n,\gamma) + \sqrt{\frac{n}{m}} I(m-1,n-1,\gamma) \quad (4a)$$

$$I(m-1,n,\gamma) = -\frac{\gamma}{\sqrt{2n}} I(m-1,n-1,\gamma) + \sqrt{\frac{m}{n}} I(m-2,n-1,\gamma) \quad (4b)$$

$$I(0,n) = \sqrt{\frac{S^n}{n!}} \exp(-\frac{S}{2}) \quad (4c)$$

For our purposes, $n = m + n_0$, where n_0 is $\Delta E / \hbar\omega$ rounded to the nearest integer. Using these recursion relations, and taking $\hbar\omega_1$ and $\hbar\omega_2$ from the list of Raman-active vibrations (Table 5), the best fit (Figure 15) was $\hbar\omega_1$= 283 cm^{-1}, $H_{AB,1}$ = 21 cm^{-1}, $\hbar\omega_2$= 388 cm^{-1}, $\Delta E_2 / \hbar\omega = 0$, S_2 = 8.4, $H_{AB,2}$ = 0.36 cm^{-1}. Electronic coupling between $^1A_{2u}$ and $^3A_{2u}$ is weak, and even weaker between $^1A_{2u}$ and the strongly displaced, (nearly) isoenergetic deactivating state of channel 2. Electronic coupling is weak because such transitions are spin- and/or symmetry-forbidden.

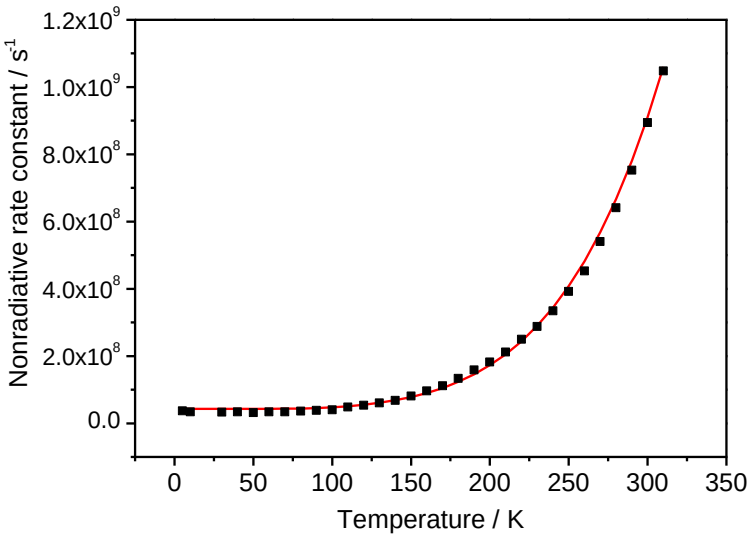

Figure 14. Temperature dependence of the nonradiative decay rate constant of the $^1A_{2u}$ excited state of Pt(pop-BF_2). Red: Fit to eq. 1: E_a = 2026 cm^{-1}; $\hbar\langle\omega\rangle$ = 367±17 cm^{-1}; $\left(C^2/\hbar\right)\left(4\pi/\lambda\hbar\langle\omega\rangle\right)^{1/2}$ = 2.57×10^{12} s^{-1}.

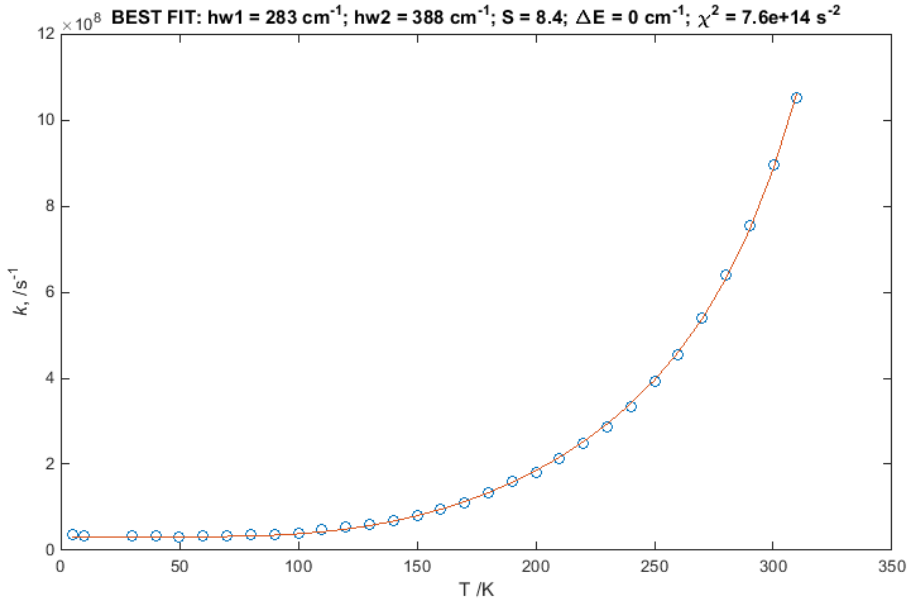

Figure 15. Temperature dependence of the nonradiative decay rate constant of the $^1A_{2u}$ excited state of Pt(pop-BF_2). Red: Fit to eq. 2, 3, and 4 (see text for details).

$^3A_{2u} \rightarrow {}^1A_{1g}$ phosphorescence: characterization of the lowest triplet excited state

High-resolution phosphorescence spectrum of Pt(pop-BF_2) is shown in Figure 16, together with the corresponding excitation spectrum that matches the spin-forbidden absorption band $^1A_{1g} \rightarrow {}^3A_{2u}$ observed in the absorption spectrum (*vide supra*). The phosphorescence vibronic progression (123 cm^{-1}) matches the ground-state ν(Pt-Pt) Raman band, while the excitation progression of 168±7 cm^{-1} accords with Pt-Pt bond strengthening in the triplet excited state. The $^3A_{2u}$ energy (E_{00} of 20460 cm^{-1}) is obtained from overlapping origins of the excitation and phosphorescence spectra at 10 K. Upon decreasing the temperature from 10 to 1.3 K, the phosphorescence band shifts by ca. 220 cm^{-1} to lower energies. The origin of this shift is discussed later.

At all temperatures between 1.3 and 310 K, the phosphorescence decay of Pt(pop-BF_2) follows first-order kinetics: the lifetime, which remains largely unchanged at 8.6 ms in the 1.5-8 K range, decreases by three orders of magnitude to ca. 8 μs at 100 K and then stays nearly constant upon further temperature increase (Figure 16). The data can be fit to eq. 5, which assumes emission from a nondegenerate state and a higher-lying, thermally populated, doubly degenerate state that can be identified as A_{1u} and E_u, respectively, based on symmetry considerations and analogy with Pt(pop).[12, 21-23]

$$\tau_{ph} = \frac{1 + 2\exp\left(-\frac{\Delta E_{zfs}}{k_B T}\right)}{\frac{1}{\tau(\mathrm{A_{1u}})} + \frac{1}{\tau(\mathrm{E_u})}\exp\left(-\frac{\Delta E_{zfs}}{k_B T}\right)} \qquad (5)$$

(This conclusion remains valid even if the upper state is not strictly degenerate in the actual C_s or C_{2h} molecular symmetry, so long as the E_u splitting does not exceed the

experimental resolution of a few cm^{-1}. No satisfactory fit can be found assuming nondegeneracy for both states.) Fitting to eq. 5 yields lifetimes $\tau(A_{1u})$ and $\tau(E_u)$ of 8.6 ms and 2.3 μs, respectively (Figure 17). The energy separation ΔE_{zfs} of 40 cm^{-1} corresponds to the zero-field splitting (zfs) of the lowest triplet state ($^3A_{2u}$). This value agrees with spin-orbit DFT calculations[16] and is very close to the experimentally determined zfs of 40-50 cm^{-1} of the Pt(pop) $^3A_{2u}$ state.[6,12,21]

Radiative decay to the A_{1g} ground state is symmetry-allowed from the upper E_u state but forbidden from A_{1u}, thereby accounting for the ca. 4000-fold difference in their emission lifetimes. Whereas both E_u and A_{1u} states are populated at $T \geq 10$ K, the emission at 1.3 K originates solely from A_{1u} since the E_u population is near zero at that temperature. A_{1u} radiative decay gains intensity through spin-vibronic Herzberg-Teller coupling involving modes of E_g or A_{2g} symmetry (in D_{4h}), as proposed for Pt(pop).[21] The phosphorescence spectrum measured at 1.3 K shows a false origin shifted by 220 cm^{-1} lower from E_{00} (Figure 16 – bottom). This shift corresponds to the zfs (40 cm^{-1}) plus the energy of the HT-active vibration, ~180 cm^{-1}. Comparison with the experimental and calculated Raman spectra (Table 5) suggests the deformation vibrations calculated at 155 and 158 cm^{-1} (giving rise to the 169 cm^{-1} Raman band) and/or the Raman-inactive vibration calculated at 213-217 cm^{-1} to be the HT-active mode(s).[ii]

[ii] The phosphorescence band broadening at 1.3 K indicates that higher-lying vibrational modes could also contribute to the HT coupling.

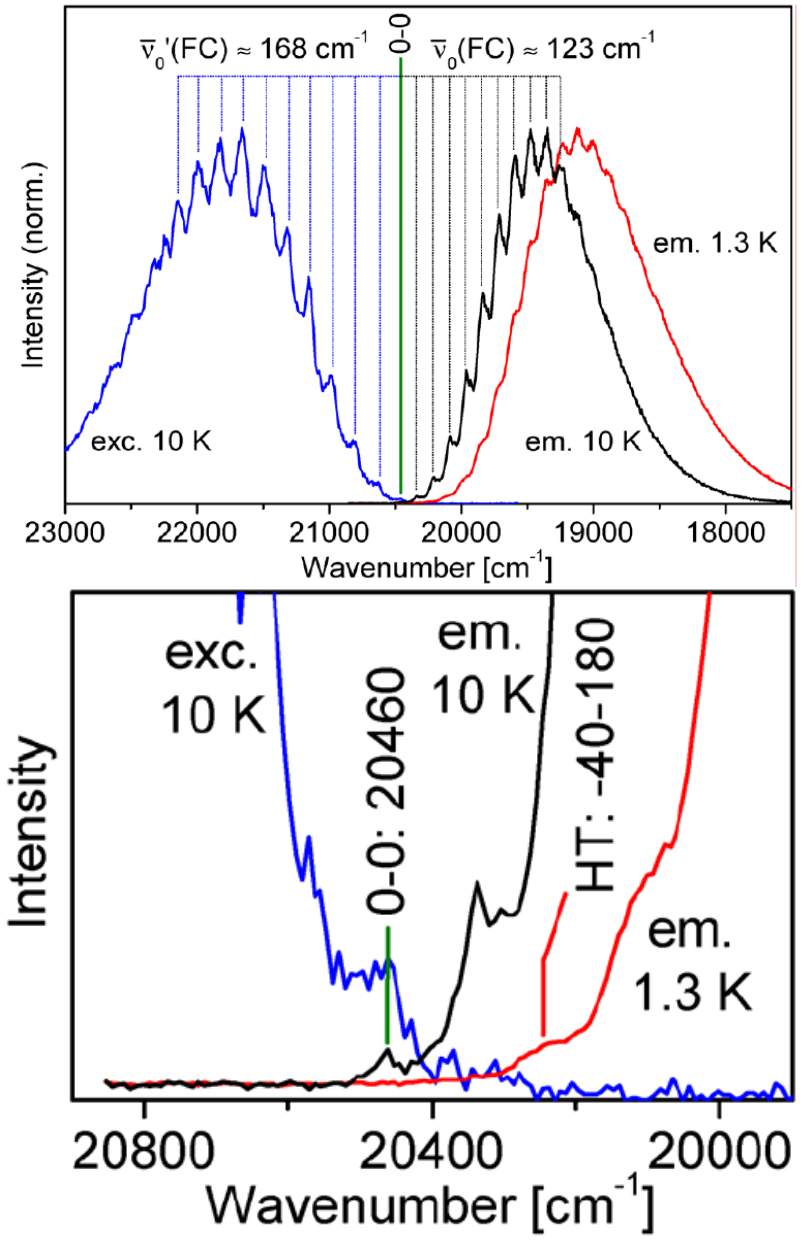

Figure 16. High-resolution emission and excitation spectra of Pt(pop-BF_2) (powder) in the range of the $^1A_{1g} \leftrightarrow {}^3A_{2u}$ transition. λ_{exc}(emission) = 300 nm, λ_{det}(excitation) = 520 nm. Top: full-range spectra. Bottom: HT: -40-180 denotes the false phosphorescence origin that is shifted by 220 cm^{-1} from the 0-0 transition. –40 cm^{-1} is the zfs, 180 cm^{-1} is the energy of the HT mode.

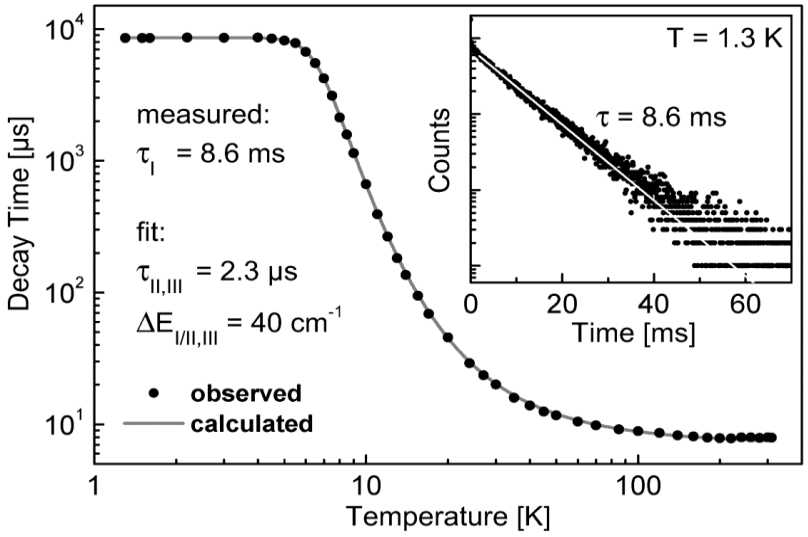

Figure 17. Temperature dependence of the phosphorescence lifetime of Pt(pop-BF_2): powder (left); MeCN solution (right). Calculated lifetimes from fitting to equation 5.

Concluding remarks

Per(difluoroboration) of Pt(pop) dramatically decreases rates of ISC such that the first singlet excited state ($^1A_{2u}$) of Pt(pop-BF_2) has a lifetime of 1.6 ns at room temperature, displaying very intense fluorescence *and* phosphorescence.

The long $^1A_{2u}$ lifetime and strong fluorescence offer a unique opportunity to investigate separately the properties and chemistry of the $d\sigma^*p\sigma$ $^1A_{2u}$ and $^3A_{2u}$ states. High-resolution spectroscopy of microcrystalline Pt(pop-BF_2) showed that Pt-Pt stretching energies in $^1A_{2u}$ (160±7) and $^3A_{2u}$ (168±7 cm^{-1}) are comparable and substantially higher than in the ground state (123 cm^{-1}), demonstrating Pt-Pt bond formation upon $d\sigma^* \rightarrow p\sigma$ excitation. Examination of fluorescence lifetimes and quantum yields over a broad temperature range showed that the ISC rate in the solid is nearly temperature-independent $(\sim 3.2\ ns)^{-1}$ up to ~150 K and increases at higher temperatures. The temperature dependence is explained using a two-channel model—$^1A_{2u}$ decay occurs via a multiphonon transition to (1) $^3A_{2u}$ and (2) to a deactivation state that subsequently undergoes very fast conversion to $^3A_{2u}$. This state is isoenergetic to (or nearly so), highly displaced (S = 8.4) from, and has very weak electronic coupling (H_{AB} = 0.36 cm^{-1}) with $^1A_{2u}$.

By contrast, the observed behavior of its $^3A_{2u}$ state is very similar to that of Pt(pop) in terms of decay kinetics and mechanism, as well as zero field splitting. Phosphorescence at T > 10 K occurs predominantly from a thermally populated E_u spin-orbit state. Emission from the A_{1u} spin-orbit state is observed at lower temperatures (1.3 K), allowed by Herzberg-Teller coupling with skeletal deformation mode(s).

Experimental Section

$[Bu_4N]_4[Pt_2(\mu\text{-}P_2O_5(BF_2)_2)_4]$ ($Pt(pop\text{-}BF_2)$) was prepared as outlined in Chapter I. Samples suitable for photophysical studies were twice recrystallized by diffusion of diethylether into a MeCN solution of the compound.

Solution Phase Spectroscopic Studies

Solutions of $Pt(pop\text{-}BF_2)$ were prepared in anhydrous MeCN (Acros Organics, Extra Dry in AcroSeal® containers, or Aldrich, SureSeal®, used as received) under anhydrous, oxygen-free conditions using drybox and/or Schlenk techniques. Samples for some of the emission experiments were further degassed with freeze-pump-thaw cycles under high vacuum (4×10^{-5} mbar).

UV–vis absorbance spectra were recorded on an Agilent 8453 UV–vis spectrometer using a cuvette containing pure solvent as the background. Steady-state emission spectra were recorded on a Jobin Yvon Spex Fluorolog-3-11. A 450 W xenon arc lamp was used as the excitation source with a single monochromator providing wavelength selection. Right-angle light emission was sorted using a single monochromator and fed into a Hamamatsu R928P photomultiplier tube with photon counting. Short and long pass filters were used where appropriate. Spectra were recorded on Datamax software. Both fluorescence and phosphorescence quantum yields were measured from optically dilute MeCN solutions using anthracene in anhydrous ethanol as a standard.

Fluorescence decay and phosphorescence rise were measured using two independent experimental setups: time correlated single photon counting (TCSPC) and a

streak camera in a photon-counting mode. The two techniques produced virtually identical results.

TCSPC: an IBH 5000 U instrument equipped with a cooled Hamamatsu R3809U-50 microchannel plate photomultiplier was used. Samples were excited at 370 nm with an IBH NanoLED-03 diode laser (~80 ps FWHM, repetition rate 500 kHz). For fluorescence decay measurements, the emission monochromator was set to 405±4 nm, preceded by a 390 nm longpass cut-off filter to remove all stray excitation light. Phosphorescence rise kinetics were measured with the monochromator set at 512±16 nm, in combination with a 450 nm longpass cut-off filter that removed both the excitation stray light and residual fluorescence. Magic angle between the excitation and emission polarization directions was used for all experiments. The temporal resolution was 2.89 ps/channel. Temperature dependence of the fluorescence decay was measured with a 7.07 ps/channel resolution. Data were analyzed using IBH Datastation2 or Microcal Origin 7.1 software. The sample solutions were prepared in a controlled-atmosphere (0.3 ppm O_2) glove box (Jacomex) using dry, degassed MeCN Aldrich SureSeal®. Additional high-vacuum (4×10^{-5} mbar) freeze-pump-thaw degassing was applied on solutions for all phosphorescence and some of the fluorescence measurements.

Streak camera in photon-counting mode: samples were excited with 50 ps pulses at 355 nm from the third harmonic of a regeneratively amplified mode-locked Nd:YAG laser (Vanguard 2000-HM532; Spectra-Physics) operating at 10 Hz. Emission was collected on a picosecond streak camera (Hamamatsu C5680 in photon-counting mode); singlet emission was selected by a 400-415 nm bandpass filter and triplet rise selected with a 500 nm long-

pass filter. The measurements were made under magic-angle conditions and data were collected over a 50 ns sweep range with 8,000 exposures.

To monitor triplet emission (phosphorescence), samples were excited at 355 nm with 8-ns pulses from the third harmonic of a Q-switched Nd:YAG laser (Spectra-Physics Quanta-Ray PRO-Series) operating at 10 Hz. Emission wavelengths were selected using a double monochromator (Instruments SA DH-10) with 1 mm slits. Luminescence was detected with a photomultiplier tube (PMT, Hamamatsu R928). The PMT current was amplified and recorded with a transient digitizer (Tektronix DSA 602). Short- and long-pass filters were employed to remove scattered excitation light. Decay traces were averaged over 500 laser pulses. Instruments and electronics in this system were controlled by software written in LabVIEW (National Instruments). Data manipulation was performed and plotted using MATLAB R2008a (Mathworks, Inc.). Some measurements were performed using TCSPC set as described above, except for the repetition rate (10 kHz) and time resolution (121.44 ps/channel).

High-Resolution Spectroscopic Studies of Microcrystalline Pt(pop-BF_2)

Emission spectra and decay curves were recorded with a Fluorolog 3 (Horiba Jobin Yvon) spectrometer equipped with a cooled photomultiplier tube. The spectra were corrected for the wavelength dependence of the spectrometer/detector. The decay behavior was recorded using a multi-channel scaler card (P7887, Fast ComTec) with time resolution down to 250 ps. The fluorescence decay measurements were carried out with a TCSPC module (PicoHarp 300, PicoQuant). Excitation employed the third harmonic (355 nm) of a pulsed Nd:YAG laser system (DiNy pQ, IB Laser) or a pulse diode laser (378 nm,

PicoBrite, Horiba). A cryostat (Konti IT, CryoVac) was used for variable temperature measurements. Quantum yields at ambient temperature and 77 K were determined using a C9920-02 system (Hamamatsu) with an integrating sphere as sample chamber.

Raman spectra were measured on Labram HR Raman spectrometer (Horiba Jobin-Yvon) with a resolution of about 1 cm^{-1}, excited with a 1064 nm laser. The spectrometer was interfaced to a microscope (Olympus, objective 50x). The size of the laser spot was about 1 micrometer. A solid powder sample was placed in a flat 2 mm quartz cell under dry argon atmosphere. Raman bands due to the Bu_4N^+ counter cation were identified by a separate measurement on $[Bu_4N]I$ powder, performed under identical conditions.

Density Functional Theory (DFT) Calculations

The electronic structures of the Pt(pop-BF_2) and Pt(pop) complex anions were calculated by density functional theory (DFT) methods using the Gaussian 09[24] program package. Calculations employed the hybrid Perdew, Burke, and Ernzerhof[25,26] (PBE0) exchange and correlation functional or the functional including Becke's gradient correction[27] to the local exchange expression in conjunction with Perdew's gradient correction[28] to the local correlation (BP86). For H, B, P, O, and F atoms, 6-311g(3d,3pd) polarized triple - ζ basis sets were employed;[29] quasi-relativistic small core effective core pseudopotentials and the corresponding optimized set of basis functions were used for Pt.[30,31]

Geometry optimization was followed by vibrational analysis; no imaginary frequencies were found for energy minimum of the C_{2h} conformer shown in Figure 2,

whose structure matches the crystallographic structure. (No true energy minima were obtained for C_{4h} and D_{4h} conformers.) The calculated bond lengths agree very well with the experimental values and reproduce the subtle structural changes between Pt(pop) and Pt(pop-BF_2), validating the calculation (Table 7). The match is better for the hybrid functional PBE0 than for BP86, which slightly overestimates the bond lengths.

Table 7. Experimental and DFT-calculated bond lengths for Pt(pop-BF_2) and Pt(pop).

Bond	Exp.	Calc. PBE0	Calc. BP86
$[Ph_4As]_4[Pt_2(POP\text{-}BF_2)_4]$ (cf. Chapter I, Table 1)			
Pt-Pt	2.8873(11)	2.901	2.922
Pt-P (average)	2.294	2.302	2.324
P-O(-P) (average)	1.614	1.628	1.656
$K_4[Pt_2(POP)_4]$[32]			
Pt-Pt	2.925(1)	2.929	2.948
Pt-P (average)	2.321(4)	2.351	2.374
P-O(-P) (average)	1.622(12/14)	1.644	1.674

Acknowledgements

We are indebted to Renske van der Veen for interesting discussions. Research at Caltech was supported by the NSF Center for Chemical Innovation (Powering the Planet CHE-0802907 and CHE-0947829) and CSER (Gordon and Betty Moore Foundation). Work at the J. Heyrovský Institute was funded by the Czech Ministry of Education program KONTAKT (grant ME10124). Bavaria California Technology Center provided travel funds.

References

(1) Roundhill, D. M.; Gray, H. B.; Che, C.-M. *Acc. Chem. Res.* **1989**, *22*, 55-61.
(2) Smith, D. C.; Gray, H. B. *ACS Symposium Series 394. The Challenge of d and f Electrons.*; Salahub, D. R., Zerner, M. C., Eds.; American Chemical Society: Washington, DC, 1989, 356-365.
(3) Smith, D. C.; Gray, H. B. *Coord. Chem. Rev.* **1990**, *100*, 169-181.
(4) Marshall, J. L.; Stiegman, A. E.; Gray, H. B. *Excited States and Reactive Intermediates. ACS Symposium Series.*; Lever, A. B. P., Ed.; American Chemical Society: Washington, DC, 1986; Vol. 307, 166-176.
(5) Sweeney, R. J.; Harvey, E. L.; Gray, H. B. *Coord. Chem. Rev.* **1990**, *105*, 23-34.
(6) Rice, S. F.; Gray, H. B. *J. Am. Chem. Soc.* **1983**, *105*, 4571-4575.
(7) Stiegman, A. E.; Rice, S. F.; Gray, H. B.; Miskowski, V. M. *Inorg. Chem.* **1987**, *26*, 1112-1116.
(8) Milder, S. J.; Brunschwig, B. S. *J. Phys. Chem.* **1992**, *96*, 2189-2196.
(9) van der Veen, R. M.; Cannizzo, A.; van Mourik, F.; Vlček, A., Jr.; Chergui, M. *J. Am. Chem. Soc.* **2011**, *133*, 305-315.
(10) van der Veen, R. M.; Milne, C. J.; El Nahhas, A.; Lima, F. A.; Pham, V.-T.; Best, J.; Weinstein, J. A.; Borca, C. N.; Abela, R.; Bressler, C.; Chergui, M. *Angew. Chem. Int. Ed.* **2009**, *48*, 2711 –2714.
(11) Vlček, A., Jr.; Gray, H. B. *J. Am. Chem. Soc.* **1987**, *109*, 286-287.
(12) Fordyce, W. A.; Brummer, J. G.; Crosby, G. A. *J. Am. Chem. Soc.* **1981**, *103*, 7061-7064.
(13) Stoyanov, S. R.; Villegas, J. M.; Rillema, D. P. *J. Phys. Chem. B* **2004**, *108*, 12175–12180.
(14) Novozhilova, I. V.; Volkov, A. V.; Coppens, P. *J. Am. Chem. Soc.* **2003**, *125*, 1079–1087.
(15) Pan, Q.-J.; Fu, H.-G.; Yu, H.-T.; Zhang, H.-X. *Inorg. Chem.* **2006**, *45*, 8729–8735.
(16) Záliš, S.; Lam, Y.C.; Gray, H. B.; Vlček, A., Jr. *Inorg. Chem.*, in revision.
(17) Peterson, J. R.; Kalyanasundaram, K. *J. Phys. Chem.* **1985**, *89*, 2486–2492.
(18) Che, C.-M.; Butler, L. G.; Gray, H. B.; Crooks, R. M.; Woodruff, W. H. *J. Am. Chem. Soc.* **1983**, *105*, 5492-5494.
(19) Englman, R.; Jortner, J. *Molec. Phys.* **1970**, *18*, 145-164.
(20) Ansbacher, F. *Z. Naturforschg.* **1959**, *14a*, 889-892
(21) Bär, L.; Gliemann, G. *Chem. Phys. Lett.* **1984**, *108*, 14-17.
(22) Ikeyama, T.; Yamamoto, S.; Azumi, T. *J. Phys. Chem.* **1988**, *92*, 6899-6901.
(23) Shimizu, Y.; Tanaka, Y.; Azumi, T. *J. Phys. Chem.* **1985**, *89*, 1372-1374.
(24) Frisch, M. J.; Trucks, G. W.; Schlegel, H. B.; Scuseria, G. E.; Robb, M. A.; Cheeseman, J. R.; Scalmani, G.; Barone, V.; Mennucci, B.; Petersson, G. A.; Nakatsuji, H.; Caricato, M.; Li, X.; Hratchian, H. P.; Izmaylov, A. F.; Bloino, J.; Zheng, G.; Sonnenberg, J. L.; Hada, M.; Ehara, M.; Toyota, K.; Fukuda, R.; Hasegawa, J.; Ishida, M.; Nakajima, T.; Honda, Y.; Kitao, O.; Nakai, H.; Vreven, T.; Montgomery, J. A., Jr.; Peralta, J. E.; Ogliaro, F.; Bearpark, M.; Heyd, J. J.; Brothers, E.; Kudin, K. N.; Staroverov, V. N.; Kobayashi, R.; Normand, J.; Raghavachari, K.; Rendell, A.; Burant, J. C.; Iyengar, S. S.; Tomasi, J.; Cossi, M.; Rega, N.; Millam, J. M.; Klene, M.; Knox, J. E.; Cross, J. B.; Bakken, V.; Adamo, C.;

Jaramillo, J.; Gomperts, R.; Stratmann, R. E.; Yazyev, O.; Austin, A. J.; Cammi, R.; Pomelli, C.; Ochterski, J. W.; Martin, R. L.; Morokuma, K.; Zakrzewski, V. G.; Voth, G. A.; Salvador, P.; Dannenberg, J. J.; Dapprich, S.; Daniels, A. D.; Farkas, O.; Foresman, J. B.; Ortiz, J. V.; Cioslowski, J.; Fox, D. J.; Gaussian 09, Revision C.01, Gaussian, Inc.: Wallingford CT, 2009.

(25) Perdew, J. P.; Burke, K.; Ernzerhof, M. *Phys. Rev. Lett.* **1996**, *77*, 3865-3868.

(26) Adamo, C.; Scuseria, G. E.; Barone, V. *J. Chem. Phys.* **1999**, *111*, 2889-2899.

(27) Becke, A. D. *Phys. Rev. A* **1988**, *38*, 3098.

(28) Perdew, J. P. *Phys. Rev. A* **1986**, *33*, 8822.

(29) Raghavachari, K.; Binkley, J. S.; Seeger, R.; Pople, J. A. *J. Chem. Phys.* **1980**, *72*, 650-654.

(30) Andrae, D.; Häussermann, U.; Dolg, M.; Stoll, H.; Preuss, H. *Theor. Chim. Acta* **1990**, *77*, 123-141.

(31) Martin, J. M. L.; Sundermann, A. *J. Chem. Phys.* **2001**, *114*, 3408.

(32) Filomena Dos Remedios Pinto, M. A.; Sadler, P. J.; Neidle, S.; Sanderson, M. R.; Subbiah, A.; Kuroda, R. *J. Chem. Soc., Chem. Commun.*, **1980**, 13-15. Corrections made by Marsh, R. E.; Herbstein, F. H., *Acta Cry. B* **1983**, *39*, 280-287.

Chapter III

A Mn Bipyrimidine Catalyst Predicted to Reduce CO_2 at Lower Overpotential

Y.C. Lam; R. J. Nielsen; H. B. Gray; W. A. Goddard, III

Abstract: Experimentally, $[(L)Mn(CO)_3]^-$ (where L = bis alkyl-substituted bipyridine) has been observed to catalyze the electrochemical reduction of CO_2 to CO in the presence of trifluoroethanol (TFEH). Here the products of TFEH-mediated electrochemical CO_2 reduction to CO are considered. Based on DFT calculations (B3LYP-d3 with continuum solvation), the thermodynamically favored half-reaction under standard conditions is CO_2 + 8 TFEH + 2 e^- → CO + H_2O + 2 [$F_3CCH_2O^-$ / 3 $HOCH_2CF_3$] (calculated standard reduction potential: -1.17 V vs. SCE), due to highly exergonic hydrogen bond formation between TFEH and its conjugate base. The atomistic level mechanism of complete catalytic cycles for this reaction, based on DFT calculations of the free energies of reaction and activation, as well as reduction potentials for all catalytically relevant elementary steps, is reported. In the catalytic cycle for CO formation, CO_2 coordinates to $[(L)Mn(CO)_3]^-$ (**1a**, L = bpy), and the adduct is then protonated to form $[(L)Mn(CO)_3(CO_2H)]$ (**3a**). **3a** subsequently reacts to form $[(L)Mn(CO)_4]^0$ (**5a**) via one of two pathways: (a) TFEH-mediated dehydroxylation to $[(L)Mn(CO)_4]^+$ (**4a**), followed by one-electron reduction to **5a**; or, (b) under more reducing potentials, one electron reduction to $[(L)Mn(CO)_3(CO_2H)]^-$ (**3'a**), followed by dehydroxylation to **5a**. Pathway b has a lower activation energy by 2.2

kcal mol^{-1}. Consequently maximum catalytic turnover frequency (TOF_{max}) is achieved at ~ -1.75 V vs. SCE (~ 0.6 V overpotential).

For the analogous bipyrimidine compound (not yet studied experimentally), reduction of **3b** to **3'b** occurs at a potential 0.5 V more positive than that of **3a**, and the overpotential required to achieve TOF_{max} is therefore predicted to be lower by ~ 0.5 V. This improvement is, however, achieved at the price of a lower TOF_{max}, and we predict that **1b** has superior TOF at potentials above ~ -1.6 V vs. SCE. In addition, the various factors contributing to product selectivity (CO over H_2) are discussed.

Introduction

Carbon monoxide (CO) is a versatile reagent, employed industrially in the synthesis of phosgene,[1] methanol,[2] and acetic acid,[3] and in the production of fuels via the Fischer-Tropsch process.[4] A potentially attractive method for CO production is the electrochemical reduction of carbon dioxide, preferably coupled to water oxidation and driven by renewable energy.

Towards this end, an assortment of homogeneous catalysts has been investigated experimentally and theoretically.[5,6,7,8,9] Among these are [*fac*-Mn(bpy-R)$(CO)_3$]$^-$ complexes[9e,f,h] (bpy-R = 4,4'- or 2,2'-disubstituted bipyridine; since all complexes discussed henceforth are *fac*-, the label will be omitted), produced by two sequential one-electron reductions of the corresponding Mn (I) halides. This catalytic activity is proton-dependent; indeed, unlike with the analogous Re complexes, no catalysis is observed in the absence of weak Brønsted acids such as water, methanol, or trifluoroethanol (TFEH).[9e,f] Notably, CO selectivity is quantitative (within experimental uncertainty), even in the presence of > 1 M concentration of aforementioned acids.

Extensive mechanistic investigations, both experimental[9b,d,10,11] and theoretical,[10,12,13] have elucidated plausible mechanisms for proton-dependent CO_2 electrochemical reduction to CO catalyzed by [Re(bpy-R)$(CO)_3$]$^-$ complexes. In particular, the [Re(bpy-R)$(CO)_3$]$^-$ complexes (**1**-Re) display kinetic preference for CO_2 coordination over protonation at Re, forming [Re(bpy-R)$(CO)_3(CO_2^-)$] (**2**-Re), which is protonated to [Re(bpy-R)$(CO)_3(CO_2H)$] (**3**-Re).[10,13] This complex may then undergo proton-assisted dehydroxylation to [Re(bpy-R)$(CO)_4$]$^+$ (**4**-Re), followed by one-electron reduction to [Re(bpy-R)$(CO)_4$]^0 (**5**-Re). Alternatively, at higher overpotentials, it undergoes one-

electron reduction, followed by proton-assisted dehydroxylation to form **5**-Re.[13] The latter pathway affords a lower activation free energy ($\Delta G^{\ddagger}$) for the rate-determining dehydroxylation step. **1**-Re is regenerated by electrochemical reduction accompanied by loss of CO.[13] The overall reaction is first-order in CO_2 and second-order in acid.[10]

Here, we report *ab initio* density functional theory (DFT) studies, including effects of solvation and potential, of electrochemical CO_2 reduction in the presence of TFEH catalyzed by $[(bpy)Mn(CO)_3]^-$ (**1a**), a system that has been studied experimentally. Given the noninnocent role of bpy in these reactions, we simultaneously studied the more electron-deficient bipyrimidine analog $[(bpymd)Mn(CO)_3]^-$ (**1b**; bpymd = bipyrimidine), which has not yet been studied experimentally. We predict that **1b** produces CO at lower overpotentials than **1a**.

Computational Methods

Density functional theory (DFT) calculations for geometry optimizations, electronic energy, solvation energy, and vibrational frequencies were performed using the (U)B3LYP hybrid exchange-correlation functional[14] with the D3 dispersion correction,[15] as implemented in the Jaguar software version 7.9.[16] Solvation effects were modeled using the Poisson-Boltzmann continuum (PBF) approximation[17] for acetonitrile ($\varepsilon = 37.5$, $r = 2.18$).

Geometry optimizations were performed in the gas phase (for CO_2, water, CO, and the TFEH complexes of **2a** and **2b**) or acetonitrile (all other species, including transition states) using the 6-311G**++ basis set on organics.[18] For Mn the 1s, 2s, and 2p core electrons were replaced with an *ab initio* angular momentum projected effective core

potential (ECP) of Melius and Goddard[19] using the parameters and 3-ζ valence functions optimized by Hay and Wadt[20] (LACV3P++) augmented with two *f*-functions.[21]

For the solvation calculations, default van der Waals' radii were used during optimization on all atoms, except TFEH, TFE^-, the TFE^-/TFE homoconjugate, $F_3CCH_2OCO_2^-$, **2a**, and **2b**, which were optimized with non-standard van der Waals' radii on anionic O atoms (2.0 Å in carboxylates, 2.2 Å in alkoxides) and protic (O-bonded) H atoms (0.75 Å). These radii were chosen because they correctly predicted pK_a's for various neutral organic oxy-acids (e.g., phenol) and ΔG_{solv}'s for their conjugate bases (e.g., phenoxide; see Supporting Information, SI). Finally, single-point energy calculations, including solvation with these non-standard van der Waals' radii, were performed.

Vibrational frequencies were obtained with the same basis sets but without *f*-functions (LACV3P++ for Mn). All optimized ground-state structures had no imaginary frequency. Most optimized transition state structures had one imaginary frequency; a few had an additional weak (between 30*i* and 0 cm^{-1}) imaginary frequency arising from the rotation of loosely-bound solvent molecules.

Thermodynamic parameters were calculated using the harmonic oscillator, ideal gas, and rigid rotor approximations;[22] in computing vibrational entropies, all vibrations lower than 50 cm^{-1} not associated with the reaction coordinate of a transition state were replaced with 50 cm^{-1} to avoid spurious fluctuations in entropy arising from low frequency modes. Standard reduction potentials are reported versus the standard calomel electrode (SCE, absolute potential -4.42 V).[23] Potentials vs SCE can be converted to values vs SHE by adding 0.24 V.

We performed key calculations with a variety of methods regarding solvation, basis set, and functional. As seen in Table S4, neither the replacement of B3LYP-d3 with M06 nor the exclusion of solvation during geometry optimization makes an important difference to reaction free energies or standard reduction potentials in our catalytic cycle. Replacement of B3LYP-d3 with M06 raised reduction potentials by 80-120 mV, while changes in solvation or basis set made smaller differences. The absolute barriers of the rate-limiting dehydroxylation reactions were sensitive to the functional and the atomic radii used in the continuum solvation calculations. Replacing B3LYP-d3 with M06, or employing the alternative atomic radii used throughout the paper, raised the dehydroxylation barriers several kcal/mol. However, the difference between these barriers ($\Delta G^{\ddagger}$ in entries 11 and 17, Table, below) underpinning the competition between two reaction pathways remains positive and is only quantitatively altered. Our basic mechanistic conclusions are therefore robust to the choice of computational method.

Results and Discussions

Products of CO_2 Reduction: the Fate of TFEH

The proton-dependent electrochemical reduction of CO_2 is often represented as:

$$CO_2 + 2\ H^+ + 2\ e^- \rightarrow CO + H_2O \qquad \text{(Equation 1)}$$

This representation uses solvated protons as the proton source, ignoring the actual proton source employed—usually water, an alcohol, or phenol—and consequently, the fate of its conjugate base (e.g., hydroxide, alkoxide, or phenoxide), which may undergo further reaction, is overlooked. This treatment is especially problematic for reactions in MeCN,

which solvates anions poorly due to the lack of hydrogen bond donors. (Even in water, which solvates oxyanions strongly, hydroxide and alkoxide react with CO_2 to form bicarbonate and alkylcarbonate.)

Transfer of a proton from TFEH generates TFE^-, which may react with more TFEH to form the TFE^- / TFEH homoconjugate (labeled B in Scheme 1 and Table 2, see Table 1, entry 1), or with CO_2 to form $[F_3CCH_2OCO_2]^-$ (Table 1, entry 2). These anions are further stabilized by hydrogen bonding to TFEH, with the hydrogen bonding of TFEH to $[F_3CCH_2OCO_2]^-$ substantially less exergonic than that to TFE^- / TFEH (Table 1, entries 3/5 vs. entries 4/6). (Hydrogen bonding to H_2O may be neglected since it is a weaker hydrogen bond donor than TFEH and present in low concentrations under typical experimental conditions.)

Table 1: ΔG for possible reactions of TFE^-, calculated under standard conditions (1 atm CO_2, 1 M in MeCN solution for all other reagents and products).

Entry	Reaction	ΔG / kcal mol^{-1}
1	TFE^- + TFEH → TFE^- / TFEH	-13.6
2	TFE^- + CO_2 → $[F_3CCH_2OCO_2]^-$	-14.6
3	TFE^- / TFEH + TFEH → TFE^- / 2 TFEH	-5.6
4	$[F_3CCH_2OCO_2]^-$ + TFEH → $[F_3CCH_2OCO_2]^-$ / TFEH	-1.5
5	TFE^- / 2 TFEH + TFEH → TFE^- / 3 TFEH	-3.3
6	$[F_3CCH_2OCO_2]^-$ / TFEH + TFEH → $[F_3CCH_2OCO_2]^-$ / 2 TFEH	-1.8
7	TFE^- + 3 TFEH → TFE^- / 3 TFEH	-22.5

These calculations predict that the ultimate product of TFEH deprotonation is TFE^- / 3 TFEH when [TFEH] > ca. 38 mM, and that the calculated pK_a of TFEH at 1 M (19.3) is 16.5 units lower than at infinite dilution (calculated pK_a: 35.8). Consequently, under conditions typical of a cyclic voltammetry (CV) experiment (1 atm CO_2, 0.1-1 M TFEH, negligible concentrations of H_2O and CO), the thermodynamically favored products of TFEH-mediated electrochemical CO_2 reduction to CO in MeCN are CO, H_2O (as expected from equation 1), and TFE^- / 3 TFEH (see Scheme 1 for structure). The net half-reaction is therefore:

$CO_2 + 8\ TFEH + 2\ e^- \rightarrow CO + H_2O + 2\ [F_3CCH_2O^- / 3\ HOCH_2CF_3]$ (Equation 2)

The calculated standard reduction potential is -1.17 V vs. SCE.

*Mechanisms for CO_2 Reduction at **1***

Scheme 1 outlines proposed reaction mechanisms for **1** (**1a** and **1b**), similar to what Keith *et al.* proposed for $[(bpy)Re(CO)_3]^-$.[13] TFEH was chosen as the acid in these studies because it afforded the highest TOF among the acids reported.[9f,h] (We have not considered the activation of precatalysts $[(bpy)Mn(CO)_3X]$ and $[(bpymd)Mn(CO)_3X]$, since **1a** and **4a** are isolable solids.) We have not considered the previously reported dimerization of $(L)Mn^0(CO)_3$,[9e,f] because the substitution of sufficiently bulky 6,6'-substituents precludes this reaction.[9h] Thermodynamic and kinetic parameters for all reactions are presented in Table 1, along with standard reduction potentials for reagents and reaction intermediates.

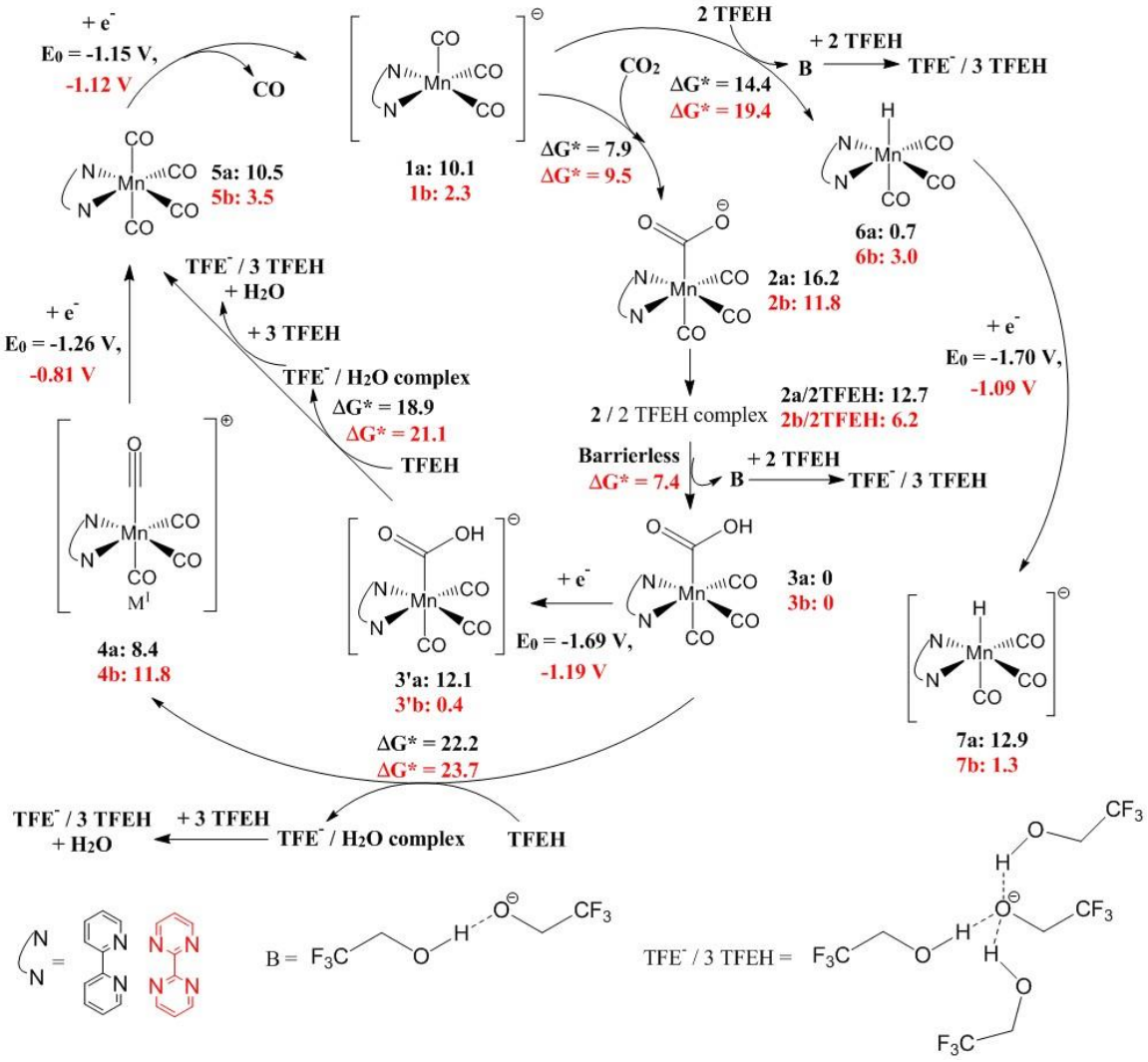

Scheme 1: Proposed electrocatalytic cycle. All reagents are in their standard states (25°C, 1 atm CO_2 and CO, 1 M for all reagents in MeCN). Gibbs free energies (kcal mol^{-1}) relative to resting state **3**, calculated at -1.17 V vs SCE (zero applied overpotential under standard conditions, see text for explanation), are reported in black for L = bpy, and in red for L = bpymd. Activation free energies are denoted ΔG*, and reported in kcal mol^{-1} relative to preceding intermediate. Standard reduction potentials are reported in V vs. SCE.

In computing proton transfer and dehydroxylation transition states, models including either one or two TFEH molecules as the proton source (*vide supra*) were considered. In the latter models, one TFEH molecule transfers its proton to the Mn complex while the other stabilizes the incipient TFE^- through hydrogen bonding. This stabilization reduces activation enthalpy at the expense of decreased activation entropy.

Agreement between calculated and experimentally derived quantities is generally quite good. In particular, the computed potential for reduction of **3a** (-1.69 V vs SCE) accords well with the potential corresponding to $i_{cat} = i_{cat,max} / 2$ in the linear scan voltammograms of both Mn(bpy-*t*Bu)$(CO)_3$Br (~ -1.7 V)[9f] and [Mn(mesbpy)$(CO)_3$(MeCN)](OTf) (~ -1.7 V)[9h]. Agreement between calculated $\Delta G^{\ddagger}$ (18.9 kcal mol^{-1} for L = bpy) and measured TOF (3000 and 5000 s^{-1}, respectively, for Mn(bpy-*t*Bu)$(CO)_3$Br and [Mn(mesbpy)$(CO)_3$(MeCN)](OTf), corresponding approximately to $\Delta G^{\ddagger}$ = 16 kcal mol^{-1}) is acceptable.

Table 2: ΔG, $\Delta G^{\ddagger}$, and standard reduction potentials for reactions in Scheme 1.

		ΔG [a]	$\Delta G^{\ddagger}$ [a]	E^{o} [b]
1	**1a** + CO_2 → **2a**	6.2	7.9	N/A
2	**1b** + CO_2 → **2b**	9.5 [c]	9.5 [c]	N/A
3	**2a** + 2 TFEH → **2a** / 2 TFEH complex	-3.6		N/A
4	**2b** + 2 TFEH → **2b** / 2 TFEH complex	-5.5		N/A
5	**2a** / 2 TFEH complex → **3a** + TFE^- / TFEH	-3.8 [d]	0 [e]	N/A
6	**2b** / 2 TFEH complex → **3b** + TFE^- / TFEH	2.6 [d]	7.4	N/A
7	**3a** + TFEH → **4a** + TFE^- / H_2O [f]	18.1	22.2	N/A
8	**3b** + TFEH → **4b** + TFE^- / H_2O [f]	21.6	23.7	N/A
9	**4a** + e^- → **5a**	N/A		-1.26
10	**4b** + e^- → **5b**	N/A		-0.81
11	**3a** + e^- → **3'a**	N/A		-1.69
12	**3b** + e^- → **3'b**	N/A		-1.19
13	**3'a** + TFEH → **5a** + TFE^- / H_2O [f]	8.1	18.9	N/A
14	**3'b** + TFEH → **5b** + TFE^- / H_2O [f]	12.8	21.1	N/A
15	**5a** + e^- → **1a** + CO	N/A		-1.09
16	**5b** + e^- → **1b** + CO	N/A		-1.12
17	CO_2 + 8 TFEH + 2 e^- → CO + H_2O + 2 TFE^- / 3 TFEH	N/A		-1.17
18	**1a** + 2 TFEH → **6a** + TFE^- / TFEH	-0.5	14.4	N/A
19	**1b** + 2 TFEH → **6b** + TFE^- / TFEH	1.8	19.4	N/A
20	**6a** + e^- → 7**a**	N/A		-1.70
21	**6b** + e^- → **7b**	N/A		-1.09

[a] In kcal mol^{-1}; [b] V vs. SCE; [c] the reverse reaction appears to be barrierless on the free energy surface because the transition state has a lower zero-point energy (ZPE) than **2b**, offsetting the higher potential energy of the former; [d] this is an upper bound because TFE^- /TFEH homoconjugate hydrogen bonds exergonically to **3**, lowering the energy of the products; [e] the transition state's lower ZPE offsets its higher potential energy; [f] the same transformation can be performed via a transition state involving two TFEH molecules: the $\Delta G^{\ddagger}$ is not significantly different, within the uncertainty of the method. See text for explanation.

*Coordination of CO_2 to Anion **1** and Protonation of the Adduct to Form **3***

At applied potentials typical of controlled potential electrolysis (CPE) experiments, anion **1** is the resting state in the absence of TFEH.[9e,f,h] CO_2 coordination to **1** (Table 2, entries 3 and 4) is endergonic but kinetically facile—the reverse reaction is almost barrierless—due to a very early transition state (Mn-C: 2.92 Å for **1a**, 2.86 Å for **1b**; see Supporting Information for coordinates). The predicted lack of reactivity between **1a** and CO_2 in the absence of a proton source accords with experimental observation.[9h] The CO_2 adduct **2** is stabilized by hydrogen bonding to two TFEH molecules (Table 2, entries 3 and 4). Such hydrogen bonding also facilitates proton transfer to form **3** (Table 2, entries 5 and 6) by stabilizing the transition state vis-à-vis CO_2 adduct **2**. The exergonic hydrogen bonding of TFEH to TFE^-/TFEH homoconjugate (Table 1) provides additional driving force for this transformation, rendering the net transformation of **1a** to **3** exergonic, in qualitative agreement with experimental observation, for which the equilibrium constant (L = Mesbpy) is ca. 46 M^{-1} ($\Delta G \sim -2.3$ kcal mol^{-1}) when MeOH is the proton source.[9h]

*Two Pathways for Dehydroxylation of **3**: Dominant Mechanism Depends on Applied Potential*

Hydroxycarbonyl complexes **3** and **3'** are converted to tetracarbonyl compounds **4** and **5** via protonolysis of the C-OH bond by the acid TFEH. In the TOF-determining transition states $TS_{\mathbf{3}\rightarrow\mathbf{4}}$ and $TS_{\mathbf{3'}\rightarrow\mathbf{5}}$, OH^- is almost fully dissociated, stabilized by strong hydrogen bonding to TFEH (Figure 1). $TS_{\mathbf{3'}\rightarrow\mathbf{5}}$ has one electron more than $TS_{\mathbf{3}\rightarrow\mathbf{4}}$, resulting in an earlier transition state with significantly shorter C28-O48 (the C-O bond being

cleaved) and longer O48-H32 (hydrogen bonding) distance (Figure 1) and reduced activation energy (by 3.3 and 2.6 kcal mol^{-1} for L = bpy and bpymd, respectively). This reduction in activation energy is attributable to the weaker C-OH bond in **3'** vis-à-vis **3** (by 10.0 and 8.7 kcal mol^{-1}, respectively, for L = bpy and bpymd; cf. Table 2, entries 7/8 vs. 13/14).

Assuming that charge transfer and mass transport are not rate-limiting, **4**, **5**, **1**, **2**, **2** / 2 TFEH complex, **3**, and **3'** interconvert on a faster timescale than dehydroxylation of **3** or **3'**. The equilibrium between **1**, **2**, **2** / 2 TFEH complex, and **3** is independent of applied potential, with **3** being dominant among these. The equilibrium between **4**, **5**, **3**, and **3'** is potential-dependent. For L = bpy, **3a** is the resting state at high applied potentials (low overpotentials); at potentials below $E_{\mathbf{3a/3'a}}$ (the reduction potential of **3a**), **3'a** becomes the resting state (Figure 2, top—note that applied potential decreases and overpotential increases to the right of the figure). Similarly, for L = bpymd, the equilibrium shifts from **3b** to **3'b** below $E_{\mathbf{3b/3'b}}$ (Figure 2, top).

As a result of these potential-dependent equilibria, for L = bpy, the flux through rate-determining dehydroxylation reactions **3a→4a** or **3'a→5a** is also a function of applied potential (Figure 2, bottom). In the potential regime where **3a** is the resting state, total TOF remains constant until **3'a** is formed in significant concentrations. The **3'a→5a** pathway begins to dominate at applied potentials higher than $E_{\mathbf{3a/3'a}}$ because it has a lower barrier than **3a→4a**, and the total TOF increases until **3'a** becomes the resting state (Figure 2, bottom). For L = bpymd, the **3'b→5b** pathway dominates at all potentials below -1.1 V.

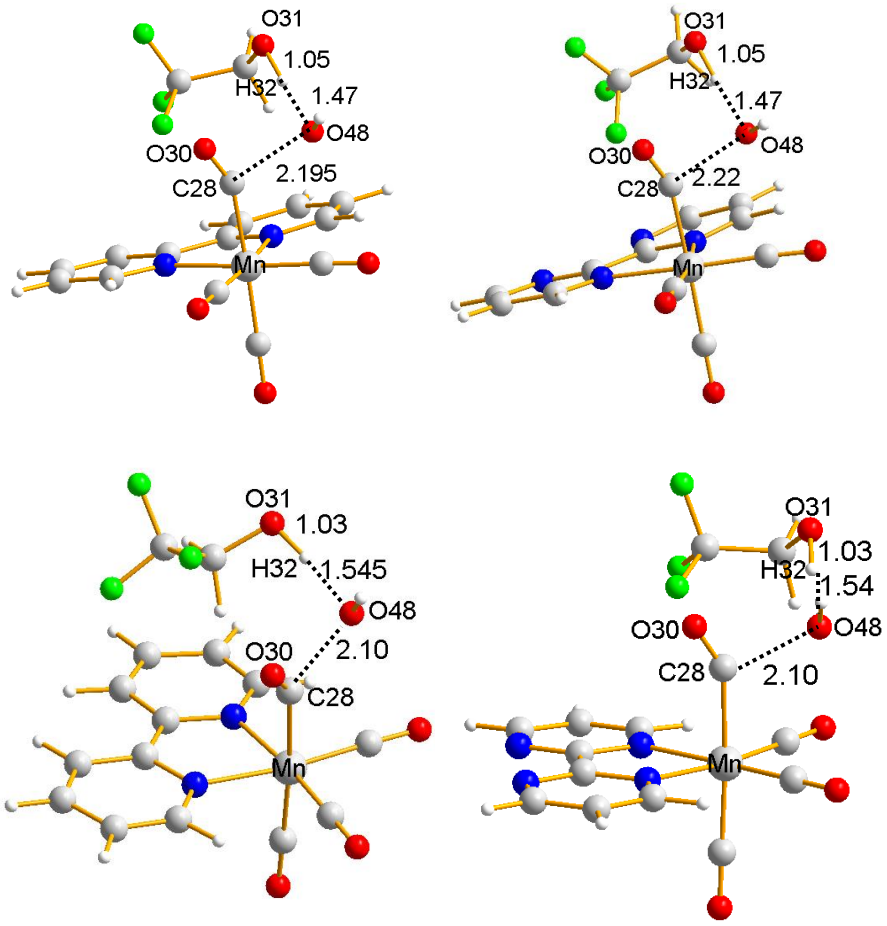

Figure 1: Optimized transition states for (top left, $TS_{\mathbf{3a}\rightarrow\mathbf{4a}}$) **3a** + TFEH → **4a** + TFE^- / H_2O, (top right, $TS_{\mathbf{3b}\rightarrow\mathbf{4b}}$) **3b** + TFEH → **4b** + TFE^- / H_2O, (bottom left, $TS_{\mathbf{3'a}\rightarrow\mathbf{5a}}$) 3'a + TFEH → **5a** + TFE^- / H_2O, and (bottom right, $TS_{\mathbf{3'b}\rightarrow\mathbf{5b}}$) **3'b** + TFEH → 5b + TFE^- / H_2O. All interatomic distances are reported in Å.

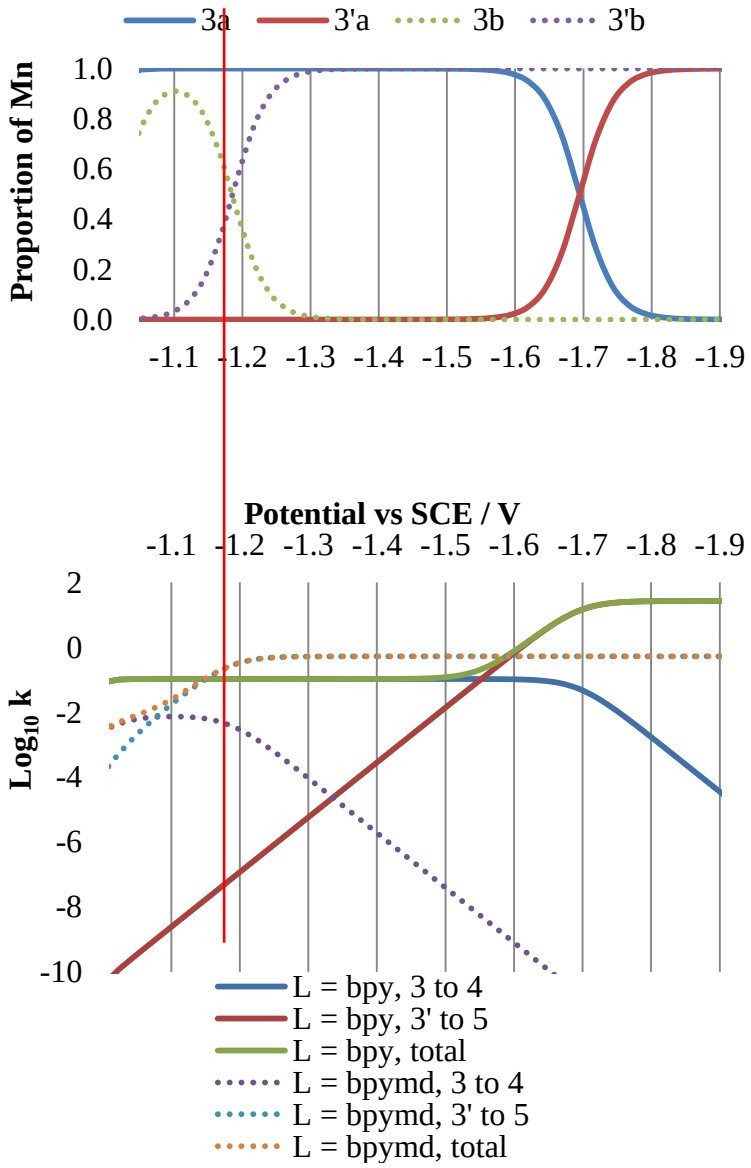

Figure 2: (Top) Concentration of species **3** and **3'** as a proportion of total Mn concentration, and (Bottom) rates for **3→4**, **3'→5** and the complete catalytic cycle, as a function of applied potential (vs. SCE), for L = bpy (solid lines) and L = bpymd (dotted lines). The computed standard thermodynamic reduction potential (-1.17 V) is marked with a vertical red line.

*Comparison of **1a** and **1b** as Catalysts for Electrochemical CO_2 Reduction*

The bipyrimidine complexes are more easily reduced than their bipyridine analogs because bipyrimidine is more electron-deficient and hence a better electron acceptor—reduction potentials of **3b** and **4b** are higher by 0.51 and 0.50 V, respectively, than those of **3a** and **4a** (Scheme 1). The SOMOs of **3'a** and **3'b** (as well as those of tetracarbonyl intermediates **5a** and **5b**) are ligand-based (Figure 3). The more facile reduction of bipyrimidine leads directly to a higher reduction potential for **3b** vis-à-vis **3a**.

The dehydroxylation reactions of **3b** and **3'b** have slightly higher $\Delta G^{\ddagger}$ (by 1.5 and 2.2 kcal mol^{-1}, respectively) than those of **3a** and **3'a**, reflecting slightly stronger (by 3.4 and 4.7 kcal mol^{-1}, respectively) C-OH bonds in the bipyrimidine complexes. The magnitude of this difference is small compared to the difference in reduction potentials.

The cumulative effect of these two differences is that whether catalyst **1a** or **1b** affords higher TOFs depends on the applied potential (Figure 2). At potentials above ~ -1.6 V, **1b** provides higher TOFs, because **3b** is exergonically reduced to **3'b**, accessing the faster dehydroxylation pathway from **3'b** to **5b**. However, when E < -1.6 V, **3a** begins to undergo reduction to **3'a**, and the lower (by 2.2 kcal mol^{-1}) activation energy for **3'a** dehydroxylation gives **1a** higher TOFs.

In summary, our calculations show that catalyst **1a** affords a higher maximum TOF (TOF_{max}), but at the price of a substantial overpotential (~ 0.6 V, ~ -1.75 V vs. SCE) to achieve TOF_{max}, in line with experimental results showing that i_{cat} for TFEH-mediated CO_2 reduction by Mn(bpy-*t*Bu)$(CO)_3$Br peaks at ~ -1.80 V vs. SCE.[9e,f] By contrast, catalyst **1b** is predicted to reach TOF_{max} at -1.25 V vs. SCE (< 0.1 V overpotential under standard

conditions), albeit at the expense of a lower maximum TOF_{max}. Note that the computed *standard* reduction potential of -1.49 V vs. SCE assumes the concentrations of H_2O and TFE^- / 3 TFEH to be 1 M, and the pressure of CO to be 1 atm. Under reaction conditions of a cyclic voltammetry (CV) experiment, these concentrations would be lower and the thermodynamic potential concomitantly higher.

*Electronic Structure of **1***

The open-shell singlets of **1a** and **1b** are lower in energy than their corresponding closed-shell singlets by 0.2 kcal mol^{-1},[25] well within the uncertainty of the method. The HOMOs in the closed-shell singlets are delocalized over the metal center and the ligand. In the open-shell singlets, the α-HOMOs are predominantly Mn-centered while the β-HOMOs are delocalized over the noninnocent ligand (bpy or bpymd, Figure 4). For comparison, IR, XANES, and EXAFS data, as well as DFT calculations, indicate a diamagnetic diradical singlet, $Re^0(bpy)^-$ ground state for $[(bpy\text{-}R)Re(CO)_3]^-$.[10b,13]

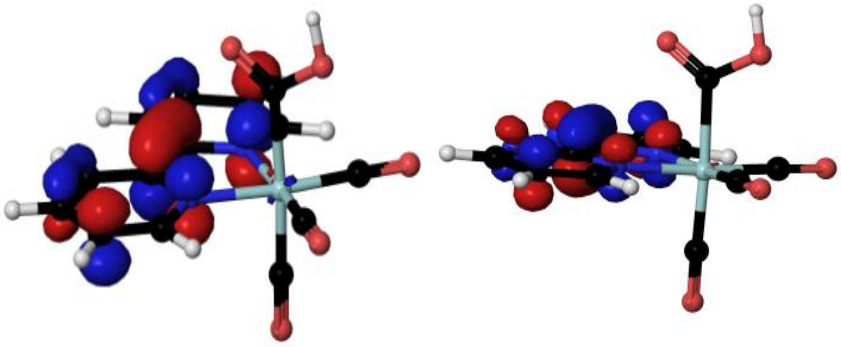

Figure 3: Calculated orbital surfaces of the SOMOs in (left) **3'a** and (right) **3'b**.

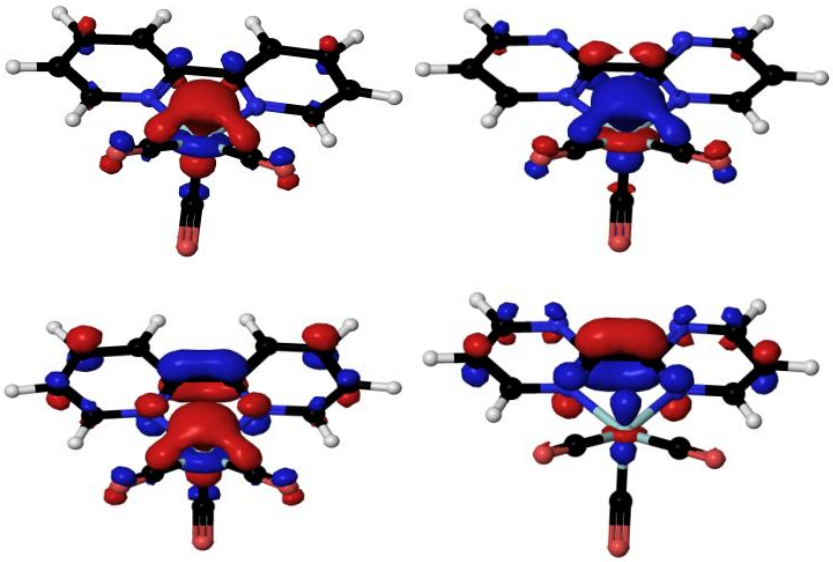

Figure 4: α-HOMOs (top) and (bottom) β-HOMOs of (left) **1a** and (right) **1b**.

Kinetic Selectivity for CO Production

Assuming protonation at Mn of **1** (to **6**) is the rate-determining step in the production of side-products (i.e., H_2), and applying the steady state approximation, the selectivity ratio S (the rate of CO formation, k_{CO}, divided by that of other products, k_{other}) for L = bpy, at potentials where dehydroxylation of **3'a** dominates over that of **3a** (*vide supra*), is given by[26]

$$S_{low-\eta} = \left[\frac{k_{1\to2}\,[CO_2]}{k_{1\to6}[TFEH]^2}\right]\frac{k_{3\prime\to5}K_{3/3\prime}[TFEH]}{k_{3\to2}\frac{[TFE^-/3\,TFEH]}{[TFEH]^4}} = \left[\frac{k_{1\to2}k_{3\prime\to5}K_{3/3\prime}}{k_{1\to6}k_{2\to1}}\right]\frac{[CO_2][TFEH]^3}{[TFE^-/3\,TFEH]} \qquad \text{L = bpy, (3a)}$$

$k_{i\to j}$ denotes the rate constant for conversion of species *i* to *j*; $K_{3/3'} = \exp\left[\frac{11600}{T}(-1.69 - E)\right]$ is the equilibrium constant for reduction of **3** to **3'**. Equation 3a applies in the low-overpotential regime, defined by $k_{3\prime\to5}K_{3/3\prime}[TFEH] \ll k_{2\to1}\frac{[TFE^-/3\,TFEH]}{[TFEH]^4}$. In the high-η regime,

$$S_{high-\eta} = \frac{k_{1\to2}}{k_{1\to6}}\frac{[CO_2]}{[TFEH]^2} \qquad \text{L = bpy, (3b)}$$

Equations (3a) and (3b) follow from the premises that (1) the rate-determining TS for conversion from **1a** to **3a** (and *vice-versa*) is the CO_2 addition transition state $TS_{\mathbf{1a}\to\mathbf{2a}}$ (Scheme 2), and (2) under operating conditions, dehydroxylation of **3'a** is TOF-limiting for CO production. In the high-η regime, the dehydroxylation of **3'a** is much faster than its conversion back to **1a**, rendering the conversion of **1a** to **3'a** irreversible. Selectivity is simply the branching ratio between conversion of **1a** to **3a** (and subsequent reduction to **3'a**) and protonation to **6a**. In the low-η regime, by contrast, a potential-dependent equilibrium between **3a** (and therefore **1a**) and **3'a** precedes TOF- and selectivity-determining dehydroxylation of **3'a**.

For the bipyrimidine complex, the rate-determining TS for conversion between **1** and **3** under standard conditions is the proton transfer transition state $TS_{\mathbf{2b}/2TFEH\rightarrow\mathbf{3b}}$ (Scheme 2). Under the same assumptions as for the bipyridine analog, in the low- η regime defined by $k_{3\prime\rightarrow5}K_{3/3\prime}[TFEH]^3 \ll k_{3\rightarrow2b/2TFEH}[TFE^-/3\,TFEH]$:

$$S_{low-\eta} = \left[\frac{k_{1\rightarrow2}k_{3\prime\rightarrow5}K_{3/3\prime}}{k_{1\rightarrow6}k_{3\rightarrow2/2TFEH}}\right]\frac{[CO_2][TFEH]^2}{[TFE^-/3\,TFEH]} \qquad \text{L = bpymd (4a)}$$

where $K_{3/3'} = \exp\left[\frac{11600}{T}(-1.19 - E)\right]$

In the high-η regime,

$$S_{high-\eta} = \left[\frac{k_{1\rightarrow2}}{k_{1\rightarrow6}}\right][CO_2] \qquad \text{L = bpymd (4b)}$$

(Note that under conditions typical of bulk electrolysis—the technique used to determine product selectivity—the concentration of products is quite low, at least initially. Consequently, the rate-determining TS for conversion between **1** and **3** may be $TS_{\mathbf{1a}\rightarrow\mathbf{2a}}$, in which case equations 3a and 3b apply for L = bpymd as well.)

Since bulk electrolysis is typically conducted at a potential which maximizes catalytic activity, the high-η regime is a better description of experimental conditions. In this regime, selectivity is independent of applied potential, unlike in the low-η regime, where increasing overpotential increases CO selectivity.

Notwithstanding that the activation energy of dehydroxylation (**3'→5**) is higher than that of protonation at Mn (**1→6**), a combination of factors allows CO to be produced selectively (Scheme 2):

(1) *All* steps between **1** and **3'** are faster than protonation of **1**: (a) the endergonic equilibration between **1** and its CO_2 adduct **2** is rapid—the

loss of CO_2 from adduct **2** is essentially barrierless (Table 1, entries 1-2), (b) homoconjugation between TFE^- and TFEH facilitates proton transfer from TFEH to **2** to form **3** (Table 2, entries 5-6).

(2) **3'**, an intermediate in the CO production pathway, is stabilized relative to **1**, a likely hydrogen evolution reaction branching point: (a) the exergonic hydrogen bonding of TFEH to TFE^- / TFEH homoconjugate (Table 1, entries 3, 5) improves the thermodynamics of the overall transformation of **1a** to **3a**, (b) under operating conditions, a low potential is applied to maximize TOF, favoring **3'**.

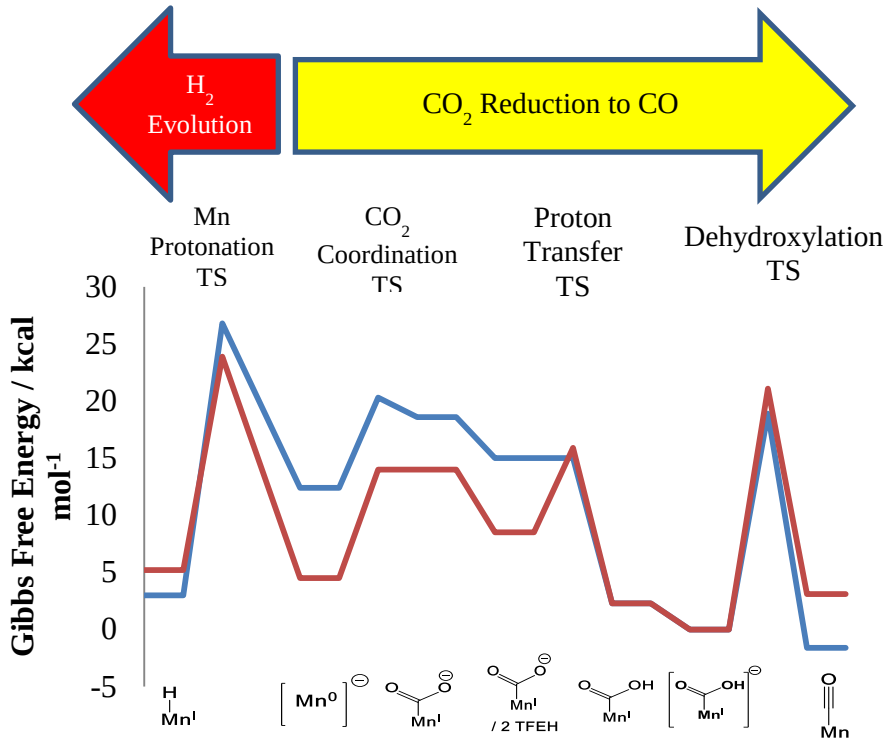

Scheme 2: Mechanistic summary showing free energies of catalytic intermediates and transition states shown in Scheme 1, at E = $E^{\circ}_{3/3}$, − 0.1, i.e., -1.79 V vs SCE for L= bpy (blue line) and at -1.29 V vs SCE for L = bpymd (red line).

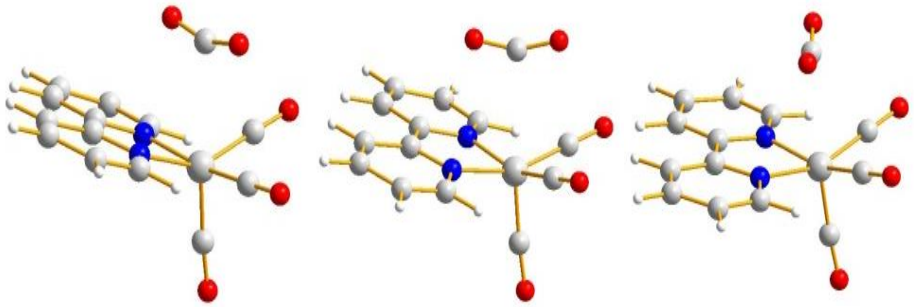

G = 0 kcal/mol +0.4 +3.7

Figure 5: Three possible configurations for the **1a** + CO_2 → **2a** transition state ($TS_{\mathbf{1a}\rightarrow\mathbf{2a}}$), with N-Mn-C-O dihedral angles fixed at different values (left, $TS_{\mathbf{1a}\rightarrow\mathbf{2a}}$': unrestricted; center, $TS_{\mathbf{1a}\rightarrow\mathbf{2a}}$'': 40°; right, $TS_{\mathbf{1a}\rightarrow\mathbf{2a}}$''': -50°).

With regard to the rapid equilibration between **1** and its CO_2 adduct, Smieja and Benson *et al.* have proposed that the delocalized electronic configuration of $[(bpy\text{-}R)Re(CO)_3]^-$ favors reaction with CO_2 over H^+, since the former involves both σ and π interactions while the latter can only involve σ interactions. [10b] If interaction of filled ligand π* orbitals with CO_2 lowers activation energy for CO_2 binding, the orientation of the CO_2 fragment with respect to the ligand in $TS_{\mathbf{1}\rightarrow\mathbf{2}}$ (the CO_2 addition transition state) should substantially affect such interactions and hence the stability of the TS. Three configurations for $TS_{\mathbf{1a}\rightarrow\mathbf{2a}}$ (Figure 5), in which the N-Mn-C-O dihedral angle was fixed at different values, were optimized. $\mathbf{TS}_{1a\rightarrow 2a}$''' (right), where the CO_2 is oriented away from the bpy ligand and has no orbital overlap with the bpy π system, was found to have a higher energy (3.7 kcal mol^{-1}), suggesting that interaction between bpy-based orbitals and CO_2 π* orbitals contributes to kinetic selectivity for CO_2 binding and hence CO production. The effect of such π overlap on selectivity is significant despite the long Mn-C distance (> 2.9 Å), CO_2-ligand distance (> 2.95 Å) in the transition state.

The foregoing discussion suggests that a delocalized electronic structure with redox-active ligands can contribute to selective CO_2 reduction to CO. This appears not to be a universal requirement, however. Neither Ni cyclam[7d] nor the phosphine complexes of Pd[8b] have redox-active ligands or delocalized electronic structures. Of equal or greater importance is the maintenance of modest proton activity in the catholyte to suppress metal hydride formation—all the catalysts referenced here[6-8a] except the Pd phosphines[8b] operate in either near-neutral aqueous solutions or polar aprotic solvents with the addition of very weak acids (water, alcohols, or phenol). In polar aprotic solvents, the highly exergonic

hydrogen bonding of these weak acids to their conjugate bases provides additional driving force for the protonation of CO_2 adducts such as **2**, permitting the use of very weak acids which protonate reduced metal centers slowly.

Conclusions

We elucidated atomistic reaction mechanisms for Brønsted acid-dependent electrochemical CO_2 reduction catalyzed by $[(bpy)Mn(CO)_3]^-$ (**1a**). It involves binding of CO_2 at the Mn center, followed by proton transfer to form $[(bpy)Mn(CO)_3(CO_2H)]$ (**3a**). Rate-determining dehydroxylation may occur from **3a**, or from once-reduced $[(bpy)Mn(CO)_3(CO_2H)]^-$ (**3'a**), and is dependent on TFEH, the Brønsted acid studied here. Depending on the applied overpotential, either pathway may dominate.

Furthermore, we studied a new compound **1b**, in which bipyridine has been substituted by bipyrimidine. We predict that **1b** catalyzes CO_2 reduction by the same mechanism. However, due to the greater electron affinity of bipyrimidine, the reduction of $[(bpymd)Mn(CO)_3(CO_2H)]$ (**3b**) occurs at a potential 0.5 V higher than that of **3a**, so that the maximum TOF of **1b** (albeit somewhat less than that of **1a**) is accessible at very low overpotentials. Tuning the electronic properties of the heterocyclic ligand should permit optimization of catalytic activity, trading activity for overpotential.

Both **1a** and **1b** were found to display kinetic preference for CO_2 addition over protonation by TFEH. Stabilization of the conjugate base trifluoroethoxide by hydrogen bonding to TFEH plays key roles in catalyst activity (by driving forward the reaction using an otherwise weak acid) and selectivity (by stabilizing states **3** and **3'** relative to the likely hydrogen evolution reaction branching point **1**). The HOMOs of both **1a** and **1b** are

delocalized over the Mn center and the chelating ligand; interaction of CO_2 with the ligand appears to play a significant role in stabilizing the CO_2 addition transition state.

Acknowledgements

Yan Choi Lam, who performed the calculations and data analysis, was supported by the National Science Foundation (NSF) through the Centers for Chemical Innovation (CCI): Solar Fuels grant CHE-1305124, as was Prof. Harry B. Gray. Dr. Robert J. Nielsen and Prof. William A. Goddard, III, who developed the computational methods required for the calculations, are supported by the Joint Center for Artificial Photosynthesis, a DOE Energy Innovation Hub, supported through the Office of Science of the U.S. Department of Energy under Award Number DE-SC0004993. We gratefully acknowledge Professor Clifford P. Kubiak for helpful discussions.

References

(1) Schneider, W.; Diller, W.; *Ullmann's Encyclopedia of Industrial Chemistry*; Wiley-VCH: Weinheim, **2005**.
(2) Wilhelm, D. J.; Simbeck, D. R.; Karp, A. D.; Dickenson, R. L.; *Fuel Process. Tech.*, **2001**, *71*, 139-148.

(3) Sunley, G. J.; Watson, D. J.; *Cat. Today*, **2000**, *58*, 293-307.

(4) Dry, M. E.; *Appl. Cat. A*, **1996**, *138*, 319-344.
(5) Reviews: (a) Costentin, C.; Robert, M.; Savéant, J-M.; *Chem. Soc. Rev.*, **2013**, *42*, 2423-2436; (b) Windle, C. D.; Perutz, R. N.; *Coord. Chem. Rev.*, **2012**, *256*, 2562-2570; (c) Finn, C.; Schnittger, S.; Yellowlees, L. J.; Love, J. B.; *Chem. Commun.* , **2012**, *48*, 1392-1399; (d) Benson, E. E.; Kubiak, C. P.; Sathrum, A. J.;Smieja, A. J.; *Chem. Soc. Rev.*, 2009, **38**, 89-99.
(6) Fe-porphyrins: (a) Bhugun, I.; Lexa, D.; Savéant, J. M.; *J. Phys. Chem.*, **1996**, *100*, 19981-19985; (b) Bhugun, I.; Lexa, D.; Savéant, J. M.; *J. Am. Chem. Soc.* **1994**, *116*, 5015-5016; (c) Bhugun, I.; Lexa, D.; Savéant, J. M.; *J. Am. Chem. Soc.* **1996**, *118*, 1769-1776; (d) Costentin, C.; Drouet, S.; Robert, M.; Savéant, J. M.; *Science*, **2012**, *338*, 90–94.
(7) Co and Ni heterocycles and macrocycles: (a) Fisher, B. J.; Eisenberg, R.; *J. Am. Chem. Soc.*, **1980**, *102*, 7361–7363; (b) Lieber, C. M.; Lewis, N. S.; *J. Am. Chem. Soc.*, **1984**, *106*, 5033-5034; (c) Beley, M.; Collin, J.-P.; Ruppert, R.; Sauvage, J.-P.; *J. Chem. Soc., Chem. Commun.*, **1984**, 1315-1316; (d) Froehlich, J. D.; Kubiak, C. P.; *Inorg. Chem.*, **2012**, *51*, 3932–3934; (e) Tinnemans, A. H. A.; Koster, T. P. M.; Thewissen, D. H. M. W.; Mackor, A.; *Recl. Trav. Chim. Pays-Bas.* **1984**, *103*, 288-295.
(8) Phosphine complexes: (a) Szymaszek, A.; Pruchnik, F. P.; *J. Organomet. Chem.*, **1989**, *376*, 133-140; (b) DuBois, M. R.; DuBois, D. L.; *Acc. Chem. Res.*, **2009**, *42*, 1974-1982.

(9) Complexes with bipyridine and related ligands: (a) Hawecker, J.; Lehn, J. –M.; Ziessel, R.; *J. Chem. Soc., Chem. Commun.*, **1984**, 328-330; (b) Patrick Sullivan, B.; Bolinger, C. M.; Conrad, D.; Vining, W. J.; Meyer, T. J.; *J. Chem. Soc., Chem. Commun.*, **1985**, 1414-1416; (c) O'Toole, T. R.; Margerum, L. D.; Westmoreland, T. D.; Vining, W. J.; Murray, R. W.; Meyer, T. J.; *J. Chem. Soc., Chem. Commun.*, **1985**, 1416-1417; (d) Smieja, J. M.; Kubiak, C. P.; *Inorg. Chem.* **2010**, *49*, 9283-9289; (e) Bourrez, M.; Molton, F.; Chardon-Noblat, S.; Deronzier, A.; *Angew. Chem., Int. Ed.* **2011**, *50*, 9903-9906; (f) Smieja, J. M.; Sampson, M. D.; Grice, K.A.; Benson, E.E.; Froehlich, J.D.; Kubiak, C.P.; *Inorg. Chem.*, **2013**, *52*, 2484-2491; (g) Bruce, M. R. M.; Megehee, E.; Sullivan, B. P.; Thorp, H.; O'Toole, T. R.; Downard, A.; Meyer, T. J.; *Organometallics* **1988**, *7*, 238-240; (h) Sampson, M.D.; Nguyen, A. D.; Grice, K. A.; Moore, C. E.; Rheingold, A. L.; Kubiak, C. P., *J. Am. Chem. Soc.* **2014**, *136*, 5460-5471; (i) Zeng, Q.; Tory, J.; Hartl, F.; *Organometallics* **2014**, *33*¸5002-5008.

(10) (a) Smieja, J. M.; Benson, E. E.; Kumar, B.; Grice, K. A.; Seu, C. S.; Miller, A. J. M.; Mayer, J. M.; Kubiak, C. P.; *Proc. Natl. Acad. Sci. U. S. A.* **2012**, *109*, 15646-15650;

(b) Benson, E. E.; Sampson, M. D.; Grice, K. A.; Smieja, J. M.; Froehlich, J. D.; Friebel, D.; Keith, J. A.; Carter, E. A.; Nilsson, A.; Kubiak, C. P.; *Angew. Chem., Int. Ed.* **2013**, *52*, 4841-4844; (c) Sampson, M. D.; Froehlich, J. D.; Smieja, J. M.; Benson, E. E.; Sharp, I. D.; Kubiak, C. P.; *Energy Environ. Sci.*, **2013**, *6*, 3748-3755.

(11) Wong, K.–Y.; Chung, W.-H.; Lau, C.-P.; *J. Electroanal. Chem.* 1998, **453,** 161-169.

(12) Agarwal, J.; Sanders, B, C.; Fujita, E.; Schaefer, H. F.; Harrop, T. C.; Muckerman, J. T.; *Chem. Commun.*, **2012**, *48*, 6797-6799.
(13) Keith, J. A.; Grice, K. A.; Kubiak, C. P.; Carter, E. A.; *J. Am. Chem. Soc.*, **2013**, *135*, 15823–15829.
(14) Becke, A. D.; *J. Chem. Phys.*, **1993**, *98*, 5648-5652.
(15) Grimme, S.; Antony, J.; Ehrlich, S.; Krieg, H.; *J. Chem. Phys.*, **2010**, *132*, 154104-154119.
(16) Jaguar; Schrödinger, LLC: New York, NY, 2012.
(17) Marten, B.; Kim, K.; Cortis, C.; Friesner, R. A.; Murphy, R. B.; Ringnalda, M. N.; Sitko, D.; Honig, B.; *J. Phys. Chem.*, **1996**, *100*, 11775-11788.
(18) (a) Krishnan, R.; Binkley, J. S.; Seeger, R.; Pople, J.A. *J. Chem. Phys.*, **1980**, *72*, 650-654 ; (b) Clark, T.; Chandrasekhar, J.; Spitznagel, G. W.; Schleyer, P. V. R *J. Comput. Chem.* **1983**, *4*, 294-301.
(19) (a) Melius, C. F.; Goddard, W. A. III, *Phys. Rev. A* **1974**, *10*, 1528-1540; (b) Melius, C. F.; Olafson, B. D.; Goddard, W. A. III; *Chem. Phys. Lett.*, **1974**, *28*, 457-462.
(20) Hay, P. J.; Wadt, W. R.; *J. Chem. Phys.* **1985**, *82*, 270-283.
(21) Martin, J. M. L.; Sundermann, A.; *J. Chem. Phys.* **2001**, *114*, 3408-3420.
(22) McQuarrie, D. A. *Statistical Mechanics*; University Science Books: Sausalito, CA, **2000.**
(23) Isse, A. A.; Gennaro, A.; *J. Phys. Chem. B* **2010**, *114*, 7894-7899. Treating an electron at SCE as a reactant yields an effective free energy (relative to an electron at rest in vacuum, the reference state of QM calculations) of (23.06 kcal/mol/eV * -4.42 V * $1e^-$) = -102.0 kcal/mol.
(24) In the context of the hydrogen evolution reaction, Fourmond and coworkers have pointed out the importance of accounting for homoconjugation in determining overpotential. See Fourmond, V.; Jacques, P-A.; Fontecave, M.; Artero, V.; *Inorg. Chem.* **2010**, *49*, 10338–10347.
(25) Since the DFT-computed energy of the open-shell singlet is an upper bound on the energy of the true (spin-uncontaminated) singlet, the latter is lower in energy than the closed-shell singlet.
(26) Note that throughout this article, the reference concentration for CO_2, $[CO_2]_0$, is 1 atm, or ca. 0.28 M in acetonitrile.

Supporting Information

Calculation of pK_as for Neutral Organic Acids and ΔG_{solv}s for their Conjugate Bases

Since proton transfer is an integral part of the catalytic cycles, computational methods were benchmarked against experimentally determined pK_a values for neutral organic oxyacids, including TFE, and ΔG_{solv}s of their anionic conjugate bases. For the calculation of pK_as, the free energy of H^+ at 1 M in MeCN (G = -264.6 kcal/mol) was taken to be its gas-phase value ($G(H^+, 1atm) = H - TS = 2.5\ k_BT - T * 26.04$ = -6.3 kcal/mol) plus the empirical solvation energy in acetonitrile ($\Delta G(1atm \rightarrow 1M,MeCN) = -260.2 + k_BTln(24.5)$).[S1]

The default van der Waals' radii in Jaguar 7.9 gave rather unsatisfactory agreement with experimental results (Figure S1, Table S1)—pK_as were underestimated by 12.5±0.9 units and ΔG_{solv}s were overestimated (too exergonic). Increasing the van der Waals' radii on anionic oxygen atoms decreased ΔG_{solv}s—a radius of 2.0 Å gave excellent agreement with experimental values for phenoxide, and satisfactory agreement for acetate (Figure S2, Table S2). Decreasing the van der Waals' radius on protic hydrogen atoms increased pK_as by increasing the exergonicity of solvation for the acid—a radius of 0.75 Å gave satisfactory to excellent values for phenol, acetic acid, and TFE (Figure S3, Table S3).

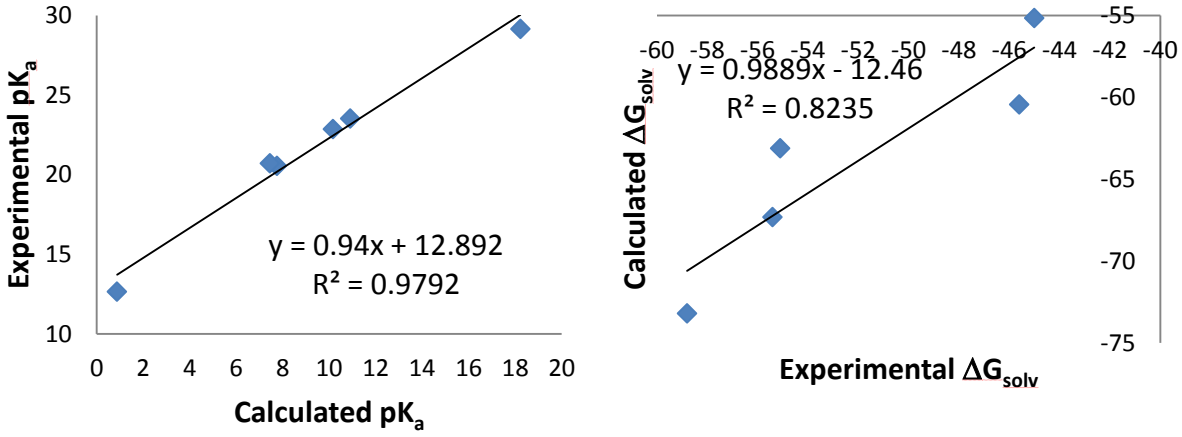

Figure S1: Calculations using default van der Waals' radii in Jaguar 7.9 underestimate pK_as and overestimate the exergonicity of anion solvation in acetonitrile.

Table S1: Calculations using default van der Waals' radii in Jaguar 7.9 underestimate pK_as and overestimate the exergonicity of anion solvation in acetonitrile.

pK_a			**ΔG_{solv}**		
Acid	**Calculated**	**Experimental**[S2]	**Anion**	**Calculated**	**Experimental**[S3]
PhOH	18.2	29.4	PhO^-	-63.1	-55.1
AcOH	10.9	23.5	AcO^-	-73.2	-58.8, -62.7 [S4]
4-nitro-phenol	10.2	22.9	4-nitro-phenoxide	-55.2	-45
PhCOOH	7.4	20.7	Benzoate	-67.3	-55.4
$(F_3C)_3COH$	7.8	20.6	$(F_3C)_3CO^-$	-50.8	Not available
F_3CCOOH	0.9	12.7	F_3CCOO^-	-60.5	-45.6

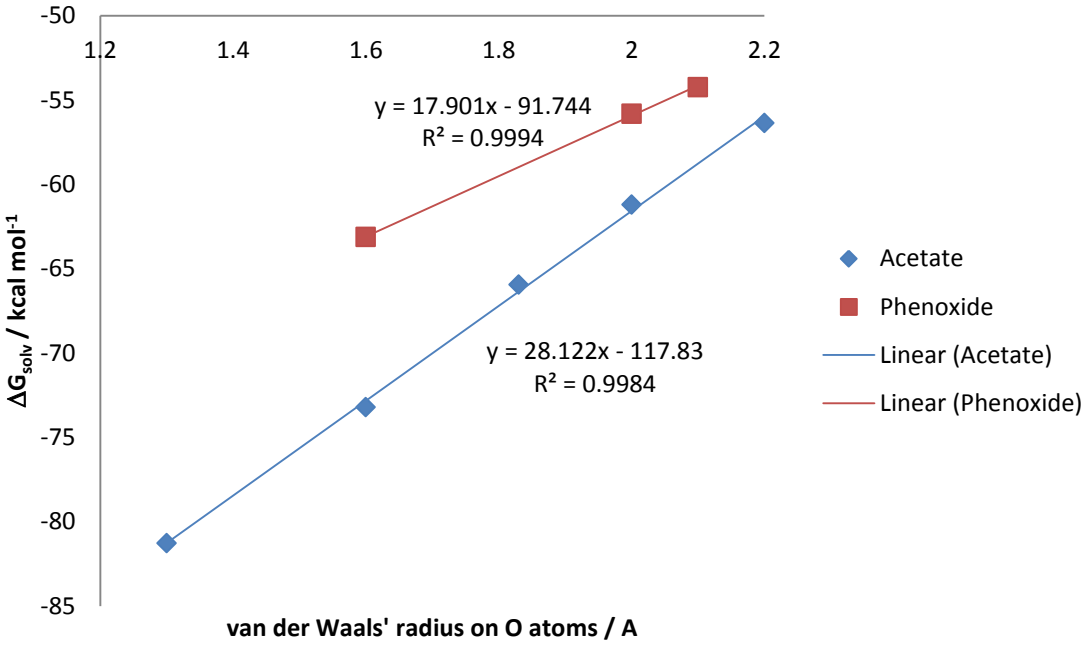

Figure S2: Increasing the van der Waals' radii on oxygen atoms decreased the calculated exergonicity of solvation in acetonitrile.

Table S2: Increasing the van der Waals' radii on oxygen atoms decreased the calculated exergonicity of solvation in acetonitrile.

	Acetate		**Phenoxide**	
	ΔG_{solv} / kcal mol^{-1}			
van der Waals' radius on O / Å	**Calculated**	**Experimental**	**Calculated**	**Experimental**
1.3	-81.3	-56.9, [S2] -62.7 [S3]	N/A	-55.1 [S3]
1.6	-73.2		-63.1	
1.83	-65.9		N/A	
2	-61.2		-55.8	
2.1	N/A		-54.3	
2.2	-56.4		N/A	

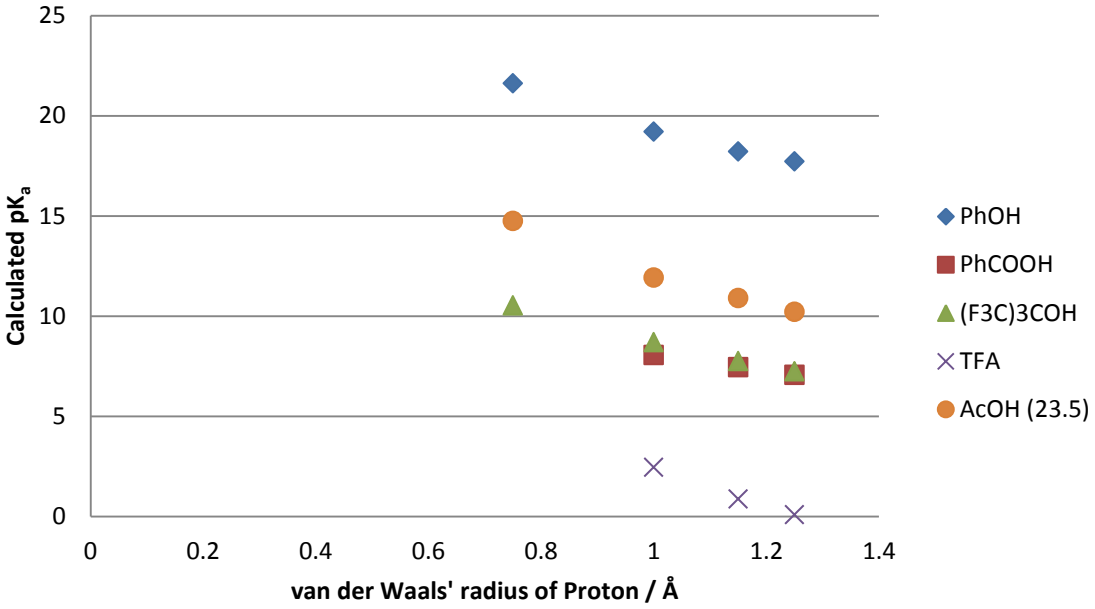

Figure S3: Decreasing the van der Waals' radius of the protic hydrogen increases calculated pK_a. Calculations were performed in acetonitrile with standard van der Waals' radii on all other atoms.

Table S3: pK_as calculated in acetonitrile with different van der Waals' radii on oxygen atoms and protons.

		Van der Waals' radius of Proton / Å				
Acid	**Van der Waals' radius of O / Å**	**1.25**	**1.15 (default)**	**1.0**	**0.75**	**Experimental pK_a** [S2]
AcOH	1.3	4.3	5.0	6.0	8.8	23.5
	1.6	10.2	10.9	11.9	14.8	
	2.0	19.0	19.7	20.7	23.5	
	2.2	22.6	23.2	24.3	27.1	
PhOH	1.6	17.7	18.2	19.2	21.6	29.1
	2.0	23.1	23.6	24.6	27.0	
	2.1	24.2	24.7	25.7	28.1	
TFEH	1.6	N/A	22.1	N/A	26.2	35.4 [S5]
	2.0	N/A	29.2	N/A	33.3	
	2.2	N/A	31.7	N/A	35.8	

Comparison of computational methods

Table S4: Key thermodynamic values calculated with a variety of methods regarding solvation, basis set, and functional.

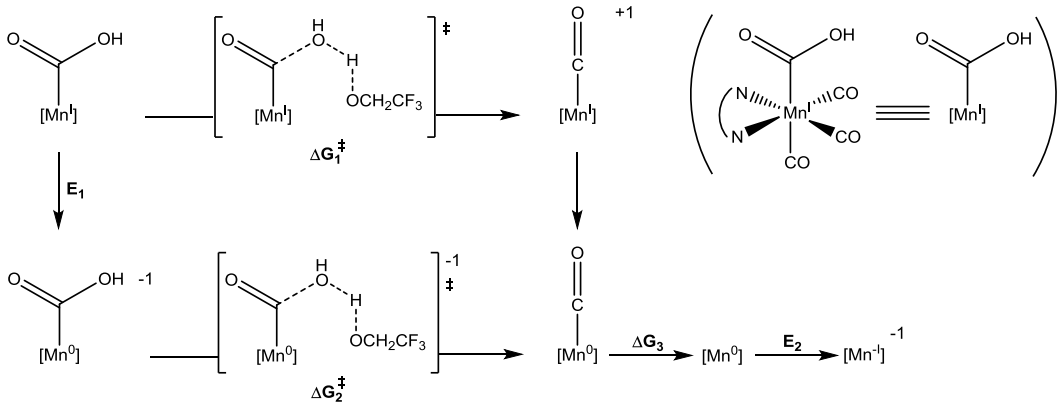

Geometry		Energy		$\Delta G^{\ddagger}_1$	$\Delta G^{\ddagger}_2$	ΔG_3	E_1	E_2
Functional	**Basis/solvation**	**Functional**	**Basis/solvation**	**kcal/mol**			**(V vs SCE)**	
B3LYP-d3	6-31G** vacuum	B3LYP-d3	6-311G**++ MeCN	19.4	15.4	-2.0	-1.58	-1.20
		B3LYP-d3	6-311G**++ MeCN (alt. radii)	26.7	24.1		-1.58	
		B3LYP-d3	6-311G**++(+2f) MeCN			-2.0	-1.57	-1.19
		M06	6-311G**++ MeCN	25.6	21.5	-1.9	-1.50	-1.08
B3LYP-d3	6-311G**++ MeCN	B3LYP-d3	6-311G**++ MeCN			-2.5	-1.59	-1.21
B3LYP-d3	6-311G**++ MeCN (alt. radii)	B3LYP-d3	6-311G**++ MeCN (alt. radii)	27.8	26.8		-1.54	
B3LYP-d3	6-311G**++(+2f) MeCN	B3LYP-d3	6-311G**++(+2f) MeCN			-2.5	-1.58	-1.20
M06	6-311G**++ MeCN	M06	6-311G**++ MeCN			-2.8	-1.50	-1.09

References

(S1) Kelly, C.P.; Cramer, C. J.; Truhlar, D.G.; *J. Phys. Chem. B* **2007**, *111*, 408-422.

(S2) Kütt, A.; Leito, I.; Kaljurand, I.; Sooväli, L.; Vlasov, V. M.; Yagupolskii, L. M.; Koppel, I. A.; *J. Org. Chem.*, **2006**, *71*, 2829–2838, unless otherwise noted.

(S3) Marenich, A. V.; Kelly, C. P.; Thompson, J. D.; Hawkins, G. D.; Chambers, C. C.; Giesen, D. J.; Winget, P.; Cramer, C. J.; Truhlar, D. G.; Minnesota Solvation Database – version 2012, University of Minnesota, Minneapolis, 2012., unless otherwise noted.

(S4) Böes, E. S.; Livotto, R. S.; Stassen, H.; *Chem. Phys.*, **2006**, *331*, 142-158

(S5) Personal correspondence with Prof. Ivo Leito. Estimated by correlation analysis from pK_a values measured in dimethylsulfoxide (DMSO)— pK_a values in acetonitrile and DMSO are known to be well-correlated—with an estimated uncertainty of ca. 1.0 pK_a units.

Cartesian coordinates (in Å) for optimized structures of species discussed in the text

CO_2

C	0.0000000000	0.0000000000	0.0000000000
O	0.0000000000	0.0000000000	1.1611091236
O	0.0000000000	0.0000000000	-1.1611091236

CO

C	0.0000000000	0.0000000000	0.6443005121
O	0.0000000000	0.0000000000	-0.4833790194

TFEH

O	0.15551597	2.0342135324	0.0000000000
C	0.93278282	0.8469239510	0.0000000000
C	-0.00654804	-0.3451943424	0.0000000000
F	-0.81477911	-0.3806472090	1.0850575988
F	-0.81477911	-0.3806472090	-1.0850575988
F	0.70815521	-1.4967544041	0.0000000000
H	1.56029966	0.7540145054	0.8936374264
H	1.56029966	0.7540145054	-0.8936374264
H	0.75200128	2.7997573239	0.0000000000

TFE^-

O	0.20376031	2.1280314461	0.0000000000
C	0.88181018	0.9381760810	0.0000000000
C	-0.00300825	-0.3145609790	0.0000000000
F	-0.81771586	-0.4037617888	1.0884259988
F	-0.81771586	-0.4037617888	-1.0884259988
F	0.74561570	-1.4593420781	0.0000000000
H	1.53812989	0.7668817364	0.8818140461
H	1.53812989	0.7668817364	-0.8818140461

B, i.e., TFE^- / TFEH

O	-2.044092708	2.3706356443	-1.5992894256
C	-1.215435634	3.4632634181	-1.3172400466
H	-0.790317615	3.9290636381	-2.2123496255
H	-1.768069660	4.2336460431	-0.7668742321
C	-0.031822681	3.0871045355	-0.4355218213
F	-0.413394990	2.6230400425	0.7831027604
F	0.756626039	2.1325197622	-0.9770057600
F	0.761526295	4.1704899844	-0.2070505003
O	-1.295831713	1.0135935125	-3.5926631293
H	-1.676227373	1.8167742858	-2.4155212250
C	-1.056952571	1.8354930126	-4.6706855399
H	-1.272229390	1.3691048627	-5.6498055780
H	-1.630895871	2.7835782650	-4.6559231483
C	0.398126944	2.2930980803	-4.7998625914
F	0.825900075	3.0464308057	-3.7523425373
F	1.276238619	1.2633766678	-4.9069952685
F	0.578780493	3.0670315396	-5.9142717688

$ROCO_2^-$, R= F_3CCH_2

O	-0.08167804	0.9347311084	0.0000000000
C	0.62403242	-0.2977216735	0.0000000000
C	-0.41535896	-1.4000495269	0.0000000000
F	-1.22259070	-1.3630693007	1.0855738052
F	-1.22259070	-1.3630693007	-1.0855738052
F	0.19194249	-2.6134445982	0.0000000000
H	1.24471643	-0.4246386497	0.8922036682
H	1.24471643	-0.4246386497	-0.8922036682
C	0.69558987	2.1234099624	0.0000000000
O	-0.011914954	3.1504953864	0.0000000000
O	1.934669951	1.9911930827	0.0000000000

TFE^- / 2 TFEH

O	0.5881021460	6.7203398219	-0.3493166939
H	0.8507368476	7.4891896964	0.2951918571
O	1.1841387164	8.6292108241	1.2216490030
C	0.2718294646	9.6631641262	1.1092864205
H	0.6367941969	10.6190197479	1.5250765503
H	-0.0312033216	9.8638039732	0.0659885358
C	-1.0432023299	9.3977464224	1.8437468662
F	-1.6793470098	8.2728780929	1.4154914853
F	-0.8886434641	9.2571081339	3.1900878979
F	-1.9261664381	10.4286913779	1.6671590767
O	2.5835987412	8.3691440693	3.3731636239
H	1.9586054703	8.4618989311	2.5631988557
C	1.8604498752	8.2336503004	4.5683127351
H	2.5217063449	8.4186065687	5.4229451505
H	1.0090723122	8.9212020218	4.6388835448
C	1.2977712042	6.8294143532	4.7632798418
F	0.4080390568	6.4714089183	3.8045392670
F	2.2606113353	5.8717642737	4.7807489897
F	0.6401454029	6.7454998586	5.9593372799
C	-0.0509873821	5.7230090250	0.4030920760
H	-0.8830251814	5.2753129429	-0.1565625545
H	-0.4367114400	6.1037929385	1.3555268750
C	0.8999838937	4.5840898888	0.7448361404
F	1.9843042473	4.9907664372	1.4493392954

$ROCO_2^-$ / TFEH, R= F_3CCH_2

O	-4.7885731689	-0.2381355131	-2.5544955341
C	-3.5488096620	-0.6306923218	-1.9848495544
H	-3.0991496416	-1.4100462990	-2.6084011514
H	-2.8597591118	0.2111294139	-1.8804351639
C	-3.7919391418	-1.2174630752	-0.6026612195
F	-4.3855329128	-0.3350854966	0.2404620726
F	-4.5870280076	-2.3191556409	-0.6331826039
F	-2.6167585062	-1.5927423955	-0.0302241767
O	-6.9901248654	3.9282062808	-3.0332583096
H	-6.7347679820	2.9636771395	-3.0203809072
C	-5.8766318092	4.6782960744	-3.4649282335
H	-5.9766863994	5.7148581074	-3.1250299023
H	-4.9322924936	4.2638451788	-3.0942382883
C	-5.7792499546	4.7153162180	-4.9844546328
F	-5.6264364013	3.4803159313	-5.5287401388
F	-6.8765207273	5.2637978478	-5.5705640352
F	-4.7077337610	5.4585071904	-5.3806775655
C	-5.1117715172	1.1424349956	-2.5877336860
O	-4.2437264026	1.9722767179	-2.2650201355
O	-6.2979942168	1.3227245431	-2.9787160513

F	0.2702134394	3.6342057539	1.4959391999				
F	1.3753090816	3.9482934073	-0.3632073389				
TFE^- / 3 TFEH				$ROCO_2^-$ / 2 TFEH, R= F_3CCH_2			
O	0.3470660901	6.8711277555	-0.0885710156	O	0.7960608239	6.3439941803	-0.5585850483
H	0.5896485191	7.6105911300	0.5651240688	H	0.9202835598	7.1874176744	-0.0550980117
O	0.9628850989	8.8037922101	1.5385918581	O	1.1590800474	8.5600660362	1.0034498540
C	0.1169250909	9.8713805484	1.2539563537	O	2.3927389287	7.9400182062	3.3519479987
H	0.4545597051	10.8224280819	1.6992125254	H	1.8764350155	8.1516780990	2.5297158225
H	-0.0105023297	10.0432285780	0.1715349062	C	1.5210831147	7.8743382623	4.4570380705
C	-1.2896728684	9.6443804529	1.7967165693	H	2.0719352241	8.1093184862	5.3748090400
F	-1.8639992763	8.5049893900	1.3261401144	H	0.6733644747	8.5611771803	4.3600528880
F	-1.3262984398	9.5545581680	3.1560665226	C	0.9451413706	6.4759564223	4.6362775317
F	-2.1247133209	10.6708957513	1.4573104907	F	0.1840298682	6.0856313829	3.5792833277
O	1.7153386313	8.9842564034	4.0601782325	F	1.9048079359	5.5279475379	4.7931218646
H	1.4419357523	8.8568688248	3.0941412965	F	0.1477482038	6.4204822872	5.7379585613
C	0.9702505250	8.1241997684	4.8822613231	C	0.2913257669	9.4887000737	0.9751902856
H	1.0139499411	8.4745804160	5.9200318805	O	-0.1568694683	10.1119732486	-0.0023760904
H	-0.0834322602	8.0524997933	4.5851745948	O	-0.1700679746	9.8056726810	2.2524249258
C	1.5184874082	6.7023291513	4.8778548700	C	-1.1216155749	10.8591479326	2.3492715919
F	1.4663941959	6.1235667117	3.6536671898	H	-0.6707323048	11.8380765855	2.1501421418
F	2.8099049117	6.6310699370	5.2918767508	H	-1.9773239809	10.7116375912	1.6826149572
F	0.7919779161	5.9085112579	5.7212968258	C	-1.6305243655	10.8509874856	3.7781590589
C	-0.1323403201	5.7748747954	0.6471051254	F	-2.2729233004	9.7015644802	4.1001887942
H	-1.0797730718	5.3983385996	0.2379933726	F	-0.6381177655	11.0119807146	4.6912641563
H	-0.2805086455	6.0133550725	1.7065038016	F	-2.5118134238	11.8686224593	3.9620661431
C	0.8551654430	4.6180759635	0.5870027719	C	0.0533115566	5.4451333242	0.2365166798
F	2.0801775673	4.9399713123	1.0686436372	H	0.1797493069	4.4286578062	-0.1505040071
F	0.4064179704	3.5558805012	1.3144760839	H	0.3565978203	5.4628134059	1.2884699703
F	1.0462152648	4.1676168347	-0.6842307931	C	-1.4366947076	5.7610835275	0.1996072226
O	3.2097029847	9.0997426766	0.2143274852	F	-1.7161858851	7.0037221323	0.6679503302
H	2.3633955974	9.0214802002	0.7651753823	F	-1.9567672584	5.6909477466	-1.0538339386
C	3.7135814274	7.8026998242	-0.0060409418	F	-2.1340429565	4.8787197861	0.9677188753
H	4.3187849553	7.7845494377	-0.9199709964				
H	2.9175192748	7.0543833314	-0.0932937653				
C	4.6191611876	7.3525475717	1.1329147658				
F	3.9846153895	7.3164372606	2.3265451648				
F	5.1063659002	6.1000330974	0.8978048357				
F	5.7016617810	8.1659633808	1.2920492643				
1a $[(bpy)Mn(CO)_3]^-$				**1b** $[(bpymd)Mn(CO)_3]^-$			
Mn	0.0429656104	1.6719999167	1.6534183620	Mn	0.0309058255	1.6784487527	1.6367640675
C	2.7118959135	0.6514890637	1.1017961628	C	2.7068930024	0.6465546914	1.1109823771
C	2.7544955039	2.9793244706	1.4096980549	C	2.7573724848	2.9650551200	1.3752505724
C	4.1136597280	3.0315415675	1.2335819218	C	4.1180897457	2.9588838870	1.1985040129
C	4.8241059497	1.8311037854	0.9710041048	C	4.7403463371	1.7037017886	0.9754970347
C	4.1149867183	0.6549704807	0.9138211477	N	4.0571525784	0.5780779619	0.9391990049
C	-0.3115996109	-1.3072289927	1.3082542014	C	-0.2981428333	-1.3062962631	1.2627961087
N	0.5400204958	-0.2366388796	1.2881649516	N	0.5299286021	-0.2274772719	1.2722667400
C	1.8837959661	-0.5067696051	1.0735526016	C	1.8852448802	-0.5023018198	1.0819286074
C	2.3383075516	-1.8298014683	0.8555632683	N	2.3908161060	-1.7516909456	0.8803313936
C	1.4531101512	-2.8814559831	0.8607075879	C	1.5459523167	-2.7621479975	0.8601284228
C	0.0820005801	-2.6047889980	1.1007879766	C	0.1518604968	-2.5855641705	1.0524757306
N	2.0161928362	1.8292113218	1.3382980275	N	2.0039672302	1.8337327633	1.3249044784
H	2.1943600844	3.8802874750	1.6234066801	H	2.2261828982	3.8887943589	1.5686593326
H	4.6235347504	3.9859820123	1.2981096221	H	4.6916491731	3.8769690772	1.2340933069
H	5.8985111445	1.8407868249	0.8249907962	H	5.8156190449	1.6374496354	0.8326180324
H	4.6289390770	-0.2803552658	0.7244803024	H	-1.3489323902	-1.1080322807	1.4347922097
H	-1.3494237182	-1.0735284260	1.5069872490	H	1.9598068813	-3.7531758243	0.6942681508
H	3.3939124203	-2.0091545446	0.6865774670	H	-0.5323479524	-3.4250844470	1.0399909085
H	1.7947525111	-3.8967038345	0.6926543484	C	-0.1626365076	1.7685344927	3.3906271572

H	-0.6575287824	-3.3970831062	1.1255141811	O	-0.3233437749	1.8527247086	4.5445037998
C	-0.1691219539	1.7489698405	3.4015507750	O	-0.4880148665	4.5460784491	1.1475665760
O	-0.3728595282	1.8433728933	4.5529688974	C	-0.2684777239	3.4142007788	1.3342261039
O	-0.4761673397	4.5285586452	1.1102262472	O	-2.8350117782	1.2573089725	1.0524149782
C	-0.2533495904	3.3973495301	1.3225020926	C	-1.6988963963	1.4103591962	1.2762114945
O	-2.7990228128	1.2710409462	0.9552293254				
C	-1.6671574872	1.4146584652	1.2270874327				
$TS_{1a \rightarrow 2a}$				$TS_{1b \rightarrow 2b}$			
Mn	-4.2483749169	1.9966879917	-0.3938834533	Mn	-4.1401511689	2.2512475353	-0.7999806440
C	-3.0537110516	-0.5541921167	-1.0986277785	C	-3.1064671105	-0.3431567190	-1.5608356604
C	-1.8813527244	0.4593567100	0.6535727368	C	-1.7445504070	0.6208257264	0.0545121975
C	-0.9813266981	-0.5798610592	0.7245617464	C	-0.9113434651	-0.4696756752	0.0061434141
C	-1.1214448118	-1.6665122040	-0.1655653515	C	-1.2467669571	-1.5023568190	-0.8977610569
C	-2.1613479299	-1.6479896313	-1.0697182420	N	-2.3272234414	-1.4451148172	-1.6575071760
C	-6.0238499859	0.8844840729	-2.5722332283	C	-6.1653924438	1.1285778245	-2.7378740664
N	-4.9056544099	0.7309148254	-1.7981144554	N	-4.9820077383	0.9774649942	-2.0849284064
C	-4.1840067714	-0.4346484051	-1.9759664054	C	-4.3091367957	-0.2040273316	-2.3220023893
C	-4.5550459657	-1.3937520064	-2.9396710640	N	-4.7228663388	-1.1651306567	-3.1797577258
C	-5.6718842856	-1.1983822640	-3.7239282289	C	-5.8604937989	-0.9669372310	-3.8236988054
C	-6.4296440050	-0.0223257246	-3.5200465237	C	-6.6434939485	0.1913625699	-3.6192931531
N	-2.9042863176	0.5050767784	-0.2397800967	N	-2.8451475960	0.7311660431	-0.7357695628
H	-1.8113387669	1.3029812775	1.3289949533	H	-1.5549493902	1.4420398486	0.7344450734
H	-0.1859505796	-0.5508968058	1.4606844316	H	-0.0357107533	-0.5336013405	0.6414368274
H	-0.4305898918	-2.5023070430	-0.1348178621	H	-0.6235612969	-2.3884314139	-0.9848557586
H	-2.2978518166	-2.4744584054	-1.7571050505	H	-6.7201344957	2.0338833385	-2.5260528952
H	-6.5925701652	1.7884989365	-2.4016382274	H	-6.1827434307	-1.7401195906	-4.5160678902
H	-3.9594527582	-2.2911987193	-3.0595402290	H	-7.5869055127	0.3366592763	-4.1322577364
H	-5.9657418070	-1.9309461868	-4.4676599339	C	-5.0731965267	2.0136765812	0.6758031971
H	-7.3258298697	0.1780994156	-4.0970957951	O	-5.6892026672	1.9090113313	1.6625328418
C	-5.0045209805	1.7283447197	1.1714577626	O	-2.2302154792	4.1898945993	0.3499709330
O	-5.4800331876	1.6254807112	2.2404259650	C	-2.9755443266	3.4156738981	-0.0980133265
O	-2.3079493943	4.0867645323	0.3661132323	O	-5.6889571089	4.5751446934	-1.7633887053
C	-3.0662603604	3.2501571948	0.0464080666	C	-5.0908224875	3.6500097438	-1.3880364119
O	-6.0941360426	4.1788032402	-1.1319914593	C	-2.6423804338	2.8485830938	-3.1692283904
C	-5.3761776731	3.3056492489	-0.8423900817	O	-2.5589165422	4.0354664906	-3.2146809291
C	-2.9246111932	2.6432770080	-2.9181347426	O	-2.4326336657	1.7587312564	-3.5861504916
O	-2.1043909714	1.7946035273	-2.9494018059				
O	-3.5318449657	3.5805190515	-3.3101683729				
2a $[(bpy)Mn(CO)_3(CO_2)]^-$				**2b** $[(bpymd)Mn(CO)_3(CO_2)]^-$			
Mn	-4.3506265444	2.1392017947	-0.2694496046	Mn	0.2267110040	1.6820694481	1.4483448778
C	-2.8499676167	-0.2476188540	-0.9971959759	C	2.8469704313	0.7500834829	0.6441974778
C	-1.9292251550	0.7193023299	0.9074956812	C	2.9462877271	3.0077884366	1.1176120426
C	-0.9318164625	-0.2370341252	0.9771140603	C	4.2746715003	3.0274936323	0.7449271432
C	-0.8873893091	-1.2358283650	-0.0034813507	C	4.8322967563	1.8224408476	0.2966751063
C	-1.8591707887	-1.2411206625	-0.9906165254	N	4.1314417338	0.6916947019	0.2623591891
C	-6.0055243201	0.7927565243	-2.4403207571	C	0.0046020392	-1.3532174880	1.3613818984
N	-4.8713995663	0.7758252611	-1.7088571540	N	0.7653828498	-0.2535377456	1.1698405616
C	-3.9797328390	-0.2275812378	-1.9247745983	C	2.0316383312	-0.4586168052	0.7122744322
C	-4.2010549236	-1.2006007660	-2.9112334332	N	2.5494670665	-1.6546027207	0.3952538414
C	-5.3581828840	-1.1574278401	-3.6714500770	C	1.7693566168	-2.7210042344	0.5539165357
C	-6.2891099829	-0.1419100100	-3.4202249360	C	0.4676064911	-2.6183591967	1.0626920049
N	-2.8678536435	0.7392152121	-0.0621142952	N	2.2052732651	1.8803795456	1.0506830941
H	-1.9973622410	1.5000042876	1.6541790121	H	2.4489228212	3.8980389043	1.4819649895
H	-0.2096958119	-0.2003899736	1.7851794544	H	4.8577599961	3.9392017450	0.7997593754
H	-0.1184110649	-2.0008726813	0.0154643494	H	5.8683975510	1.7714975120	-0.0256959233
H	-1.8578492898	-2.0177172146	-1.7453899216	H	-0.9878754004	-1.1962607431	1.7650358607
H	-6.7069776497	1.5859843582	-2.2157250146	H	2.1901128285	-3.6856447844	0.2847595678
H	-3.4785306033	-1.9909942065	-3.0723737726	H	-0.1529135973	-3.4930622016	1.2177725067
H	-5.5434787739	-1.9060632758	-4.4344229691	C	0.3390328398	1.7076252884	3.2247259139

H	-7.2213313560	-0.0759146852	-3.9700941383
C	-5.4099323592	1.4814187512	1.0032411618
O	-6.1192101515	1.1236884224	1.8576287261
O	-3.0559540922	4.1453200441	1.4646507136
C	-3.5596734598	3.3514443511	0.7819038607
O	-6.2545486293	4.2055411840	-1.1708928332
C	-5.5064010363	3.3879491462	-0.8216468901
C	-2.9546509281	3.1230689203	-1.9436895848
O	-2.8923500641	4.3677717668	-1.9841941847
O	-2.4023706438	2.2624360127	-2.6417243540

2a/2TFEH [(bpy)Mn(CO)$_3$(CO$_2$)]$^-$/2TFEH

Mn	-4.9623026159	2.4588117984	-0.7657750295
C	-2.5199023193	1.6377052574	0.5920886221
C	-3.6733066906	3.1840363577	1.8755950460
C	-2.6664451620	3.2225766555	2.8245087567
C	-1.5294819353	2.4354926169	2.6303739524
C	-1.4611032127	1.6314954045	1.5075518706
C	-3.7391571141	0.3808531636	-2.5724808173
N	-3.6601565143	1.0445578355	-1.3974255520
C	-2.5467713872	0.8503683412	-0.6330167907
C	-1.5134819041	-0.0003295129	-1.0387698037
C	-1.6055295095	-0.6647566826	-2.2487870957
C	-2.7504995647	-0.4683152913	-3.0291223571
N	-3.6129120114	2.4200282776	0.7741998686
H	-4.5591244099	3.7964277861	1.9742435009
H	-2.7636668299	3.8760545972	3.6824679872
H	-0.6997604122	2.4687109134	3.3253699897
H	-0.5733929778	1.0483986244	1.3085598474
H	-4.6222796811	0.5747934869	-3.1629517521
H	-0.6281875393	-0.1045015628	-0.4282097130
H	-0.8019402514	-1.3098273626	-2.5837321386
H	-2.8709803770	-0.9548368212	-3.9892741660
C	-6.1711656214	1.5112343284	0.1785552695
O	-6.9773917879	0.9448371793	0.7902231076
O	-5.9641833699	5.1664418176	-0.1376523992
C	-5.5821177891	4.1007166272	-0.3799634099
O	-6.7073607571	2.4149675303	-3.1540830681
C	-6.0118761701	2.4373552392	-2.2336355578
C	-3.4505362400	3.6109717903	-1.9286250126
O	-2.4675049119	4.0029535872	-1.2306613677
O	-3.5745549102	3.6394063186	-3.1537384978
O	-0.3262085312	2.9716967354	-2.0248906097
H	-1.1597225443	3.4680696055	-1.6726775390
C	-0.4067957579	2.9068109550	-3.4216924028
H	-0.5068395564	1.8728475946	-3.7756143116
H	-1.2583720141	3.4851254173	-3.7969466318
C	0.8687342919	3.4585689998	-4.0233736608
F	1.0933800183	4.7486387195	-3.7006952776
F	1.9690152879	2.7630304802	-3.6139689558
F	0.8448652644	3.3791644197	-5.3811444691
O	1.2380908652	1.4794737726	-0.5208906508
H	0.5655412615	1.9298222972	-1.0941848640
C	2.2199307098	2.4360912966	-0.2488048574
H	3.1586143252	1.9380389282	0.0102480421
H	2.3953753714	3.1073156963	-1.0963603570
C	1.8423699225	3.3118989559	0.9374031525
F	0.6869935226	3.9659590827	0.7497540722
F	1.7134731203	2.5909545943	2.0862314031
F	2.8123350735	4.2404972987	1.1710565420
O	0.3628527362	1.7581192899	4.3878115448
O	-0.3612465717	4.5626737755	1.1778559227
C	-0.1221625832	3.4326696584	1.2858628413
O	-2.6741805744	1.1370917184	1.3774019455
C	-1.5329607522	1.3428787227	1.4072985181
C	-0.0118047320	1.7051871169	-0.9570828658
O	-0.9795655645	2.3293053694	-1.4093844811
O	0.8979396060	1.0633968139	-1.4847224159

2b/2TFEH [(bpymd)Mn(CO)$_3$(CO$_2$)]$^-$/2TFEH

Mn	-3.3050652207	1.9690937522	-1.9435717567
C	-2.5032775348	-0.1189889319	-0.0209452268
C	-1.1370921634	1.7127211034	0.2160216592
C	-0.4794275629	1.0835933926	1.2603747728
C	-0.9031023818	-0.2003591819	1.6016305747
N	-1.9197790071	-0.7960746862	0.9652992739
C	-5.3399065873	-0.2874397799	-2.2525563099
N	-4.2353154286	0.1474043219	-1.6249249943
C	-3.6866233756	-0.6798148368	-0.7123823204
N	-4.1487910099	-1.8874303125	-0.3891802244
C	-5.2499621813	-2.3116629536	-1.0234573790
C	-5.8925950643	-1.5274321448	-1.9780749747
N	-2.1454166823	1.1141600544	-0.4445564329
H	-0.8780242134	2.7137154666	-0.0939372955
H	0.3189133242	1.5819123358	1.7995888706
H	-0.4317175265	-0.7565295745	2.4069453207
H	-5.7958095665	0.3884347288	-2.9574106453
H	-5.6242266325	-3.2952053940	-0.7542341090
H	-6.7940505957	-1.8633195920	-2.4786337829
C	-4.3302600534	2.8281388011	-0.7112327015
O	-4.9701431375	3.4306706120	0.0401703420
O	-1.7493113654	4.4069235748	-2.5419764885
C	-2.3234627467	3.4447080016	-2.2664659739
O	-5.0766190366	2.8773850307	-4.1220253765
C	-4.3798826737	2.4993915086	-3.2857850603
C	-2.0649523867	1.0273848787	-3.4455315176
O	-0.8177415081	1.2950179299	-3.5114043836
O	-2.5944579566	0.2503634789	-4.3002688980
O	1.3902622158	1.8443272873	-2.1720024137
H	0.4733144678	1.7187572463	-2.5392203235
C	1.8469521380	3.1355011029	-2.4804413454
H	2.8807904181	3.1106298261	-2.8425695972
H	1.2246237963	3.6392015437	-3.2272203392
C	1.8482254301	4.0181507057	-1.2358279742
F	0.6018404985	4.2646183207	-0.7521330826
F	2.5446809871	3.4689060677	-0.2152152089
F	2.4067401088	5.2276340875	-1.5106576759
O	-3.6541175654	1.3274212288	-6.5652028360
H	-3.3567640387	0.9198187030	-5.7150596548
C	-4.5700671036	0.4762386778	-7.1981282730
H	-4.6198888743	0.7318942472	-8.2613121670
H	-4.3203378162	-0.5879144243	-7.1072876101
C	-5.9751558040	0.6572968680	-6.6430943000
F	-6.0655386679	0.2997654090	-5.3393380728
F	-6.4177546809	1.9318692825	-6.7325737879
F	-6.8602782081	-0.1174398003	-7.3268323592

$TS_{2a/2TFEH \rightarrow 3a}$			
Mn	-4.0878739468	2.5095479924	-1.2391346112
C	-2.4683978609	0.1336701433	-0.5669618284
C	-1.6266851628	2.0058609264	0.5131215338
C	-0.6789062917	1.2489806377	1.1905122947
C	-0.6264304842	-0.1232380010	0.9614313678
C	-1.5338595076	-0.6873758111	0.0716765264
C	-5.3808593325	0.1973770889	-2.7316741675
N	-4.3822256757	0.5740927980	-1.9164959005
C	-3.5145563450	-0.3684962249	-1.4733272418
C	-3.6443225467	-1.7113144160	-1.8396063408
C	-4.6922258363	-2.0951339535	-2.6681173990
C	-5.5778434807	-1.1202052772	-3.1235812129
N	-2.5036223173	1.4719271777	-0.3522973482
H	-1.6872778400	3.0707828691	0.6628317451
H	0.0061989489	1.7392923233	1.8712253656
H	0.1017609399	-0.7461969718	1.4707649950
H	-1.5211070366	-1.7549521778	-0.1082011984
H	-6.0486547309	0.9758569252	-3.0732181937
H	-2.9406336864	-2.4514947128	-1.4794294186
H	-4.8136981111	-3.1353707738	-2.9497254686
H	-6.4134078832	-1.3664687930	-3.7688542248
C	-5.0599398355	2.2599419539	0.2770330126
O	-5.6951385188	2.1663039653	1.2378954903
O	-3.3037416241	5.2513957784	-0.4654701258
C	-3.5845946163	4.1691130372	-0.7452849307
O	-6.3973779230	3.7423551881	-2.6006656606
C	-5.4941951970	3.2489815679	-2.0762608022
C	-3.0588030337	2.8621473605	-3.0816780146
O	-1.9276825872	3.5497990747	-3.1279576595
O	-3.5736544624	2.5349888259	-4.1708482156
O	-0.1930103218	3.4543283302	-1.4501075973
H	-1.1936635408	3.5441633118	-2.2335929425
C	0.5634220081	2.3809863991	-1.8935611837
H	1.0470707181	1.8382381776	-1.0686964704
H	-0.0256969551	1.6468948701	-2.4661582571
C	1.6914590680	2.8171819365	-2.8168020487
F	1.2497469212	3.4107547227	-3.9516611243
F	2.5362152595	3.7006062027	-2.2308879142
F	2.4524156338	1.7511253967	-3.2061519292
O	1.2667269815	4.1858061399	0.6422995685
H	0.6630280316	4.0100403355	-0.1361387598
C	1.0828959684	5.4942674391	1.1116137380
H	1.9940985045	5.8439485815	1.6084097709
H	0.8201205374	6.2092425130	0.3244499085
C	-0.0277601142	5.5402496970	2.1497569721
F	-1.2290159932	5.1832870413	1.6354920800
F	0.2065414037	4.7059219502	3.1924100421
F	-0.1727204106	6.7875501477	2.6681788518

$TS_{2b/2TFEH \rightarrow 3b}$			
Mn	-4.1297118237	2.5247517206	-1.1756945530
C	-2.4707703496	0.1733330828	-0.5375872755
C	-1.6477841806	2.0108630042	0.5667478102
C	-0.7092074175	1.2062422624	1.1955631719
C	-0.7120997144	-0.1462801742	0.8758510705
N	-1.5922830512	-0.6657457671	0.0084606689
C	-5.3411959617	0.1983755083	-2.7490242089
N	-4.3824916027	0.6028672031	-1.8965467656
C	-3.5091655753	-0.3335346051	-1.4666842023
N	-3.5314147782	-1.6207731543	-1.8038033049
C	-4.4994543883	-2.0174969523	-2.6391033335
C	-5.4393356716	-1.1254254946	-3.1481706067
N	-2.5373839537	1.5006830457	-0.3031555127
H	-1.7100483416	3.0679996347	0.7642073923
H	0.0051244769	1.6276670425	1.8909911533
H	0.0004343304	-0.8319523244	1.3248505530
H	-6.0380988509	0.9449757673	-3.1044866679
H	-4.5197350077	-3.0704522387	-2.9025466106
H	-6.2215332243	-1.4460908041	-3.8261791160
C	-5.1120138661	2.2469074426	0.3331990493
O	-5.7481825714	2.1347301304	1.2900433157
O	-3.4323476608	5.2880968190	-0.3949938334
C	-3.6705066159	4.1952202322	-0.6711585294
O	-6.4499950218	3.7227982912	-2.5519072264
C	-5.5441922598	3.2457431557	-2.0208222165
C	-3.0760648734	2.9120553536	-2.9947899499
O	-1.9199032685	3.5509225879	-3.0097294649
O	-3.5984176428	2.6272301800	-4.0924701410
O	-0.1782014710	3.2585349170	-1.3656272371
H	-1.1680875684	3.4558755763	-2.1206972428
C	0.5622281012	2.2342743222	-1.9355221968
H	1.0315335835	1.5826606452	-1.1823756852
H	-0.0362376561	1.5945091808	-2.6007525076
C	1.7046514386	2.7650318200	-2.7895306087
F	1.2805423888	3.5380980910	-3.8168293385
F	2.5841013398	3.5176399543	-2.0826880529
F	2.4221465047	1.7426836583	-3.3388147681
O	1.2678396312	3.9052490968	0.7775043753
H	0.6938292565	3.7217948410	-0.0187769082
C	1.2203752465	5.2808260291	1.0561344447
H	2.1099741902	5.5801173636	1.6192196118
H	1.1510671533	5.9016512017	0.1548505578
C	0.0123554047	5.6074323380	1.9199325462
F	-1.1535651220	5.2671898890	1.3164197196
F	0.0331594873	4.9526931476	3.1081361740
F	-0.0558185330	6.9332286696	2.2009841420

3a [(bpy)Mn(CO)$_3$(CO$_2$H)]			
Mn	0.19615489	1.7061251249	1.5740837495
C	2.89303502	0.7466417746	0.9721644297
C	2.93868660	3.0439680495	1.3231300512
C	4.29714459	3.1118447203	1.0423104707
C	4.96665702	1.9396648238	0.6962948811
C	4.25755590	0.7442999044	0.6682284699
C	-0.01756614	-1.3470365761	1.5783765612
N	0.77997490	-0.2787426148	1.4079342467
C	2.06916289	-0.4758168321	1.0407614983

3b [(bpymd)Mn(CO)$_3$(CO$_2$H)]			
Mn	0.1848420447	1.7013046715	1.3165985138
C	2.8679578653	0.7535025098	0.6776303873
C	2.9525342495	3.0214960837	1.0596650227
C	4.2949235451	3.0265862105	0.7127472460
C	4.8558396696	1.8106959925	0.3289824863
N	4.1487966967	0.6737066245	0.3265748593
C	-0.0079676208	-1.3696014633	1.3081479293
N	0.7641130830	-0.2804580429	1.1481496438
C	2.0378637643	-0.4773858393	0.7475377822

C	2.567221885	-1.7597101214	0.7998919394	N	2.5752775571	-1.6596583367	0.4583994757
C	1.730450176	-2.8585415874	0.9570673014	C	1.7902069930	-2.7365924290	0.5867124717
C	0.414836637	-2.6497807063	1.3666100776	C	0.4742396569	-2.6401506172	1.0330938081
N	2.242647105	1.8952489270	1.2779580558	N	2.2271437508	1.8898981499	1.0237785995
H	2.392436259	3.9379157177	1.5971061134	H	2.4473523515	3.9281204323	1.3699023520
H	4.808169903	4.0665492003	1.0960304358	H	4.8759438281	3.9414308728	0.7364038054
H	6.025780778	1.9519416729	0.4614141957	H	5.8958847068	1.7424595755	0.0234481720
H	4.766817612	-0.1776529791	0.4174965962	H	-1.0205891905	-1.2155244552	1.6605516853
H	-1.033453650	-1.1543393565	1.8998977311	H	2.2292450902	-3.6970160465	0.3327025669
H	3.596349029	-1.9061217246	0.4969387231	H	-0.1524120202	-3.5159666741	1.1573748482
H	2.103866423	-3.8603691187	0.7722426847	C	0.3775739564	1.6769562047	3.1371018273
H	-0.272255758	-3.4741314531	1.5214632976	O	0.4782570546	1.6752324658	4.2822736985
C	0.415301427	1.6701866570	3.3874951518	O	-0.3954009347	4.6014693505	1.2914705161
O	0.533947619	1.6619839935	4.5325071121	C	-0.1633277766	3.4739307878	1.2978852209
O	-0.391565408	4.6029807796	1.5743761371	O	-2.7167620916	1.1556333149	1.4924780140
C	-0.154457932	3.4748407094	1.5702497101	C	-1.5865039331	1.3617774919	1.4206511264
O	-2.703895241	1.1764070472	1.7871428352	C	0.0696679606	1.6581827333	-0.7776341154
C	-1.571341228	1.3730319216	1.6996082441	O	-0.9718254328	2.3289822208	-1.3867821991
C	0.048633980	1.6836563849	-0.5174452468	O	0.8644382103	1.0795477950	-1.5099292665
O	-1.012551492	2.3711599744	-1.0892731581	H	-0.8857663329	2.2181531612	-2.3567376957
O	0.818149482	1.1215457146	-1.2867902059				
H	-0.945519923	2.2804556846	-2.0620906411				
3'a [(bpy)Mn(CO)$_3$(CO$_2$H)]$^-$				**3'b** [(bpymd)Mn(CO)$_3$(CO$_2$H)]$^-$			
Mn	0.18811058	1.7133533449	1.5373514995	Mn	0.1791207471	1.7033195277	1.2622492260
C	2.89676867	0.7176456446	0.9971864573	C	2.8841052186	0.7024670188	0.7140945167
C	2.93177001	3.0603357175	1.2237793414	C	2.9311401332	3.0194421812	0.9434727557
C	4.29829998	3.1326906124	1.0124538250	C	4.3074248236	3.0278915684	0.7168564996
C	4.99592596	1.9219491239	0.7599697135	C	4.9036571513	1.7813668025	0.4665116038
C	4.30106511	0.7371435339	0.7544372041	N	4.2313607010	0.6402141218	0.4622632421
C	-0.03422933	-1.3487894628	1.4793324731	C	-0.0214463070	-1.3571080771	1.1898634508
N	0.75450580	-0.2714669194	1.3383903229	N	0.7446595017	-0.2793854065	1.0585763113
C	2.10529201	-0.4590030711	1.0660614006	C	2.0924476386	-0.4705271901	0.7793688946
C	2.605558183	-1.7830780048	0.9010516630	N	2.6426872677	-1.7134080295	0.5915780992
C	1.773515848	-2.8672086971	1.0364627897	C	1.8396565541	-2.7591862161	0.7190262758
C	0.404526644	-2.6552235986	1.3461484339	C	0.4756457426	-2.6510786177	1.0349373956
N	2.226635284	1.9177758033	1.2104341363	N	2.2150677523	1.9000623613	0.9351029855
H	2.370168932	3.9674995168	1.4180476294	H	2.3984915223	3.9435618306	1.1390420489
H	4.802856800	4.0908209740	1.0413171620	H	4.8774145961	3.9480576212	0.7294672313
H	6.066290495	1.9286009824	0.5789376062	H	5.9709514769	1.7165174232	0.2653610721
H	4.826628071	-0.1927099436	0.5715817670	H	-1.0660416211	-1.1923061824	1.4299042531
H	-1.074517467	-1.1530678910	1.7151119425	H	2.2898794713	-3.7381145947	0.5679004022
H	3.653984514	-1.9356125830	0.6737883848	H	-0.1608088563	-3.5192530190	1.1481705428
H	2.162704764	-3.8729424844	0.9132667775	C	0.4706573533	1.6098970195	3.0627080118
H	-0.288539939	-3.4773234216	1.4757825403	O	0.6345106337	1.5637712643	4.2026544244
C	0.507232720	1.6042625675	3.3276674135	O	-0.3860110712	4.5999738078	1.3859298860
O	0.710271886	1.5370425977	4.4614204069	C	-0.1568574089	3.4688184191	1.3272789079
O	-0.366669393	4.6094170452	1.6834738354	O	-2.7055173751	1.1595966521	1.5912700605
C	-0.144624929	3.4755523364	1.6142309418	C	-1.5767517117	1.3635947535	1.4521164732
O	-2.694435717	1.1671630798	1.8649337059	C	-0.0446599350	1.7364409341	-0.8165621905
C	-1.563438725	1.3726634113	1.7281073467	O	-1.1500159273	2.4260932643	-1.3197574204
C	-0.036492953	1.7402942601	-0.5451962892	O	0.6877142669	1.2163389735	-1.6503950571
O	-1.098248154	2.5024472235	-1.0509524982	H	-1.1270109179	2.3594310750	-2.2962501053
O	0.649661460	1.1689669291	-1.3845444447				
H	-1.082976419	2.4243147175	-2.0263721146				
$TS_{3a \rightarrow 4a}$				$TS_{3b \rightarrow 4b}$			
Mn	-4.5873188586	2.2440365976	-0.8015528248	Mn	-4.6103766319	2.2848524595	-0.9118338172
C	-2.7892058683	-0.0517787744	-0.4707232941	C	-3.0537668286	-0.1954645786	-0.7215530507
C	-2.7949207322	1.2559511669	1.4544317371	C	-2.7463595285	1.0526829838	1.1888513577
C	-1.9549682563	0.3679644664	2.1162853577	C	-1.9387919663	0.0479909596	1.7036771177

C	-1.5329807234	-0.7790712837	1.4487828432
C	-1.9499769322	-0.9879215334	0.1376177852
C	-4.4385139626	0.9054444622	-3.5679673848
N	-4.0259012676	0.8820310116	-2.2890136228
C	-3.2479268519	-0.1475348375	-1.8703833741
C	-2.9001004372	-1.1914689446	-2.7303531600
C	-3.3413521506	-1.1667067171	-4.0492265432
C	-4.1164600438	-0.0927734867	-4.4798973028
N	-3.2161382713	1.0492075152	0.1970855208
H	-3.1239127299	2.1674770537	1.9302371682
H	-1.6443528319	0.5849112195	3.1320087052
H	-0.8800130158	-1.4973174253	1.9339225302
H	-1.6177480339	-1.8670420524	-0.4001943879
H	-5.0465808031	1.7471576703	-3.8741623333
H	-2.2913421185	-2.0163270692	-2.3817053272
H	-3.0801285648	-1.9723302193	-4.7276533867
H	-4.4770723240	-0.0217571038	-5.5000784859
C	-5.9565640515	1.1061115995	-0.3040945566
O	-6.8203036519	0.4199772357	-0.0055776384
O	-5.2118836718	4.0638083885	1.4671448865
C	-4.9507035243	3.3600391372	0.6035960679
O	-6.4813758884	3.7684308276	-2.5015482000
C	-5.7480514054	3.1793231738	-1.8451972316
C	-3.1588933882	3.4963662209	-1.4107648464
O	-2.6809023778	4.1624345818	-2.2113438109
O	0.3051212208	3.5309065747	-0.4804719684
H	-0.6644782287	3.7706633208	-0.1483980277
C	0.4296050438	2.1387077323	-0.4886146669
H	1.4257210075	1.8214233544	-0.1579381006
H	-0.3116827616	1.6499527431	0.1538119538
C	0.2433029350	1.5439150752	-1.8782099382
F	-0.9795961710	1.7922503247	-2.4045926375
F	1.1493385138	2.0091233962	-2.7731409610
F	0.3811364035	0.1899331764	-1.8434712024
O	-2.0122608383	4.0374971053	0.3810470720
H	-2.1440855465	4.9879160693	0.2618706290

C	-1.7665056001	-1.0935481928	0.9259137982
N	-2.3160587884	-1.2114013623	-0.2909286283
C	-4.7607859721	0.9621868634	-3.7156761764
N	-4.2922238369	0.8998851826	-2.4547672265
C	-3.6117183792	-0.2140273386	-2.1024554013
N	-3.3955299374	-1.2599630977	-2.8920974142
C	-3.8770845878	-1.1982209020	-4.1409683982
C	-4.5661842773	-0.0819241381	-4.6081583038
N	-3.3204851111	0.9256572010	-0.0188339325
H	-2.9215402364	1.9758110725	1.7213032416
H	-1.4715589001	0.1533703216	2.6765394744
H	-1.1707880221	-1.9309130495	1.2780778250
H	-5.2974670846	1.8558755004	-4.0102796706
H	-3.7044640753	-2.0611614635	-4.7779304876
H	-4.9450063541	-0.0273846394	-5.6226655105
C	-6.0845614857	1.3040333527	-0.3633116597
O	-7.0077647406	0.7204961238	-0.0310934096
O	-4.9512797135	4.0875584494	1.4340448290
C	-4.7864887667	3.3935740150	0.5412505681
O	-6.3723422508	4.0699240510	-2.4990734950
C	-5.6941604014	3.3808233109	-1.8843738712
C	-3.0521176776	3.3427586562	-1.5584803848
O	-2.4469294720	3.8820624310	-2.3652471424
O	0.4487619482	3.6094816267	-0.5155361403
H	-0.5517412575	3.7291407378	-0.2044594171
C	0.8156429476	2.2770778098	-0.3106934685
H	1.8986900250	2.1818856829	-0.1737678428
H	0.3255444054	1.8303533982	0.5645496491
C	0.4624921290	1.3888711154	-1.4972258555
F	-0.8666630477	1.3869672466	-1.7749654634
F	1.0896681904	1.7590134472	-2.6389621231
F	0.8065700011	0.0952407676	-1.2554713542
O	-1.9255764406	3.8381982371	0.2949932118
H	-2.1337717195	4.7823693809	0.3084139105

4a $[(bpy)Mn(CO)_4]^+$

Mn	-1.34459633	1.7005029884	0.9600376218
C	0.52771293	0.2630818486	2.7106996081
C	0.66806627	2.5544602436	3.1137391308
C	1.64516422	2.3719898555	4.0847539814
C	2.07177368	1.0773694610	4.3698881228
C	1.50646858	0.0125718986	3.6753137287
C	-1.71149336	-1.2684196693	0.2742288617
N	-1.06048788	-0.3653404026	1.0301221676
C	-0.13226248	-0.7975656274	1.9225467167
C	0.156057836	-2.1571185264	2.0632072494
C	-0.518950892	-3.0854283379	1.2767469830
C	-1.470727149	-2.6339478239	0.3659618422
N	0.117829765	1.5290715033	2.4382328252
H	0.320160778	3.5517811434	2.8763282036
H	2.054067231	3.2348073520	4.5987292615
H	2.832917497	0.8942506970	5.1214020892
H	1.828744334	-0.9992706007	3.8876887255
H	-2.447893417	-0.8941157804	-0.4256503581
H	0.897925911	-2.4950527078	2.7760640812
H	-0.302128391	-4.1439700396	1.3769379234
H	-2.024072755	-3.3168861073	-0.2692063739
C	-2.677756356	1.5379891237	2.2909190893

4b $[(bpymd)Mn(CO)_4]^+$

Mn	-1.3510837440	1.7098853347	0.9530965435
C	0.5213923852	0.2788034671	2.7070143997
C	0.6929424778	2.5397003816	3.1255682701
C	1.6602128485	2.2822392229	4.0853557774
C	2.0081381958	0.9508395277	4.2981401307
N	1.4385394080	-0.0465623553	3.6085007222
C	-1.6931622864	-1.2932819238	0.2784597088
N	-1.0645628664	-0.3601707127	1.0199032269
C	-0.1444575647	-0.7915920054	1.9112834804
N	0.1864618289	-2.0605886855	2.1105648770
C	-0.4396618768	-2.9860424119	1.3711242686
C	-1.4032900190	-2.6414430399	0.4269164744
N	0.1173724480	1.5386038042	2.4307153979
H	0.3761401499	3.5530185237	2.9112056668
H	2.1215355061	3.0896063349	4.6429178370
H	2.7570575284	0.6739702027	5.0343825602
H	-2.4329325063	-0.9577115181	-0.4380212522
H	-0.1611093910	-4.0218426820	1.5415730727
H	-1.9106043826	-3.3899052264	-0.1712656156
C	-2.6875765493	1.5501279476	2.2867775275
O	-3.4916070719	1.4590321694	3.0809137394
O	-1.5473114390	4.6817442726	1.0779575038

O	-3.482411273	1.4446635485	3.0856504465	C	-1.4715699496	3.5449586820	1.0307613380
O	-1.558262692	4.6709923695	1.0572775984	O	-3.4348042879	1.6377912239	-1.1776628668
C	-1.470726270	3.5330538613	1.0262731904	C	-2.6379335069	1.6671199320	-0.3627852331
O	-3.421559428	1.6623786094	-1.1756304056	C	0.0089135099	1.8384922596	-0.3598125575
C	-2.625758636	1.6706195070	-0.3570941644	O	0.8182878828	1.9202368570	-1.1495517632
C	0.020350442	1.8199011803	-0.3426184582				
O	0.835217781	1.8957230869	-1.1287147105				
$TS_{3'a \rightarrow 5a}$				$TS_{3'b \rightarrow 5b}$			
Mn	-4.4022698380	2.1647187317	-0.6753011832	Mn	-3.9735333772	1.9847702362	-0.9307192375
C	-2.7355550954	-0.2524899749	-0.6788812598	C	-3.2793478813	-0.8308466106	-1.4593171995
C	-2.5239738502	0.8794212110	1.3809057289	C	-2.2351992261	-0.1206935726	0.4970437804
C	-1.6620822601	-0.0717294218	1.8892992332	C	-1.6917339715	-1.3871263672	0.6840100493
C	-1.3140925289	-1.1721966759	1.0615959558	C	-1.9941672062	-2.3469312262	-0.2962128837
C	-1.8462861805	-1.2558503526	-0.2003627420	N	-2.7632552060	-2.0953073077	-1.3439070137
C	-4.8100170514	0.8578408296	-3.4301406547	C	-5.4491381109	1.1774139228	-3.5117127045
N	-4.2022607490	0.8038285299	-2.2295362265	N	-4.6282008716	0.8194113173	-2.5245033578
C	-3.3380406273	-0.2525252039	-1.9646927297	C	-4.1503103440	-0.4879149863	-2.5236587927
C	-3.1118324749	-1.2404509422	-2.9643367339	N	-4.4990819448	-1.4077753549	-3.4781937413
C	-3.7444050918	-1.1605982086	-4.1798539870	C	-5.3203339960	-1.0108898790	-4.4362416582
C	-4.6272164730	-0.0780335131	-4.4302169946	C	-5.8375845960	0.2945853919	-4.5154371554
N	-3.0514313234	0.8285740088	0.1413994851	N	-3.0068697403	0.1812895454	-0.5459307011
H	-2.8028192500	1.7346631274	1.9848208298	H	-2.0461226493	0.6690950547	1.2140344335
H	-1.2651739662	0.0372928288	2.8907900235	H	-1.0660402842	-1.6131057202	1.5373904234
H	-0.6352790276	-1.9392834602	1.4199435340	H	-1.5958743256	-3.3562640554	-0.2165207207
H	-1.5885370037	-2.0913304060	-0.8401915072	H	-5.8129494634	2.1988564587	-3.5060204538
H	-5.4757451330	1.6973517931	-3.5929795404	H	-5.5911149289	-1.7543814706	-5.1831473735
H	-2.4316076114	-2.0593212251	-2.7642179022	H	-6.5066685471	0.6002035971	-5.3093390933
H	-3.5679489691	-1.9167019101	-4.9384075082	C	-5.3898939011	1.4013494167	0.0819001621
H	-5.1510238524	0.0266608469	-5.3724777295	O	-6.2786352187	1.0425823319	0.7098628097
C	-5.7391901934	1.1525063980	0.0452424229	O	-2.7290526835	3.4089267810	1.3537813972
O	-6.5801521421	0.5062117627	0.4824065324	C	-3.2167471876	2.8659899485	0.4674786445
O	-4.3947406152	4.0340225025	1.6285229410	O	-5.4266761284	4.4488372683	-1.7080939307
C	-4.3779910224	3.3111773842	0.7357006445	C	-4.8630936535	3.4923472486	-1.4118177564
O	-6.3955545403	3.8696395916	-2.0471235605	C	-2.4867651146	2.5411219625	-2.1725844387
C	-5.6115431516	3.2106419250	-1.5188540198	O	-1.8957265784	2.3453900674	-3.1398982337
C	-2.9622066279	3.2169093791	-1.6717623054	O	0.6145629723	4.2383338459	-0.7645322717
O	-2.5893437942	3.5123713861	-2.7213797653	H	-0.3717133736	4.2843562145	-1.0818099047
O	0.4260532938	3.1381922201	-0.1882207149	C	0.7441948352	3.2882057170	0.2564379381
H	-0.4439572222	3.6864861629	-0.2601243001	H	1.6051094348	3.5223573060	0.8916011763
C	0.1156170281	1.8546879190	-0.6624132369	H	-0.1422239262	3.2258574449	0.8988335108
H	0.5925364496	1.0783500391	-0.0560169657	C	0.9835155306	1.8855266120	-0.2866831737
H	-0.9602698163	1.6757476271	-0.6601859470	F	-0.0334026118	1.4405339831	-1.0584482188
C	0.5744705154	1.6266158481	-2.0939011849	F	2.1083496705	1.8019879257	-1.0415437961
F	0.1760595940	2.6002149163	-2.9419454845	F	1.1244743568	0.9909613600	0.7292816848
F	1.9300566179	1.5519651837	-2.2083063463	O	-1.8201723898	4.4423293723	-1.5473295449
F	0.0760973455	0.4552422643	-2.5713170700	H	-1.7125617221	4.8103418155	-2.4357342917
O	-1.8048951682	4.4061312675	-0.3908170674				
H	-1.5902159504	5.0723507786	-1.0593433641				
5a $[(bpy)Mn(CO)_4]^0$				**5b** $[(bpymd)Mn(CO)_4]^0$			
Mn	-1.4364191210	1.8201146673	0.8817653905	Mn	-1.3558179696	1.7126281196	0.9489874807
C	0.6034136365	0.1833663901	2.7835869786	C	0.5049540318	0.2536453858	2.6865446771
C	0.7490785659	2.4572677532	3.1936036738	C	0.6718923558	2.5463327418	3.1080560242
C	1.7310011035	2.2812236521	4.1638941319	C	1.6438476299	2.3087005642	4.0718508315
C	2.1574584097	0.9836444058	4.4414694837	C	2.0001468533	0.9640072462	4.2859774723
C	1.5882829630	-0.0782103114	3.7450231768	N	1.4578896900	-0.0436389465	3.6233842427
C	-1.6238573886	-1.3629976253	0.3492956639	C	-1.6988373955	-1.2676515407	0.2738775534
N	-0.9806760124	-0.4625117338	1.1006193440	N	-1.0796312006	-0.3395704680	1.0071824762
C	-0.0627294932	-0.8845894790	1.9907140142	C	-0.1291986518	-0.7648916400	1.9308402857
C	0.2292776182	-2.2462541794	2.1439079859	N	0.1850374756	-2.0851253603	2.1104645873

C	-0.4429198627	-3.1784294222	1.3592127700	C	-0.4508867316	-2.9726658235	1.3645962262
C	-1.3907279387	-2.7317839929	0.4404025906	C	-1.4228089774	-2.6226112445	0.4085127377
N	0.1995382958	1.4405098140	2.5204995270	N	0.0998146084	1.5576622461	2.4165645327
H	0.3847040020	3.4470909635	2.9410149246	H	0.3487159964	3.5582087231	2.8910553121
H	2.1446344790	3.1400859614	4.6812138625	H	2.0983326193	3.1200659635	4.6254564631
H	2.9220499573	0.7972938515	5.1888696826	H	2.7556225454	0.7093819347	5.0261560710
H	1.9123595261	-1.0902521301	3.9535294360	H	-2.4370214531	-0.9248017535	-0.4423860194
H	-2.3517490231	-0.9660957394	-0.3495648576	H	-0.1885734296	-4.0166774852	1.5210178898
H	0.9674616419	-2.5833626001	2.8610492901	H	-1.9327649769	-3.3642082798	-0.1927893818
H	-0.2277827336	-4.2367540258	1.4660134653	C	-2.6644345515	1.5275138191	2.2951709397
H	-1.9393761848	-3.4201325095	-0.1932144582	O	-3.4466964201	1.4114444315	3.1111342784
C	-2.7352122567	1.6473214358	2.1944066997	O	-1.5557929202	4.6784726416	1.0679569242
O	-3.5449423300	1.5490137086	3.0045768957	C	-1.4751808734	3.5377260771	1.0263056651
O	-1.6148060268	4.7725152432	1.0221480006	O	-3.4353603600	1.6595239320	-1.1779926556
C	-1.4812078594	3.6174662281	1.0335212794	C	-2.6352704162	1.6722875414	-0.3602729063
O	-3.4953714597	1.7353449720	-1.2444337137	C	0.0205667484	1.8151455479	-0.3367896928
C	-2.6824094713	1.6760335140	-0.4152418972	O	0.8550899305	1.8724226390	-1.1058199780
C	-0.0850683430	1.9309392464	-0.3832914560				
O	0.7474919162	2.0077103418	-1.1726536599				
6a [(bpy)MnH(CO)$_3$]				**6b** [(bpymd)MnH(CO)$_3$]			
Mn	-4.5330392464	2.0390186902	0.2707679218	Mn	-4.5272514999	2.0560528502	0.2728453129
C	-2.8124915850	-0.0512513883	-0.8643845250	C	-2.8373107721	-0.0681496582	-0.8385134242
C	-2.1642738154	0.4162259763	1.3167638510	C	-2.1597409030	0.3858418644	1.3108346271
C	-1.1201446544	-0.4978522899	1.2566654363	C	-1.1503895542	-0.5563084302	1.1878907358
C	-0.9178520786	-1.2061978488	0.0732421662	C	-1.0461096335	-1.2232568282	-0.0303085514
C	-1.7769776460	-0.9823327956	-0.9962279733	N	-1.8924887316	-0.9843181114	-1.0391430591
C	-5.7087556643	1.4296849959	-2.4825386851	C	-5.7053564436	1.4087678532	-2.4965453695
N	-4.7406983627	1.1494105064	-1.5927036884	N	-4.7516564157	1.1510550874	-1.5823093117
C	-3.7991895344	0.2313269856	-1.9225064122	C	-3.8296613304	0.2186372327	-1.9046842501
C	-3.8022300956	-0.3998887821	-3.1708049110	N	-3.7725039470	-0.4401246286	-3.0600288230
C	-4.7987784339	-0.0934431316	-4.0900061442	C	-4.7132013303	-0.1631333165	-3.9708540271
C	-5.7766157187	0.8346784867	-3.7358389538	C	-5.7229756958	0.7637471594	-3.7234769393
N	-2.9906068310	0.6498985364	0.2822717091	N	-3.0034129037	0.6465194223	0.2948523363
H	-2.3508633413	0.9766295740	2.2239364768	H	-2.3028488268	0.9377489701	2.2313047102
H	-0.4862281589	-0.6440999679	2.1241292199	H	-0.4736785632	-0.7607118708	2.0096076693
H	-0.1101936239	-1.9252382783	-0.0150064561	H	-0.2742389573	-1.9677067749	-0.2016557280
H	-1.6422956982	-1.5318892609	-1.9194758348	H	-6.4623540547	2.1376092686	-2.2352626187
H	-6.4557965154	2.1510473468	-2.1768476710	H	-4.6578781214	-0.6993063165	-4.9135727923
H	-3.0396243611	-1.1253947232	-3.4250864802	H	-6.4938347453	0.9763218426	-4.4552731872
H	-4.8135536432	-0.5754716493	-5.0618828905	C	-5.7385120820	0.9780094527	1.1067317579
H	-6.5821962609	1.0999452069	-4.4114701827	O	-6.5286696676	0.3516210197	1.6676852405
C	-5.7224354672	0.9269938467	1.0864045556	O	-3.6570252591	3.4548859457	2.7196235101
O	-6.5005802219	0.2763039281	1.6393924192	C	-4.0119231749	2.8864891432	1.7791657488
O	-3.7166997309	3.4287956382	2.7399231030	O	-6.4211560778	4.2542837655	-0.2563145742
C	-4.0443062172	2.8621965851	1.7871301340	C	-5.7030802061	3.3760644430	-0.0404284290
O	-6.4695115861	4.2119206135	-0.2012954613	H	-3.4731371177	3.0315275276	-0.4471574437
C	-5.7313724162	3.3417715950	-0.0157077355				
H	-3.4870438622	3.0302036809	-0.4443741461				
$TS_{\mathbf{1a}\rightarrow\mathbf{6a}}$				$TS_{\mathbf{1b}\rightarrow\mathbf{6b}}$			
Mn	-3.3116850936	2.3988995093	-0.0381108574	Mn	-3.3963209738	2.4491908138	-0.1832716594
C	-2.0571491629	-0.0165752542	-1.1634975518	C	-2.2431562618	0.0050163738	-1.3198666979
C	-1.0441554764	0.5392397871	0.8516341087	C	-1.0769003681	0.5865668113	0.5783329309
C	-0.2127161697	-0.5653283901	0.7961327340	C	-0.2926526272	-0.5393876205	0.4388696242
C	-0.3113457316	-1.4350293676	-0.2959347148	C	-0.5535423467	-1.3773103790	-0.6523194492
C	-1.2435151992	-1.1513708711	-1.2814752548	N	-1.5249014002	-1.1059370685	-1.5219184486
C	-4.7841127076	1.8603645492	-2.6333203865	C	-5.0602741972	1.8274344645	-2.6553184112
N	-3.7951419120	1.4629310638	-1.8074439668	N	-4.0150225334	1.4760202360	-1.8750109530
C	-3.0813271898	0.3557495336	-2.1388251012	C	-3.3421665297	0.3506473156	-2.2245709211
C	-3.3360782646	-0.3522590760	-3.3210904185	N	-3.6237541952	-0.4173288800	-3.2830351101

C	-4.3464052914	0.0733822838	-4.1691219026
C	-5.0912942410	1.2018183131	-3.8124556202
N	-1.9610555859	0.8313026248	-0.1006686427
H	-0.9870110070	1.2247433581	1.6865750529
H	0.4972915194	-0.7393925631	1.5973856609
H	0.3221688591	-2.3125932454	-0.3716337301
H	-1.3433409862	-1.8094691231	-2.1358264660
H	-5.3397130198	2.7352488347	-2.3208123344
H	-2.7485892165	-1.2257529342	-3.5754840904
H	-4.5542472368	-0.4642534556	-5.0885057563
H	-5.8982610158	1.5688041012	-4.4367141219
C	-4.7480072844	1.7675585421	0.7600511102
O	-5.7558376707	1.4731318868	1.2820021243
O	-2.3595588565	3.5146402601	2.5215914558
C	-2.7227435226	3.0765404080	1.5056835399
O	-4.2291764381	5.0887281933	-0.8499131914
C	-3.7595357394	4.0243044120	-0.5752627004
O	-1.1841850563	4.5855835918	-1.5930170908
H	-2.3760493702	3.9011050913	-0.9655474306
C	-0.4218251470	3.4703845188	-1.8560265288
H	0.6674909692	3.6305072555	-1.7824501751
H	-0.6614095872	2.6290155680	-1.1807325783
C	-0.6431813611	2.8997020153	-3.2578152346
F	-1.9439376974	2.8630910384	-3.6241400474
F	0.0012699005	3.6063196076	-4.2357685091
F	-0.1799588342	1.6152796703	-3.3522597715

C	-4.6470387902	-0.0470495939	-4.0532024661
C	-5.4114949758	1.0894552636	-3.7690324616
N	-2.0665583757	0.8883464954	-0.2991761143
H	-0.9279270968	1.2702863140	1.4040464606
H	0.4934389887	-0.7631993814	1.1513277250
H	0.0269670006	-2.2798484147	-0.8205999845
H	-5.6119722367	2.7119550670	-2.3621070094
H	-4.8690990202	-0.6724548574	-4.9131903222
H	-6.2496031753	1.3808243573	-4.3914364282
C	-4.7225946128	1.8082950737	0.8020922355
O	-5.6469041475	1.5114045115	1.4508059991
O	-2.1267771174	3.6660766590	2.1901183008
C	-2.6231727867	3.1924967711	1.2539406465
O	-4.4681018028	5.0702806291	-1.0111687346
C	-3.9834136488	4.0315027392	-0.7091489103
O	-1.4399155852	4.6476961409	-1.8709575789
H	-2.5972920753	3.8310982093	-1.2158365346
C	-0.4033257011	3.7848536485	-1.6098222249
H	0.5697334479	4.2741743366	-1.4284833034
H	-0.5985714738	3.1393839788	-0.7317243822
C	-0.1413336987	2.7928880499	-2.7420729269
F	-1.2691361794	2.2059036534	-3.2091355640
F	0.4612905348	3.3607428854	-3.8268996051
F	0.6809353752	1.7762967932	-2.3408741647

$TS_{1a \rightarrow 2a}$, closed shell			
Mn	-4.2497194616	1.9953186778	-0.3936890016
C	-3.0538508721	-0.5546783248	-1.0985132805
C	-1.8803827270	0.4602660383	0.6520483499
C	-0.9797226832	-0.5784269164	0.7226657628
C	-1.1199908019	-1.6654007895	-0.1669325076
C	-2.1607348285	-1.6478067408	-1.0701937080
C	-6.0245909510	0.8826312283	-2.5721762016
N	-4.9077979946	0.7284401034	-1.7962952445
C	-4.1850483437	-0.4360572317	-1.9749636334
C	-4.5554708277	-1.3953624406	-2.9386558936
C	-5.6715280751	-1.1998739048	-3.7239966852
C	-6.4292148977	-0.0237129745	-3.5210798296
N	-2.9042412627	0.5050548620	-0.2403744202
H	-1.8100201896	1.3042670109	1.3269315998
H	-0.1836501394	-0.5486177636	1.4580349175
H	-0.4286368520	-2.5008176287	-0.1365038737
H	-2.2973950915	-2.4748267177	-1.7569207306
H	-6.5941318599	1.7860777716	-2.4011235588
H	-3.9599625229	-2.2929717213	-3.0577552858
H	-5.9648693972	-1.9325144189	-4.4679026664
H	-7.3246643680	0.1770342705	-4.0992259460
C	-5.0062130494	1.7278176574	1.1715754028
O	-5.4821477596	1.6265918814	2.2405868346
O	-2.3083872170	4.0857865793	0.3632863468
C	-3.0669501268	3.2487402605	0.0450639973
O	-6.0919116647	4.1789987003	-1.1360888725
C	-5.3759333949	3.3048081602	-0.8445810736
C	-2.9192311028	2.6491091788	-2.9165143043
O	-2.1159748985	1.7851828016	-2.9596736925
O	-3.5097567767	3.6019253665	-3.2961820276

$TS_{1b \rightarrow 2b}$, closed shell			
Mn	-4.1415843338	2.2508576487	-0.7980799168
C	-3.1080484500	-0.3441425637	-1.5585241583
C	-1.7477636163	0.6194544225	0.0581333035
C	-0.9134401768	-0.4701280725	0.0089273353
C	-1.2477633525	-1.5025017988	-0.8951342738
N	-2.3283544234	-1.4457575541	-1.6551645123
C	-6.1638340289	1.1303372221	-2.7421806083
N	-4.9824155936	0.9780241701	-2.0851680969
C	-4.3098696488	-0.2038651408	-2.3217892221
N	-4.7213425391	-1.1638505873	-3.1815947292
C	-5.8564562076	-0.9643457095	-3.8295614991
C	-6.6389819559	0.1945351970	-3.6267877282
N	-2.8476677973	0.7291162646	-0.7326695265
H	-1.5599309073	1.4404513714	0.7387588164
H	-0.0376020834	-0.5331914256	0.6437445718
H	-0.6237819003	-2.3879209168	-0.9822631545
H	-6.7193272572	2.0353889923	-2.5312026358
H	-6.1769199043	-1.7368496953	-4.5234035776
H	-7.5800139023	0.3415598935	-4.1434471667
C	-5.0630874555	2.0147624905	0.6846672599
O	-5.6720788122	1.9119605428	1.6760449621
O	-2.2227406667	4.1956927964	0.3253589501
C	-2.9716881010	3.4180507306	-0.1111630641
O	-5.7030724508	4.5718082069	-1.7470015628
C	-5.0999855404	3.6476087759	-1.3769253099
C	-2.6473792457	2.8444076332	-3.1694402832
O	-2.5624715436	4.0313513473	-3.2181628017
O	-2.4379923577	1.7550111369	-3.5876390877

$TS_{1a \rightarrow 2a}$''			
Mn	-4.2686905479	1.9906283600	-0.4140562243

$TS_{1a \rightarrow 2a}$'''			
Mn	-4.2469588101	1.9925978011	-0.4283104087

C	-3.0590201149	-0.5380942658	-1.1438044528	C	-3.0646957134	-0.5758158838	-1.1196414211
C	-1.8367575463	0.4974992319	0.5610224667	C	-1.7819188873	0.5235183443	0.4958358034
C	-0.9219206540	-0.5276758141	0.6007450753	C	-0.8840016879	-0.5168467325	0.5636130451
C	-1.0725076375	-1.6181306988	-0.2859250859	C	-1.0820628659	-1.6522207234	-0.2509110349
C	-2.1475438384	-1.6156991702	-1.1474675304	C	-2.1794949299	-1.6720976332	-1.0858964844
C	-6.1420270057	0.8024421128	-2.4585257367	C	-6.0645351326	0.8427792607	-2.5345416675
N	-4.9774306712	0.6840876799	-1.7588293983	N	-4.9334773265	0.6886565355	-1.7894799038
C	-4.2311545290	-0.4541072402	-1.9670170055	C	-4.2333124380	-0.4873299441	-1.9496410348
C	-4.6308312690	-1.4340409867	-2.9008785933	C	-4.6538017274	-1.4776956345	-2.8598969710
C	-5.7970104761	-1.2753044298	-3.6170421475	C	-5.7943335044	-1.2893412916	-3.6128328795
C	-6.5788857306	-0.1221219937	-3.3769259809	C	-6.5192829411	-0.0911895786	-3.4361509575
N	-2.8930271661	0.5370449871	-0.3002223466	N	-2.8646676543	0.5360212226	-0.3314111358
H	-1.7518317229	1.3377477025	1.2380021147	H	-1.6586363196	1.3953244558	1.1243843696
H	-0.1038998519	-0.4861712626	1.3114582119	H	-0.0427508617	-0.4510566668	1.2444814999
H	-0.3678241366	-2.4426197406	-0.2796176791	H	-0.3945037298	-2.4903441690	-0.2167304556
H	-2.3000980284	-2.4461789380	-1.8266680030	H	-2.3660301134	-2.5331557820	-1.7168035289
H	-6.7278397690	1.6879260942	-2.2483832601	H	-6.6118203556	1.7621153407	-2.3764143153
H	-4.0184626912	-2.3156708855	-3.0500839223	H	-4.0775737782	-2.3894778536	-2.9663621995
H	-6.1126213284	-2.0223903860	-4.3373237898	H	-6.1264823056	-2.0439455388	-4.3175804472
H	-7.5145784698	0.0451994063	-3.8992479729	H	-7.4272457059	0.1066089589	-3.9951297744
C	-5.2604714411	1.7034644896	1.0057273385	C	-5.2279853672	1.6474789623	0.9880437693
O	-5.9254676984	1.5960154832	1.9677910760	O	-5.8869889401	1.5011111596	1.9486558639
O	-2.4906793734	4.0317200372	0.7653497156	O	-2.5126268961	4.0403159968	0.8059344136
C	-3.1860850103	3.2123763321	0.3033310055	C	-3.1927716175	3.2228670047	0.3176600259
O	-5.8228056116	4.2524354254	-1.5052164740	O	-5.8549410722	4.2612984827	-1.4240349493
C	-5.2163717338	3.3471974822	-1.0799508207	C	-5.2209533532	3.3558829544	-1.0394458865
C	-2.5940493090	2.7322890851	-2.7827549808	C	-2.6649493599	2.7940431831	-2.7837335609
O	-2.3858438535	1.6447110252	-3.1860814729	O	-1.5641123107	2.8038228726	-2.3481441505
O	-2.5387140109	3.9144889712	-2.7546915767	O	-3.4949384612	2.9031005593	-3.6193254857

[1] Schneider, W.; Diller, W.; *Ullmann's Encyclopedia of Industrial Chemistry*; Wiley-VCH: Weinheim, **2005**.

[2] Wilhelm, D. J.; Simbeck, D. R.; Karp, A. D.; Dickenson, R. L.; *Fuel Process. Tech.*, **2001**, *71*, 139-148.

[3] Sunley, G. J.; Watson, D. J.; *Cat. Today*, **2000**, *58*, 293-307.

[4] Dry, M. E.; *Appl. Cat. A*, **1996**, *138*, 319-344.

[5] Reviews: (a) Costentin, C.; Robert, M.; Savéant, J-M.; *Chem. Soc. Rev.*, **2013**, *42*, 2423-2436; (b) Windle, C. D.; Perutz, R. N.; *Coord. Chem. Rev.*, **2012**, *256*, 2562-2570; (c) Finn, C.; Schnittger, S.; Yellowlees, L. J.; Love, J. B.; *Chem. Commun.* , **2012**, *48*, 1392-1399; (d) Benson, E. E.; Kubiak, C. P.; Sathrum, A. J.;Smieja, A. J.; *Chem. Soc. Rev.*, 2009, **38**, 89-99.

[6] Fe-porphyrins: (a) Bhugun, I.; Lexa, D.; Savéant, J. M.; *J. Phys. Chem.*, **1996**, *100*, 19981-19985; (b) Bhugun, I.; Lexa, D.; Savéant, J. M.; *J. Am. Chem. Soc.* **1994**, *116*, 5015-5016; (c) Bhugun, I.; Lexa, D.; Savéant, J. M.; *J. Am. Chem. Soc.* **1996**, *118*, 1769-1776; (d) Costentin, C.; Drouet, S.; Robert, M.; Savéant, J. M.; *Science*, **2012**, *338*, 90–94.

[7] Co and Ni heterocycles and macrocycles: (a) Fisher, B. J.; Eisenberg, R.; *J. Am. Chem. Soc.*, **1980**, *102*, 7361–7363; (b) Lieber, C. M.; Lewis, N. S.; *J. Am. Chem. Soc.*, **1984**, *106*, 5033-5034; (c) Beley, M.; Collin, J.-P.; Ruppert, R.; Sauvage, J.-P.; *J. Chem. Soc., Chem. Commun.*, **1984**, 1315-1316; (d) Froehlich, J. D.;Kubiak, C. P.; *Inorg. Chem.*, **2012**, *51*, 3932–3934; (e) Tinnemans, A. H. A.; Koster, T. P. M.; Thewissen, D. H. M. W.; Mackor, A.; *Recl. Trav. Chim. Pays-Bas.* **1984**, *103*, 288-295.

[8] Phosphine complexes: (a) Szymaszek, A.; Pruchnik, F. P.; *J. Organomet. Chem.*, **1989**, *376*, 133-140; (b) DuBois, M. R.; DuBois, D. L.; *Acc. Chem. Res.*, **2009**, *42*, 1974-1982.

[9] Complexes with bipyridine and related ligands: (a) Hawecker, J.; Lehn, J. –M.; Ziessel, R.; *J. Chem. Soc., Chem. Commun.*, **1984**, 328-330; (b) Patrick Sullivan, B.; Bolinger, C. M.; Conrad, D.; Vining, W. J.; Meyer, T. J.; *J. Chem. Soc., Chem. Commun.*, **1985**, 1414-1416; (c) O'Toole, T. R.; Margerum, L. D.; Westmoreland, T. D.; Vining, W. J.; Murray, R. W.; Meyer, T. J.; *J. Chem. Soc., Chem. Commun.*, **1985**, 1416-1417; (d) Smieja, J. M.; Kubiak, C. P.; *Inorg. Chem.* **2010**, *49*, 9283-9289; (e) Bourrez, M.; Molton, F.; Chardon-Noblat, S.; Deronzier, A.; *Angew. Chem., Int. Ed.* **2011**, *50*, 9903-9906; (f) Smieja, J. M.; Sampson, M. D.; Grice, K.A.; Benson, E.E.; Froehlich, J.D.; Kubiak, C.P.; *Inorg. Chem.*, **2013**, *52*, 2484-2491; (g) Bruce, M. R. M.; Megehee, E.; Sullivan, B. P.; Thorp, H.; O'Toole, T. R.; Downard, A.; Meyer, T. J.; *Organometallics* **1988**, *7*, 238-240; (h) Sampson, M.D.; Nguyen, A. D.; Grice, K. A.; Moore, C. E.; Rheingold, A. L.; Kubiak, C. P., *J. Am. Chem. Soc.* **2014**, *136*,

5460-5471; (i) Zeng, Q.; Tory, J.; Hartl, F.; *Organometallics* **2014**, *33*, 5002-5008.

[10] (a) Smieja, J. M.; Benson, E. E.; Kumar, B.; Grice, K. A.; Seu, C. S.; Miller, A. J. M.; Mayer, J. M.; Kubiak, C. P.; *Proc. Natl. Acad. Sci. U. S. A.* **2012**, *109*, 15646-15650; (b) Benson, E. E.; Sampson, M. D.; Grice, K. A.; Smieja, J. M.; Froehlich, J. D.; Friebel, D.; Keith, J. A.; Carter, E. A.; Nilsson, A.; Kubiak, C. P.; *Angew. Chem., Int. Ed.* **2013**, *52*, 4841-4844; (c) Sampson, M. D.; Froehlich, J. D.; Smieja, J. M.; Benson, E. E.; Sharp, I. D.; Kubiak, C. P.; *Energy Environ. Sci.*, **2013**, *6*, 3748-3755.

[11] Wong, K.–Y.; Chung, W.-H.; Lau, C.-P.; *J. Electroanal. Chem.* 1998, **453,** 161-169.

[12] Agarwal, J.; Sanders, B. C.; Fujita, E.; Schaefer, H. F.; Harrop, T. C.; Muckerman, J. T.; *Chem. Commun.*, **2012**, *48*, 6797-6799.

[13] Keith, J. A.; Grice, K. A.; Kubiak, C. P.; Carter, E. A.; *J. Am. Chem. Soc.*, **2013**, *135*, 15823–15829.

[14] Becke, A. D.; *J. Chem. Phys.*, **1993**, *98*, 5648-5652.

[15] Grimme, S.; Antony, J.; Ehrlich, S.; Krieg, H.; *J. Chem. Phys.*, **2010**. *132*, 154104-154119.

[16] Jaguar; Schrödinger, LLC: New York, NY, 2012.

[17] Marten, B.; Kim, K.; Cortis, C.; Friesner, R. A.; Murphy, R. B.; Ringnalda, M. N.; Sitko, D.; Honig, B.; *J. Phys. Chem.*, **1996**, *100*, 11775-11788.

[18] (a) Krishnan, R.; Binkley, J. S.; Seeger, R.; Pople, J.A. *J. Chem. Phys.*, **1980**, *72*, 650-654 ; (b) Clark, T.; Chandrasekhar, J.; Spitznagel, G. W.; Schleyer, P. V. R *J. Comput. Chem.* **1983**, *4*, 294-301.

[19] (a) Melius, C. F.; Goddard, W. A. III, *Phys. Rev. A* **1974**, *10*, 1528-1540; (b) Melius, C. F.; Olafson, B. D.; Goddard, W. A. III; *Chem. Phys. Lett.*, **1974**, *28*, 457-462.

[20] Hay, P. J.; Wadt, W. R.; *J. Chem. Phys.* **1985**, *82*, 270-283.

[21] Martin, J. M. L.; Sundermann, A.; *J. Chem. Phys.* **2001**, *114*, 3408-3420.

[22] McQuarrie, D. A. *Statistical Mechanics*; University Science Books: Sausalito, CA, **2000.**

[23] Isse, A. A.; Gennaro, A.; *J. Phys. Chem. B* **2010**, *114*, 7894-7899. Treating an electron at SCE as a reactant yields an effective free energy (relative to an electron at rest in vacuum, the reference state of QM calculations) of (23.06 kcal/mol/eV * -4.42 V * 1e$^-$) = -102.0 kcal/mol.

Chapter IV

Mn Catalyst with Pendant Alcohol Reduces CO_2 80,000 Times Faster

Y.C. Lam; R. J. Nielsen; H. B. Gray; W. A. Goddard, III

Abstract: Previously (see Chapter III) we showed that substituting bipyrimidine (bpymd) for bipyridine (bpy) in $[(L)Mn(CO)_3]^-$ reduced turn-on overpotential at the expense of turnover frequency (TOF). Here we present computational evidence (B3LYP-d3 / 6-311G**++, LACV3P++ with 2 *f*-functions for Mn / PBF implicit solvation in MeCN) that appending a single alcohol moiety to the bipyrimidine ligand increases TOF ca. 80,000 times, while preserving very low turn-on overpotential and improving CO selectivity over H_2. Crucially, the appended alcohol and solution trifluoroethanol (TFEH) work in concert, the external TFEH acidifying the appended alcohol by stabilizing the incipient alkoxide through hydrogen bonding. This synergistic effect reduces (by 6.8 kcal mol^{-1} relative to simple bipyrimidine) the barrier for dehydroxylation of $[(L)Mn(CO)_3(CO_2H)]^-$.

Introduction

The reduction of carbon dioxide (CO_2) to such useful chemicals as carbon monoxide (CO), formic acid, or methanol (MeOH) invariably couples the gain of electrons to the gain of protons and/or loss of base. As a result, (electro)catalytic CO_2 reduction either requires or is significantly accelerated by the presence of a Brønsted acid.[1-4]

This observation has given rise to attempts to further enhance catalytic activity by appending Brønsted acidic sites to the catalyst. This strategy has been successfully employed in catalysts that evolve and/or oxidize H_2, for example, metal phosphine complexes with pendant proton relays such as amines.[5-16] For electrochemical CO_2 reduction, the only (to our knowledge) catalysts to successfully employ this strategy are the Fe tetraphenylporphyrin catalysts "*bearing prepositioned phenol functionalities*" reported by Savéant and co-workers.[17-19] Initially, these pendant phenols were conceived as proton sources at very high effective concentrations, facilitating proton transfer and proton-dependent dehydroxylation.[17, 19] Later investigations indicated that these pendant phenol groups also serve to stabilize the initial CO_2 adduct by hydrogen bonding and/or protonation, thereby increasing the rate of CO_2 binding.[18, 19]

Using DFT methods, we previously predicted that the turn-on overpotential for trifluoroethanol (TFEH)-mediated CO_2 reduction to CO by $[(bpymd)Mn(CO)_3]^-$ (bpymd = bipyrimidine) is < 0.1 V (see Chapter III). Its catalytic activity, however, was predicted to be ca. 40 times lower than its bipyridine analog, which experimental studies had shown displays turnover frequencies (TOFs) of up to 5000 s^{-1}.[3, 20] Here, we demonstrate using the same methods that appending an alcohol functionality to bpymd increases TOF by up to

80,000 times, while introducing complexities, not seen with the parent system, that call for careful catalyst design.

Results and Discussions

As shown in Scheme 1 and Table 1, the pendant alcohol in catalyst **1t** serves two important functions.

(1) CO_2 coordination to $[(L)Mn(CO)_3]^-$ (Table 1, entries 2-3) becomes substantially less endergonic (by 5.1 kcal mol^{-1}) and somewhat more facile ($\Delta G^{\ddagger}$ decreases by 1.9 kcal mol^{-1}), because the pendant alcohol hydrogen bonds strongly to the coordinated CO_2 in complex **2t** and less strongly to the bent CO_2 fragment in transition state $TS_{\mathbf{1t\rightarrow 2t}}$ (Figure 1). Stabilization of the CO_2 adduct and facilitation of its formation were also observed in Constentin and Savéant's phenol-appended Fe porphyrins. In those catalysts, for which the TOF-determining step is CO_2 binding, this stabilization directly improved TOFs.[18, 19]

(2) Since the alcohol-mediated dehydroxylation of $[(L)Mn(CO)_3(CO_2H)]^-$ (**4**) to $[(L)Mn(CO)_4]^0$ (**5**) is the TOF-determining step in these reactions, the more significant function is that the pendant alcohol substantially lowers the dehydroxylation barrier of **4t** vis-à-vis **4b**. In the dehydroxylation transition states, the C-O bond (> 2.1 Å) is almost completely broken, and the dissociated OH^- is stabilized by hydrogen bonding to an alcohol. This hydrogen bonding lengthens the alcohol H-O bond (Figure 2, H32-O31)

and increases electron density on the alcohol O, resulting in an incipient alkoxide. (With very strong hydrogen bonding, a proton is transferred from the alcohol to OH^-, forming a water-alkoxide complex.) For this reason, a more acidic alcohol, whose conjugate alkoxide is more stable, leads to a more stable $TS_{\mathbf{3}\rightarrow\mathbf{5}}$.

In $TS_{\mathbf{4t}\rightarrow\mathbf{5t}}$ (Figure 2 right), an external TFEH increases the acidity of the appended alcohol by hydrogen bonding to and hence stabilizing the incipient alkoxide. This stabilizes the dehydroxylation TS, resulting in a significantly lower (by 6.7 kcal mol^{-1}) $\Delta G^{\ddagger}$ for the dehydroxylation of **4t** when compared with **4b**. An analogous transition state for **4b** involving two molecules of (external) TFEH is likewise stabilized—the electronic component of $\Delta G^{\ddagger}$ decreases by ca. 4.3 kcal mol^{-1}—but this effect is offset, at least at low TFEH concentrations,[1] by the entropic penalty of incorporating an additional TFEH molecule into the transition state. As noted in Table 1 (footnote f), the net result is that $\Delta G^{\ddagger}$ is not significantly lower. At higher TFEH concentrations, however, $\Delta S^{\ddagger}$ increases, and this pathway (in which two TFEH molecules act in concert) predominates.

[1] The dimerization constant for TFEH in CCl_4 is 0.875 M^{-1}, and the "multimerization" constant is 3.03 M^{-1} (298 K, *Spec. Chim. Acta. A* **2000**, *57*, 2763-2774). This suggests that the entropic cost for bringing two TFEH molecules is overestimated, since almost half exists as dimer at 1 M.

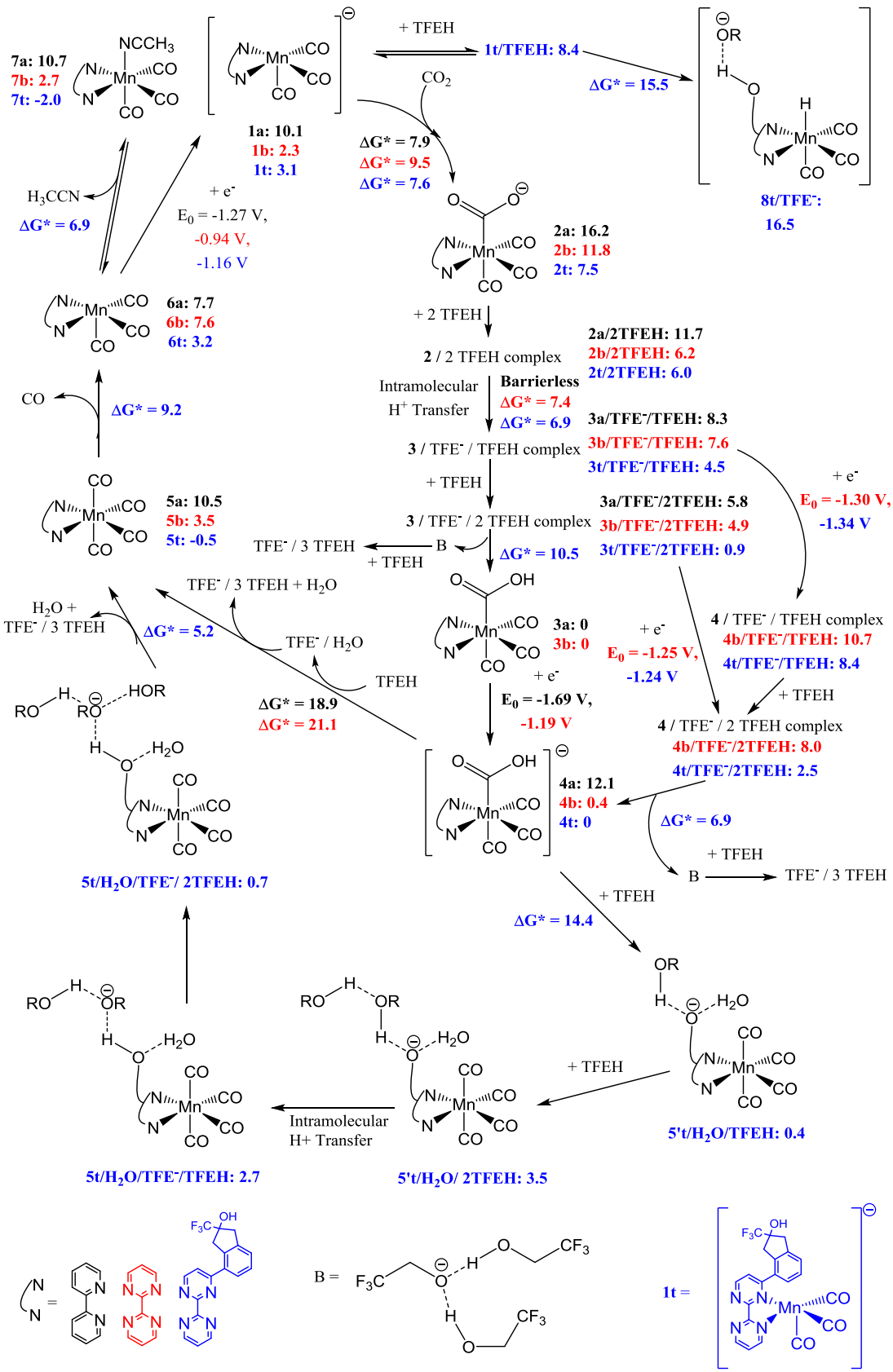
7a: 10.7
7b: 2.7
7t: -2.0
NCCH3
1a: 10.1
1b: 2.3
1t: 3.1
+ TFEH
1t/TFEH: 8.4
ΔG* = 15.5
8t/TFE-:
16.5
CO2
ΔG* = 7.9
ΔG* = 9.5
ΔG* = 7.6
2a: 16.2
2b: 11.8
2t: 7.5
H3CCN
ΔG* = 6.9
+ e-
E0 = -1.27 V,
-0.94 V,
-1.16 V
6a: 7.7
6b: 7.6
6t: 3.2
+ 2 TFEH
2 / 2 TFEH complex
2a/2TFEH: 11.7
2b/2TFEH: 6.2
2t/2TFEH: 6.0
Intramolecular
H+ Transfer
Barrierless
ΔG* = 7.4
ΔG* = 6.9
3a/TFE-/TFEH: 8.3
3b/TFE-/TFEH: 7.6
3t/TFE-/TFEH: 4.5
3 / TFE- / TFEH complex
CO
ΔG* = 9.2
+ TFEH
3a/TFE-/2TFEH: 5.8
3b/TFE-/2TFEH: 4.9
3t/TFE-/2TFEH: 0.9
+ e-
E0 = -1.30 V,
-1.34 V
5a: 10.5
5b: 3.5
5t: -0.5
3 / TFE- / 2 TFEH complex
TFE- / 3 TFEH
B
+ TFEH
ΔG* = 10.5
TFE- / 3 TFEH + H2O
H2O +
TFE- / 3 TFEH
ΔG* = 5.2
TFE- / H2O
TFEH
3a: 0
3b: 0
+ e-
E0 = -1.25 V,
-1.24 V
4 / TFE- / TFEH complex
4b/TFE-/TFEH: 10.7
4t/TFE-/TFEH: 8.4
+ e-
E0 = -1.69 V,
-1.19 V
ΔG* = 18.9
ΔG* = 21.1
4 / TFE- / 2 TFEH complex
4b/TFE-/2TFEH: 8.0
4t/TFE-/2TFEH: 2.5
4a: 12.1
4b: 0.4
4t: 0
ΔG* = 6.9
+ TFEH
B
TFE- / 3 TFEH
5t/H2O/TFE-/ 2TFEH: 0.7
+ TFEH
ΔG* = 14.4
5't/H2O/TFEH: 0.4
+ TFEH
Intramolecular
H+ Transfer
5t/H2O/TFE-/TFEH: 2.7
5't/H2O/ 2TFEH: 3.5
B =
1t =

Scheme 1: Comparison between catalytic cycles for CO_2 reduction by **1b** (bpymd, in red) and **1t** (bpymd with pendant alcohol, bpymd-OH in blue). Gibbs free energies (kcal mol^{-1}), relative to resting state **3** (for L = bpy or bpymd) or **4** (for L = bpymd-OH), are calculated at -1.17 V vs SCE, i.e., at zero applied overpotential under standard conditions (half reaction is in Table 1, entry 1, see Chapter III for explanation), and reported in black for L = bpy, in red for L = bpymd and in blue for bpymd-OH. (Data for L = bpy are included for comparison only, and are not discussed in the text.) Activation free energies are denoted ΔG^*, and reported in kcal mol^{-1} relative to preceding intermediate. Standard reduction potentials are reported in V vs. SCE. All reagents are in their standard states (25°C, 1 atm CO_2 and CO, 1 M for all reagents in MeCN).

Table 1: ΔG, $\Delta G^{\ddagger}$, and standard reduction potentials for reactions in Scheme 1.

		ΔG [a]	$\Delta G^{\ddagger}$ [a]	E^{o} [b]
1	CO_2 + 8 TFEH + 2 e^- → CO + H_2O + 2 TFE^- / 3 TFEH	N/A	N/A	-1.17
2	**1b** + CO_2 → **2b**	9.5 [c]	9.5 [c]	N/A
3	**1t** + CO_2 → **2t**	4.4	7.6	N/A
4	**2b** + 2 TFEH → **2b** / 2 TFEH [d]	-5.5	N/A [e]	N/A
5	**2t** + 2 TFEH → **2t** / 2 TFEH [d]	-1.6	N/A [e]	N/A
6	**2b** / 2 TFEH complex → **3b** / TFE^- / TFEH [d]	1.4	7.4	N/A
7	**2t** / 2 TFEH complex → **3t** / TFE^- / TFEH [d]	-1.5	6.9	N/A
8	**3b** / TFE^- / TFEH + TFEH → **3b** / TFE^- / 2 TFEH [d]	-1.5	N/A [e]	N/A
9	**3t** / TFE^- / TFEH + TFEH → **3t** / TFE^- / 2 TFEH [d]	-3.6	N/A [e]	N/A
10	**3b** / TFE^- / 2 TFEH → **3b** + TFE^- / 2 TFEH [d]	-2.9		N/A
11	**3t** / TFE^- / 2 TFEH → **3t** + TFE^- / 2 TFEH [d]	5.1	10.5	N/A
12	**3b** + e^- → **4b**	N/A	N/A	-1.19
13	**3t** + e^- → **4t**	N/A	N/A	-1.05
14	**3b** / TFE^- / TFEH + e^- → **3b** / TFE^- / TFEH [d]	N/A	N/A	-1.30
15	**3t** / TFE^- / TFEH + e^- → **3t** / TFE^- / TFEH [d]	N/A	N/A	-1.34
16	**4b** / TFE^- / TFEH + TFEH → **4b** / TFE^- / 2 TFEH [d]	-2.7	N/A [e]	N/A
17	**4t** / TFE^- / TFEH + TFEH → **4t** / TFE^- / 2 TFEH [d]	-5.8	N/A [e]	N/A
18	**4b** / TFE^- / 2 TFEH → **4b** + TFE^- / 2 TFEH [d,f]	-4.3		N/A
19	**4t** / TFE^- / 2 TFEH → **4t** + TFE^- / 2 TFEH [d]	0.8	6.9	N/A
20	**4b** + TFEH → **5b** + TFE^- / H_2O [d]	12.8	21.1	N/A
21	**4t** + TFEH → **5t' /** TFEH / H_2O [d,g]	0.4	14.4	N/A
22	**5t' /** TFEH / H_2O + TFEH → **5t'** / H_2O / 2 TFEH [d,g]	3.2	N/A [e]	N/A
23	**5t'** / H_2O / 2 TFEH → **5t** / H_2O / TFE^- / TFEH [d]	-0.8		N/A
24	**5t** / H_2O / TFE^- / TFEH + TFEH → **5t** / H_2O / TFE^- / 2 TFEH [d]	-2.0	N/A [e]	N/A
25	**5t** / H_2O / TFE^- / 2 TFEH → **5t** / TFE^- / 2 TFEH [d] + H_2O	0.7		N/A
26	**5t** / TFE^- / 2 TFEH → **5t** + TFE^- / 2 TFEH [d]	1.3	5.2	N/A

27	**5b** → **6b** + CO	4.1		N/A
28	**5t** → **6t** + CO	3.7	9.2	N/A
29	**7b** → **6b** + MeCN	4.9		N/A
30	**7t** → **6t** + MeCN	5.2	6.9	N/A
31	**6b** + e^- → **1b**	N/A	N/A	-0.94
32	**6t** + e^- → **1t**	N/A	N/A	-1.16
33	**1b** + 2 TFEH → **8b** + TFE^- / TFEH [d]	1.8	19.4	N/A
34	**1t** + TFEH → **1t** / TFEH [d]	-2.5	N/A	N/A
	1t / TFEH complex + TFEH → **8t** / TFE^- [d]	8.1	15.5	N/A

[a] In kcal mol^{-1}

[b] V vs SCE

[c] The reverse reaction appears to be barrierless on the free energy surface, because the transition state has a lower zero-point energy (ZPE) than **2b**, offsetting the higher potential energy of the former

[d] X / Y / Z denotes a hydrogen bonded complex consisting of fragment X, Y, and Z; for example, **2b** / 2 TFEH (entry 4) consists of 2 TFEH molecules hydrogen bonded to **2b**; similarly, **3b** / TFE^- / TFEH (entry 6) consists of **3b** hydrogen bonded to TFE^-, which is in turn hydrogen bonded to a TFEH molecule

[e] TFEH association events are assumed not to be rate-limiting, although owing to loss of entropy, they are not barrierless; indeed, some association events, where this loss of entropy exceeds the exothermicity of hydrogen bond formation, are endergonic (entry 22).

[f] The same transformation can be performed via a transition state involving two TFEH molecules; at 1 M TFEH, the $\Delta G^{\ddagger}$ is similar, within the uncertainty of the method

[g] **t'**: the pendant alcohol is deprotonated

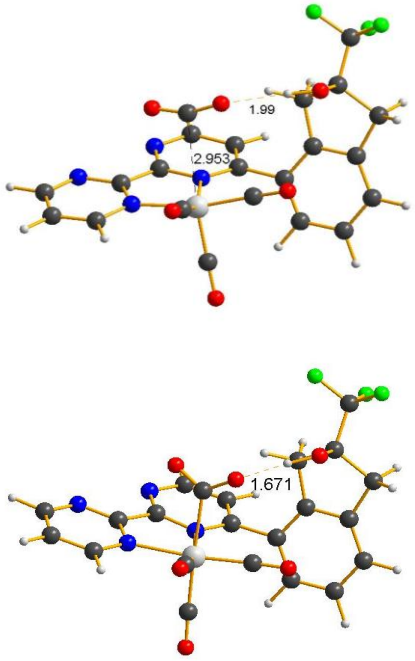

Figure 1: Hydrogen bond between the pendant alcohol and the CO_2 fragment in the TS for CO_2 addition to **1t** (top) and in CO_2 adduct **2t** (bottom).

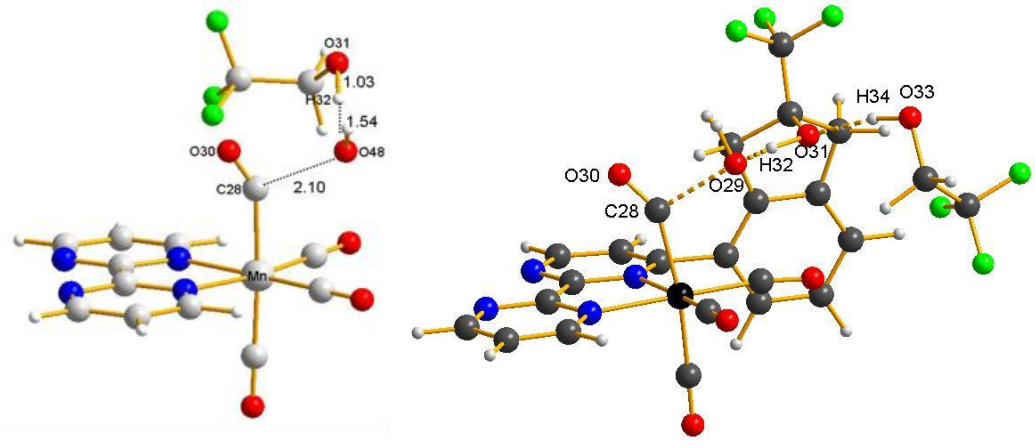

Figure 2: Optimized transition states for dehydroxylation of $[(L)Mn(CO)_3(CO_2H)]^-$ (3'). (Left) $TS_{3'b \rightarrow 5b}$, C28-O29: 2.10 Å, O29-H32: 1.54 Å, H32-O31: 1.03 Å. (Right) $TS_{3't \rightarrow 5t'/H2O/TFEH}$, C28-O29: 2.12 Å, O29-H32: 1.30 Å, H32-O31: 1.14 Å, O31-H34: 1.65 Å, H34-O33: 1.00 Å.

An attractive feature of **1t**-catalyzed electrochemical CO_2 reduction is high CO selectivity under operating conditions. Indeed, **1t** is predicted to have ca. 6-fold higher CO selectivity, defined as the ratio of CO production to H_2 production, than **1b**. This is because $\Delta G^{\ddagger}$ (**1t** → **5t'**/TFEH/H_2O) - $\Delta G^{\ddagger}$ (**1t** → **8t' /** TFEH) = -1.7 kcal mol^{-1}, compared with $\Delta G^{\ddagger}$ (**1b** → **5b**) - $\Delta G^{\ddagger}$ (**1b** → **8b**) = -0.6 kcal mol^{-1}, as calculated at zero overpotential and standard concentrations (Scheme 1). (Selectivity under operating conditions is greater than suggested by the numbers here, because the low concentrations of H_2O and TFE^- / 3 TFEH shift the equilibrium between **1** and **4** towards **4**.) The large improvement in the kinetics of **4** dehydroxylation, and hence of CO production, more than offsets the increase in rates of H_2 production via protonation of **1**.

In CO_2 reduction catalyzed by **1t**, the pendant alcohol needs to be regenerated by protonation and removal of hydrogen bonded species such as TFE^- / 2 TFEH, leading to complexities not seen with the catalytic cycle of **1b**. For example, the dehydroxylation of **4t** generates **5t'** / H_2O / TFEH (Table 1, entry 21), in which the pendant alcohol is deprotonated. H_2O and TFEH are hydrogen bonded to this pendant alkoxide. The pendant alcohol is regenerated through a sequence involving TFEH association, intramolecular proton transfer, and dissociation of H_2O and TFE^- / 2 TFEH (Table 1, entries 22-26, see also Scheme 1), finally generating **5t**. Dissociation of TFE^- / 2 TFEH is endothermic because a relatively strong hydrogen bond between an oxyanion and an alcohol is broken. Consequently, such dissociations, as well as intramolecular proton transfers, may involve substantial activation energies and introduce significant kinetic barriers to pendant alcohol regeneration. Careful ligand design can mitigate these barriers, and our calculations predict

that pendant alcohol regeneration is not rate-limiting in **1t**-catalyzed CO_2 reduction (Scheme 1).

Conclusions

Using DFT methods, a pendant alcohol has been shown to increase rates of CO_2 reduction ca. 80,000-fold vis-à-vis $[(bpymd)Mn(CO)_3]^-$ (**1b**). In the TOF-determining dehydroxylation TS, the dissociating OH^- is stabilized by hydrogen bonding to the pendant alcohol, a stabilization enhanced by an external TFEH hydrogen bonding to the incipient pendant alkoxide. This mode of TS stabilization suggests that a similar acceleration may be observed by substituting TFEH with a diol, with one alcohol functionality hydrogen bonding directly to the dissociating OH^- while the other, located at a suitable distance, hydrogen bonds to the incipient alkoxide. This approach obviates the need for catalyst elaboration with a pendant alcohol and should prove more amenable to experimental demonstration.

Acknowledgements

Yan Choi Lam, who performed the calculations and data analysis, was supported by the National Science Foundation (NSF) through the Centers for Chemical Innovation (CCI): Solar Fuels grant CHE-1305124, as was Prof. Harry B. Gray. Dr. Robert J. Nielsen and Prof. William A. Goddard, III, who developed the computational methods required for the calculations, are supported by the Joint Center for Artificial Photosynthesis, a DOE Energy Innovation Hub, supported through the Office of Science of the U.S. Department of Energy under Award Number DE-SC0004993.

Computational Methods

Density functional theory (DFT) calculations for geometry optimizations, electronic energy, solvation energy, and vibrational frequencies were performed using the (U)B3LYP hybrid exchange-correlation functional[21] with the D3 dispersion correction,[22] as implemented in the Jaguar software version 7.9.[23] Solvation effects were modeled using the Poisson-Boltzmann continuum (PBF) approximation[24] for acetonitrile (ε = 37.5, r = 2.18).

For all new species, i.e., those not carried over from Chapter III, geometry optimizations were performed in the gas phase (for MeCN) or in acetonitrile (all other species, including transition states) using the 6-31G**++ basis set on organics.[25, 26] For Mn the 1s, 2s, and 2p core electrons were replaced with the *ab initio* angular momentum projected effective core potential (ECP) of Melius and Goddard[27, 28] using the parameters and 3-ζ valence functions optimized by Hay and Wadt (LACV3P++).[29]

For solvation calculations, default van der Waals' radii were used during optimization on all atoms. A set of non-standard van der Waals' radii on anionic O atoms (2.0 Å in carboxylates, 2.2 Å in alkoxides) and protic (O-bonded) H atoms (0.75 Å) were previously found to correctly predict pK_a's for various neutral organic oxy-acids (e.g., phenol) and ΔG_{solv}'s for their conjugate bases (e.g., phenoxide; see Supporting Information in Chapter III). Single-point energy calculations including solvation with these non-standard van der Waals' radii were performed, using the 6-311G**++/LACV3P++ basis sets, the latter augmented with two *f*-functions.[30]

Vibrational frequencies were obtained with the 6-31G**++/LACV3P++ basis sets. Most optimized ground-state structures had no imaginary frequency, and most optimized transition state structures had one; a few had additional weak (between 50*i* and 0 cm^{-1}) imaginary frequencies arising from the rotation of loosely-bound solvent molecules.

Thermodynamic parameters were calculated using the harmonic oscillator, ideal gas, and rigid rotor approximations;[23] in computing vibrational entropies, all vibrations lower than 50 cm^{-1} that were not associated with the reaction coordinate of a transition state were replaced with 50 cm^{-1} to avoid spurious fluctuations in entropy arising from low frequency modes. Standard reduction potentials are reported versus the standard calomel electrode (SCE, absolute potential -4.42 V).[31]

References

1. Bourrez, M., et al., *Mn(bipyridyl)(CO)$_3$Br : An Abundant Metal Carbonyl Complex as Efficient Electrocatalyst for CO2 Reduction.* Angewandte Chemie-International Edition, 2011. **50**(42): p. 9903-9906.
2. Bhugun, I., D. Lexa, and J.M. Saveant, *Catalysis of the electrochemical reduction of carbon dioxide by iron(O) porphyrins: Synergystic effect of weak Bronsted acids.* Journal of the American Chemical Society, 1996. **118**(7): p. 1769-1776.
3. Smieja, J.M., et al., *Manganese as a Substitute for Rhenium in CO_2 Reduction Catalysts: The Importance of Acids.* Inorganic Chemistry, 2013. **52**(5): p. 2484-2491.
4. Wong, K.Y., W.H. Chung, and C.P. Lau, *The effect of weak Bronsted acids on the electrocatalytic reduction of carbon dioxide by a rhenium tricarbonyl bipyridyl complex.* Journal of Electroanalytical Chemistry, 1998. **453**(1-2): p. 161-169.
5. Wilson, A.D., et al., *Hydrogen Oxidation and Production Using Nickel-Based Molecular Catalysts with Positioned Proton Relays.* Journal of the American Chemical Society, 2005. **128**(1): p. 358-366.
6. Helm, M.L., et al., *A Synthetic Nickel Electrocatalyst with a Turnover Frequency Above 100,000 s^{-1} for H_2 Production.* Science, 2011. **333**(6044): p. 863-866.
7. Wiese, S., et al., *[$Ni((P_2N_2^{Ph})_2](BF_4)_2$ as an Electrocatalyst for H_2 Production.* Acs Catalysis, 2012. **2**(5): p. 720-727.
8. Raugei, S., et al., *The Role of Pendant Amines in the Breaking and Forming of Molecular Hydrogen Catalyzed by Nickel Complexes.* Chemistry-a European Journal, 2012. **18**(21): p. 6493-6506.
9. O'Hagan, M., et al., *Proton Delivery and Removal in $[Ni((P_2N_2^R)]^{2+}$ Hydrogen Production and Oxidation Catalysts.* Journal of the American Chemical Society, 2012. **134**(47): p. 19409-19424.
10. Stewart, M.P., et al., *High Catalytic Rates for Hydrogen Production Using Nickel Electrocatalysts with Seven-Membered Cyclic Diphosphine Ligands Containing One Pendant Amine.* Journal of the American Chemical Society, 2013. **135**(16): p. 6033-6046.
11. Fernandez, L.E., S. Horvath, and S. Hammes-Schiffer, *Theoretical Design of Molecular Electrocatalysts with Flexible Pendant Amines for Hydrogen Production and Oxidation.* Journal of Physical Chemistry Letters, 2013. **4**(3): p. 542-546.
12. Yang, J.Y., et al., *Two Pathways for Electrocatalytic Oxidation of Hydrogen by a Nickel Bis(diphosphine) Complex with Pendant Amines in the Second Coordination Sphere.* Journal of the American Chemical Society, 2013. **135**(26): p. 9700-9712.
13. Lense, S., et al., *A proton channel allows a hydrogen oxidation catalyst to operate at a moderate overpotential with water acting as a base.* Chemical Communications, 2014. **50**(7): p. 792-795.
14. Franz, J.A., et al., *Conformational Dynamics and Proton Relay Positioning in Nickel Catalysts for Hydrogen Production and Oxidation.* Organometallics, 2013. **32**(23): p. 7034-7042.

15. Dutta, A., et al., *Minimal Proton Channel Enables H_2 Oxidation and Production with a Water-Soluble Nickel-Based Catalyst.* Journal of the American Chemical Society, 2013. **135**(49): p. 18490-18496.
16. Das, P., et al., *Controlling proton movement: electrocatalytic oxidation of hydrogen by a nickel(II) complex containing proton relays in the second and outer coordination spheres.* Dalton Transactions, 2014. **43**(7): p. 2744-2754.
17. Costentin, C., et al., *A Local Proton Source Enhances CO_2 Electroreduction to CO by a Molecular Fe Catalyst.* Science, 2012. **338**(6103): p. 90-94.
18. Costentin, C., et al., *Ultraefficient homogeneous catalyst for the CO_2-to-CO electrochemical conversion.* Proceedings of the National Academy of Sciences of the United States of America, 2014. **111**(42): p. 14990-4.
19. Costentin, C., et al., *Pendant Acid-Base Groups in Molecular Catalysts: H-Bond Promoters or Proton Relays? Mechanisms of the Conversion of CO_2 to CO by Electrogenerated Iron(0)Porphyrins Bearing Prepositioned Phenol Functionalities.* Journal of the American Chemical Society, 2014. **136**(33): p. 11821-11829.
20. Sampson, M.D., et al., *Manganese Catalysts with Bulky Bipyridine Ligands for the Electrocatalytic Reduction of Carbon Dioxide: Eliminating Dimerization and Altering Catalysis.* Journal of the American Chemical Society, 2014. **136**(14): p. 5460-5471.
21. Becke, A.D., *DENSITY-FUNCTIONAL THERMOCHEMISTRY .3. THE ROLE OF EXACT EXCHANGE.* Journal of Chemical Physics, 1993. **98**(7): p. 5648-5652.
22. Grimme, S., et al., *A consistent and accurate ab initio parametrization of density functional dispersion correction (DFT-D) for the 94 elements H-Pu.* Journal of Chemical Physics, 2010. **132**(15).
23. *Jaguar*. 2012, Schrodinger, LLC: New York, NY.
24. Marten, B., et al., *New model for calculation of solvation free energies: Correction of self-consistent reaction field continuum dielectric theory for short-range hydrogen-bonding effects.* Journal of Physical Chemistry, 1996. **100**(28): p. 11775-11788.
25. Krishnan, R., et al., *SELF-CONSISTENT MOLECULAR-ORBITAL METHODS .20. BASIS SET FOR CORRELATED WAVE-FUNCTIONS.* Journal of Chemical Physics, 1980. **72**(1): p. 650-654.
26. Clark, T., et al., *Efficient diffuse function-augmented basis sets for anion calculations. III. The 3-21+G basis set for first-row elements, Li–F.* Journal of Computational Chemistry, 1983. **4**(3): p. 294-301.
27. Melius, C.F., B.D. Olafson, and W.A. Goddard, *FE AND NI AB-INITIO EFFECTIVE POTENTIALS FOR USE IN MOLECULAR CALCULATIONS.* Chemical Physics Letters, 1974. **28**(4): p. 457-462.
28. Melius, C.F. and W.A. Goddard, *AB-INITIO EFFECTIVE POTENTIALS FOR USE IN MOLECULAR QUANTUM-MECHANICS.* Physical Review A, 1974. **10**(5): p. 1528-1540.
29. Hay, P.J. and W.R. Wadt, *ABINITIO EFFECTIVE CORE POTENTIALS FOR MOLECULAR CALCULATIONS - POTENTIALS FOR K TO AU INCLUDING THE OUTERMOST CORE ORBITALS.* Journal of Chemical Physics, 1985. **82**(1): p. 299-310.

30. Martin, J.M.L. and A. Sundermann, *Correlation consistent valence basis sets for use with the Stuttgart–Dresden–Bonn relativistic effective core potentials: The atoms Ga–Kr and In–Xe.* The Journal of Chemical Physics, 2001. **114**(8): p. 3408-3420.
31. Isse, A.A. and A. Gennaro, *Absolute Potential of the Standard Hydrogen Electrode and the Problem of Interconversion of Potentials in Different Solvents.* Journal of Physical Chemistry B, 2010. **114**(23): p. 7894-7899.

Cartesian Coordinates for Optimized Structures of Species Discussed in Text

Note: Refer to Supporting Information section of Chapter III for species discussed therein; L = bpymd-OH.

1t [(L)Mn(CO)$_3$]$^-$

Mn1	-4.5275948981	1.8217119822	-0.7441517616
C2	-3.0508056157	-0.5555293682	-1.5274509758
C3	-2.2163418203	0.2046965061	0.5172571455
C4	-1.3527826033	-0.8688911794	0.5470049184
C5	-1.3875126021	-1.7792577694	-0.5273027788
N6	-2.2124795133	-1.6219618735	-1.5386792834
C7	-5.6484334741	1.0491581342	-3.4288281857
N8	-4.7558313033	0.8088065094	-2.4101551439
C9	-3.9563330052	-0.3222641046	-2.5870698676
N10	-4.0139896240	-1.1331138411	-3.6735769473
C11	-4.8694101460	-0.8538089279	-4.6302991704
C12	-5.7406646921	0.2659591708	-4.5420136944
N13	-3.0995454952	0.3966387277	-0.5109629976
H14	-0.6571895118	-0.9908389222	1.3668794328
H15	-0.7232338869	-2.6393721782	-0.5526189489
H16	-6.2886382181	1.9111876272	-3.3088515427
H17	-4.8902985541	-1.5131925888	-5.4939662124
H18	-6.4513760555	0.4937314972	-5.3266933495
C19	-5.4544757248	1.3829302613	0.6849279975
O20	-6.0760619539	1.1184960835	1.6359826305
O21	-3.1259728545	4.1520846313	0.3632633324
C22	-3.6282360764	3.1778847407	-0.0540810295
O23	-6.5201653627	3.8364491284	-1.5428295335
C24	-5.7339371981	3.0330259289	-1.2365689118
O27	-0.3335824858	4.7181320834	-0.0240320544
H28	-1.2748135565	4.5590492859	0.1558268665
C29	0.4358676467	3.7727476336	0.7070816797
C30	1.8665839651	3.9809189180	0.2254351824
F31	1.9951102407	3.7321641263	-1.0980610918
F32	2.2979901446	5.2451093869	0.4373467959
F33	2.7285809969	3.1558321486	0.8666405682
C36	-1.7287597666	3.0966736760	3.6694321417
C37	-0.8832715280	3.0769891641	2.5664456202
C38	-1.0657733208	2.1355241395	1.5516863181
C39	-2.1014006921	1.2079110537	1.6096232714
C40	-2.9416046725	1.2147727936	2.7268168094
C41	-2.7582066878	2.1522744301	3.7436371171
H42	-1.6002689048	3.8334333504	4.4563048752
H43	-3.4275824040	2.1496785158	4.5973155484

H44	-3.7448893168	0.4925889891	2.7931351681
C46	-0.0529950423	2.3257505550	0.4497936019
H47	-0.4653429534	2.2273232471	-0.5565266173
H48	0.7676998312	1.6075745283	0.5462755113
C48	0.2809368817	3.9829896274	2.2374656533
H49	1.1818128395	3.6636816377	2.7713879274
H50	0.1070924095	5.0359450092	2.4646147390

$TS_{1t \rightarrow 2t}$

Mn1	-4.2283584684	1.9241742081	-0.8076717068
C2	-3.0692588962	-0.6373420572	-1.4941385482
C3	-2.1140504231	0.0967884574	0.5015479351
C4	-1.2826334490	-0.9992068195	0.4829703546
C5	-1.3684376513	-1.8884835804	-0.6049257490
N6	-2.2665705919	-1.7167390643	-1.5545172448
C7	-5.7936628653	0.9664535764	-3.1937821985
N8	-4.7806095654	0.7453625734	-2.3169873143
C9	-4.0688560167	-0.4173264183	-2.4876250701
N10	-4.2824317649	-1.2915999264	-3.4970384203
C11	-5.2472567789	-1.0283573746	-4.3571811066
C12	-6.0667530228	0.1139084566	-4.2338881998
N13	-2.9947007048	0.3587130610	-0.5233807486
H14	-0.5851269560	-1.1697871900	1.2933735170
H15	-0.7156902931	-2.7540202142	-0.6781118263
H16	-6.3857261841	1.8569904115	-3.0295325648
H17	-5.3975493301	-1.7389940060	-5.1659886470
H18	-6.8764613641	0.3101845025	-4.9253723617
C19	-5.5873312411	1.7034719814	0.2866150013
O20	-6.4865482786	1.5881884259	1.0215003312
O21	-3.0049185077	4.0147442563	0.8812047986
C22	-3.4267027101	3.1269083672	0.2689347026
O23	-5.2246111372	4.2875196073	-2.2587988133
C24	-4.8298239314	3.3525416912	-1.6837155618
C25	-1.7990902248	2.3618125406	-2.4293144039
O26	-1.9503131885	1.5029857948	-3.2159893122
O27	0.2210914253	4.3290990788	0.4264340529
H28	-0.2246062721	3.9366462336	-0.3372739642
C29	0.8567984135	3.3195720847	1.1961430093
C30	2.3548421265	3.4234037263	0.9156670211
F31	2.6290330972	3.1936535904	-0.3913278282
F32	2.8443463967	4.6481912469	1.2145034116
F33	3.0742209222	2.5261158096	1.6334222741
O34	-1.2775348793	3.2832802954	-1.8981820707
C36	-1.7622793034	2.8321415655	3.7991480143
C37	-0.7670178707	2.7390995125	2.8357100670

C38	-0.8854177123	1.8266707160	1.7851163299
C39	-2.0173143224	1.0330221549	1.6471221148
C40	-3.0248417617	1.1266423696	2.6171237450
C41	-2.8902041817	2.0083021772	3.6873354528
H42	-1.6813175296	3.5428936986	4.6157545563
H43	-3.6788670193	2.0712583035	4.4298219222
H44	-3.9160238177	0.5178701521	2.5183183536
C46	0.3090877769	1.9141658692	0.8687859835
H47	0.0772477242	1.8044107803	-0.1916982621
H48	1.0485288958	1.1465287055	1.1190183943
C48	0.5049103305	3.5430945172	2.6875949218
H49	1.2940764445	3.1545402475	3.3397718286
H50	0.3826705897	4.6061730225	2.8995447211

2t $[(L)Mn(CO)_3(CO_2)]^-$

Mn1	-4.1880604177	1.9574924944	-0.7491131359
C2	-3.0704723362	-0.6554093186	-1.3481879057
C3	-2.2110941669	0.0056836451	0.6839817054
C4	-1.4053260087	-1.1287513812	0.6871588165
C5	-1.5021382766	-1.9999330204	-0.3868547272
N6	-2.3348301867	-1.7616952996	-1.4006305879
C7	-5.5459866747	1.0828882251	-3.3367613982
N8	-4.6837755893	0.7854255803	-2.3493558687
C9	-3.9693325517	-0.3484736471	-2.4792883066
N10	-4.0415952290	-1.1806163999	-3.5177107174
C11	-4.8723172843	-0.8575433454	-4.5101915858
C12	-5.6698026588	0.2827657835	-4.4588121552
N13	-3.0681505119	0.2476583108	-0.3346806834
H14	-0.7131551081	-1.3068372633	1.5003046655
H15	-0.8946077027	-2.8982670351	-0.4445518754
H16	-6.1351554457	1.9826449539	-3.2236064511
H17	-4.9028599649	-1.5312452579	-5.3617805910
H18	-6.3537526585	0.5387830451	-5.2583711384
C19	-5.6535802785	1.5109232409	0.2020896100
O20	-6.5994951574	1.2777949498	0.8284806061
O21	-3.3384097456	3.9419783233	1.2620164257
C22	-3.6148301903	3.0945490922	0.5340305916
O23	-5.2902658429	4.3508717669	-2.0468755267
C24	-4.8778824101	3.4023237687	-1.5251758446
C25	-2.3735896193	2.4352489417	-1.7963599204
O26	-1.9580111318	1.5786605984	-2.6063841042
O27	0.1374228364	4.2662396207	0.1608657224
H28	-0.5260532512	3.8707491452	-0.4617809545
C29	0.7751697960	3.2826579341	0.9424306556
C30	2.2610258717	3.3264898713	0.5850203191

F31	2.4778229284	3.0187301978	-0.7136793518
F32	2.7963949381	4.5524583434	0.7933485401
F33	2.9943093888	2.4509524614	1.3205722790
O34	-1.7627138871	3.5223541816	-1.5303219537
C36	-1.6113409084	2.9011688598	3.7931838836
C37	-0.7142684600	2.7780076112	2.7389711858
C38	-0.9184457757	1.8192760360	1.7455767877
C39	-2.0424788601	0.9972133753	1.7730780606
C40	-2.9479154011	1.1155421067	2.8335403125
C41	-2.7268199496	2.0578516823	3.8372669712
H42	-1.4604377767	3.6519895887	4.5625029914
H43	-3.4415253968	2.1502815121	4.6482340366
H44	-3.8270586631	0.4818225166	2.8595306021
C46	0.1818509758	1.8709292228	0.7129148057
H47	-0.1550452310	1.7432723995	-0.3170512980
H48	0.9315410915	1.0991701039	0.9133978860
C48	0.5334973592	3.5767114343	2.4480166715
H49	1.3689335923	3.2263076398	3.0630985684
H50	0.4192173858	4.6489830207	2.6125248666

2t / 2 TFEH $[(L)Mn(CO)_3(CO_2)]^-$ / 2 TFEH

Mn1	-3.4698061506	2.3053221951	-0.6110563836
C2	-3.0929009613	-0.4699325524	-1.4689344328
C3	-2.0093164767	-0.2279673248	0.5584343531
C4	-1.6014423952	-1.5606878765	0.4728846363
C5	-1.9710321145	-2.2873737113	-0.6568134672
N6	-2.7222169433	-1.7445438481	-1.6229300720
C7	-5.3264020932	1.9318863619	-3.0192447506
N8	-4.4095431989	1.3868300398	-2.1959036985
C9	-4.0014185553	0.1292885812	-2.4724942513
N10	-4.4039770191	-0.5980327085	-3.5211417166
C11	-5.2833417823	-0.0307624233	-4.3573905917
C12	-5.7971411070	1.2498749923	-4.1334462966
N13	-2.7551632719	0.3362919716	-0.4266144297
H14	-1.0002580460	-2.0038404339	1.2614487999
H15	-1.6628817171	-3.3225452183	-0.7901438581
H16	-5.6817524546	2.9275843280	-2.7767303606
H17	-5.5915551264	-0.6195132800	-5.2190564723
H18	-6.5303313737	1.6980814937	-4.7973105451
C19	-4.8855568713	2.0265649554	0.4868653188
O20	-5.7939223784	1.8980728574	1.2073472780
O21	-2.1816949228	3.8255630574	1.5757363298
C22	-2.6007352351	3.1487139526	0.7329216448
O23	-4.2846447595	5.0037518168	-1.5055916783
C24	-3.9751942604	3.9370002575	-1.1507079733

C25	-1.7801692612	2.5871952571	-1.9753088889
O26	-1.6392331137	1.7472643826	-2.9048205804
O27	0.6587779178	3.8436479633	0.2019332285
C29	1.3321007754	2.7104030005	0.7160146255
C30	2.7355747303	2.6968013423	0.1014822643
F31	2.6912600936	2.5689633397	-1.2490824649
F32	3.4182489046	3.8382345393	0.3711284196
F33	3.4932047757	1.6660021187	0.5686169378
C34	-0.6097992679	2.1538950318	3.8666703412
C37	0.1033089288	2.0879636786	2.6715094550
C38	-0.3588866709	1.2990739207	1.6120450664
C39	-1.5582407675	0.5939459129	1.7143262655
C40	-2.2801014606	0.6522996014	2.9185667355
C41	-1.8036664349	1.4250421378	3.9844379228
H42	-0.2622737679	2.7734580264	4.6900296879
H43	-2.3761938940	1.4725176802	4.9081847981
H44	-3.2148907053	0.1051850881	3.0148071076
C46	0.5697285343	1.3923660119	0.4256677468
H47	0.0663775456	1.4187942893	-0.5424949238
H48	1.2624508677	0.5404412384	0.4131828478
C48	1.3691364298	2.8109832746	2.2647913644
H49	2.2563026100	2.3110467503	2.6742899259
H50	1.3946171713	3.8546970373	2.5807267804
O50	0.4244337560	6.4701627491	0.7165828920
H51	0.6404648896	5.5070936835	0.6581306007
C52	-0.9444889936	6.6159345551	0.3702026810
H53	-1.0666166253	7.3605743699	-0.4253232432
H54	-1.3754370592	5.6677538801	0.0399684205
C55	-1.7352769299	7.1061610072	1.5731219445
F56	-1.5781686291	6.3337366440	2.6680539092
F57	-1.3589861369	8.3678924879	1.9404377308
F58	-3.0630035788	7.1548975094	1.2907007067
O57	-0.9694266436	3.5842531928	-1.8208978067
H58	0.0518027704	3.6504975157	-0.5837045406
H60	1.2883294301	7.3320589773	2.1048342613
O61	1.8788164532	7.7966996454	2.7382109797
C65	1.2935763450	7.8521236762	4.0210731883
H67	1.8361207036	8.5897759133	4.6215900506
H68	0.2321127323	8.1259263943	3.9988063043
C64	1.3982406778	6.5164945591	4.7473859422
F65	0.7381440642	5.5250447387	4.0986138475
F66	2.6810264243	6.0989212009	4.8967567893
F67	0.8592482062	6.6056855583	5.9939587127

Proton Transfer TS: $TS_{\mathbf{2t}/2\ TFEH \rightarrow \mathbf{3t}/TFE^-/TFEH}$

Mn1	-3.3730018629	2.2402549621	-0.9765287352
C2	-3.1066841716	-0.6300363366	-1.6132111705
C3	-2.2041787506	-0.3396767343	0.4939211263
C4	-1.8879430877	-1.7014500025	0.5162788204
C5	-2.1898608402	-2.4651337531	-0.6070543630
N6	-2.8159123759	-1.9321386343	-1.6648220304
C7	-5.0533169565	1.7932094160	-3.4996012641
N8	-4.2109488238	1.2590440142	-2.5943751203
C9	-3.9239848479	-0.0529282377	-2.7126353260
N10	-4.3864596888	-0.8565639295	-3.6757532405
C11	-5.2122829698	-0.3150340713	-4.5830006308
C12	-5.5922300505	1.0280442833	-4.5271071621
N13	-2.7953888955	0.2176103339	-0.5976626216
H14	-1.4125687086	-2.1394969038	1.3888693858
H15	-1.9421615212	-3.5237493630	-0.6580179441
H16	-5.3030640625	2.8428833703	-3.3872704606
H17	-5.5861377661	-0.9759346109	-5.3624622781
H18	-6.2807079648	1.4602255388	-5.2474064717
C19	-4.9755245807	2.0364907915	-0.1291096192
O20	-6.0027314814	1.9512803117	0.4096146058
O21	-2.8004591439	3.7105191003	1.5291854446
C22	-2.8487369692	3.0778545866	0.5601447316
O23	-3.8738845130	4.9567106817	-2.0253599151
C24	-3.7030381571	3.8786037763	-1.6190339598
C25	-1.5913221855	2.4170362678	-2.1352237796
O26	-1.4552557948	1.7170107372	-3.1659183083
O27	-0.0519754105	3.9287300114	0.4044200391
C29	0.7545785170	2.9760874555	1.0322382543
C30	2.2039488164	3.2183329924	0.5928391576
F31	2.3591543569	3.0832097659	-0.7509098752
F32	2.6252165581	4.4681559664	0.9133292190
F33	3.0928304727	2.3515206362	1.1680390783
C34	-1.3881533847	2.0748804450	3.9691164537
C37	-0.5504684816	2.1324219454	2.8581344920
C38	-0.7824217398	1.3122659765	1.7451117437
C39	-1.9064763138	0.4885156426	1.6939101587
C40	-2.7549511056	0.4236628982	2.8160166884
C41	-2.4879657306	1.2024376108	3.9466042786
H42	-1.2110038151	2.7099611089	4.8341812816
H43	-3.1542359334	1.1468019887	4.8050014214
H44	-3.6279826103	-0.2247840692	2.7940717563
C46	0.2898333618	1.5260995329	0.7055892117
H47	-0.0479301050	1.4251507432	-0.3241162179
H48	1.1069027134	0.8086540850	0.8641327910
C48	0.6220458645	3.0472254022	2.5866508606

H49	1.5317135646	2.6776953887	3.0783405364
H50	0.4534246958	4.0714366584	2.9163223819
O50	-0.2030176637	6.3978770952	1.1796770804
H51	-0.1038094782	5.4150212455	0.9259667506
C52	-1.5334647541	6.6784238655	1.5435941994
H53	-1.7951462891	7.7051387781	1.2623147131
H54	-2.2416922980	5.9898631288	1.0759624620
C55	-1.7423583552	6.5704614843	3.0504508220
F56	-1.4076823495	5.3641124548	3.5556214408
F57	-1.0124072795	7.4948205409	3.7389237607
F58	-3.0489308973	6.7910847720	3.3674792632
O57	-0.6447680580	3.3060752642	-1.8646414625
H58	-0.4308427170	3.6113631735	-0.7442654858
H60	1.1186473984	7.4973947612	1.6734843533
O61	1.8340170341	8.1583422028	1.8361560407
C65	2.0978529464	8.2721103907	3.2172412960
H67	2.8155211623	9.0840179385	3.3731956028
H68	1.1994817333	8.4790192497	3.8106861712
C64	2.7193493076	7.0000923487	3.7799132381
F65	1.9102177697	5.9230413347	3.6264836103
F66	3.9025709506	6.6874985015	3.1950628326
F67	2.9566799674	7.1324513285	5.1157171377

3t / TFE^- / TFEH [(L)$MnCO_3CO_2H$ / TFE^- / TFEH]

Mn1	-4.3888153378	1.8969958192	-1.6286585433
C2	-3.1882638754	-0.7609957064	-1.4830571956
C3	-2.3331598994	0.4695993698	0.2805918126
C4	-1.3876636199	-0.5416119785	0.4862272058
C5	-1.4134286433	-1.6463448848	-0.3612571695
N6	-2.3436103989	-1.7785402403	-1.3193381988
C7	-6.1406825943	0.1132952648	-3.4165237626
N8	-5.0611887535	0.2108762452	-2.6144880034
C9	-4.2862097969	-0.8868521001	-2.4781074212
N10	-4.4790670276	-2.0452298176	-3.1131402974
C11	-5.5360700637	-2.1247832650	-3.9363450962
C12	-6.4218706015	-1.0581089597	-4.1084892892
N13	-3.1927641713	0.3898936176	-0.7636648147
H14	-0.6845991424	-0.4805863424	1.3117274370
H15	-0.7010228639	-2.4613069391	-0.2480811615
H16	-6.7822336932	0.9847696614	-3.4975882815
H17	-5.6804084693	-3.0671412874	-4.4612116243
H18	-7.2912682590	-1.1329604610	-4.7552404357
C19	-5.6822618216	1.7156580010	-0.3404429481
O20	-6.5075015137	1.6229153368	0.4671700692
O21	-3.4771114670	4.4056719170	-0.3213735338

C22	-3.7427078932	3.3888807069	-0.7996485602
O23	-6.0325275856	3.7495614756	-3.2549737508
C24	-5.3887570428	3.0189894970	-2.6215196000
O25	-2.2694359642	0.9789007137	-3.5179941568
O26	-0.6952235246	5.4372213838	0.1287656840
C27	-0.1034208782	4.4834488793	0.9742522307
C28	1.4147237532	4.7018417466	0.9159303785
F29	1.9010374541	4.5537490885	-0.3474871066
F30	1.7709653129	5.9392820718	1.3309679370
F31	2.1040282002	3.8149841593	1.6952559483
C32	-2.7096692936	3.3626669523	3.4497033202
C33	-1.7090780433	3.5206853291	2.4910250556
C34	-1.5918192077	2.6298601014	1.4145992169
C35	-2.4761041328	1.5527942109	1.2961492139
C36	-3.4927544566	1.3975307870	2.2583472360
C37	-3.6106992638	2.2969354464	3.3217737324
H38	-2.7924331022	4.0548847081	4.2832799795
H39	-4.3994517631	2.1573735250	4.0577982743
H40	-4.1767832766	0.5558605628	2.1827190984
C41	-0.4661189195	3.0419509821	0.4930958857
H42	-0.7606749481	3.0706688433	-0.5596163000
H43	0.3859827641	2.3564265432	0.5815555509
C44	-0.6230063720	4.5671499043	2.4381571281
H45	0.1709523663	4.3181243641	3.1531852295
H46	-0.9629703735	5.5769642293	2.6655214032
O47	-1.5883110806	7.5594248500	1.2599780180
H48	-1.0105931176	6.2687214312	0.6415398538
C49	-2.9454250636	7.4988658955	1.5078474607
H50	-3.5242717801	8.3211778720	1.0450538056
H51	-3.3978321953	6.5525817663	1.1647895914
C52	-3.2991607956	7.5875328323	2.9931721627
F53	-2.7333795098	6.6125443911	3.7523034374
F54	-2.9238514829	8.7707814045	3.5611405885
F55	-4.6504810516	7.4856185951	3.1850374496
O56	-0.1527598583	9.5758685541	1.8247104934
C57	0.1576679195	9.6922090917	3.1867247102
H58	0.6670247263	10.6456921444	3.3722116107
H59	-0.7250010915	9.6424258298	3.8375178706
C60	1.1014920911	8.5973697472	3.6728347677
F61	0.5514901646	7.3612363987	3.6213966952
F62	2.2593957029	8.5431275462	2.9652728876
F63	1.4480232199	8.8156795128	4.9793455669
H64	-0.7714374074	8.7599950319	1.6518175405
C65	-2.8905942734	1.9591702071	-3.0926397961
O66	-2.5848999830	3.1780900327	-3.6571088977

H67	-1.8888302651	3.0416918394	-4.3372878986

3t / TFE^- / 2 TFEH [(L)$MnCO_3CO_2H$ / TFE^- / 2 TFEH]

Mn1	-4.5483446357	1.7418660129	-1.6391840101
C2	-3.0718419802	-0.7904472635	-1.4970428860
C3	-2.3743302821	0.4964417849	0.2910413104
C4	-1.3555979353	-0.4355388984	0.5245822095
C5	-1.2743013016	-1.5424128697	-0.3133287983
N6	-2.1561610700	-1.7395085709	-1.3044640519
C7	-5.9236533150	-0.1352633300	-3.6621758133
N8	-4.9448468766	0.0355473077	-2.7489028198
C9	-4.0860999870	-0.9907696972	-2.5655182524
N10	-4.1161021793	-2.1474589738	-3.2326244607
C11	-5.0779530231	-2.3014814007	-4.1544099063
C12	-6.0275227450	-1.3072802801	-4.4021681092
N13	-3.2043993403	0.3474019948	-0.7695624057
H14	-0.6752079942	-0.3084957027	1.3612831866
H15	-0.5085608673	-2.3026504140	-0.1732507195
H16	-6.6282862054	0.6782844575	-3.7974807820
H17	-5.0897106431	-3.2432755426	-4.6994148562
H18	-6.8132187226	-1.4374301987	-5.1407694416
C19	-5.8417035750	1.3074239120	-0.4118540453
O20	-6.6609408919	1.0387892509	0.3638024669
O21	-3.8936921990	4.2479128322	-0.1679914039
C22	-4.0823087072	3.2460097301	-0.7107017680
O23	-6.4248926648	3.4263144694	-3.1963719877
C24	-5.6793981063	2.7706445143	-2.5935713185
O25	-2.1941295326	1.2505288512	-3.3940539923
O26	-0.8426237518	5.3197069015	0.1366911587
C27	-0.1413960118	4.4357599147	0.9728902807
C28	1.3529077137	4.7513425688	0.8345413061
F29	1.7944016309	4.5990000970	-0.4379863538
F30	1.6273082844	6.0317041862	1.1962305387
F31	2.1353030412	3.9513052013	1.6164817273
C32	-2.8108625635	3.4528394652	3.3917450211
C33	-1.7587880329	3.5381665703	2.4823082088
C34	-1.6410017639	2.6264903208	1.4242285696
C35	-2.5688312568	1.5919839019	1.2807056243
C36	-3.6372656234	1.5058213967	2.1943473608
C37	-3.7607443920	2.4328042444	3.2336801728
H38	-2.8957757732	4.1632242196	4.2103011017
H39	-4.5910366642	2.3506381043	3.9315702640
H40	-4.3568187075	0.6969077934	2.1034527897
C41	-0.4604634247	2.9756883128	0.5448597722
H42	-0.6882814550	2.9408614732	-0.5238028223

H43	0.3880556095	2.3050368149	0.7324667441
C44	-0.6140211037	4.5222152537	2.4486896529
H45	0.1780235356	4.2049102631	3.1396020709
H46	-0.8988710833	5.5394672559	2.7107825155
C47	-3.0443364596	7.1013757576	1.8193029031
H48	-3.8578014601	7.6422641097	1.3054444828
H49	-3.2536175212	6.0245725902	1.7153554582
C50	-3.2146926584	7.4098852154	3.2999816373
F51	-2.2320745773	6.8476939609	4.0598455479
F52	-3.1947733978	8.7415124039	3.5762901738
F53	-4.3975935359	6.9281523941	3.7807175712
O54	-0.1778639727	9.0227595769	2.7135069655
C55	0.6466922984	8.1790005999	3.4752678934
H56	0.4121855688	8.2149520196	4.5489462719
H57	0.5951496307	7.1382857869	3.1420341471
C58	2.0985842110	8.5990134609	3.3328058972
F59	2.5400933104	8.5596153188	2.0529119293
F60	2.3224791965	9.8640297461	3.7830418467
F61	2.9054799506	7.7749288429	4.0597322733
C62	-3.0272389435	2.0855612285	-3.0256980085
O63	-2.9665901833	3.3324734258	-3.6042565998
H64	-2.2160676763	3.3606840018	-4.2381359143
O65	-1.3575846544	9.0757372517	-0.5712660173
C66	0.0177006287	8.7933282089	-0.6998125020
H67	0.2275081023	7.7172306917	-0.6410649818
H68	0.6261426415	9.3036714249	0.0600583064
C69	0.5095369904	9.2602369542	-2.0525903048
F70	0.3174369119	10.5928955424	-2.2516001715
F71	1.8480932350	9.0337654228	-2.1730030805
F72	-0.0938743376	8.6239423574	-3.0872821609
O73	-1.7731158122	7.4417517662	1.3695651615
H74	-0.8354386714	8.4411085614	2.2179437957
H75	-1.1462151131	6.1407523619	0.6369006686
H76	-1.6752510536	8.4595981186	0.1694292430

4t / TFE^- / TFEH [(L)Mn$CO_3CO_2H^-$ / TFE^- / TFEH]

Mn1	-4.4010814218	1.8924701100	-1.6775902461
C2	-3.1916130629	-0.7832052720	-1.4894200621
C3	-2.3454524950	0.5129164225	0.2620578760
C4	-1.3954751787	-0.4895935798	0.5272373343
C5	-1.4038445421	-1.6205141368	-0.3062190181
N6	-2.2936116500	-1.7987277789	-1.2739907534
C7	-6.1268607386	0.0268631978	-3.4026039569
N8	-5.0517055040	0.1691103573	-2.6283105315
C9	-4.2378603612	-0.9391836833	-2.4333300805

N10	-4.4383198844	-2.1331902537	-3.0871468613
C11	-5.5019530687	-2.2227662811	-3.8774604993
C12	-6.4195382626	-1.1702180995	-4.0639624908
N13	-3.1746751523	0.4231991058	-0.7848638261
H14	-0.7162532004	-0.4029196829	1.3680252115
H15	-0.6795868960	-2.4212890262	-0.1551439521
H16	-6.7771313546	0.8913415314	-3.5052456397
H17	-5.6479715250	-3.1747858962	-4.3879024163
H18	-7.2943783997	-1.2694772219	-4.6969343732
C19	-5.6680924389	1.6623753361	-0.3789040804
O20	-6.4873273517	1.5375767504	0.4356318247
O21	-3.5542582377	4.4401845798	-0.4078787877
C22	-3.7942519190	3.4056409628	-0.8711648462
O23	-6.1545957014	3.6566552373	-3.2803103762
C24	-5.4590748704	2.9572462463	-2.6579258713
O25	-2.2251897266	1.1101235360	-3.6125490368
O26	-0.6818226634	5.4819469758	0.1265536598
C27	-0.1039954651	4.5133038493	0.9680185008
C28	1.4163592535	4.7118677809	0.9186719061
F29	1.9111059984	4.5628352439	-0.3416104112
F30	1.7876255338	5.9429578568	1.3413129228
F31	2.0896467050	3.8126252922	1.6989396576
C32	-2.7467751269	3.4320309994	3.4161634217
C33	-1.7348027546	3.5746387369	2.4679505245
C34	-1.6205608336	2.6829660397	1.3922248356
C35	-2.5059150315	1.6099883596	1.2651433553
C36	-3.5315450156	1.4703457349	2.2197280437
C37	-3.6575630926	2.3757595306	3.2774858431
H38	-2.8304651759	4.1279445106	4.2464933298
H39	-4.4592647091	2.2491230740	4.0020442094
H40	-4.2232896302	0.6362132238	2.1374508340
C41	-0.4848823514	3.0816132933	0.4788042273
H42	-0.7779435679	3.1159493869	-0.5739027562
H43	0.3554569522	2.3820333961	0.5671254771
C44	-0.6273342357	4.5978616673	2.4298925487
H45	0.1590656272	4.3231708555	3.1441806613
H46	-0.9433168778	5.6128256080	2.6663193616
O47	-1.5730714733	7.5987561937	1.2921993882
H48	-0.9937886512	6.3046543368	0.6487469979
C49	-2.9289761014	7.5268056413	1.5443666056
H50	-3.5165554034	8.3429592487	1.0821666947
H51	-3.3733248721	6.5761618980	1.2027057379
C52	-3.2834562818	7.6154941239	3.0297846310
F53	-2.7188021876	6.6423312190	3.7918175501
F54	-2.9084157659	8.8001119598	3.5972574378

F55	-4.6358015324	7.5142303071	3.2202991766
O56	-0.0994342701	9.5637584574	1.9070938588
C57	0.2193884905	9.6432338893	3.2693095594
H58	0.7430720396	10.5844081657	3.4746176555
H59	-0.6606847164	9.5895835872	3.9235902948
C60	1.1514290134	8.5255608831	3.7263097172
F61	0.5810099401	7.2996329410	3.6647027223
F62	2.2998280272	8.4640729935	3.0039278342
F63	1.5179767227	8.7183629639	5.0315750021
H64	-0.7388087800	8.7656915240	1.7168865075
C65	-2.9255270981	2.0204228033	-3.1596437473
O66	-2.7192770785	3.2763909080	-3.7255332982
H67	-2.0146684865	3.1866053677	-4.4042557134

4t / TFE^- / 2 TFEH [$(L)MnCO_3CO_2H^-$ / TFE^- / 2 TFEH]

Mn1	-4.7508723574	1.6033803928	-1.5377560638
C2	-3.0409930623	-0.8011451614	-1.5659046489
C3	-2.3343336943	0.5555589695	0.2015202728
C4	-1.2150298749	-0.2784946004	0.3768709060
C5	-1.0899925504	-1.3776886788	-0.4844569983
N6	-1.9831316780	-1.6653613375	-1.4222485218
C7	-5.9814284425	-0.3268069804	-3.5956097343
N8	-5.0164999875	-0.0943985228	-2.7054720937
C9	-4.0284138384	-1.0583940073	-2.5521742019
N10	-3.9873880877	-2.2093584383	-3.3075468295
C11	-4.9602710816	-2.3950508101	-4.1914822572
C12	-6.0151856526	-1.4825553916	-4.3829902733
N13	-3.2145837944	0.3444446393	-0.7860497339
H14	-0.5012062272	-0.0870850896	1.1699060348
H15	-0.2414516782	-2.0555035087	-0.3906604981
H16	-6.7544335452	0.4295688282	-3.6950317582
H17	-4.9121804429	-3.3107675883	-4.7812752570
H18	-6.8032823068	-1.6527098297	-5.1085634855
C19	-5.9105511300	0.9650375601	-0.2728339376
O20	-6.6519274167	0.5775021055	0.5352659823
O21	-4.2122211329	4.1242580034	-0.0526017102
C22	-4.3747770379	3.1118440359	-0.5924232646
O23	-6.8999626820	3.0768914928	-2.9411284768
C24	-6.0457212063	2.5058717343	-2.3891703215
O25	-2.3862210133	1.5749128555	-3.3841313292
O26	-0.8040293330	5.3940963243	0.0372366226
C27	-0.1309614592	4.5044671566	0.8926146530
C28	1.3705839627	4.7984320187	0.7832545344
F29	1.8404288884	4.6218400291	-0.4759609964
F30	1.6584521390	6.0796724061	1.1340986945

F31	2.1240505557	3.9979061172	1.5934100997
C32	-2.8145150386	3.5223956641	3.3024275267
C33	-1.7611080625	3.6095219853	2.3950624995
C34	-1.6303480919	2.6895665976	1.3459958792
C35	-2.5411542796	1.6385024182	1.2064878120
C36	-3.6001009427	1.5445998418	2.1293485415
C37	-3.7428180993	2.4813588599	3.1573295398
H38	-2.9158318789	4.2478132536	4.1059302892
H39	-4.5746607817	2.3951566565	3.8527249904
H40	-4.3082075938	0.7263510749	2.0436658164
C41	-0.4510923110	3.0446650414	0.4675060685
H42	-0.6792981846	3.0057763091	-0.6007835312
H43	0.3986293567	2.3756470533	0.6532079582
C44	-0.6305741419	4.6088172381	2.3595456750
H45	0.1562531966	4.3185890371	3.0683053933
H46	-0.9376131147	5.6264233726	2.5979050940
C47	-3.0349589144	7.2232306245	1.6700846290
H48	-3.8036702513	7.7758866324	1.1026921778
H49	-3.2691869884	6.1499362180	1.5741490585
C50	-3.2848023243	7.5668963840	3.1333888127
F51	-2.3855614847	6.9753486371	3.9709348981
F52	-3.2151906984	8.9024724016	3.3876417010
F53	-4.5211133309	7.1577013503	3.5423016921
O54	-0.0897963162	9.0019861526	2.6580286417
C55	0.6125337178	8.1104537747	3.4839415368
H56	0.2635239826	8.1311254476	4.5264462817
H57	0.5603785501	7.0802711647	3.1204941592
C58	2.0862395430	8.4690297426	3.5108124055
F59	2.6620816872	8.4495757206	2.2857869432
F60	2.3166604224	9.7067734791	4.0295319622
F61	2.7723043433	7.5834194127	4.2887738055
C62	-3.3533183075	2.2087473727	-2.9545439304
O63	-3.5356778775	3.4805743365	-3.4914993022
H64	-2.7976608561	3.6548148535	-4.1149026735
O65	-1.0838578373	9.1402896560	-0.6355502595
C66	0.2925633228	8.8295656513	-0.6426001846
H67	0.4751543041	7.7494443559	-0.5767737181
H68	0.8382165575	9.3202782053	0.1748233339
C69	0.9152314621	9.2993181415	-1.9393483897
F70	0.7813985857	10.6402700209	-2.1336634334
F71	2.2518063507	9.0341164625	-1.9447536636
F72	0.3882904717	8.6968829180	-3.0343430177
O73	-1.7331253579	7.5225694315	1.2826121414
H74	-0.7816677199	8.4623904569	2.1563078694
H75	-1.1117502061	6.2124266438	0.5349528054

H76	-1.4859562180	8.5385915865	0.0718181668

3t [(L)$MnCO_3CO_2H$]

Mn1	-3.9820795723	2.0322228739	-0.8429931118
C2	-3.0753328388	-0.7084833480	-1.3206150724
C3	-2.2107621973	-0.0552718525	0.7122228195
C4	-1.4922400135	-1.2476004389	0.7629160759
C5	-1.6178117529	-2.1274496964	-0.2997762337
N6	-2.4207961087	-1.8612496285	-1.3331993725
C7	-5.5188461204	1.0773338740	-3.3203950489
N8	-4.6279748285	0.7854005673	-2.3582051295
C9	-3.9960162270	-0.3989087763	-2.4443243046
N10	-4.1645148282	-1.2838519630	-3.4193603021
C11	-5.0303972490	-0.9763817010	-4.3893314045
C12	-5.7550763958	0.2101647657	-4.3744530110
N13	-2.9978873401	0.2307366803	-0.3489694246
H14	-0.8510652452	-1.4669989040	1.6071230741
H15	-1.0705921666	-3.0645256460	-0.3268542145
H16	-6.0429584416	2.0199244758	-3.2436719611
H17	-5.1460306905	-1.7009483608	-5.1893743066
H18	-6.4690139509	0.4536682954	-5.1509578270
C19	-5.4354215799	1.6227924120	0.1905605224
O20	-6.3415096833	1.3839710955	0.8544719296
O21	-3.1183370668	3.9891893595	1.1989055446
C22	-3.3772929855	3.1670446159	0.4414094196
O23	-5.2181407568	4.4116049952	-2.0640118590
C24	-4.7458598603	3.4782567001	-1.5824548096
C25	-2.3116996078	2.3234742657	-2.0378040625
O26	-1.8899544968	1.5133617233	-2.8466714141
O27	-0.1009946284	4.3063638107	0.3896572088
H28	-0.5565249665	3.9468196052	-0.3909425026
C29	0.6651404760	3.3141650191	1.0496149719
C30	2.1140964569	3.4753444506	0.5913109436
F31	2.2279727480	3.2724231685	-0.7443048780
F32	2.5943395458	4.7116686449	0.8487348911
F33	2.9457713074	2.5937030492	1.1981758287
O34	-1.5893066123	3.5146413310	-1.9360627190
H35	-0.9152022324	3.5064968068	-2.6439321617
C36	-1.6408464055	2.7511689714	3.9111392225
C37	-0.7428546422	2.6763433103	2.8542067912
C38	-0.9413925459	1.7571351661	1.8231361894
C39	-2.0529202827	0.9218770296	1.8169962583
C40	-2.9642488914	0.9939935743	2.8782717818
C41	-2.7529333473	1.9010135468	3.9164747789
H42	-1.4980733007	3.4703698109	4.7111690579

H43	-3.4688234463	1.9539027305	4.7297639002
H44	-3.8329500449	0.3451187303	2.8865341749
C46	0.1364742629	1.8869941538	0.7766735259
H47	-0.2116559456	1.7711482113	-0.2510460464
H48	0.9271956996	1.1461733542	0.9360561181
C48	0.4857728102	3.5117325535	2.5743663421
H49	1.3515730001	3.1301312585	3.1258012200
H50	0.3668074361	4.5684275922	2.8166024846

4t [(L)$MnCO_3CO_2H^-$]

Mn1	-3.8845108283	2.0494721318	-0.9134985499
C2	-3.1079791493	-0.7685668062	-1.3426380111
C3	-2.2281115900	-0.0916214801	0.7102297961
C4	-1.6356584498	-1.3526869601	0.8584928275
C5	-1.7863850128	-2.2617638087	-0.1973424414
N6	-2.5048058372	-1.9978810706	-1.2743140423
C7	-5.4739576668	1.0610234714	-3.3338292344
N8	-4.5699592626	0.7826032195	-2.3996247338
C9	-3.9950579790	-0.4759877372	-2.4084412257
N10	-4.2765692271	-1.4141463951	-3.3691238847
C11	-5.1702251395	-1.0908669428	-4.2914072309
C12	-5.8316037336	0.1468548405	-4.3228394067
N13	-2.9271500449	0.2329712988	-0.3827678981
H14	-1.0658721841	-1.5953382696	1.7455852105
H15	-1.3074510369	-3.2379304505	-0.1539927135
H16	-5.9350382595	2.0415637526	-3.2991176963
H17	-5.3843915513	-1.8447614658	-5.0460597150
H18	-6.5711240091	0.3885949744	-5.0752065234
C19	-5.3127269651	1.6042322928	0.1319761583
O20	-6.2129749433	1.3475232843	0.8024221199
O21	-3.1224489735	4.0017351373	1.1710403706
C22	-3.3162890640	3.1810564152	0.3862981477
O23	-5.1762762323	4.4307448321	-2.0688977767
C24	-4.6823778796	3.4861261453	-1.6210135601
C25	-2.2630738416	2.4244501174	-2.1878480309
O26	-1.9012640920	1.7662555104	-3.1501176431
O27	-0.1429898240	4.4363995270	0.4553370833
H28	-0.5847491570	4.1074075881	-0.3495335068
C29	0.6025885289	3.3989857207	1.0755466676
C30	2.0571732982	3.5544356541	0.6289617309
F31	2.1788102372	3.4184708634	-0.7144331355
F32	2.5623083437	4.7674769689	0.9517608233
F33	2.8712220668	2.6275788236	1.1938843965
O34	-1.5070053944	3.6033371657	-1.9586441132
H35	-0.8647521088	3.6841636549	-2.6929409315

C36	-1.6031761693	2.6389951258	3.9904843500
C37	-0.7600180053	2.6511299584	2.8858400427
C38	-0.9754145337	1.7778275255	1.8175850116
C39	-2.0454739553	0.8881207839	1.8206047185
C40	-2.8960695922	0.8732569124	2.9347950642
C41	-2.6768986387	1.7414662413	4.0060664987
H42	-1.4416206537	3.3183507392	4.8224295542
H43	-3.3499617649	1.7194252060	4.8575730053
H44	-3.7311264543	0.1807501599	2.9597544380
C46	0.0555534344	1.9889546849	0.7386859402
H47	-0.3469388543	1.9408837420	-0.2728851935
H48	0.8495204971	1.2377291487	0.8108446196
C48	0.4365926438	3.5329191349	2.6098095027
H49	1.3222462371	3.1588664746	3.1352390357
H50	0.2938073215	4.5775126789	2.8935489548

Dehydroxylation TS: $TS_{\mathbf{4t}\rightarrow\mathbf{5t'}/H2O/TFEH}$

Mn1	-3.9551113771	2.1422861116	-1.0467379972
C2	-3.0777664548	-0.6807455899	-1.2065833621
C3	-2.2900372194	0.1967275086	0.8119836322
C4	-1.7112110552	-1.0424726358	1.1058716431
C5	-1.8339172169	-2.0587378319	0.1485067014
N6	-2.4970091129	-1.8999502818	-0.9826443622
C7	-5.1780216293	0.9878131892	-3.6120729472
N8	-4.4266214166	0.7733635351	-2.5316250359
C9	-3.8585923892	-0.4811639522	-2.3742564584
N10	-4.0336895565	-1.4925994056	-3.2833888728
C11	-4.7823456570	-1.2377625200	-4.3435071581
C12	-5.3979629400	0.0057514802	-4.5713018459
N13	-2.9585758147	0.4044073789	-0.3321519655
H14	-1.1696311280	-1.1916017569	2.0305058049
H15	-1.3741830430	-3.0306260321	0.3164976052
H16	-5.6182257021	1.9721103005	-3.7219627837
H17	-4.9103125459	-2.0506874999	-5.0550579985
H18	-6.0086950553	0.1963455919	-5.4441305125
C19	-5.4439139420	1.6205939066	-0.1021667778
O20	-6.3635003501	1.2728312298	0.4852185811
O21	-3.4861930748	4.2294671517	1.0260282225
C22	-3.5541438674	3.3753722994	0.2685077227
O23	-5.3419479845	4.4005337970	-2.3704116528
C24	-4.8103183924	3.5152756084	-1.8659161790
C25	-2.3307982725	2.4288987071	-2.1864110501
O26	-1.6056901718	1.9933635758	-2.9649160514
O27	-0.5357199935	4.8303990050	0.1650837790
H28	-1.0148309636	4.5711681814	-0.8322652664

C29	0.3118604049	3.9027713612	0.7680152324
C30	1.7178455195	4.1168965093	0.2067206960
F31	1.7458384464	3.9105172107	-1.1354288723
F32	2.1647914055	5.3787496567	0.4211098393
F33	2.6465287581	3.2814205962	0.7482722110
O34	-1.6286982459	4.4168087168	-1.9649537482
H35	-0.9245711647	4.4251518273	-2.6277333156
C36	-1.6669989049	3.1903144826	3.8450193103
C37	-0.8828647786	3.1745573934	2.6982814044
C38	-1.1101790217	2.2298793800	1.6932647837
C39	-2.1219659215	1.2814209137	1.8203851838
C40	-2.9106674507	1.2928936726	2.9803617910
C41	-2.6899639671	2.2441579432	3.9770815575
H42	-1.4983224343	3.9279385141	4.6235006825
H43	-3.3174044192	2.2457809775	4.8632486049
H44	-3.6974751806	0.5545114295	3.0975544856
C46	-0.1493613805	2.4335761418	0.5508521817
H47	-0.5930595579	2.2991472514	-0.4315138244
H48	0.6952036990	1.7394479420	0.6318477592
C48	0.2627986491	4.0793722239	2.3108603425
H49	1.1924983765	3.7374620890	2.7811453651
H50	0.1079276470	5.1235402498	2.5759327275
O51	-0.6355001914	7.4517226115	0.4036621980
H52	-0.4628007748	6.4721010243	0.3480351378
C53	-1.9990179396	7.6046422056	0.7149805997
H55	-2.3652487293	8.5641393736	0.3381712163
H56	-2.6125774003	6.7998088164	0.2981870849
C56	-2.2362327914	7.5987993166	2.2172688488
F57	-1.8781621413	6.4361261542	2.8022585969
F58	-1.5501536560	8.5820591135	2.8560057395
F59	-3.5539263923	7.7950371657	2.4946921607

5t' / H_2O / TFEH [(L')Mn$(CO)_4$ / H_2O / TFEH]$^-$, L' = bpymd-O$^-$ (pendant alcohol deprotonated)

Mn1	-4.6661453141	1.7244807213	-1.0325885472
C2	-3.0150360254	-0.6597692296	-1.5457101147
C3	-2.0590703937	0.5106800300	0.2461730120
C4	-0.9831550646	-0.3827348026	0.2281644650
C5	-0.9952790137	-1.3975918594	-0.7375018389
N6	-1.9834485070	-1.5555615297	-1.6008347478
C7	-6.2169711968	0.0068115751	-3.0615065553
N8	-5.1211285280	0.1570720064	-2.3138301608
C9	-4.1292607394	-0.8089645725	-2.4107935982
N10	-4.2139895544	-1.8689874657	-3.2751456238
C11	-5.3086119835	-1.9742411270	-4.0090481201

C12	-6.3761835758	-1.0603504736	-3.9367992824
N13	-3.0566636340	0.4105349257	-0.6467978160
H14	-0.1882738140	-0.3003506104	0.9570054310
H15	-0.1765484790	-2.1117604825	-0.7923969259
H16	-6.9924107574	0.7580573326	-2.9646714669
H17	-5.3574280008	-2.8197772086	-4.6917634512
H18	-7.2693347582	-1.1686535031	-4.5383367486
C19	-5.6625730753	0.8582458200	0.3042623753
O20	-6.2627682454	0.3153940862	1.1036716862
O21	-4.0801195962	4.0392642921	0.7636183603
C22	-4.2297094255	3.1134572650	0.1141338203
O23	-7.0109315626	3.3414619147	-1.8816259035
C24	-6.1089739856	2.7151490689	-1.5566594581
C25	-3.5894400704	2.4751029568	-2.3928131508
O26	-2.9291199435	2.9238526200	-3.2011419268
O27	0.5057113543	5.3954413444	0.3039471970
H28	1.3579323985	5.8581499256	-1.0821285290
C29	0.6024385762	4.2352359662	1.0253246001
C30	2.0872330090	3.8380566697	1.1317885792
F31	2.6704298086	3.6704379006	-0.0831398021
F32	2.8311700177	4.7676476919	1.7861183753
F33	2.2782755372	2.6589590557	1.8060286456
O34	1.8632521571	6.2563542357	-1.8503639719
H35	2.7257283166	6.4810023358	-1.4765762440
C36	-2.0126167431	3.1863643194	3.6050480875
C37	-1.1140914254	3.3717395505	2.5561904335
C38	-1.1748815039	2.5729882753	1.4115946128
C39	-2.0967792802	1.5208367553	1.3406143962
C40	-2.9815378135	1.3189034291	2.4103100222
C41	-2.9560097105	2.1599449966	3.5227748750
H42	-1.9695478408	3.8207753506	4.4857237925
H43	-3.6559520621	1.9954133586	4.3361059493
H44	-3.6755103534	0.4860124719	2.3787173796
C46	-0.1722484322	3.0193455483	0.3784260625
H47	-0.6597226914	3.3949586501	-0.5252559938
H48	0.4877314842	2.2036774306	0.0720034690
C48	0.0306595471	4.3433079430	2.4910635082
H49	0.7780548435	4.0784655147	3.2461602304
H50	-0.2739533663	5.3699350984	2.6838388766
O51	0.1548287089	7.6305971648	1.3964340230
H52	0.3586035873	6.6846256980	1.0065336646
C53	-1.0756624927	8.0318302961	0.8601850239
H55	-1.1339253379	9.1236444363	0.7849423082
H56	-1.2580706644	7.6051096671	-0.1330892626
C56	-2.2488979494	7.6037661983	1.7327760685

F57	-2.3491777875	6.2686677673	1.8857081114
F58	-2.1791850109	8.1307636108	2.9869565351
F59	-3.4292805805	8.0303555690	1.1995044229

5t' / H_2O / 2 TFEH [(L')Mn$(CO)_4$ / H_2O / 2 TFEH]$^-$, L' = bpymd-O$^-$ (pendant alcohol deprotonated)

Mn1	-4.8994643809	1.3532358790	-1.0721455058
C2	-2.9149219189	-0.7799473093	-1.5332678530
C3	-2.0708059561	0.6259818541	0.1454141202
C4	-0.8546471316	-0.0666336938	0.0896739727
C5	-0.7448622979	-1.1165186157	-0.8373124021
N6	-1.7460808141	-1.4897283975	-1.6211553924
C7	-6.2952808619	-0.7957292197	-2.8079801741
N8	-5.1861110585	-0.3917478069	-2.1746673834
C9	-4.0449565499	-1.1783627593	-2.2960518823
N10	-3.9997611752	-2.3004717467	-3.0857999769
C11	-5.1112435084	-2.6555709784	-3.7137988166
C12	-6.3238573287	-1.9426775392	-3.5987362673
N13	-3.0845671592	0.3228403480	-0.6888189390
H14	-0.0472847128	0.1834727784	0.7681668573
H15	0.1837493573	-1.6803529778	-0.9224671653
H16	-7.1861829115	-0.1869220996	-2.6872589103
H17	-5.0527523429	-3.5457206841	-4.3398329112
H18	-7.2271228741	-2.2560271363	-4.1107953719
C19	-5.6581662480	0.4581078999	0.4013231730
O20	-6.1120942549	-0.1255978301	1.2771146947
O21	-4.4810154702	3.8909983729	0.4580116298
C22	-4.5808929650	2.8876956020	-0.0968027947
O23	-7.5524702399	2.4725290227	-1.8512715824
C24	-6.5211535657	2.0465784142	-1.5565412231
C25	-4.0505046045	2.0981400080	-2.5832000698
O26	-3.5230582385	2.5418886646	-3.4987149459
O27	0.2213126559	5.7756507456	0.0159484549
H28	1.5963434979	6.0565154024	-0.9654407633
C29	0.0310590209	4.6842295412	0.8485455412
C30	1.4191883859	4.2073262389	1.3375845524
F31	2.2147284671	3.7909692506	0.3101855608
F32	2.1073518337	5.1878161995	1.9765607633
F33	1.3538210941	3.1528094744	2.2084200313
O34	2.3538870913	6.3692881636	-1.5396463599
H35	3.0310869250	6.6686885524	-0.9143014754
C36	-2.4646669142	3.3903364911	3.4249061580
C37	-1.6740584732	3.7279082601	2.3252591169
C38	-1.5605895706	2.8616928440	1.2269774032
C39	-2.2469635239	1.6424715998	1.2200812072

C40	-3.0361593462	1.2980863926	2.3347848267
C41	-3.1465057618	2.1647495231	3.4251148508
H42	-2.5425615965	4.0607842734	4.2787922747
H43	-3.7461011732	1.8725760143	4.2845073962
H44	-3.5308311435	0.3307302388	2.3582766416
C46	-0.6802145045	3.4670077062	0.1577780789
H47	-1.2823011575	3.8734056767	-0.6644855091
H48	0.0218336494	2.7530222490	-0.2826349297
C48	-0.8595467619	4.9778664211	2.1095773286
H49	-0.2812812090	5.2762981612	2.9894703510
H50	-1.5044134516	5.8232124418	1.8533925168
O51	0.7300378699	7.8506434816	1.3039756939
H52	0.5027492221	6.9508324387	0.7733965062
C53	0.0048639201	8.9201087052	0.7632936063
H55	0.5416438110	9.8673273814	0.9039198716
H56	-0.1943022406	8.7929124765	-0.3092625605
C56	-1.3497164756	9.0895618181	1.4412713299
F57	-2.1542500255	8.0039235963	1.2927396946
F58	-1.2413899174	9.3126272178	2.7742382949
F59	-2.0273428587	10.1511396936	0.9137788531
O60	0.8067825493	7.3059752850	3.9905537940
H61	0.7843242538	7.5511819282	3.0345266739
C62	2.0109526959	7.7490540595	4.5576297127
H64	2.9052522063	7.3598539808	4.0487289074
H65	2.0894949493	8.8456575915	4.6111118247
C65	2.0714211827	7.2411626580	5.9867875458
F66	1.0373435797	7.6796818151	6.7480516169
F67	2.0676321567	5.8868480045	6.0685369198
F68	3.2155278476	7.6685437022	6.5942565157

5t/ H_2O / TFE^- / TFEH [(L)$Mn(CO)_4$ / H_2O / TFE^- / TFEH]

Mn1	-4.4557070257	2.1072782031	-0.1640790429
C2	-3.0283198090	-0.1646086647	-1.4212132843
C3	-1.9441269027	0.3388434037	0.5978849069
C4	-1.0444355857	-0.7067173023	0.3610819376
C5	-1.2030481884	-1.4416167189	-0.8284075258
N6	-2.1606051313	-1.1871573428	-1.7060568947
C7	-5.9173105601	1.5000471726	-2.8164247671
N8	-4.9325822686	1.1758077045	-1.9671686775
C9	-4.0735630679	0.1454845484	-2.3314410177
N10	-4.2008798358	-0.5424389217	-3.5126640020
C11	-5.1846954945	-0.1903289842	-4.3275071423
C12	-6.0981063783	0.8436688112	-4.0311080142
N13	-2.9379295859	0.6214524019	-0.2665221773
H14	-0.2509766903	-0.9237554388	1.0674193299

H15	-0.5218461296	-2.2579794183	-1.0679483715
H16	-6.5815466003	2.3071995541	-2.5243654254
H17	-5.2628392821	-0.7426640264	-5.2637945113
H18	-6.8976542426	1.1202691869	-4.7099106094
C19	-5.4941504969	0.8312021825	0.7467410652
O20	-6.0996656022	0.0219827746	1.2883392616
O21	-3.8963795459	3.6227745732	2.3524294033
C22	-4.0208282444	2.9774166032	1.4075581488
O23	-6.7322254453	4.0183600132	-0.3852577626
C24	-5.8511764189	3.2773720521	-0.3018080401
C25	-3.3061395638	3.1821728342	-1.2082744305
O26	-2.5967962126	3.7577695525	-1.8982967116
O27	1.1524585987	4.9181510071	0.3997145004
H28	2.7565861635	6.5553945618	-0.6688253149
C29	0.9005560656	3.8345013409	1.2583363622
C30	2.2827875764	3.1956654718	1.4800440113
F31	2.8698182283	2.8253578477	0.3117873617
F32	3.1476315173	4.0366193983	2.1005249540
F33	2.2103570551	2.0724859242	2.2495365946
O34	2.4947635742	7.4890538480	-0.6997185521
H35	1.6134948520	7.4984532640	-0.2307180717
C36	-1.3121797311	2.7195682651	4.1346686268
C37	-0.6768017438	3.0436230980	2.9347742029
C38	-0.8841159022	2.2664961036	1.7881399987
C39	-1.7566201175	1.1720490392	1.8191116519
C40	-2.3787703127	0.8306083642	3.0318901155
C41	-2.1570980438	1.6007066932	4.1785921593
H42	-1.1480741436	3.3150519429	5.0304952670
H43	-2.6469116723	1.3271302878	5.1104624514
H44	-3.0319898197	-0.0381262167	3.0745228930
C46	-0.0608509071	2.7731693458	0.6293254556
H47	-0.6709815106	3.2887079914	-0.1158323111
H48	0.4723349578	1.9738672489	0.1046081324
C48	0.2725818551	4.1849101913	2.6464925353
H49	1.0261570433	4.3235955550	3.4277598534
H50	-0.2703213447	5.1296831446	2.5543768972
O51	0.0892782650	7.2825971564	0.5761920156
H52	0.6738430562	5.7739146718	0.6479525828
C53	-0.9667865239	7.2266384724	-0.3241353028
H55	-1.3234977844	8.2204302310	-0.6484186205
H56	-0.7252636791	6.6546086641	-1.2366876988
C56	-2.1789285367	6.5318519068	0.2908973058
F57	-1.8973826742	5.2662270662	0.7088700252
F58	-2.6698367251	7.1870877511	1.3735966810
F59	-3.2099231956	6.4134480318	-0.5992458632

O60	-0.3726012082	9.2533368353	2.1873031469
H61	-0.2181212414	8.4474307866	1.5769733035
C62	0.5085994211	9.1543010119	3.2718693828
H64	1.4553857358	8.6644348291	3.0056221432
H65	0.7353698655	10.1499834374	3.6725226786
C65	-0.0844514122	8.3492392811	4.4245334412
F66	-1.2262503965	8.8973925893	4.9189106259
F67	-0.3843254531	7.0727787174	4.0803335858
F68	0.7988712413	8.2817005280	5.4641018668

5t/ H_2O / TFE^- / 2 TFEH [(L)Mn$(CO)_4$ / H_2O / TFE^- / 2 TFEH]

Mn1	-4.4869843323	2.2122972169	-0.0471901395
C2	-3.2240243792	-0.1023670958	-1.3986077198
C3	-1.8651322168	0.4936452878	0.4204636928
C4	-0.9616149608	-0.5116218251	0.0574406088
C5	-1.2680053346	-1.2797213029	-1.0806898319
N6	-2.3640768713	-1.0924109441	-1.7983801928
C7	-6.3453883350	1.4290211133	-2.3885456639
N8	-5.2256043733	1.1736325963	-1.6977891439
C9	-4.4072330110	0.1433801683	-2.1455003459
N10	-4.6993245592	-0.6039522129	-3.2596422248
C11	-5.8114092450	-0.3162607722	-3.9202386109
C12	-6.6990794981	0.7071113610	-3.5256349306
N13	-2.9932161207	0.7131264278	-0.2835955050
H14	-0.0631482610	-0.6841008867	0.6390840135
H15	-0.5932723698	-2.0690645280	-1.4114339999
H16	-6.9796002961	2.2336174310	-2.0302520714
H17	-6.0206829194	-0.9149527378	-4.8066055677
H18	-7.6060878965	0.9286879786	-4.0777345959
C19	-5.4253475368	1.0236237081	1.0689594038
O20	-5.9795006682	0.2695385618	1.7319796056
O21	-3.5862288259	3.8596475116	2.2797305109
C22	-3.8404431211	3.1641425112	1.3988388902
O23	-6.7209552888	4.1855308592	-0.1146992336
C24	-5.8607838073	3.4161823402	-0.0880745169
C25	-3.4336910293	3.1729400619	-1.2864925718
O26	-2.7624042792	3.6557746929	-2.0779667520
O27	1.6914498605	4.7975127232	0.0861811091
C29	1.2953907327	3.7607351446	0.9534976346
C30	2.5906432987	2.9752737689	1.2246487989
F31	3.1499427453	2.5003085503	0.0791053601
F32	3.5353091013	3.7384882685	1.8288746028
F33	2.3812663508	1.8980268000	2.0276344396
O34	2.5455818371	8.2622610634	-0.8154856801
H35	1.7110790429	7.8318292080	-0.4390788612

C36	-0.9157234463	2.8756546685	3.8864746166
C37	-0.3140759277	3.1445288704	2.6574555056
C38	-0.6077868671	2.3643740901	1.5297706485
C39	-1.5515098127	1.3332338551	1.6110839287
C40	-2.1417490723	1.0472768232	2.8554576146
C41	-1.8218109771	1.8094568611	3.9827008486
H42	-0.6764409091	3.4718727463	4.7643660516
H43	-2.2849618098	1.5745362298	4.9383297579
H44	-2.8456682647	0.2221959794	2.9363521474
C46	0.2198670119	2.8038428552	0.3422473905
H47	-0.3682025873	3.3872882266	-0.3716232554
H48	0.6595910221	1.9696030098	-0.2127038417
C48	0.6906228213	4.2202903507	2.3151012196
H49	1.4490072027	4.3734110359	3.0891233895
H50	0.1890070366	5.1783574948	2.1552341107
O51	0.4492637500	7.0490489548	0.1990617858
H52	1.1397391992	5.6556034092	0.2008932870
C53	-0.6176992832	7.0290107224	-0.6974649231
H55	-0.8981049601	8.0326116437	-1.0599074212
H56	-0.4213572234	6.4038594360	-1.5848938332
C56	-1.8736137015	6.4541263709	-0.0500608227
F57	-1.6686794070	5.2086671114	0.4604844149
F58	-2.3390888720	7.2139022655	0.9699834263
F59	-2.8978908580	6.3302576766	-0.9473549222
O60	0.0191224745	9.0465476935	1.8993436342
H61	0.1905870231	8.2492012058	1.3084330863
C62	0.3392369446	8.7423716218	3.2306858580
H64	1.2346087641	8.1155428592	3.3245164555
H65	0.5080930966	9.6710571455	3.7888008837
C65	-0.7854111777	8.0011831065	3.9483382227
F66	-1.9718541309	8.6581945365	3.8896422223
F67	-1.0013345510	6.7578562874	3.4546146214
F68	-0.4836959180	7.8475351553	5.2722826532
C68	3.6609198171	7.5894630184	-0.2830364159
H69	3.4378051490	6.5469269604	-0.0290559731
H71	4.4930373507	7.6074897176	-0.9958824343
C71	4.1578059095	8.2452561146	0.9975822057
F72	4.5219137006	9.5429943115	0.8240824009
F73	3.2248104693	8.2327489456	1.9841466361
F74	5.2517985183	7.5907752323	1.4819769315
O75	3.7108961602	4.5152919035	-2.0694559173
H76	3.0623710353	4.5599654070	-1.3389141038
H77	4.4872215176	4.0625461183	-1.7033559941

5t $[(L)Mn(CO_4)]^0$

Mn1	-4.6091912278	1.7792516514	-1.0688791081
C2	-2.9540974922	-0.5845131008	-1.6488647222
C3	-1.9604304823	0.5757739965	0.1296564072
C4	-0.8752232002	-0.3007870806	0.0736866409
C5	-0.9010416598	-1.3027240763	-0.9104815814
N6	-1.9107932922	-1.4630238482	-1.7451822135
C7	-6.2317638527	0.0347579531	-3.0149427188
N8	-5.1020003655	0.2028646779	-2.3224067507
C9	-4.1011244352	-0.7470372324	-2.4680317918
N10	-4.2089074785	-1.8045360824	-3.3306246682
C11	-5.3362444540	-1.9280970677	-4.0104867244
C12	-6.4152836459	-1.0340732797	-3.8822560064
N13	-2.9790356516	0.4786406337	-0.7406466197
H14	-0.0643435770	-0.2256050893	0.7856312043
H15	-0.0742060062	-2.0038137458	-1.0000016140
H16	-7.0140478903	0.7726537077	-2.8785938011
H17	-5.4037639087	-2.7723956970	-4.6929496009
H18	-7.3353865460	-1.1572379670	-4.4386548104
C19	-5.5424425898	0.9096549624	0.3168358318
O20	-6.0973100811	0.3643701745	1.1453835224
O21	-3.9660976724	4.1146491567	0.6717603785
C22	-4.1446424160	3.1776902338	0.0413461529
O23	-6.9927196093	3.3802791222	-1.8445142785
C24	-6.0795355209	2.7580910250	-1.5475085682
C25	-3.5861071977	2.5250319812	-2.4717927018
O26	-2.9496640117	2.9709949190	-3.3009554374
O27	0.9622057634	5.3811378278	0.1714934243
C28	0.5874624571	4.2821630768	0.9892684282
C29	1.8734551117	3.5400978040	1.4007098714
F30	2.5779252454	3.1152630585	0.3281763958
F31	2.6996275605	4.3349489039	2.1245609241
F32	1.6062651437	2.4481435949	2.1552873324
C33	-1.9832145478	3.2265756925	3.5265438386
C34	-1.2000666224	3.5263974753	2.4191345142
C35	-1.2164794793	2.7155962795	1.2787666056
C36	-2.0074131706	1.5667029702	1.2440660751
C37	-2.7941507471	1.2607090961	2.3671850012
C38	-2.7917372180	2.0862676066	3.4899512221
H39	-1.9571843156	3.8558915614	4.4113689021
H40	-3.4035241762	1.8252616868	4.3475211693
H41	-3.3881144180	0.3527347052	2.3672732967
C42	-0.3237355383	3.2994728249	0.2063344706
H43	-0.9088412441	3.8913266830	-0.5065995839
H44	0.2355073308	2.5595743331	-0.3687278064
C45	-0.2372270901	4.6756059327	2.2453380028

H46	0.3848048499	4.8565841583	3.1257853250
H47	-0.7657149901	5.6086932183	2.0196730253
H49	1.3669510210	6.0812887448	0.7103741898

CO dissociation TS: $TS_{\mathbf{5t\rightarrow 6t}}$

Mn1	-4.6556223278	1.6878202986	-1.0381942950
C2	-2.9573258300	-0.5698044267	-1.7094992698
C3	-1.8975301309	0.6422036497	-0.0365858891
C4	-0.7543996184	-0.1159113973	-0.2558175927
C5	-0.7938202098	-1.1031883076	-1.2421876247
N6	-1.9016215982	-1.3554146811	-1.9379921431
C7	-6.4134709823	-0.1544083902	-2.7077266676
N8	-5.2023337579	0.0800714407	-2.1542360716
C9	-4.2213882404	-0.8225022231	-2.4143450970
N10	-4.3574908902	-1.8950651727	-3.2028253936
C11	-5.5496783870	-2.0970235708	-3.7629411963
C12	-6.6337002547	-1.2413742486	-3.5291131792
N13	-2.9961138284	0.4683501216	-0.8232067193
H14	0.1253514803	0.0174503027	0.3611964984
H15	0.0739448296	-1.7236663165	-1.4465280974
H16	-7.2029165467	0.5498310088	-2.4756590559
H17	-5.6514914743	-2.9638327004	-4.4093372259
H18	-7.6055495014	-1.4188216073	-3.9743941147
C19	-5.6016054723	1.3963635920	0.4557447204
O20	-6.2298451580	1.2327230398	1.4123572385
O21	-3.4865888743	4.2521927739	-0.1114378001
C22	-3.8945558144	3.2219774659	-0.4373734880
O23	-6.7084748196	3.4448114263	-2.2473431834
C24	-5.9109848500	2.7507625392	-1.7777697256
C25	-3.1126817719	2.1285131870	-3.4554711646
O26	-2.7740439438	3.1235996765	-3.8839968248
O27	0.9768454086	5.4774736814	0.5157798553
C28	0.5930584191	4.3098289914	1.2270732371
C29	1.8765544868	3.5657372239	1.6413340501
F30	2.6457944506	3.2495688243	0.5754190020
F31	2.6441062998	4.3118854905	2.4725710139
F32	1.5994694421	2.4058437217	2.2852202204
C33	-2.0715345304	3.0165568066	3.5483035962
C34	-1.2394834191	3.4077301135	2.5071834012
C35	-1.1876756431	2.6887090064	1.3068494626
C36	-1.9750861032	1.5476298752	1.1416964911
C37	-2.8200726597	1.1556080105	2.1940496552
C38	-2.8704609892	1.8808597208	3.3809680308
H39	-2.0939355457	3.5748520153	4.4800039726
H40	-3.5217733191	1.5490464121	4.1829475138

H41	-3.4207145818	0.2597111177	2.0830333993
C42	-0.2552803386	3.3698064867	0.3286447725
H43	-0.8219395446	3.9981961234	-0.3664519957
H44	0.3531245338	2.6910909318	-0.2715691388
C45	-0.2974962816	4.5858265843	2.4684351882
H46	0.2780015876	4.7120702676	3.3891103908
H47	-0.8404913417	5.5208086763	2.2894954307
H49	1.3321615971	6.1438980877	1.1275231125

6t $[(L)Mn(CO)_3]^0$

Mn1	-4.7260312191	1.6009958609	-0.9698275888
C2	-2.9446646545	-0.5956931078	-1.6921901764
C3	-1.9255346529	0.6178024129	0.0019996958
C4	-0.7832428456	-0.1519874656	-0.1805166525
C5	-0.7953408878	-1.1337021854	-1.1699314015
N6	-1.8834413567	-1.3748557904	-1.9024528993
C7	-6.3829579430	-0.2138200113	-2.7671773579
N8	-5.1882736227	0.0292987050	-2.1775108815
C9	-4.1901192821	-0.8535651763	-2.4328956482
N10	-4.2858866217	-1.9052010005	-3.2518254197
C11	-5.4610537335	-2.1156114322	-3.8462731718
C12	-6.5644030177	-1.2853231240	-3.6168340044
N13	-3.0099601033	0.4409945200	-0.8067676305
H14	0.0790962600	-0.0211200678	0.4615250194
H15	0.0750426774	-1.7569455217	-1.3520588673
H16	-7.1901775473	0.4699886814	-2.5371974799
H17	-5.5314920721	-2.9679311997	-4.5153626387
H18	-7.5228904695	-1.4693462422	-4.0875276058
C19	-5.6853587857	1.2532945077	0.5058804668
O20	-6.3236639400	1.0639605383	1.4548240892
O21	-3.6458437444	4.1884213837	-0.0015423329
C22	-4.0117217418	3.1473009591	-0.3483272431
O23	-6.7789922425	3.3552401741	-2.1747164881
C24	-5.9767813866	2.6562443727	-1.7116659555
O27	1.0323134001	5.3898504654	0.3949380196
C28	0.6255386930	4.2601550943	1.1531339253
C29	1.8941509970	3.5126594742	1.6057957464
F30	2.6605465540	3.1327113681	0.5588543865
F31	2.6732055782	4.2836365396	2.4034695413
F32	1.5944909108	2.3901286262	2.3030761065
C33	-2.0888825318	3.1209717449	3.4999088391
C34	-1.2360270077	3.4503184478	2.4542675143
C35	-1.1901996727	2.6821280764	1.2852950806
C36	-2.0024818629	1.5540410546	1.1555945664
C37	-2.8638774292	1.2216466417	2.2140208911

C38	-2.9106105936	1.9967719942	3.3695446492
H39	-2.1104098638	3.7178400146	4.4073564806
H40	-3.5781244670	1.7135421085	4.1767130351
H41	-3.4848058791	0.3371596990	2.1314924029
C42	-0.2343056719	3.2992608737	0.2885902851
H43	-0.7823307021	3.9028563234	-0.4426425899
H44	0.3650495695	2.5813444016	-0.2735186354
C45	-0.2654372944	4.6033890742	2.3780362711
H46	0.3081309132	4.7480840318	3.2972472628
H47	-0.7826745698	5.5449333530	2.1617978546
H49	1.4157539323	6.0663931059	0.9775493205

7t $[(L)Mn(CO)_3(NCCH_3)]^0$

Mn1	-4.5845294311	1.7922236294	-1.0577273196
C2	-2.9453098468	-0.5347882946	-1.7734271895
C3	-1.9385330947	0.5724360563	0.0674083082
C4	-0.8211179889	-0.2683675799	-0.0451481329
C5	-0.8293648050	-1.2074424542	-1.1076878068
N6	-1.8245203475	-1.3695249718	-1.9432793494
C7	-6.2908583797	0.0502980310	-2.8948481713
N8	-5.1345136953	0.2446305849	-2.2850827085
C9	-4.0774612626	-0.6875653987	-2.5268126950
N10	-4.2238477491	-1.7054252898	-3.4944688021
C11	-5.3937734224	-1.8161132365	-4.0783407975
C12	-6.5129790197	-0.9842912025	-3.8082149804
N13	-2.9606864064	0.5156246855	-0.7814061011
H14	-0.0015868152	-0.2028287872	0.6566865101
H15	0.0325973354	-1.8608911289	-1.2484252679
H16	-7.0890740286	0.7516432852	-2.6651824314
H17	-5.4893293282	-2.6094985414	-4.8206919059
H18	-7.4629554698	-1.1067516404	-4.3121226898
C19	-5.4913166063	1.0665395318	0.3165996737
O20	-6.0813962532	0.5701309068	1.1719661349
O21	-3.7524206497	4.1827964767	0.5043060385
C22	-4.0077185870	3.2162915622	-0.0680001606
O23	-6.9003388668	3.4535098263	-1.8702160071
C24	-5.9998988832	2.8031283775	-1.5569072904
N25	-3.4790211917	2.4289276969	-2.7295138690
C26	-2.8805876366	2.6843113442	-3.6770039167
O27	0.8362550520	5.4535869108	0.3980112038
C28	0.5503210119	4.2971146430	1.1762591634
C29	1.8947946933	3.6542871728	1.5603523689
F30	2.6243583716	3.3054232433	0.4765516336
F31	2.6629904346	4.5042520322	2.2895323115
F32	1.7252855522	2.5334190775	2.3009631820

C33	-2.0309215698	3.0402539582	3.6234330950
C34	-1.2176762851	3.3944379001	2.5537495050
C35	-1.1934250085	2.6351008210	1.3778369761
C36	-1.9878506106	1.4931760071	1.2499848825
C37	-2.8034709835	1.1381620945	2.3367853725
C38	-2.8324342130	1.9005495987	3.5043758085
H39	-2.0407882102	3.6306026331	4.5356842114
H40	-3.4709391260	1.5964118344	4.3282639627
H41	-3.4118174636	0.2435644120	2.2652297041
C42	-0.2876761346	3.2814135342	0.3539868458
H43	-0.8761631342	3.8512191058	-0.3724929006
H44	0.3222238133	2.5727351341	-0.2079966774
C45	-0.2933541204	4.5837704344	2.4490536858
H46	0.3186920215	4.7416376591	3.3412055399
H47	-0.8561742428	5.5076706821	2.2744475134
H49	1.1778180325	6.1658086156	0.9634192378
C49	-2.1256638331	2.9902961898	-4.8812012165
H50	-2.8131876800	3.2519208084	-5.6906590439
H51	-1.4521203511	3.8313160233	-4.6950929130
H52	-1.5362308196	2.1184436284	-5.1809177002

MeCN dissociation TS: $TS_{\mathbf{7t\rightarrow 6t}}$

Mn1	-4.6657287791	1.7271218467	-0.9848290641
C2	-2.9139123558	-0.3972762755	-1.8672837290
C3	-1.8618311536	0.7383560724	-0.1217484195
C4	-0.6999723372	0.0416342286	-0.4076407195
C5	-0.7191533127	-0.8732765912	-1.4730309143
N6	-1.8197237393	-1.1196009816	-2.1677571176
C7	-6.4079131417	-0.0627155791	-2.7047119427
N8	-5.1848967947	0.1975314147	-2.1866145822
C9	-4.1663405872	-0.6503668760	-2.5422795478
N10	-4.2984235184	-1.6707760823	-3.4138369357
C11	-5.4998037045	-1.8825048130	-3.9332849717
C12	-6.6176218638	-1.0973314717	-3.5883194934
N13	-2.9678257769	0.5904486093	-0.9046888613
H14	0.1798531780	0.1548847871	0.2120012687
H15	0.1693730803	-1.4426250295	-1.7309776189
H16	-7.2194177201	0.5820091806	-2.3885921794
H17	-5.5962890192	-2.7031716889	-4.6386674265
H18	-7.6002992727	-1.2921612926	-4.0008376184
C19	-5.5392856962	1.3147793191	0.5072935030
O20	-6.1216350380	1.0494744639	1.4692860601
O21	-3.5544433304	4.2653326816	0.0830296392
C22	-3.9394320857	3.2479411701	-0.2962974525
O23	-6.8629234357	3.4536924745	-1.9678340362

C24	-6.0122347812	2.7736184965	-1.5857056344
N25	-3.1002999656	2.3977322124	-3.5751491110
C26	-2.4039648051	2.5720197697	-4.4789249080
O27	0.9135285196	5.5777154122	0.7480576066
C28	0.5589400388	4.3531276387	1.3744423460
C29	1.8613701398	3.6010013961	1.7060124567
F30	2.6103594265	3.3769381393	0.6030370993
F31	2.6372061698	4.2962927283	2.5736941789
F32	1.6169039428	2.3926455393	2.2678772353
C33	-2.0227559979	2.8254208438	3.6440679433
C34	-1.2268314423	3.3183354737	2.6180832168
C35	-1.1867380997	2.6949586998	1.3648409701
C36	-1.9451248814	1.5474082900	1.1268229776
C37	-2.7509106673	1.0516927010	2.1664845305
C38	-2.7940630913	1.6826800598	3.4063506179
H39	-2.0369248664	3.3086066470	4.6167761958
H40	-3.4165860130	1.2711870383	4.1943792870
H41	-3.3283003840	0.1490491245	2.0015444912
C42	-0.2925775688	3.4713561693	0.4230532704
H43	-0.8890295356	4.1398611737	-0.2065786238
H44	0.3128693074	2.8540091567	-0.2425081556
C45	-0.3112933047	4.5182069211	2.6491165849
H46	0.2799399597	4.5915828154	3.5657878576
H47	-0.8773167600	5.4512396250	2.5476843941
H49	1.2652103047	6.2024119104	1.4038366860
C49	-1.5270019737	2.7911851589	-5.6215837836
H50	-2.1274096906	2.9333693591	-6.5241563150
H51	-0.9104901036	3.6801391291	-5.4560823596
H52	-0.8752912929	1.9252221792	-5.7631565653

1t / TFEH

Mn1	-4.5592783542	1.7630361083	-0.6266098388
C2	-2.9902475638	-0.4633440918	-1.6437945176
C3	-2.1709200630	0.1312833871	0.4609157236
C4	-1.2443337829	-0.8845200128	0.3702671220
C5	-1.2365587033	-1.6747811158	-0.7955822166
N6	-2.0881301654	-1.4668652990	-1.7757962242
C7	-5.7105175350	1.1665261295	-3.3419184252
N8	-4.7818763978	0.8845754814	-2.3673020884
C9	-3.9313841974	-0.1822082230	-2.6612387241
N10	-3.9729375511	-0.8941685802	-3.8148635385
C11	-4.8649346108	-0.5769144707	-4.7256027507
C12	-5.7886784972	0.4831325230	-4.5197595707
N13	-3.0746489353	0.3783286876	-0.5371315233
H14	-0.5347354115	-1.0527859958	1.1698142729

H15	-0.5193321999	-2.4824230340	-0.9186051936
H16	-6.3930248413	1.9780511262	-3.1329618955
H17	-4.8742277932	-1.1589573698	-5.6432428272
H18	-6.5287235362	0.7419485129	-5.2668929233
C19	-5.4526849941	1.1953092372	0.7797446252
O20	-6.0698263178	0.8533404077	1.7084935868
O21	-3.1686994020	4.0426996240	0.5916812990
C22	-3.6713353317	3.0889722980	0.1257659340
O23	-6.6419669168	3.7598797345	-1.2094815704
C24	-5.8191720260	2.9645782240	-0.9916675728
O25	-0.4369926802	4.7678170384	0.4326891433
H26	-1.3850340440	4.5618058980	0.5222673728
C27	0.3281588913	3.7668706858	1.1057034292
C28	1.7685504431	4.0584952732	0.7035905023
F29	1.9551530133	3.9287101603	-0.6274419291
F30	2.1382230969	5.3196319850	1.0370246076
F31	2.6331572826	3.2172814544	1.3120309414
C32	-1.8704268407	2.6715501373	3.9250657902
C33	-1.0147643948	2.8232091942	2.8400515860
C34	-1.1322142990	1.9919974112	1.7250819256
C35	-2.1156566882	1.0091584337	1.6606972433
C36	-2.9634644094	0.8420225894	2.7596013213
C37	-2.8424735284	1.6665455548	3.8784745031
H38	-1.7922681832	3.3207415663	4.7915144028
H39	-3.5157629708	1.5268719720	4.7174770433
H40	-3.7240242745	0.0724810099	2.7337325257
C41	-0.1104764678	2.3470872586	0.6741083693
H42	-0.4983589460	2.3534352874	-0.3466442858
H43	0.7336097040	1.6506162014	0.7028965422
C44	0.1045624684	3.8191693990	2.6400565549
H45	1.0052389460	3.5056277334	3.1779817374
H46	-0.1405268081	4.8341665139	2.9585116017
O47	-0.2604617121	7.5209597720	0.2737635109
H48	-0.2054295143	6.5634285690	0.4598707513
C49	0.9262245775	8.1675957461	0.6744603552
H50	1.0139975057	8.2574147938	1.7642555460
H51	1.8272492019	7.6870096151	0.2826705297
C52	0.8938130045	9.5711510541	0.1087981608
F53	0.9519537690	9.5855723134	-1.2432636931
F54	-0.2261697822	10.2458919771	0.4573589430
F55	1.9492574503	10.2916617531	0.5592077299

TS for Protonation at Mn: $TS_{\mathbf{1t/TFEH \rightarrow 8t'/TFEH}}$

Mn1	-4.5805224462	1.9738906565	-0.5400557583
C2	-2.8705994284	-0.0960292208	-1.7466650259

C3	-2.0636719708	0.3254021594	0.3788084497
C4	-1.1982102795	-0.7497054341	0.2280342846
C5	-1.2155746039	-1.4594232320	-0.9717486912
N6	-2.0399947750	-1.1200035992	-1.9610262655
C7	-5.6874919760	1.5172287978	-3.3333520871
N8	-4.7294790009	1.2073014812	-2.4301868818
C9	-3.8323159041	0.2610278072	-2.7949689004
N10	-3.7893692270	-0.3416049399	-3.9895823008
C11	-4.7192124971	0.0008358909	-4.8814627645
C12	-5.7182151942	0.9330923178	-4.5832456516
N13	-2.9512911915	0.6594234678	-0.6087160445
H14	-0.5053835966	-1.0078771895	1.0204459352
H15	-0.5495015391	-2.3006627611	-1.1412935034
H16	-6.4262914014	2.2474501083	-3.0298981940
H17	-4.6728273360	-0.4815600148	-5.8536957171
H18	-6.4843459089	1.1957933255	-5.3035125878
C19	-5.8814143654	0.9420487101	0.0786263271
O20	-6.8237547281	0.3848043055	0.4872279844
O21	-4.4538862628	3.2172407735	2.1377032841
C22	-4.4013514842	2.6920250515	1.1076012682
O23	-6.0184139043	4.4569941842	-1.1882266752
C24	-5.4012963299	3.4763560868	-0.9590016146
O25	-1.8306439291	5.3585406626	0.5118162694
H26	-2.1933802460	5.0681493731	-0.3827008145
C27	-0.7002376273	4.5842140473	0.8439510047
C28	0.5326298485	5.2514658004	0.2233009235
F29	0.4339621122	5.3316874033	-1.1269669393
F30	0.7156895905	6.5126976385	0.6792410087
F31	1.6792882284	4.5714015590	0.4889867414
C32	-1.6434402961	2.6833019076	3.9529193835
C33	-1.2250148703	3.1729894018	2.7193592397
C34	-1.3783405048	2.4042766175	1.5671320099
C35	-1.9678481747	1.1417530629	1.6164033263
C36	-2.3750212931	0.6396751724	2.8589785517
C37	-2.2173935880	1.4088354661	4.0142044510
H38	-1.5304751151	3.2788246857	4.8545019183
H39	-2.5510480865	1.0127374064	4.9683346505
H40	-2.8317531604	-0.3432072279	2.9166374326
C41	-0.8323982908	3.1129775497	0.3606516906
H42	-1.4974826254	3.0445475553	-0.4942129365
H43	0.1375774750	2.6943999102	0.0715093611
C44	-0.5738923525	4.4960338923	2.3897658233
H45	0.4751626774	4.4952511442	2.7046591303
H46	-1.0595539724	5.3549222821	2.8573928358
O47	-2.9033743008	4.6126648416	-1.7750075107

C49	-2.1980451721	3.8880846387	-2.7125993124
H50	-1.1303177424	4.1510292030	-2.7671592542
H51	-2.2556777524	2.7977019575	-2.5351853081
C52	-2.7378889933	4.0715647231	-4.1221813183
F53	-4.0639814414	3.8185402775	-4.2177534535
F54	-2.5507091354	5.3297380390	-4.6057604053
F55	-2.1195571669	3.2227613473	-4.9983025372
H55	-3.8609631033	3.5922293742	-1.2160334564

3b / TFE^- / TFEH [(bpymd)$MnCO_3CO_2H$ / TFE^- / TFEH]

Mn1	-3.7215704499	2.4960905234	-1.2924063010
C2	-2.6755313136	-0.1425336034	-0.4833617964
C3	-1.3340642060	1.5128112387	0.3895330386
C4	-0.5237534186	0.5404577968	0.9693420558
C5	-0.8635849094	-0.7920164661	0.7453017001
N6	-1.9480192990	-1.1363502130	0.0290931249
C7	-5.7394916084	0.4268054968	-2.3419300602
N8	-4.5936350299	0.6441404420	-1.6681440996
C9	-3.9189613747	-0.4445564180	-1.2339570214
N10	-4.2953361192	-1.7118199818	-1.4170423514
C11	-5.4394476242	-1.9190480526	-2.0875424476
C12	-6.2084501410	-0.8612730126	-2.5757672792
N13	-2.4021530170	1.1766489921	-0.3590427908
H14	-1.1397502080	2.5640562377	0.5161109970
H15	0.3380358181	0.8155675752	1.5694025873
H16	-0.2673098783	-1.6046351931	1.1550974358
H18	-6.2859385060	1.2959283747	-2.6889170192
H20	-5.7425244312	-2.9537280836	-2.2323157981
H21	-7.1352042584	-1.0294126409	-3.1157725017
C22	-4.6439380973	2.7192012653	0.2754219868
O23	-5.2335591193	2.9101325359	1.2571103998
O24	-2.3023262811	5.0782043795	-0.9380712391
C25	-2.8046569885	4.0398903393	-1.0487242771
O26	-5.6970769650	4.0696086985	-2.8405066161
C27	-4.9282701044	3.4481667320	-2.2303725839
C28	-2.7263237849	2.1897591575	-3.1171638768
O29	-1.4083173695	2.4400302256	-3.2552032621
O30	-3.3004488133	1.7738342147	-4.1416082624
O31	0.1278000048	3.2077559952	-1.3655193493
H32	-0.9121291896	2.7763286150	-2.4057785977
C33	1.3098267729	2.6231320992	-1.7736850451
H34	1.9883209566	2.3631643131	-0.9395690553
H35	1.1693425588	1.7020301993	-2.3686072310
C36	2.1146508642	3.5607788908	-2.6686145595
F37	1.4590505889	3.8788528953	-3.8188108659

F38	2.4183478103	4.7400864152	-2.0636834510
F39	3.3092285432	3.0028450736	-3.0465350671
O40	0.9839362587	4.3831420501	0.7783497678
H41	0.5799211458	3.9906380390	-0.0747159048
C42	0.3004540686	5.5520690664	1.1412254178
H44	0.9951688722	6.3243692803	1.4981807112
H45	-0.2935702043	5.9730432154	0.3217815394
C45	-0.6635844610	5.2738762368	2.2874800452
F46	-1.6097615183	4.3507801291	1.9653346135
F47	-0.0326516106	4.8029030592	3.3969809768
F48	-1.3266114730	6.4029938168	2.6626525417

3b / TFE^- / 2 TFEH [(bpymd)$MnCO_3CO_2H$ / TFE^- / 2 TFEH]

Mn1	-3.4687827754	0.8052065790	-2.2241385170
C2	-2.5529642815	-0.6548729431	0.1639496355
C3	-2.3308528435	1.6093061359	0.5366155634
C4	-1.9036543061	1.3486318248	1.8341349054
C5	-1.8202692308	0.0114610379	2.2242342145
N6	-2.1404490344	-0.9892522004	1.3881212059
C7	-3.7822649670	-2.1774340048	-2.8981854645
N8	-3.3963830338	-1.2597191547	-1.9913323556
C9	-2.9601867674	-1.7140196317	-0.7959438774
N10	-2.8903789363	-2.9978810555	-0.4379945270
C11	-3.2898027728	-3.9073507928	-1.3412670600
C12	-3.7497651091	-3.5372103650	-2.6069236654
N13	-2.6632429574	0.6101487312	-0.3071485981
H14	-2.4102159197	2.6256592303	0.1687510312
H15	-1.6473090679	2.1545987765	2.5145355606
H16	-1.4935152239	-0.2669910246	3.2241918522
H17	-4.1277736104	-1.8126310979	-3.8589195273
H18	-3.2402543243	-4.9518198529	-1.0404034831
H19	-4.0738482967	-4.2740493452	-3.3360739914
C20	-5.1839095355	0.7684551562	-1.5887553737
O21	-6.2843820123	0.7575117036	-1.2205527159
O22	-3.8372805911	3.7428443929	-2.0212307097
C23	-3.5870288335	2.6201133020	-2.1461116239
O24	-4.2759359937	0.8574532612	-5.0759471008
C25	-3.9803804860	0.8299347011	-3.9534190037
C26	-1.5287707789	0.6095284538	-3.0336935611
O27	-0.5685566883	1.5605055146	-2.9383383151
O28	-1.1750013536	-0.4162930854	-3.6404796043
O29	-0.6264496251	3.9490965630	-1.9513384587
H30	-0.8130565801	2.4355198683	-2.4848687797
C31	-0.3120381329	4.7784681358	-3.0266064628
H32	0.2909642630	5.6508972173	-2.7287250797

H33	0.2421837727	4.2523656891	-3.8226572937
C34	-1.5463735292	5.3557625989	-3.7016518336
F35	-2.3186826561	4.4078973171	-4.2982838945
F36	-1.1960517734	6.2372913205	-4.6896440244
O37	-1.8430330318	4.8958566844	0.1580995646
H38	-1.4344144664	4.5956753665	-0.7195087715
C39	-0.3855773702	6.7598728278	0.6794946394
F40	0.0771110676	6.8935574741	-0.5905359624
F41	-1.4003566104	7.6528434090	0.8173917366
F42	0.6156089521	7.1685261618	1.5097469238
C43	-0.8057267931	5.3304039098	0.9985042453
H44	-1.1412396915	5.3263216689	2.0424519070
H45	0.0971500675	4.7125796560	0.9138132280
F46	-2.3426871673	6.0352959750	-2.8409450019
O47	1.7865972132	3.6426440982	-1.0300846611
H48	0.8290145871	3.7665543345	-1.3431132693
C49	1.9810975492	2.2744634676	-0.7740986521
H50	1.1512355607	1.6604102328	-1.1443756946
H51	2.9107964168	1.9108956761	-1.2311126056
C52	2.0949350933	2.0256011317	0.7217370036
F53	3.1424801655	2.6831717280	1.2838065952
F54	0.9824939953	2.4200251419	1.3994209876
F55	2.2700975109	0.7015655420	0.9893032528

4a / TFE^- / TFEH [(bpy)$MnCO_3CO_2H^-$ / TFE^- / TFEH]

Mn1	-3.6903263127	2.4769018885	-1.3165303958
C2	-2.7143116746	-0.1806738235	-0.4764943168
C3	-1.3115935184	1.4867872674	0.3407407565
C4	-0.4978462112	0.5527974126	0.9810286981
C5	-0.8085613645	-0.8031191356	0.8683424803
C6	-1.9351589852	-1.1732075024	0.1334556469
C7	-5.7548510062	0.4743866380	-2.3603132220
N8	-4.6012157049	0.6384712762	-1.6879648280
C9	-3.9526048368	-0.4617326371	-1.2287969322
C10	-4.4524735926	-1.7536785544	-1.4491097248
C11	-5.6488522686	-1.9146673393	-2.1461974877
C12	-6.3152606002	-0.7768674754	-2.6080709334
N13	-2.3901668000	1.1365649830	-0.3833019172
H14	-1.0904156533	2.5407088879	0.3879785780
H15	0.3601533984	0.8932506110	1.5534674887
H16	-0.1937030742	-1.5604115745	1.3489199898
H18	-6.2490708431	1.3739985102	-2.7065176240
H20	-6.0522726166	-2.9088547554	-2.3219161793
H21	-7.2529288310	-0.8451188370	-3.1526708877
C22	-4.6127379890	2.6944672925	0.2505406864

O23	-5.1971305038	2.8893971924	1.2361846395
O24	-2.3267401688	5.0854952111	-0.9332983333
C25	-2.7913511380	4.0292594203	-1.0530569602
O26	-5.6392949271	4.0695070692	-2.8784992893
C27	-4.8801249317	3.4385853525	-2.2618069788
C28	-2.6719513851	2.1806088541	-3.1305184625
O29	-1.3847247217	2.5606460753	-3.2932128835
O30	-3.2021981958	1.6745519865	-4.1389506975
O31	0.1481317051	3.4139724738	-1.4438591694
H32	-0.8971080441	2.9460033841	-2.4568741603
C33	1.2920684697	2.7290248327	-1.7986066648
H34	1.9252793684	2.4364164739	-0.9391872324
H35	1.0971327556	1.8052705945	-2.3751525354
C36	2.1968574312	3.5708975192	-2.6944724771
F37	1.5935796700	3.9378594669	-3.8589764109
F38	2.6102377047	4.7234494826	-2.1007548779
F39	3.3354565696	2.8912557876	-3.0492293098
O40	0.9837635036	4.6031181205	0.7084306996
H41	0.5776499709	4.2086303740	-0.1444823694
C42	0.2185135482	5.6781993536	1.1788785518
H44	0.8635710045	6.4648745966	1.5936413259
H45	-0.4195450804	6.1266711682	0.4079826031
C45	-0.7012012786	5.2447384612	2.3154937014
F46	-1.5945932150	4.2911416542	1.9447148693
F47	-0.0156882771	4.7347424651	3.3755390962
F48	-1.4245482473	6.2996040835	2.7886936152
H17	-2.2041475656	-2.2207368320	0.0477537008
H19	-3.9195656989	-2.6247462923	-1.0821880101

4b / TFE^- / TFEH [(bpymd)$MnCO_3CO_2H^-$ / TFE^- / TFEH]

Mn1	-3.7102468639	2.5010715211	-1.3365496531
C2	-2.7034469608	-0.1529444802	-0.5192615886
C3	-1.3586407307	1.5201830833	0.3897082308
C4	-0.5548514161	0.5533534963	1.0062888171
C5	-0.8874126086	-0.7867630197	0.7578566107
N6	-1.9341360599	-1.1559236519	0.0214620836
C7	-5.7647859999	0.4375863541	-2.3113484444
N8	-4.6121815047	0.6606618416	-1.6866138233
C9	-3.8996615838	-0.4422689909	-1.2251030911
N10	-4.3269887807	-1.7387266166	-1.4061758765
C11	-5.4836367444	-1.9144759790	-2.0377394271
C12	-6.2707570072	-0.8526382105	-2.5179037730
N13	-2.3951292164	1.1966107351	-0.3809266428
H14	-1.1542824143	2.5717948901	0.5119729523
H15	0.2908146066	0.8357628664	1.6233126327

H16	-0.2847500583	-1.5916935586	1.1789441858
H18	-6.3128606921	1.3076736104	-2.6588809178
H20	-5.8102484394	-2.9457942748	-2.1719930308
H21	-7.2156718247	-1.0162412591	-3.0247076666
C22	-4.6124834451	2.6897652064	0.2414230012
O23	-5.1785312325	2.8343825285	1.2476347690
O24	-2.3048722966	5.0821676157	-0.9145680698
C25	-2.7979975301	4.0406157461	-1.0667997559
O26	-5.7135767264	4.0370797573	-2.8834658778
C27	-4.9232235860	3.4333074229	-2.2740287697
C28	-2.6927550747	2.1501214660	-3.1324813410
O29	-1.3571268735	2.3703503651	-3.2288923869
O30	-3.2217645096	1.7259202499	-4.1793364408
O31	0.1598668500	3.3123470546	-1.3536112833
H32	-0.9166227675	2.7634550672	-2.3899333390
C33	1.3185648493	2.6940179870	-1.7682053214
H34	2.0074125470	2.4333635450	-0.9420949655
H35	1.1458240383	1.7635128055	-2.3401672250
C36	2.1243600409	3.5965069485	-2.6971475462
F37	1.4406850065	3.9359331234	-3.8243709616
F38	2.4948097105	4.7678217936	-2.1100720225
F39	3.2856998517	2.9974748949	-3.1184343924
O40	0.9500213135	4.3325406416	0.8351033141
H41	0.5631194123	3.9619687733	-0.0558530751
C42	0.2877979502	5.5131884436	1.1874569120
H44	0.9910892961	6.2796711487	1.5431548572
H45	-0.2973655910	5.9385908654	0.3631735494
C45	-0.6853325349	5.2693393442	2.3351109473
F46	-1.6505087487	4.3644669274	2.0329855074
F47	-0.0628356933	4.8076227271	3.4557540352
F48	-1.3236944471	6.4214853671	2.6937216044

4a / TFE^- / 2 TFEH [(bpy)$MnCO_3CO_2H^-$ / TFE^- / 2 TFEH]

Mn1	-3.4415116862	0.7796343753	-2.1995822964
C2	-2.5211820813	-0.7362726085	0.1520002938
C3	-2.2345787776	1.5455813759	0.5183591369
C4	-1.7844329077	1.3287391184	1.8187677435
C5	-1.6939298732	0.0187129056	2.2920218605
C7	-3.8622351822	-2.1545365591	-2.9225521112
N8	-3.4167237288	-1.2880571440	-1.9957413654
C9	-2.9736407646	-1.7666496488	-0.8057195610
C11	-3.4484785664	-4.0333269605	-1.4870343016
C12	-3.8994388687	-3.5310904373	-2.7104244745
N13	-2.6046762366	0.5424498064	-0.3016840565
H14	-2.3057229736	2.5530362488	0.1275730122

H15	-1.5129391207	2.1751146619	2.4414807926
H16	-1.3458417684	-0.1884554295	3.3010254589
H17	-4.2073678504	-1.7302541041	-3.8582611781
H18	-3.4662219672	-5.1006120599	-1.2813160531
H19	-4.2794846701	-4.1843790612	-3.4908434401
C20	-5.1397589821	0.7570044195	-1.5282547879
O21	-6.2327399720	0.7577467759	-1.1330862359
O22	-3.7835963800	3.7184676636	-1.9595062884
C23	-3.5398294971	2.5944707316	-2.0965244502
O24	-4.3053251376	0.8899455463	-5.0324450720
C25	-3.9827266447	0.8395975122	-3.9159923526
C26	-1.5089409223	0.5807462334	-3.0199551620
O27	-0.5573131240	1.5469951446	-2.9377076438
O28	-1.1379534158	-0.4452165491	-3.6168517718
O29	-0.6517314531	3.9514274586	-1.9607903107
H30	-0.8193634135	2.4196215767	-2.4956993375
C31	-0.3290786375	4.7618318596	-3.0457543849
H32	0.2658080083	5.6435036221	-2.7591858629
H33	0.2387471249	4.2232321561	-3.8243303213
C34	-1.5530964138	5.3198659816	-3.7560853786
F35	-2.3381658968	4.3513440284	-4.2986249353
F36	-1.1809454100	6.1373640250	-4.7916490859
O37	-1.8988983234	4.9004444658	0.1355588032
H38	-1.4866086702	4.5954919277	-0.7384443559
C39	-0.4185657868	6.7489761804	0.6192686088
F40	0.0319097319	6.8367179931	-0.6582521049
F41	-1.4149858656	7.6648354886	0.7428385848
F42	0.5992551797	7.1597386770	1.4278840075
C43	-0.8614478701	5.3375483785	0.9741081204
H44	-1.2033693770	5.3621618509	2.0155176989
H45	0.0330712872	4.7070556566	0.9087330709
F46	-2.3456690514	6.0653584370	-2.9457020094
O47	1.7526750341	3.6823474412	-1.0173822532
H48	0.7921408476	3.7909312249	-1.3308993496
C49	1.9515718259	2.3323123401	-0.6834995430
H50	1.1164432669	1.6962258387	-1.0017718500
H51	2.8739030345	1.9413966413	-1.1331149795
C52	2.0976616721	2.1714986362	0.8221078004
F53	3.1598931400	2.8588744263	1.3202808215
F54	1.0059767866	2.6069331987	1.5045188840
F55	2.2788657308	0.8646842846	1.1602026268
C55	-2.9759921135	-3.1407532677	-0.5256447947
H56	-2.6213441419	-3.5132426081	0.4298014310
C56	-2.0619880092	-1.0258992030	1.4451139215
H57	-2.0005086365	-2.0505515742	1.7964578686

4b / TFE^- / 2 TFEH [(bpymd)$MnCO_3CO_2H^-$ / TFE^- / 2 TFEH]

Mn1	-3.5741258056	0.7881918475	-2.3599442949
C2	-2.3509587072	-0.4756676177	0.0094025920
C3	-2.2929017566	1.8458469359	0.2314373108
C4	-1.7089595072	1.7211141828	1.4955319203
C5	-1.4507547354	0.4128923531	1.9400092155
N6	-1.7583245204	-0.6708403404	1.2349089813
C7	-3.8254495662	-2.2440839717	-2.7558905683
N8	-3.3768465975	-1.2478155977	-1.9966113119
C9	-2.7783535825	-1.5721018110	-0.7834962923
N10	-2.6293138371	-2.8683544273	-0.3462546182
C11	-3.0989453297	-3.8322081612	-1.1323171055
C12	-3.7191627771	-3.5864535309	-2.3706947059
N13	-2.6023166189	0.7882880709	-0.5184299326
H14	-2.5053131422	2.8198263814	-0.1891618779
H15	-1.4359355903	2.5902008686	2.0811409747
H16	-0.9775596251	0.2441076169	2.9072259971
H17	-4.2938229983	-1.9719306875	-3.6967145713
H18	-2.9848105429	-4.8528553857	-0.7669858097
H19	-4.1008534748	-4.3872757003	-2.9946559577
C20	-5.1942540470	0.7241254380	-1.5230976983
O21	-6.2368764334	0.6890573367	-1.0084633309
O22	-4.0164121135	3.7221300932	-2.5205951681
C23	-3.7504652567	2.5929376971	-2.4753580160
O24	-4.6987323702	0.5183414016	-5.0860653594
C25	-4.2684148551	0.6186153000	-4.0074954880
C26	-1.6991531135	0.6577830877	-3.2934319125
O27	-0.7397590846	1.6048193590	-3.0821151360
O28	-1.3419247836	-0.2604899770	-4.0524798326
O29	-0.9870461548	3.9212725504	-1.8014750335
H30	-1.0451703679	2.3747518196	-2.5162956367
C31	-0.3409646501	4.6791740515	-2.7712644529
H32	0.3831000959	5.3934061651	-2.3473350290
H33	0.2018237850	4.0592219122	-3.5061633511
C34	-1.3059703334	5.5202229593	-3.5953681708
F35	-2.1342597844	4.7790743813	-4.3775980067
F36	-0.6210693660	6.3505121783	-4.4468129560
O37	-2.2172847777	5.2931304197	0.1084528492
H38	-1.7893795493	4.8351616369	-0.6837248652
C39	-0.4633124271	6.8026590012	0.8489810464
F40	0.2015390129	6.8029319485	-0.3352708136
F41	-1.2610350192	7.9043102429	0.8428822569
F42	0.4674610329	6.9976024556	1.8256730714
C43	-1.2352143359	5.5110700687	1.0908811930

H44	-1.7089039717	5.6122324566	2.0747127886
H45	-0.4886138569	4.7079894649	1.1324951713
F46	-2.0976411454	6.3186304550	-2.8345204058
O47	0.9576089172	3.3320683819	-0.2317214370
H48	0.1638325768	3.5387627611	-0.8369963401
C49	1.2950317253	1.9835684481	-0.4039440343
H50	0.4286044421	1.3117252928	-0.3506743903
H51	1.8225788790	1.7858315830	-1.3491822932
C52	2.2310071079	1.5679519331	0.7107193111
F53	3.3915338198	2.2784952669	0.7172491600
F54	1.6864753492	1.7070210653	1.9452923721
F55	2.5729304713	0.2544500603	0.5749417482

6a $[(bpy)Mn(CO)_3]^0$

Mn1	0.0279358905	1.6821911194	1.5905194754
C2	2.7260515310	0.6670274986	1.1053563865
C3	2.7784862977	2.9690411844	1.4537759227
C4	4.1516580242	3.0146537029	1.2788723577
C5	4.8340332388	1.8282571160	0.9964340648
C6	4.1124392994	0.6450954495	0.9145548356
C7	-0.2969933609	-1.3296975387	1.3424633204
N8	0.5533003601	-0.2810483393	1.3049777481
C9	1.8724640097	-0.5264069104	1.0748939330
C10	2.3463666788	-1.8246455351	0.8537053113
C11	1.4583754175	-2.8914669518	0.8779564749
C12	0.1083115459	-2.6377151134	1.1345297046
N13	2.0621178458	1.8279056619	1.3604232110
H14	2.2208448808	3.8679995488	1.6814565773
H15	4.6704322104	3.9627319777	1.3617109785
H16	5.9085589728	1.8264605588	0.8483833340
H17	4.6239603552	-0.2864338477	0.7069186787
H18	-1.3334125447	-1.0994225972	1.5516462465
H19	3.3983584225	-2.0014681105	0.6676166148
H20	1.8111911851	-3.9025884196	0.7057258416
H21	-0.6230314887	-3.4368582836	1.1726532219
C22	-0.1756854462	1.7721291268	3.3701733109
O23	-0.3449159292	1.8566927093	4.5170534163
O24	-0.5048092737	4.5545299769	1.1292635952
C25	-0.2781454401	3.4268389478	1.3023091757
O26	-2.8458939705	1.2781965113	1.0200496948
C27	-1.7116901931	1.4210931821	1.2355823744

Appendix A

Co-Upgrading of Light Alkanes and Olefins by Tandem Olefin Dimerization-Transfer Hydrogenation

Y.C. Lam; D. C. Leitch; J. A. Labinger; J. E. Bercaw

Abstract: Light alkane-olefin mixtures are produced in various petrochemical processes, but of limited value owing to their volatility and complex composition. These mixtures can conceivably be upgraded into heavier alkanes by olefin dimerization operating in tandem with alkane-olefin transfer hydrogenation: light olefin dimerization produces a heavier olefin, which then undergoes transfer hydrogenation with the light alkane to produce a heavy alkane and light olefin, the latter reentering the dimerization cycle. The net result is the production of a heavy alkane from the light alkane-olefin mixture. Here we present preliminary results extending this concept to a silica-supported Ir transfer hydrogenation catalyst working in tandem with a $Cp^{*}TaCl_2(C_2H_4)$ olefin dimerization catalyst. Olefin dimer was formed under reaction conditions; however, this did not undergo transfer hydrogenation with the light alkane, probably owing to the steric bulk of the olefin dimer. It is proposed that the organometallic Ta catalyst be replaced by a Ni-exchanged zeolite, permitting operation at higher temperatures and selectivity for less highly branched dimers. Both these factors are expected to favor transfer hydrogenation.

Introduction

Modern refinery operations depend heavily on the cracking of heavy hydrocarbons to increase the yield of lighter hydrocarbons in the gasoline to diesel range. These cracking processes often produce a variety of products differing in both degree of unsaturation and carbon number. For example, fluid catalytic cracking (FCC) using Y zeolite produces ca. 20% cycloalkanes, 45% aromatics, 15% olefins, and 20% paraffins by volume.[1] The light fractions are particularly olefin-rich—using XZ-25 zeolite, the C3 fraction is 90% propylene while the C4 fraction is ca. 50% butenes, most of the balance being isobutane.[1] While isobutane and the light olefins are sent to an alkylating unit to produce high-octane gasoline, the remaining light olefin-alkane mixture is of limited value.

In light of this, we have attempted the conversion of olefin-alkane mixtures into heavier alkanes—an exothermic but entropically disfavored reaction that is exergonic at temperatures below ca. 250°C (Figure 1)—through tandem olefin dimerization and olefin-alkane transfer hydrogenation (Scheme 1).[2] Employing $Cp^*TaCl_2(C_2H_4)$ to catalyze the former[3-6] and $(PCP)IrH_4$ to catalyze the latter,[7-9] we demonstrated tandem formation of olefin dimers and hydrogen transfer from light alkane to light olefin, as evidenced by the formation of C13 and C14 olefins from a 1-hexene/heptane mixture.[2, 10] Unfortunately, no heavy alkane was formed, indicating that the olefin dimer did not undergo hydrogen transfer.[2, 10] Nevertheless, the tandem operation of the olefin dimerization and transfer hydrogenation is a substantial achievement—most olefin dimerization/oligomerization catalysts require strongly Lewis or Brønsted acidic activators, while the Ir transfer hydrogenation catalysts are highly sensitive to impurities, including traces of boranes and even N_2.[8]

Heterogeneous catalysts offer numerous intrinsic advantages over homogeneous ones, including facile separation of product and catalyst and operation of the reaction in continuous mode. Here, we present preliminary attempts to employ heterogeneous catalysts in tandem olefin dimerization-transfer hydrogenation. In particular, ($^{t\text{-Bu}}$POCOP)Ir(C_2H_4) supported on calcined silica was tried as a transfer hydrogenation catalyst.[11, 12] In combination with (dissolved) $Cp^*TaCl_2(C_2H_4)$, both olefin dimerization and transfer hydrogenation activity were observed. As with our previously reported system, the olefin dimer did not undergo transfer hydrogenation.

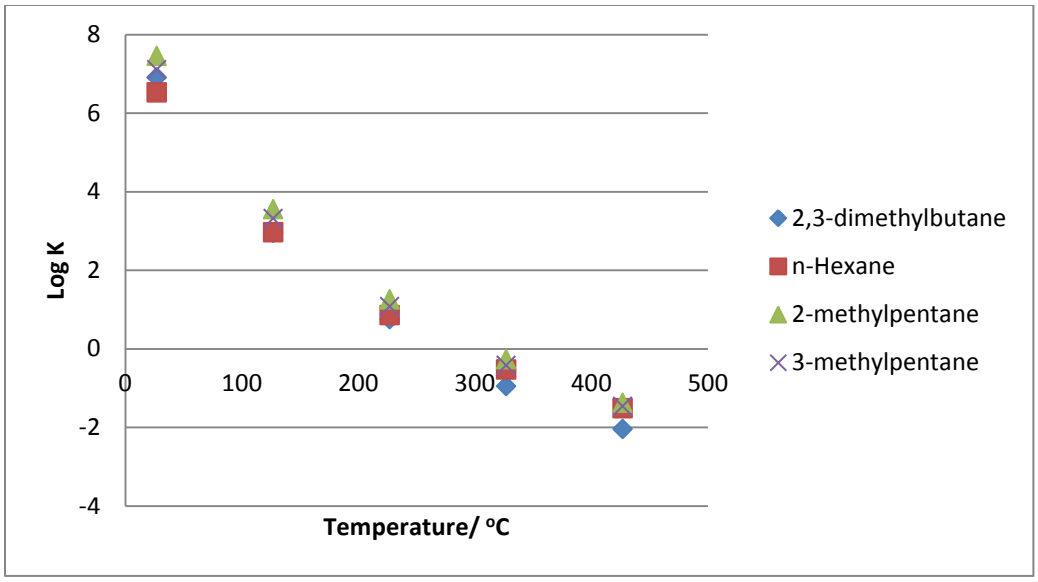

Figure 1: Thermodynamics, at 1 atm, of adding propane to propylene to produce various hexane isomers.[13] The vertical axis is $\log_{10}$ [K_{eq} (atm^{-1})].

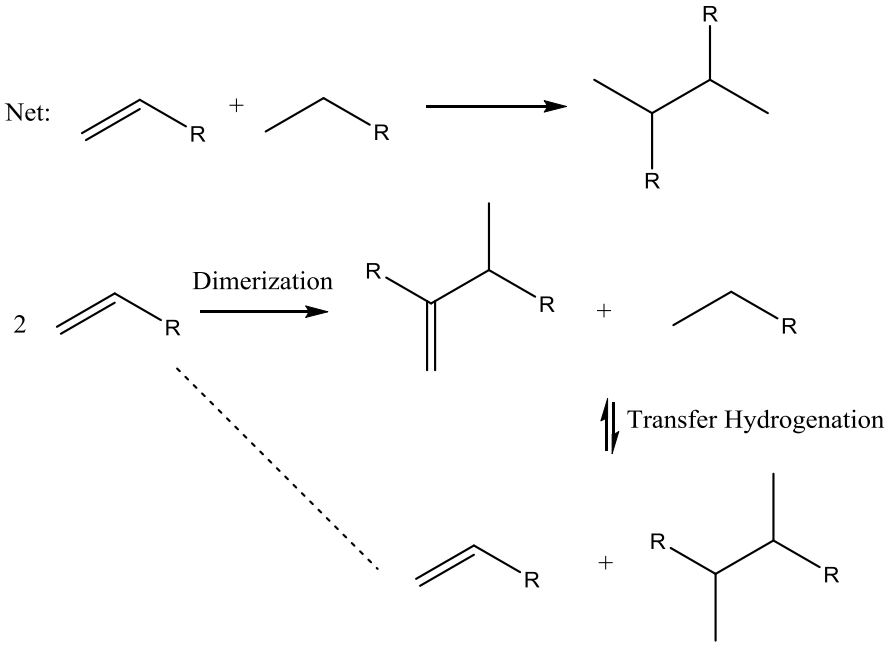

Scheme 1: Co-upgrading of light olefin and alkane by tandem olefin dimerization-transfer hydrogenation.

Results and Discussions

Silica, either dried at 150ºC or calcined at 500ºC, discolored 1-octene solutions of $Cp^*TaCl_2(C_2H_4)$. The silica acquired a yellow coloration reminiscent of the metallocycles formed by reaction of $Cp^*TaCl_2(C_2H_4)$ with α-olefins, presumably through surface Si-OH groups. In any event, the product(s) of such reaction showed no dimerization activity towards 1-hexene, raising doubts about the compatibility of organometallic dimerization catalysts with silica-supported transfer hydrogenation catalysts.

However, under a dry N_2 atmosphere, the presence of ($^{t\text{-Bu}}$POCOP)Ir(C_2H_4) immobilized on calcined silica did not prevent quantitative dimerization of neat 1-octene by $Cp^*TaCl_2(C_2H_4)$ (Figure 2). Since the covalent immobilization of the Ir catalyst involves reaction with free Si-OH groups (Scheme 2),[11] these free silanols were presumably "protected" by the Ir catalyst, enabling $Cp^*TaCl_2(C_2H_4)$ to remain catalytically active. The presence of N_2,[i] and the high olefin concentration, inhibited transfer hydrogenation and olefin isomerization by ($^{t\text{-Bu}}$POCOP)Ir(C_2H_4), accounting for the absence of octene isomers. It is also possible that under the fairly severe reaction conditions (overnight at 125ºC) the octene isomers were in equilibrium, and all eventually formed (via 1-octene) the olefin dimer, which acted as a thermodynamic sink.

The same catalyst mixture of $Cp^*TaCl_2(C_2H_4)$ and silica-supported ($^{t\text{-Bu}}$POCOP)Ir(C_2H_4) produced C12 products and a smaller quantity of C16 products, *n*-hexane, and perhaps C14 products—along with large amounts of hexene isomers and unreacted octane and 1-hexene—from a mixture of 1-hexene and octane (Figure 3).[ii] As with our previous results,[2, 10] the formation of

[i] Contrary to what Vicente *et al*. reported in reference 11, we did not observe any transfer hydrogenation, even between *tert*-butylethylene and cyclooctane, under a N_2 atmosphere. This inhibition by N_2 was previously reported for homogeneous analogs of these catalysts, refs. 7-9.

[ii] The very modest yield of dimer (C12-C16) products is due in part to the extensive isomerization of 1-hexene, and in part to an impure sample of $Cp^*TaCl_2(C_2H_4)$.

C16 products indicates transfer hydrogenation between 1-hexene and octane and the dimerization of 1-hexene and 1-octene operating in tandem.

This observation, while admittedly preliminary, hints at the possibility of co-upgrading light alkanes and olefins using heterogeneous catalysts. One limitation is that the olefin dimer does not accept hydrogen from a light alkane, precluding utilization of the light alkane. This limitation, also seen with our previous system using homogeneous catalysts, [2, 10] might conceivably be overcome through designing a Ir catalyst with a more open coordination site, probably by using less bulky alkyl substituents on the pincer ligand.

Another approach to overcome this limitation is to replace $Cp^*TaCl_2(C_2H_4)$ with Ni-exchanged zincosilicate olefin oligomerization catalysts, two of which have been shown to dimerize propylene (with some trimer also observed).[14] The C6 fraction comprises exclusively of olefins, with a slight selectivity for linear over mono-branched isomers; di-branched isomers are not formed.[14] Such dimers undergo transfer hydrogenation with light alkanes more readily than the di-branched olefins formed with $Cp^*TaCl_2(C_2H_4)$—the aforementioned formation of C16 products from a mixture of hexenes and octane is an indication of such hydrogen transfer. It may reasonably be hoped that the use of such Ni-zincosilicate materials in conjunction with supported Ir pincer catalysts will close the cycle in Scheme 1 and enable co-utilization of light alkanes and olefins.

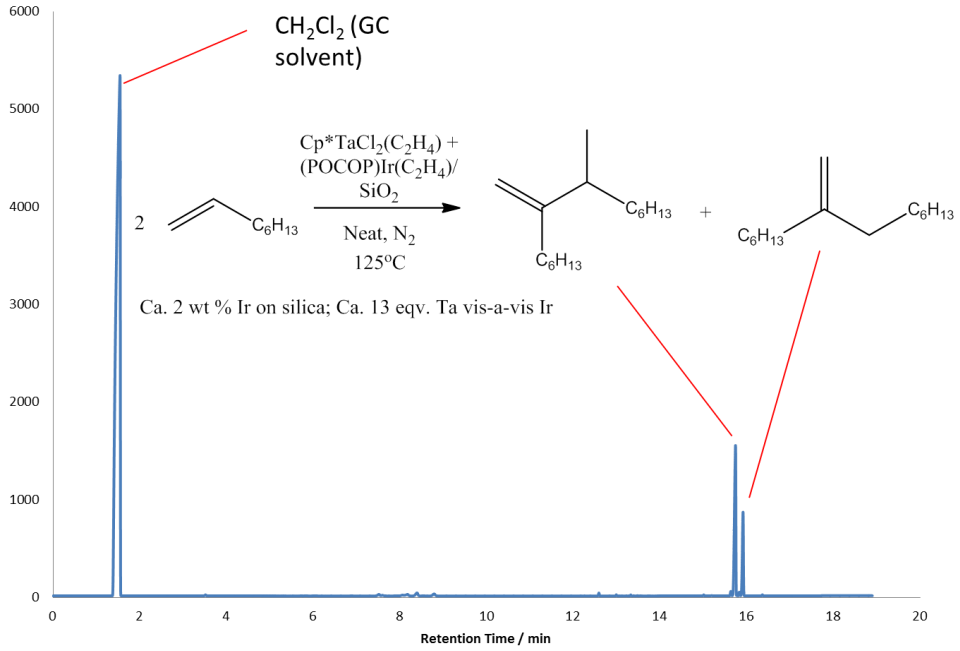

Figure 2: Gas chromatogram (GC) of mixture of 1-octene, ($^{t\text{-Bu}}$POCOP)Ir(C_2H_4) supported on calcined silica and $Cp^*TaCl_2(C_2H_4)$ after overnight reaction at 125ºC under a N_2 atmosphere. Note the quantitative conversion of 1-octene into octene dimers.

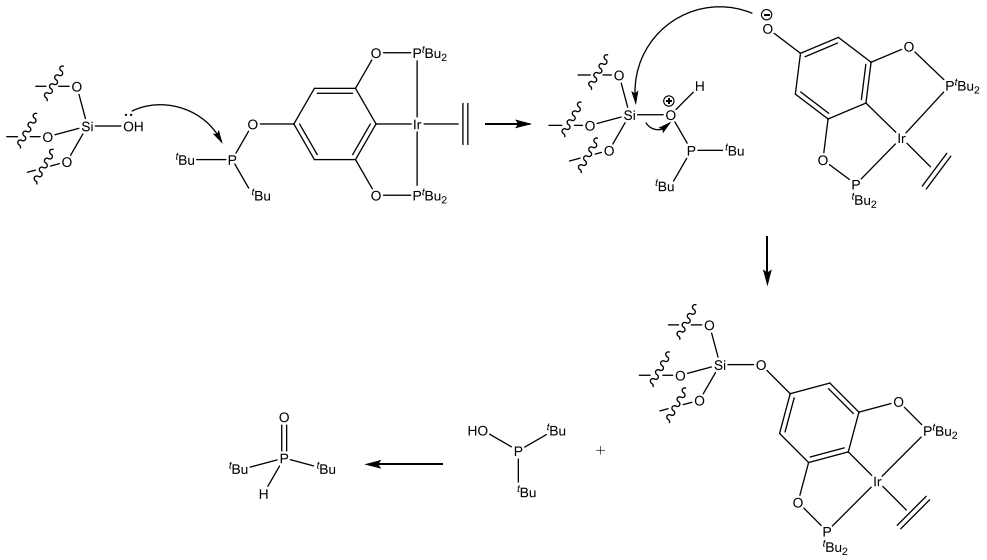

Scheme 2: Proposed scheme for reaction of ($^{t\text{-Bu}}$POCOP)Ir(C_2H_4) with surface Si-OH groups of calcined silica.

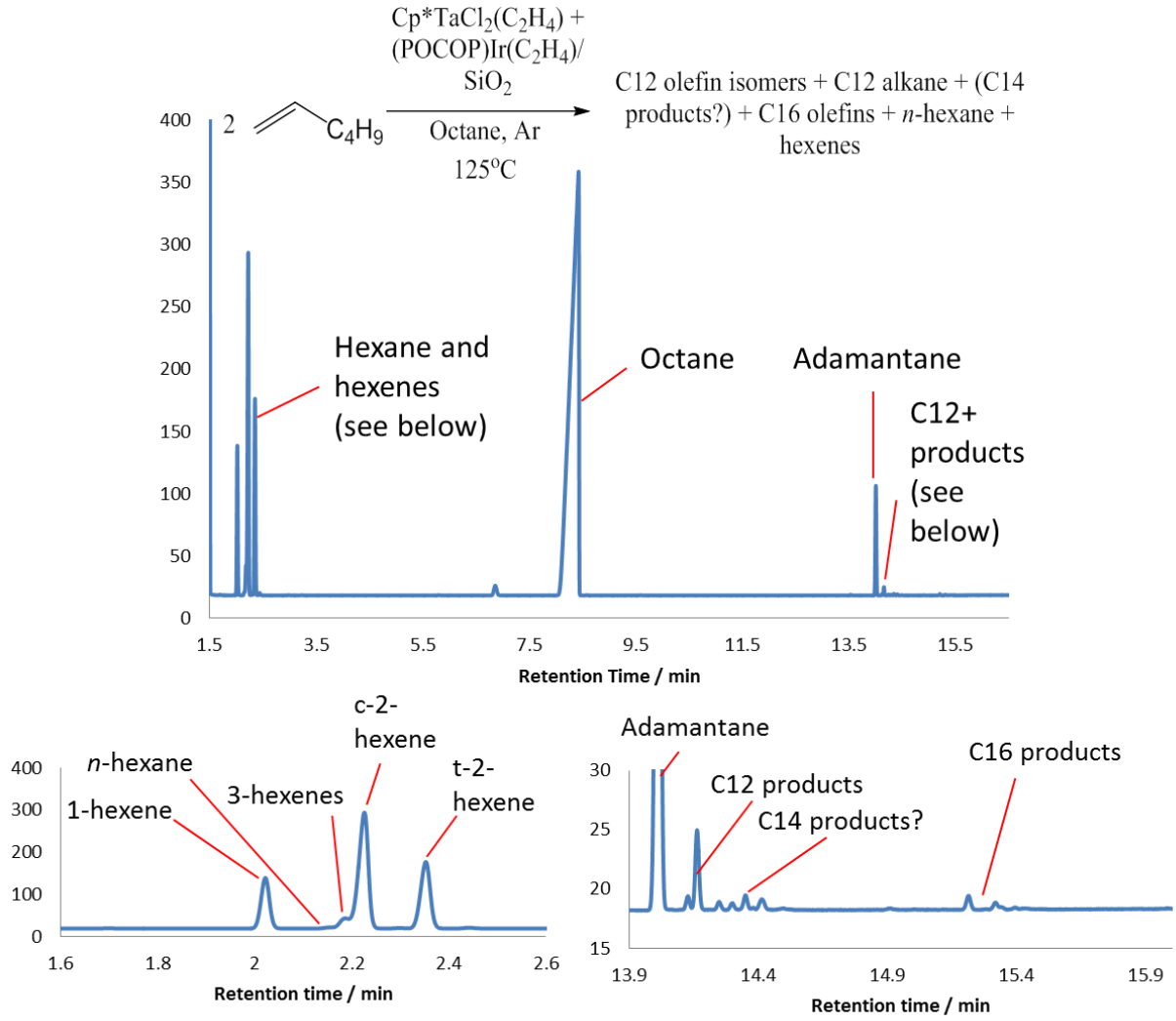

Figure 3: Gas chromatogram (GC) of mixture of 1-hexene and octane with catalytic $Cp^{*}TaCl_2(C_2H_4)$ and ($^{t\text{-Bu}}$POCOP)Ir(C_2H_4) supported on calcined silica, after overnight reaction at 125ºC under an Ar atmosphere. Adamantane was added as calibration standard.

Acknowledgements

The authors would like to thank BP for financial support through the XC^2 program, and Prof. Mark E. Davis and his group for helpful discussions.

Materials and Methods

All experiments were performed under inert atmospheres using standard Schlenk line, high vacuum line, and dry box techniques. $Cp^*TaCl_2(C_2H_4)$[5] and ($^{t\text{-Bu}}$POCOP)$Ir(C_2H_4)$[12] were synthesized as previously described. Silica Aerosil-380 (Evonik Industries, 363 m^2 g^{-1}) was heated under dynamic vacuum overnight at 500ºC,[11] then cooled under an Ar atmosphere. Silica-supported ($^{t\text{-Bu}}$POCOP)$Ir(C_2H_4)$ (32 mg ($^{t\text{-Bu}}$POCOP)$Ir(C_2H_4)$ on 0.39 g calcined silica, 105 μmol / g, 2.0 wt % Ir) was prepared as previously described.[11] Octane and 1-octene were dried over activated 3 Å molecular sieves, while 1-hexene was distilled from CaH_2 under argon.

For the dimerization of neat 1-octene, 6.1 mg $Cp^*TaCl_2(C_2H_4)$ (15 μmol, 1.5 mol %) and 11 mg silica-suported ($^{t\text{-Bu}}$POCOP)$Ir(C_2H_4)$ (1.2 μmol Ir) were added to 109 mg 1-octene (0.97 mmol), and the mixture was heated overnight at 125ºC. The resultant mixture was filtered through a plug of silica and diluted in CH_2Cl_2 for gas chromatographic (GC) analysis on an Agilent 6890N instrument equipped with a flame ionization detector and a DB-1 capillary column (10 m length, 0.10 mm diameter, 0.40 μm film).

Similarly, the tandem dimerization-transfer hydrogenation reaction was carried out with 480 mg 1-hexene (5.70 mmol), 715 mg octane (6.26 mmol), 5.5 mg $Cp^*TaCl_2(C_2H_4)$ (13 μmol), and 25 mg silica-suported ($^{t\text{-Bu}}$POCOP)$Ir(C_2H_4)$ (2.6 μmol Ir). The mixture was heated at 125ºC for one day and then at 200ºC for three days, and analyzed by GC as above.

References

1. P. B. Venuto, E.T.H., Jr., *Fluid Catalytic Cracking with Zeolite Catalysts*. 1979, New York: M. Dekker.
2. Leitch, D.C., et al., *Upgrading Light Hydrocarbons via Tandem Catalysis: A Dual Homogeneous Ta/Ir System for Alkane/Alkene Coupling.* Journal of the American Chemical Society, 2013. **135**(28): p. 10302-10305.
3. McLain, S.J., J. Sancho, and R.R. Schrock, J. Am. Chem. Soc., 1979. **101**: p. 5451.
4. McLain, S.J., J. Sancho, and R.R. Schrock, J. Am. Chem. Soc., 1980. **102**: p. 5610.
5. McLain, S.J. and R.R. Schrock, J. Am. Chem. Soc., 1978. **100**: p. 1315.
6. McLain, S.J., C.D. Wood, and R.R. Schrock, J. Am. Chem. Soc., 1979. **101**: p. 4558.
7. Gupta, M., et al., Chem. Commun., 1996: p. 2083.
8. Jensen, C.M., Chem. Commun., 1999: p. 2443.
9. Liu, F., et al., J. Am. Chem. Soc., 1999. **121**: p. 4086.
10. Leitch, D.C., J.A. Labinger, and J.E. Bercaw, *Scope and Mechanism of Homogeneous Tantalum/Iridium Tandem Catalytic Alkane/Alkene Upgrading using Sacrificial Hydrogen Acceptors.* Organometallics, 2014. **33**(13): p. 3353-3365.
11. Vicente, B.C., et al., *Reactions of phosphinites with oxide surfaces: a new method for anchoring organic and organometallic complexes.* Dalton Transactions, 2011. **40**(16): p. 4268-4274.
12. Huang, Z., et al., *Highly Active and Recyclable Heterogeneous Iridium Pincer Catalysts for Transfer Dehydrogenation of Alkanes.* Advanced Synthesis & Catalysis, 2009. **351**(1-2): p. 188-206.
13. M. Frenkel, G.J.K., K. N. Marsh, G. N. Roganov, R. C. Wilhoit, *Thermodynamics of Organic Compounds in the Gas State*. 1994, College Station, TX: Thermodynamics Research Center.
14. Deimund, M.A., J. Labinger, and M.E. Davis, *Nickel-Exchanged Zincosilicate Catalysts for the Oligomerization of Propylene.* ACS Catalysis, 2014. **4**(11): p. 4189-4195.